Computer Simulation of Fire-Sprinkler Interaction

By

Nicole Andrea Hoffmann

BSc, GIMA

Thesis submitted to the Council for National Academic Awards in partial fulfilment of the requirements for the Degree of Doctor of Philosophy

Centre of Numerical Modelling and Process Analysis
School of Mathematics, Statistics and Computing
Thames Polytechnic
London

Ove Arup and Partners, London

June 1990

Abstract

The research work presented herein addresses the problem of the mathematical modelling of fire and fire-sprinkler scenarios. This involved the numerical simulation of two-phase, three-dimensional, buoyant, turbulent, recirculating flows. The simulations were carried out in two successive and distinct stages.

The first stage dealt with the modelling of buoyant hot turbulent gas flows generated by a fire within room-sized compartments. These single phase studies were based on the field modelling approach to fire simulation.

The second part of the study involved the introduction of the cold water droplets through a single sprinkler head, thus, extending the scenario into the more complex two-phase regime. This led to expanding the single-phase fire model to take account of two concurrently present phases, ie. gas/liquid. The strategy used to model the two-phase process was the Eulerian-Eulerian technique or volume-fraction method. In order to take into account the physics involved in this process, interphase friction or drag was considered. Furthermore, due to the large difference in temperatures between the hot gases and the cold water droplets it was necessary to introduce interphase heat transfer. Due to the subsequent evaporation of the water droplets interphase mass transfer was also accounted for.

Models for both steady-state and time-dependent situations were developed, whereby experimental results of transient fire-sprinkler tests were used for validation. The simulations performed indicated the creation of extremely complex flow fields within the compartments both prior and during sprinkler activation. Phenomena such as the significant cooling of the hot combustion gases caused by the active sprinkler and the evaporation of water droplets have also been predicted. This has been verified by the experimental data. Thus, it can be concluded that the models outlined herein are capable of simulating the complex two-phase fire-sprinkler scenarios.

The need for subsequent investigative studies into such areas as the effect of using different auxiliary relationships eg. heat transfer, sprinkler characteristics and grid-spacing has been highlighted. In order to complete the validation process, further experimental data needs to be made available.

This two-phase technique has proven to be very computationally intensive with simulations requiring days of CPU time. This is clearly unacceptable. However, it is suggested that parallel computing technology may provide a means for reducing the CPU time involved to hours.

It can be concluded that though the model developed requires further investigation and refinements, it provides a basis for a practical and useful fire engineering tool.

Acknowledgements

I would like to express my sincere gratitude to my supervisor Dr. Edwin Galea for the keen interest and support he has shown during this project and preparation of this thesis.

I would also like to thank Professor Nikos Markatos for his initial guidance of this project. Thanks are also due to the staff of the Fire Research Station. In particular I would like to thank Mr. Geoff Cox and Dr. Suresh Kumar for their initial training and continued interest shown.

My sincerest thanks go to my mum and belated dad, brother Michael and sisters Gaby and Daniela, to whom this thesis is dedicated. Thank you for all the moral support and encouragement given to me during all my studies. I would like to extend my thanks to my fiance Steve Rix for all his patience and assistance given during the research and preparation of this thesis.

I also wish to thank all my friends and colleagues at Thames Polytechnic for their assistance and advice. I would like to thank the staff of the Computer Centre, in particular Mr. Robert Paynter and Ms. Moira Jarvis for providing me with the vital computer resources.

I would also like to express my appreciation for the financial support of Ove Arup and Partners and the SERC. Finally, I would like to thank CHAM Ltd. for their kind permission to use PHOENICS.

Table Of Contents

List of Tables

Chapter 1

Introduction

Chapter 1 Introduction

1.1 The Problem Considered

The destructive powers of uncontrolled fires can be seen daily. These result in around a thousand deaths and millions of pounds worth of property loss a year in the United Kingdom alone. An obvious method to limit these grim statistics is to reduce the possibility of the outbreak and spread of fires.

In 1812, the first prototype sprinkler system was installed in the Theatre Royal, Drury Lane, London [Nash (1973)]. Its life safety and property protection potential were quickly recognised and developed. Today the automatic sprinkler system is widely accepted as the most efficient form of automatic fire detection and extinguishment. Insurance statistics show that only four percent of losses occur on sprinklered premises [Anon,i (1984)]. In fact sprinklers successfully control or extinguish a fire in 98.5% of the cases [Anon,ii (1984)]. Due to this high success rate insurance companies encourage the installation of sprinkler systems by reducing the premiums payable [Tye and Genasis(1986)].

In the nineteenth century the newly formed insurance companies, like the Mutual Fire Insurance Company in Britain (now the Fire Offices' Committee) were the driving force behind the development and subsequent setting of the rules and regulations for sprinkler installations. They published their first edition of the Sprinkler Rules in 1888 [Round (1987)]. Today research and testing into every aspect of the fire phenomena, from collecting fire statistics, understanding the physical and chemical interactions and examining the processes involved in activating and subsequent

workings of a sprinkler are carried out at the Fire Research Station, Borehamwood.

For several decades a considerable amount of research has been concentrated on gaining a clearer understanding of the complex fire phenomena occurring within a variety of enclosures, such as nuclear containment cells, hospital rooms, aircraft cabins, and shopping malls.

In order to obtain the details concerning the fire dynamics involved and the potential fatal hazards responsible for preventing the occupants from escaping, simulations of possible fire scenarios are performed. These are either experimental fire tests or numerically based mathematical models.

Fire tests fall into two main categories; *full-scale* and *scale* models, whereby the former represents the ideal case. However, the amount of human and financial resources required to carry out full-scale fire tests within a completely fitted enclosure, such as a room can be extremely expensive (from around £10,000 for one *simple* full-scale compartment to around £100,000 for a series of full-scale compartment fire tests) and sometimes, impossible. The other problem is that it is not always possible to conduct enough fire tests to adequately deal with all eventualities, such as the positioning of the fire source, ventilation or material and positioning of the furniture. Full-scale tests are however still carried out to examine individual fire disasters such as the Stardust disco disaster in Dublin in 1981 which killed 48 people, or the King's Cross disaster of 1987 which claimed 32 lives.

The *scale* model approach is a useful technique used in several branches of engineering to test smaller models before developing full-scale systems. Hence,

various details such as flow characteristics can be analysed without the expense of constructing a full-sized model. However, this approach also has its disadvantages. In fire modelling complete similarity between full- and scale-models cannot be preserved [Williams (1969)] especially for the modelling of temperature distributions [Lee (1972)].

However, a mathematical model of the system under investigation potentially provides the fire engineer with a cheaper and more general alternative. The types of models currently available and still being developed can be divided into two main research areas, or fields of interest. Firstly there is the general fire scenario which only treats the pre-flashover case. The second area of interest is the initiation of the sprinkler and the subsequent fire-sprinkler scenario. These are two very distinct research fields and as such will be treated separately within this chapter.

1.2 Fire Modelling

Many attempts have been made to model fire phenomena mathematically. These fire models can be divided into two main groups; the stochastic and the deterministic models. The first type, based on fire statistics, evaluates the fire risk within a compartment by associating probabilities to all controlling parameters such as design features, distribution and the combustible nature of materials [Beard (1984/85)]. However, this method is not able to provide detailed transient or spatial developments of fire characteristics such as temperature or concentration. Nor is it able to assess the importance of dominant phenomena such as radiation or convection which are necessary for the determination of fire safety device activation. Hence, this review and

the work carried out uses a more fundamental approach and treats the fire as a physio-chemical fluid dynamic system of heat and mass transfer. This concept is embodied within the deterministic models.

Deterministic fire modelling of pre-flashover fire conditions have been carried out for over a decade using two distinct methods. These have become known as zone and field models; though a more apt description would be empirical and fundamental models. During this period several reviews have been published detailing the advantages and disadvantages of each model. Some of the most noteworthy reviews have been made by Kumar (1983), Galea and Markatos (1987,ii) and Galea (1989).

As a fire in a compartment grows due to the radiative heat feedback from the flames above the fuel, the hot combustion products start collecting below the ceiling in a distinct layer. This phase, known as the pre-flashover phase, is an important stage for determining life safety requirements. Once the hot layer temperature reaches around 600°C and the radiant heat to the fuel in the room reaches around 2 W/cm^2 there is a very rapid involvement of the whole room in flaming combustion. This stage is known as flashover and once this situation has occurred life within the compartment would no longer be possible.

1.2.1 Zone Models

For pre-flashover fire conditions zone models divide the fire compartment into several well defined zones or regions of fire behaviour. There are typically about four or five zones, see figure 1.1, which might be the fire's combustion zone, the rising thermal plume, as well as the hot upper layer accumulating below the ceiling containing the

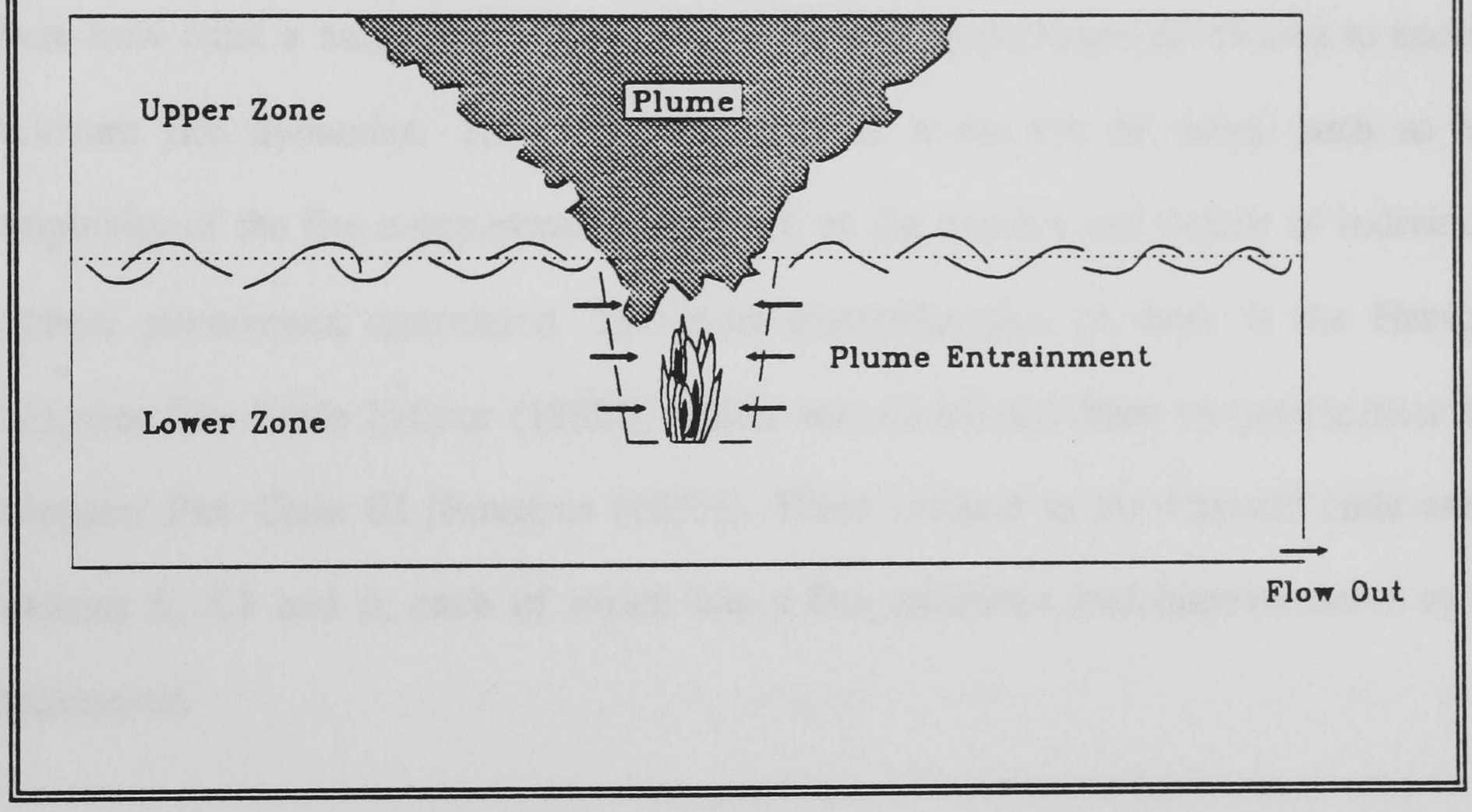

Figure 1.1 Schematic of a Zone Model (ASET) [Cooper and Stroup (1982)]

hot combustion products. Within the lower layer the gases are still cold and uncontaminated. These two layers are separated by a sharp interface.

Each zone is treated in isolation and experimentally based expressions are used to describe the physical processes within the zone. The output of one zone is used as the input to another, whereby the fundamental rules of conservation for energy and mass are maintained. The solution of these equations can be carried out within minutes on a medium sized computer such as a DEC VAX 11/780.

There now exist a number of different zone modelling packages developed to predict enclosure fire dynamics. These models differ in a number of ways, such as the complexity of the fire compartments analysed, or the number and details of individual physical phenomena considered. The most comprehensive of these is the Harvard Computer Fire Code [Mitler (1985)], which was developed from its predecessor the Computer Fire Code III [Emmons (1979)]. Three variants to the Harvard code exist; Versions 5, 5.3 and 6, each of which has a few additions and improvements to its predecessor.

The basic one-room zone model, given in version 5, is capable of using up to eight zones to obtain predictions which are to within ten percent of experimental values. Version 5.3 is basically the same as version 5 except that forced-ventilation along with a point-source plume rather than an area-source plume can be considered. The predictions of this new version were validated with experimental results obtained from the Lawrence Livermore Laboratory for a vented compartment [Mitler (1984)]. Version 6 does everything version 5 is capable of but on a larger scale. This version has been extended to simulate a multi-room lay-out of up to five interconnecting

rooms. This code has been used to simulate the events in the 1977 Beverley Hills Supper Club Fire in which 165 people died [Emmons (1983)].

Blomqvist and Andersson (1985) used Version 5 to simulate a full-scale three-seater sofa fire within a room with an open door. From their results they suggested that the fire plume model should be improved, whereby the model they were working with was compared with the FOVER zone model developed by Hägglund. A further study carried out by Takeda (1987) also used Harvard 5 for comparison purposes. He proposed a simple one-zone, transient model to simulate the fire growth process within a compartment in order to be able to determine the timing and conditions for flashover. From his results he was able to conclude that his one-zone model predicted the same behaviour as the Harvard 5 code.

Following the termination of the Harvard code project in 1983 the National Bureau of Standards (now the National Institute of Standards and Technology, NIST) started to develop their own zone model, FIRST (FIRe Simulation Technique) [Mitler and Rockett (1987)] using Harvard 5 and its improvements as a basis. The code they developed was only specific to a single compartment. However, with the new extensions the code is capable of simulating three different types of fire growth, as well as combustion products, and the effect of forced ventilation. The other important point is that it can be run on an IBM-PC (Personal Computer), making it more widely available.

The ASET (Available Safe Egress Time) zone model [Cooper and Stroup (1982)] is specific to determining the time available for occupants to safely evacuate the fire compartment. It calculates the egress time interval by determining the time of fire

detection to the time when hazardous conditions prevail within the compartment.

Another code which is specific to aircraft fires is DACFIR (Dayton Aircraft Cabin Fire Model) [Reeves and MacArthur (1976)]. It models the cabin atmosphere within wide body aircrafts caused by a seat fire.

The CCFM (Consolidated Compartment Fire Model) [Cooper and Forney (1987)] computer code is a prototype developed at the National Bureau of Standards. Its aim is to simulate the fire environment developing in a single room of a multi-room lay-out with a single opening like a vent, and is mainly used for fire and venting simulations.

There also exist zone models capable of describing the fire behaviour within a multi-compartment building. The first of these was developed by Tanaka which can be said to be the most comprehensive of the zone models. Figure 1.2 [Cox (1987)] shows the results of a typical calculation for a ten-storey building after a one minute simulation. The numbers under the ceiling represents the temperature rise (in degrees Kelvin) of the upper gas layer, whilst the numbers at the arrows refer to the mass flow rate of the hot gases or air.

FAST (transport of Fire And Smoke and Toxic gases) is another multi-room/multi-level model. However, it is only able to deal with the fire and the transport of the gases from room to room. It is not able to deal with forced ventilation or heating of target items [Cooper et al(1985), Walton et al(1985)].

Although these models are widely used and still subject of research and development in the U.S.A., Britain and Japan, several weaknesses are apparent. Firstly, the

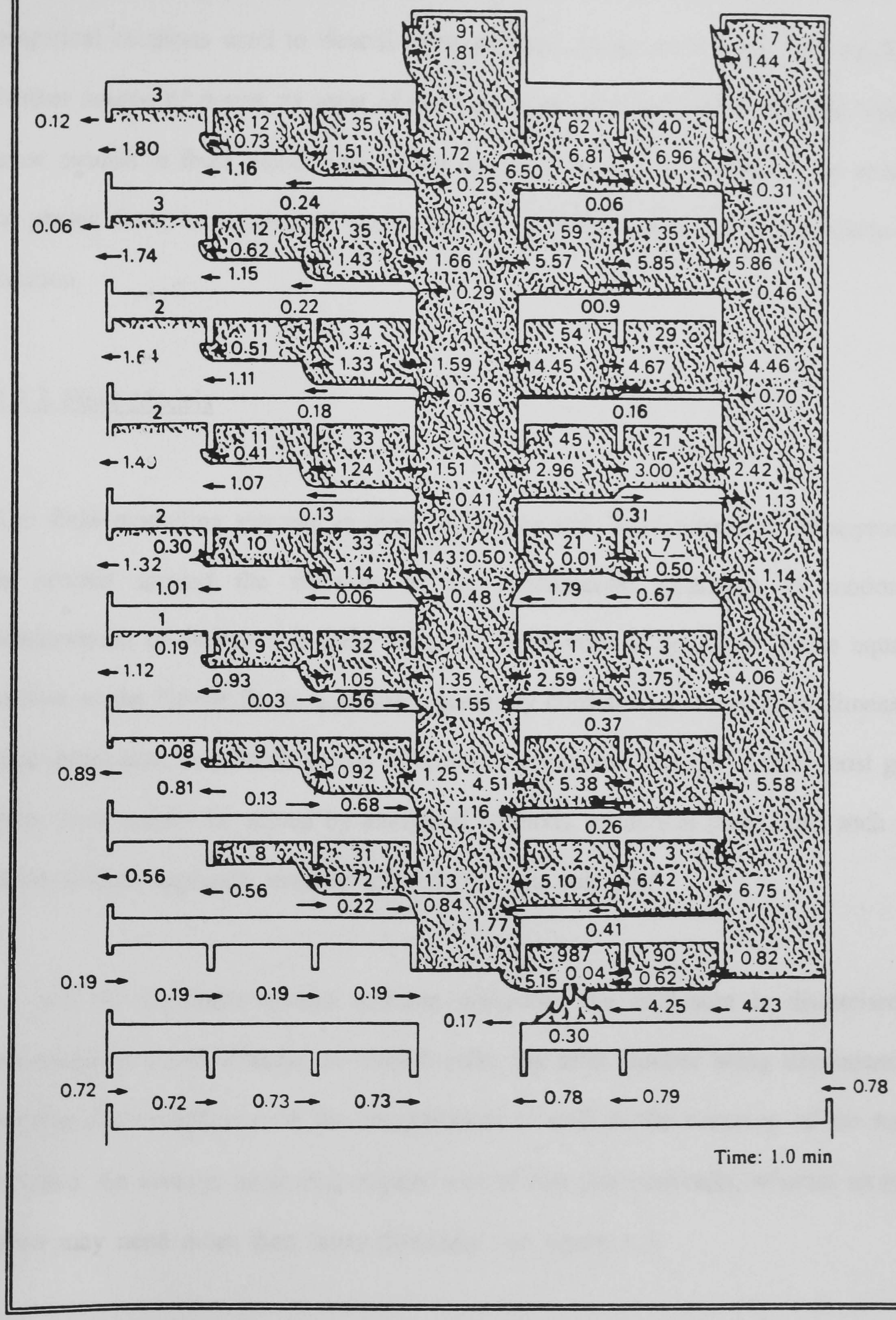

Figure 1.2 Typical results obtained with Tanaka's Zone Model [Cox (1987)]

assumption of a uniform field of temperature or species concentration is very idealised. Full-scale experiments have shown very clearly that temperature and concentration gradients exist within each region of the zone itself. The validity of the empirical relations used to describe the physical behaviour within each region is a further source of doubt, as most of the experimental experience employed within the zone models is from wood fires within domestic sized rooms. Hence, the simulation of plastic fires, large areas of enclosures or tall buildings should be approached with caution.

1.2.2 Field Models

The field modelling strategy is more ambitious and sophisticated in its approach. It is centred around the solution of the fundamental equations of motion and conservation of energy and mass using the finite-volume approach. These equations, known as the Navier-Stoke equations, generally consist of a set of three-dimensional, time-dependent, non-linear partial differential equations. Though in their most general form these cannot be solved by analytical methods, numerical procedures such as the finite-volume approach may be utilised for their solution.

As part of the finite-volume solution procedure the enclosure is discretised into thousands of small volumes or control cells, the total number being dependent upon the size and complexity of the compartment as well as the accuracy of the solution required. An average room may require around two thousand cells, whereas an aircraft cabin may need more than thirty thousand; see figure 1.3.

The governing equations are solved for simultaneously at the centre of each cell

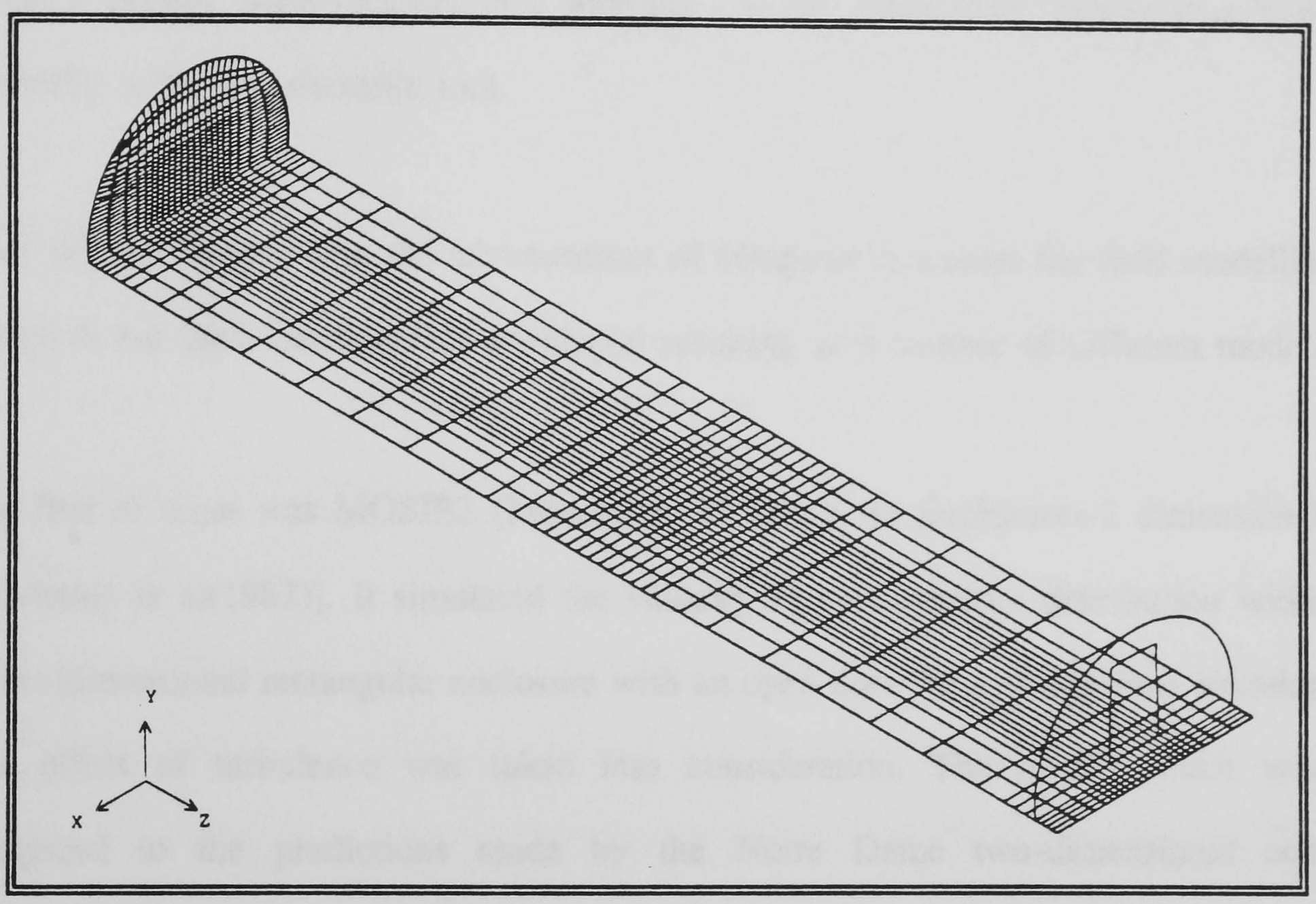

Figure 1.3 Schematic of a body-fitted aircraft cabin grid used in the SAFEAIR code [Galea and Markatos (1987)]

calculating the various fire parameters of interest such as temperature, pressure, and gas concentrations. In that way a more detailed perspective of conditions occurring within the compartment can be obtained.

Due to the vast amount of calculations performed, computer resources can be stretched to their limits, both in terms of speed and storage. However, the field-model's greater sophistication and minimal use of empiricism makes it a more generally valid and versatile tool.

Over the last decade with the advancement of computer resources the field modelling approach has been considerably developed resulting in a number of different models.

The first of these was MOSIE2 (Movement Of Smoke In Enclosures-2 dimensional) [Markatos et al(1982)]. It simulated the velocity and temperature distribution within a two-dimensional rectangular enclosure with an open door for a steady-state situation. The effect of turbulence was taken into consideration. The results which were compared to the predictions made by the Notre Dame two-dimensional code UNDSAFE as well as experimental data indicated the correct trends and even gave reasonable agreement with the experimental data. However, in order to validate the model thoroughly it was suggested that either, more two-dimensional experimental data was needed or that a three-dimensional version of the model should be developed.

In the early 1980s the Fire Research Station, Borehamwood, England, realising the potential of a computer fire model, started to develop their in-house field model JASMINE (Analysis of Smoke Movement IN Enclosures) by extending the two-

dimensional model MOSIE2. The model's first demonstration of its potential was made in 1982 with a simulation of a shopping mall [Markatos and Cox (1982)] where the results indicated the correct trends. However, further work particularly in grid-refinement studies and comparisons with experimental data were required. A further validation test was carried out on a nuclear containment cell [Cox (1983)] resulting in the same conclusions.

Further experimental data in the form of a fire within a road tunnel was made available for validation tests [Kumar and Cox (1985)]. In order to improve realism, the added effect of combustion was also included in this validation study. A simple one-step chemical reaction model was used to characterise the combustion process. The effect of natural and forced ventilation on the temperature distribution within the tunnel was also studied, whereby better agreement between the steady-state predictions and the experimental data were obtained remote from the fire source and with low ventilation. Close to the fire and with increased ventilation the agreements were less satisfactory. Though more work is required to improve on the agreement close to the fire this validation study demonstrated the usefulness of a computer model to study design features.

This basic framework of JASMINE was also validated for fires in hospital wards [Kumar et al(1985,1986,i,ii)], forced ventilated enclosures [Cox and Kumar (1987)] and an air-supported structure [Pericleous et al(1987)]. During these studies more points were raised which required further research. The first was concerned with modelling the turbulent diffusion flame. As a first approximation the fire source is represented as a volumetric heat source. However, Markatos et al (1986) developed a two-fluid steady-state model to simulate turbulent flames, which also allows for

chemical reactions to take place. The results they obtained were qualitatively realistic, but the cost of obtaining these results were paid for in the form of excessive computational time.

Further improvements to JASMINE were made by accounting for the effects of radiative heat transfer as well as momentum and convective heat losses to rough surfaces. These consequences were tested out on the tunnel fire problem [Kumar and Cox (1985)]. The new model TUNFIRE [Kumar and Cox (1988)] with the inclusion of the six-flux radiation model, improved the predictions remote from the fire source. However, Kumar et al did not think that the model was adequate in dealing with the effect close to the fire source and suggested that further validation and testing needed to be carried out.

During the period of developing JASMINE another general field model, UNDSAFE (University of Notre Dame Smoke And Fire in Enclosures), was developed by the University of Notre Dame in Indiana. It too was originally confined to two-dimensional compartment studies, but further modifications and versions have resulted in three-dimensional studies such as an aircraft cabin fire [Galea (1989)].

The importance of mathematical fire models as design tools for architects can be seen in the paper by Waters (1986) of Ove Arup and Partners. He used the general computer code PHOENICS to study air and smoke movement generated by a fire within very large buildings, such as airport terminals or department stores. With the aid of this model he was able to assess the environmental conditions within the building and hence the life safety aspects in the event of a fire.

A field model designed specifically for aircraft cabin fires was developed by Galea and Markatos (1987,i). It is a steady-state and time-dependent, three dimensional model which uses a body-fitted co-ordinate system to accurately model the interior of an aircraft, which is neither cartesian nor polar-cylindrical. It has been partially validated and is now used as a research tool to investigate design features of aircraft such as the effect of the air-conditioning system on the temperature distribution within a burning fuselage [Galea and Markatos (1989)].

Gupta et al (1988) developed a one-dimensional transient model to simulate the behaviour of the fire plume during the pre-flashover phase. It also calculates the fire plume characteristics under steady-state conditions.

Though field models, such as those mentioned above, provide the fire engineer with a useful investigative tool, the accuracy obtained is paid for by the excessive amount of CPU time required to perform the simulations. Partially due to the overheads involved in the calculation of the models and the limited amount of experimental data available, thorough validation of these models still needs to be carried out. Other problems associated with the field models, at this current stage of development, concerns the treatment of various physical phenomena which are present during a fire. The areas which need further research involve the processes concerned with turbulent flow, combustion as well as the spread of fire over a solid fuel.

The exact equations governing the turbulent flow of hot fluids are known, however their solution for practical purposes are not possible. The problem lies in the very nature of turbulence. The physical process which controls the growth and decay of turbulent motion are occurring on scales much smaller than the overall flow scales.

In order to describe this flow, it would be necessary to work down to this scale. However, tremendously large computer overheads would be incurred. To overcome this problem semi-empirical turbulence models have been developed, which consist of differential or algebraic equations and associated constants. One such model, the two-equation k-ε model [Harlow and Nakayama (1967)] is generally applied to simulate the re-circulating turbulent flow conditions occurring during a fire scenario.

The combustion process is very complex, due to the number of intermediate reactions and the formation of short lived species taking place. Turbulence further complicates this situation by mixing the reactants and products. Hence, it is assumed that combustion follows a one-step chemical reaction, whereby the fuel reacts with the oxidant to give the product. This approach, while only approximating the combustion process, produces satisfactory results for relatively simple fuels such as polyurethane foam [Kumar et al(1986,i,ii)].

This in turn leads on to the method of dealing with fire-spread across solid surfaces. At present it is assumed that the fire source is positioned across a fixed area or volume. However, solid fires travel along a surface increasing the fire area and replenishing their fuel. Hence, with improved combustion models the area close to the fire source can be predicted more accurately leading to the development of fire spread models.

However, these effects could be modelled using a combination of a field-zone model. This hybrid model employing the empiricism inherent in the zone model and the fundamental approach of the field model could simulate combustion, flame length and spread.

1.3 Sprinkler Modelling

While fire models were being researched and developed complementary efforts to quantify and model fire suppression were also initiated. As in the case for fire modelling, two distinct approaches, the empirical and the fundamental, have been developed to deal with various aspects of fire-sprinkler interaction. These are discussed below, though further details and research areas concerning the sprinklers themselves can be found in Appendix 1.

1.3.1 Empirical Models

A considerable amount of research has been carried out into characterising sprinkler activation for a variety of fire conditions, which has led to the setting of standards and regulations. However, the need was felt in the U.S.A. to *computerise* this system and use existing expertise to calculate the response time for arbitrary fires. Evans and Stroup (1985,1986) wrote DETACT-T2 capable of calculating the time required for a ceiling mounted heat and smoke detector to respond to a growing fire. The results of the calculated response times are to within five percent of the published standard figures. However, the correlations used for the code were obtained from experiments using large un-confined ceilings. For confined ceilings, these correlations are no longer valid due to the accumulation of fire products beneath the ceiling. Cooper (1982) though has developed a calculation procedure to deal with those situations.

A further restriction of the code was, that the fire to be detected could only increase its energy release rate proportionally with the square of time from ignition. This restriction was overcome in the BASIC version of the code, DETACT-QS [Evans and

Stroup (1985,1986)]. A fire can now have an arbitrary energy release rate which must be represented by a series of connecting linear approximations.

The model developed by Gardiner (1988) has taken up a position some way between the empirical and the fundamental models. He describes it as a quasi-zone-field model capable of describing the interaction between sprinklers and the thermally buoyant layers of fire gases. It is a three-dimensional steady-state model taking into account the geometry of the compartment and the position and characteristics of the sprinkler head(s). As it is assumed that the sprinkler is remote from the fire, three different methods to generate the smoke flow are provided within the model.

1.3.2 Fundamental Models

From the fundamentalist's point of view the simulation of a sprinkler falls into the category of a multi-phase process. Two-phase, and multi-phase flow in general play an important role in a wide range of environmental, industrial and engineering disciplines. Some typical examples are fluidisation [Patel et al (1989)], pneumatic conveying [Mason et al (1987)], sedimentation, air and water pollution and spray drying and cooling [Soo (1975)].

Particulate gas-liquid, solid-liquid and solid-gas flows form one class of two-phase flows, and are usually referred to as dispersed flows. The simulation of these particulate flows is of interest in many engineering applications such as droplet combustion, spray drying and cooling, and cyclone separators. In these fields the importance of adding particles into a fluid is shown by the drastic increase of particle surface area which can subsequently accelerate the reaction rate between the two

phases. The advantage can best be seen in the areas concerning heat and mass transfer as well as chemical reactions.

If the particles of a particulate two-phase flow are small enough then they follow the fluid motion and hence the whole flow can be treated as a homogeneous flow which is basically a single phase flow. However, in the present study it is assumed that the particles are large enough for there to exist a slip velocity between the two phases. Studying these types of flows provides us with a clearer understanding of the effects of engineering flow parameters such as pressure drop, and heat and mass transfer coefficients. They are also essential as they help us to understand the physical phenomena which could limit the performance of the equipment, aid in economic design, optimise operating conditions and also provide us with an insight into the reliability and safety of the system.

Over the last decade considerable progress has been made in the numerical study of single-phase flow, both laminar and turbulent. With the advent of increased capacity, speed and availability of computer resources particular interest has now been focused on solving two-phase flow phenomena numerically. Particulate two-phase flow can be dealt with using two distinct approaches. One method treats the fluid phase as a continuum and the particulate second phase as individual particles. The momentum and transport of these discrete particles are calculated using the various forces acting on the particles. The effect of the particles on the gas phase is taken into account by introducing appropriate source terms in the gas phase conservation equations. This approach is known as the Lagrangian or particle tracking method.

Treating both phases as a continuum and solving for the appropriate continuity

equations for the fluid and the particulate phases is the approach employed by the Eulerian method.

These distinct approaches have been fully reviewed by several authors, detailing the method's individual algorithms, merits and disadvantages. Crowe (1982) reviewed the methods for one- and two-dimensional flows. He concluded that the most difficult aspect of gas-particle modelling is the treatment of turbulence and that more studies, both experimentally and numerically are needed.

Durst et al (1984) discusses the differences between the two methods. However, this review is made more complete by comparisons obtained by simulating two two-dimensional particulate flows using both methods. From these studies the main conclusion was that the two approaches are very similar from a numerical rather than a physical point of view, whilst the main difference lies in the treatment of the particle phase. The Lagrangian approach provides more detailed information on the particle phase. However, convergence problems can occur for flows with high particle loadings. These are not observed when using the Eulerian methods.

A third review by Sirignano (1986) also compares the merits and demerits of the two methods. However, he also introduces a third technique of formulating the second phase as a set of probability density functions. This approach can be used for a wide range of resolutions relative to the droplet size. Furthermore, his decision criteria on which method to use is dependent on the resolution scale and the droplet spacing. Hence prefering the Lagrangian formulation which limits the number of droplets considered on the computer resources.

In the following sections brief details of the different treatments of the motion of the dispersed particles and their interaction with the continuum for both phases are presented, along with their advantages and disadvantages. However, details of the mathematical equations employed by the schemes will not be given as these have been cited in the review papers and the papers highlighted in the following sections. The treatment of the continuous phase is not described here as both methods deal with it in the same fashion; as described in chapter 2 for the single-phase fire simulation.

Any model, simulating suspended droplets within a gas field, needs to account for the effect of three distinct phenomena. As droplets are introduced into a gas field a drag force will be exerted on the gas and the droplets, accelerating or decelerating the overall flow accordingly. This momentum transfer between the phases is one of the first *coupling* phenomena to be considered.

If the gas phase and the particles are initially at different temperatures heat will be transferred between the two phases. The affect of this phenomena is that the densities can be altered and hence the overall flow field of the two phases can be affected. The last mode of coupling is mass transfer. If, as for the case of particles evaporating, the mass of the second phase is decreasing. This decrease in mass needs to be accounted for, due to the conservation of mass, by adjusting the gas phase accordingly.

The Lagrangian Method

The concept of two superimposed continua occupying the same control-volume was first formulated by Migdal and Agosta (1967). They derived a system of differential

equations from the basic laws of mass conservation and thermodynamics, to describe the dynamics of gas-particle systems. Within this system the particles, which are assumed to be finely dispersed, are treated as a continuous system of sources/sinks to the gas phase. The gas phase, which is treated as a continua is evaluated using partial differential equations whilst the particulate phase is solved for using ordinary differential equations. In their paper from 1967, an application to one-dimensional flow is given, but no solution or comparisons are provided. However, this paper has proven to be a stepping stone for a considerable amount of work ir two-phase simulations. Some of the developments and results with this approach to two-phase modelling are presented below.

In the early 1970s Crowe and Pratt (1972) presented a two-dimensional gas-particle flow model using the *tank and tube* formulation, where the finite-difference volume represented the tank and the particles traversing the volume, the tube. This formulation required the differential equations to be formulated as vorticity and stream functions. The disadvantage this causes is that mass transfer was not permitted. It also implied that particles were assumed to occupy negligible volume.

Crowe et al presented a two-dimensional gas-droplet model in 1975. This model is based on the concept first developed by Migdal and Agosta (1967) and treats droplets as a source of mass, momentum and energy to the gas phase. Hence, it is known as the particle-source-in-cell (PSI-Cell) model. Since it was first presented it has been applied to simulate a variety of processes; spray drying, electrostatic precipitators, cyclone separators, combustors, and coal-fired furnaces [Lockwood et al(1980)].

Recently a modified version of the original PSI-Cell model was used in a study on

the flow characteristics and convective heat transfer of a freely falling curtain of spherical particles [Hruby et al(1988)]. This modification took into account the buoyancy effect on the air and temperature dependent properties as well as the effect of radiation. The predictions, which were compared with experimental results obtained as part of the study, gave the correct trends for the velocity and temperatures for isothermal air-particles. However, over-predictions were observed for the non-isothermal case. These were shown to be reduced with an adjustment of the drag-coefficient used.

The viability of using two-phase mathematical models as design tools for gas-particle flow meters was recently demonstrated by Sharma and Crowe (1989). The gas-particle flow through a venturi was analysed using the quasi-one-dimensional model CONVAS (CONservative VAriable And Source) whilst the PSI-Cell model was used to simulate the two-dimensional orifice flow. This in itself shows how far mathematical models have developed. Two-phase models are used as design tools to improve the design of measurement techniques which, in turn are used to obtain better measurements to model two-phase flow.

Several other groups have also been working with and developing particle tracking routines. Boysan et al (1982) developed their own code to simulate cyclone separators. As part of this model and due to the highly swirling flows associated with cyclone separators account was made for turbulence modelling. However, it was assumed that there existed no coupling effects between the gas and the particles due to the small slip velocities and isothermal conditions. With this model good results were obtained for the two primary design features of a cyclone separator; the pressure drop and the grade-efficiency curve.

In recent years the group has been involved in a variety of two-phase calculations using the commercially available code FLUENT [Swithenbank et al(1987)]. This computer package is capable of simulating three-dimensional, laminar or turbulent flows including chemical reactions and radiant heat transfer as well as all three modes of phase coupling.

Other researchers have included Abou Ellail and Khalil (1980) who presented a combustion model for kerosene spray flames in which the droplets evaporated due to convective heat transfer. The liquid fuel within a cylinder of a spark ignition engine was simulated by Low and Baruah (1981) using a one-dimensional transient particle tracking model. On e again all three modes of coupling were taken into account. Another one-dimensional model used to predict the pressure distribution in air-drilling systems as used within the oil industry was presented by Sharma (1987).

These above examples show how diverse the field of two-phase modelling is, as well as the complexities that some models can handle. However, with respect to fire-sprinkler modelling the most notable work using particle tracking has been carried out by Alpert [Alpert and Mathews (1979), Alpert (1985,1986)]. He used an extended version of TEACH-T [Gosman and Pun (1973)], capable of dealing with two phases, to simulate a range of steady-state two-dimensional axisymmetric interactions of fires with droplet water sprays. The three modes of coupling were taken into consideration. In the series of investigations carried out he studied the effects of sprinkler spray characteristics such as mass flow, inlet velocities and droplet diameters. He concluded that the plume penetration is controlled by the ratio between spray and plume thrust as well as a ratio of median spray dropsize to critical dropsize that can be stopped from falling by the plume.

The Eulerian Method

The Eulerian-Eulerian two-phase approach is an extension to the one-phase Eulerian method, whereby account has to be made of the volume that each phase occupies within a single control-cell.

For the single-phase Eulerian approach, the complete volume or space of the control-cell consists of the fluid under consideration; gas, liquid or solid. In the case of the two phase approach the volume of a single control-cell is made up of a mixture of gas and liquid, gas and solid, or liquid and solid, depending on the process simulated. In that way, assuming that the cell does not consist of blockages, a simple *space sharing* equation can be used to take into account the volume fraction of the cell consisting of the various phases. This equation is:

$$r_1 + r_2 = 1.0 \qquad (1.2\text{-}1)$$

where r_1 is the volume fraction taken up by the first phase and r_2 the volume fraction of the second phase. In that way if a control-cell consists of only one-phase, the set of partial differential equations for the two phases converts to a single-phase system.

This approach has been embedded into the workings of two powerful computational fluid dynamic code solvers; PHOENICS [Spalding (1981), Rosten and Spalding (1986)] and CASCADE [Patel and Cross (1989), Patel et al(1989)]. PHOENICS is a commercially available code capable of modelling steady and transient, turbulent, three-dimensional two-phase problems. CASCADE has been developed to be able to simulate steady and transient, turbulent, two-dimensional multi-phase problems. The

three modes of coupling are included in both codes.

The capabilities of both codes can be seen by the variety of applications they have been used for. Gosman et al (1976) simulated steady-state recirculating flow assuming no momentum interaction. Kostamis (1987) performed a three-dimensional steady-state study of the flow characteristics in the off-gas ducting system of a modern industrial steel making plant. In this study he included the effects of turbulence on the gas phase, chemical reactions and two-phase thermal radiation. Fenech (1987) simulated an iron blast furnace using a two-dimensional steady-state model taking into account heat transfer and momentum coupling.

These three cases used PHOENICS as their main equation solver, whilst the following two examples utilised the capabilities of CASCADE. The processes carried out within a fluidised bed were simulated by Patel and Cross (1989), who used the multi-phase capabilities by modelling the effect of up to four different sized particles. Other multi-phase problems simulated using the code include blast furnaces and iron ore pellet induration systems [Patel et al(1989)].

None of the above cases were concerned with diminishing particles or droplets. However, in the case of a liquid phase, evaporation sometimes needs to be accounted for. In those cases the approach outlined above needs to be extended in order to satisfy the laws of conservation. In 1982 Spalding published this extension calling it the *shadow volume fraction* method. In this approach a volume fraction is evaluated which represents the volume fraction which the liquid phase would have possessed in the absence of evaporation. The velocities remain unchanged. To obtain these two distinct liquid volume fractions two separate steps need to be performed. Firstly the

conservation law of the second phase is evaluated including the mass transfer effect, $\dot{m}$. This is given by:

$$r_1 \Sigma g_{1o} = r_{1i} \Sigma g_{2i} - \dot{m} \qquad (1.2\text{-}2)$$

where r_1 is the volume fraction of the liquid and g_2 is the mass flow rate of the second phase. The subscripts i and o denote inflow and outflow from a control volume.

The second step involves the calculation of the *shadow* volume fraction, whereby equation (1.2-2) is evaluated but excluding the effect of the mass transfer. Hence, the equation solved for is:

$$r_s \Sigma g_{1o} = r_{si} \Sigma g_{2i} \qquad (1.2\text{-}3)$$

where r_s is the *shadow* volume fraction.

This capability, which has been *built in* to the algorithms employed within PHOENICS, has been used to simulate the steady-state effect of spray cooling of combustion products [Kircaldy and Markatos (1982)]. It has also been employed to investigate the ignition of granulated propellants within a gun barrel [Markatos and Kircaldy (1982)].

The latter model is able to predict the formation of the pressure waves generated within a gun barrel as well as the spread of flames along a bed of small grain propellants. Due to the combustion and hence diminishing size of the powder the

space-sharing equation was implemented. The results obtained were physically realistic however no experimental data was available for comparison.

The work carried out by Kircaldy and Markatos (1982) on spray cooling of combustion products was with respect to the exit of hot gases from a combustor. It was proposed to cool these by spraying cooler water into the very hot gas stream. The flow considered was two-dimensional two-phase steady-state with interphase heat and mass transfers. This study was used as an initial basis for the three-dimensional steady-state two-phase model and calculations presented in chapter 4 and 5 respectively.

Summary

It is clear that a considerable amount of research has been carried out implementing the two distinct two-phase methods. A brief summary of the methods is given below.

The Lagrangian methods uses Newton's law of motion to calculate the velocities of every individual particle within the flow field of a continuous fluid. Integration of the velocity with time gives the trajectories, so that the particle velocities and locations can be used to obtain the mass, momentum and energy transfers of the solid to the fluid and vica versa. However, the actual volume of the particle is neglected in order for the general equations of the fluid not to be weighted.

Hence, it can be concluded that this approach provides more details on the particle phase, yielding the trajectories and residence time of the particles within the flow. Furthermore, a range of particle sizes can be solved for concurrently. However,

convergence problems occur in cases when particle loadings are high [Durst et al(1984)].

The Eulerian approach treats the dispersed particles as a continuum. This implies that there are two fluids present differentiated by considering the volume concentration of each phase. Hence, the resulting set of general transport equations are weighted by this factor in order to take into account the two fluids flowing through each control volume.

One of the main advantages of the Eulerian approach is that it is able to provide converged solutions fo flows with high particle concentrations and density differences between the particles and the fluid. A drawback experienced with this technique is that generally only an average droplet diameter can be solved for. Though the extension to IPSA by Patel and Cross (1989) enables the effect of multi-sized particles to be solved for but at the expense of computing storage and time.

1.4 Contributions of the Present Study

As the field of fire modelling and experimentations have now reached a stage where models are used as design tools and a plethora of data has been collected, attention is beginning to be focused on the sprinkler system. It has become apparent over the last few years that not enough is known about the processes of sprinkler activation, the effect of flow rate on the smoke layers, the effect of droplet characteristics and overall cooling effects of the fire atmosphere. However, wide interest has now been focused both in the U.K and the U.S.A. on studying the distinct aspects which are

part of the sprinkler process. Just as mathematical models were developed alongside, or following full-scale fire experiments, sprinkler models and fire-sprinkler interaction simulations are now developed utilising the data as it becomes available.

In the short review on current sprinkler models and the mathematical techniques available for dealing with concurrent gas and water phases, it could be seen that a variety of different models have already been developed. However, as yet no model using the volume fraction approach has been developed to simulate the fire-sprinkler interaction phenomena. The amount of computer resources available was probably a major hinderance. Now, as suitable computer power with the development of parallel computer technology becomes more readily available, this method can be further developed and researched.

The work presented was carried out to show that this alternative approach is now available as well as to develop a prototype. It can only be described as a prototype due to the knowledge and data available during this project. However, as more experiments are carried out, vital data for further validation is obtained. Hence, the prototype presented within the following chapters can be modified in order for its future versions to be used as a design tool by architects and fire engineers.

1.5 Outline of Thesis

This thesis consist of six chapters.

Chapter 2 is devoted to single-phase fire modelling. For completeness, outlines of the

physical and mathematical modelling of a steady-state as well as transient fire within a compartment are provided. This includes the single-phase governing partial-differential equations along with the auxiliary equations, such as heat losses to the walls, turbulence and boundary conditions. The numerical solution procedure, SIMPLEST, employed to solve the set of equations is highlighted. A derivation of the finite-domain equations is given.

The predictions obtained implementing the fire models are presented in chapter 3, whereby comparisons with experimental data are made whenever possible. For the steady-state simulation a fire within an open office-sized room was used. The cases considered for the transient studies were a bed fire within a closed hospital ward room and a corner fire within an open office-sized compartment.

The two-phase steady-state and transient fire-sprinkler models are presented in chapter 4, whereby the outline of the chapter closely follows that of chapter 2. Due to the more complex nature of the phenomena investigated, the auxiliary equations now also include interphase heat and mass transfer and interphase friction. For the two-phase model the solution procedure IPSA was employed. This algorithm is outlined, along with details concerning the computer resources utilised.

The results obtained by implementing the two-phase models are detailed in chapter 5. The format and order of the results presented closely follows that of chapter 3 to ease comparisons with the single-phase results.

In the final chapter the main conclusions of this study are presented along with some suggestions for future work.

Chapter 2

Single-Phase Modelling

Chapter 2 Single Phase Modelling

2.1 Introduction

The modelling of fire spread within a compartment presents a formidable challenge due to the number of underlying physical processes such as turbulent buoyant convection, radiative heat transfer and combustion which are difficult to model. A considerable amount of numerical computations have already been carried out to study the various aspects of the fire phenomena [Markatos et al(1982), Kumar and Cox (1985), Hoffmann and Markatos (1988), Galea and Markatos (1989)]. Within the studies carried out for this thesis the physical pr blem concerns the movement of combustion products within single three-dimensional enclosures, though the theories can equally well be applied to multi-compartment lay-outs. The flow is dominated by buoyancy and the turbulence serves to promote the rate of diffusion of heat, mass and momentum.

Radiative heat transfer and combustion have not been included in any part of the simulations. There are several reasons for these omissions. Firstly, an earlier study [Hoffmann and Markatos (1988)] showed that radiation for enclosure fires with a maximum heat release rate of about 80kW was not a significant factor of heat transfer. Furthermore, at this early stage of model development the priority was to obtain gas temperature stratifications and velocity flow fields which were used as initial conditions for the second stage of this study. Combustion could be added at a later stage once confidence in the model has been obtained.

The starting point of the present analysis is the set of partial differential equations

that express the conservation of mass, momentum and energy and other fluid variables. These differential and empirical relations are presented both for steady-state and transient conditions in this chapter.

For completeness and clarity the chapter has been divided into six main sections. Sections 2.2 and 2.3 are devoted to the steady-state and time-dependent equations and relations, respectively. Within each of these sections the dependent and independent variables are highlighted; the equations for conservation of mass, momentum, and energy are presented in the general form. The auxiliary equations necessary for completeness of the model are also illustrated.

Within section 2.4, prior to presenting the solution procedure, the set of conservation equations are integrated over a typical control-volume to form a set of algebraic equations. For completeness, the time-dependent equations are discretised in full and the steady-state discretisations quoted. These equations can be solved for iteratively.

The solution procedure SIMPLEST was used to evaluate the algebraic equations. Its algorithm used for solving the set of differential equations is described in section 2.5 along with the computer package PHOENICS used for this study.

2.2 The Steady-State Fire Model

2.2.1 Introduction

The partial differential and auxiliary equations used to model a steady-state single

phase fire scenario within a single three-dimensional compartment are presented within this section. Additional information on physical processes covered will be given as necessary.

2.2.2 The Dependent and Independent Variables

The independent variables used are the width, height and length; x, y and z of a cartesian co-ordinate system.

The dependent variables solved for are the velocities of the gas in the three space directions u, v, and w, the pressure p, the gas enthalpy H and the turbulence kinetic energy k and its dissipation rate ε.

2.2.3 The General Differential Equations

A physical situation involving fluid flow is governed by the conservation principles of mass, momentum, energy etc. These principles can be expressed in terms of differential equations which possess a common form. The form of the steady-state generalised conservation equation is:

$$\text{div}(\rho V\Phi - \Gamma_\Phi \text{grad}\Phi) = S_\Phi \qquad (2.2\text{-}1)$$

$$\uparrow \qquad \uparrow \qquad \uparrow$$

convection diffusion source

where Φ represents the dependent variables such as H, k, etc. ρ represents the density of the phase, V is the velocity vector of the three velocity components. Γ_Φ is the diffusion coefficient which represents the general fluid properties such as viscosity

or conductivity. The source term S_Φ deals with the general forces acting on the fluid such as heat generation or heat losses.

Although the behaviour of any dependent variable Φ is governed by equation (2.2-1), the mass flow rate must satisfy an additional equation.

This is the continuity equation of the flow field which is:

$$\text{div}(\rho V) = 0 \qquad (2.2\text{-}2)$$

In that way the pressure field which enters the source terms of the momentum equations must adjust so that the resulting velocity field satisfies the continuity equation [Patankar (1981)].

2.2.4 The Conservation of Mass Equations

In order to satisfy the mass-conservation principle, the density and velocities obey the following equation:

$$\text{div}(\rho V) = S \qquad (2.2\text{-}3)$$

where ρ represents the density of the gas phase, and V is the velocity vector of the three velocity components. S represents the source/sink term of the equation. In this particular situation, as no mass is created or destroyed S is taken to be zero.

2.2.5 The Conservation of Momentum Equations

The conservation equation of momentum for the gas phase is given by:

$$\text{div}(\rho V\Phi - \Gamma_{\Phi}\text{grad}\Phi) = S_{\Phi} \qquad (2.2\text{-}4)$$

where Φ stands for u, v, and w. Γ_{Φ} is the diffusion coefficient. The source terms for the three velocities, S_{Φ}, are given in Table 1.

2.2.6 The Conservation of Energy Equations

Let H stand for the gas enthalpy per unit mass. Then the conservation of energy equation for the gas phase is given by:

$$\text{div} (\rho VH - (\lambda/Cp)\ \text{gradH}) = S_H \qquad (2.2\text{-}5)$$

The term on the right hand side is the source term which prescribes the rate of heat released by the fire source.

2.2.7 The Auxiliary Relations

In order to complete the mathematical formulation the above set of differential equations have to be solved for in conjunction with the algebraic relations and correlations observing the constraints on the values of the variables. These relations deal with the setting of the fire source, the modelling of the turbulence and general boundary conditions such as heat losses through the walls. These are essential to

obtain realistic predictions and are presented below. Other physical flow constants such as density are detailed in Appendix 2.

Fire Source

The source of fire was modelled as a volumetric source of heat. No combustion of the burning material was considered. For the steady-state simulation a constant heat release rate was assumed. The exact details can be found in section 3.2. The effect of radiative heat transfer was not taken into consideration as previous studies [Hoffmann and Markatos (1988)] showed that radiation was not a significant factor for heat transferred within an enclosure fire of this nature.

It should be noted here that the general flow of heat was calculated in terms of enthalpy. However, it is more convenient to think in terms of temperature. Hence, the enthalpy was converted into temperature using the following relationship:

$$H = Cp * T \qquad (2.2\text{-}6)$$

where Cp is given by the equations [Kumar (1985)]:

if $275.0 \leq T_g \leq 550.0$

$$Cp = 1005.7 *(2.325E\text{-}2 * (H_g/H_{g0})^2 - 2.794E\text{-}2 * (H_g/H_{g0}) + 1.004)$$

if $550.0 < T_g \leq 1300.0$

$$Cp = 1005.7 *(-5.454E\text{-}3 * (H_g/H_{g0})^2 + 8.449E\text{-}2 * (H_g/H_{g0}) + 0.8934) \qquad (2.2\text{-}7)$$

Turbulence Modelling

Turbulence is the most complicated type of fluid motion making its precise definition difficult [Bradshaw (1978)]. However, it is this phenomena which forms a significant part in most flow processes, including the present one. A fire produces flow dominated by buoyancy. The turbulence created serves to promote the rate of diffusion of heat, mass and momentum.

It is generally accepted that turbulence can be described by the Navier-Stoke equations, which express the principle of viscous stress directly proportional to the rate of strain. Though this is the simplest description of turbulence, in practice the evaluation of these equations is not always feasible. As turbulence is a fully three-dimensional phenomena, with processes such as the creation of eddies taking place in very small time- and space-scales prohibitively large computer processing time and storage would be required.

Hence, with the advancement of high-speed computers the turbulence phenomena has now become an important research area in its own right. The main aims of these projects are to obtain a clearer understanding of the processes involved as well as to obtain mathematical relationships which could simulate this complex phenomena.

A number of different types of turbulent models have already been developed aimed at simulating as much detail of the turbulent motion as possible. These models fall into several broad categories; zero-, one-, and two-equation models, stress-equation models, large-eddy simulation or even the relatively new area of two-fluid model analysis. The difference in their approaches as well as their validity have been

reviewed by several authors including Launder and Spalding (1972), Reynolds and Cebeci (1978), Markatos (1984/85) and Leschziner (1989). Kumar (1983) in a review concerning mathematical modelling of the fire phenomena, discusses the distinct approaches to turbulence modelling from a fire engineers point of view.

In order to account for the effect of the turbulence created by the fire the *popular* two-equation k-ε turbulence model [Markatos (1984/5)] suggested by Harlow and Nakayama (1967) was used. This model involves two transport equations for the turbulence characteristics. One of these equations governs the distribution through the fluid of the local kinetic energy of fluctuating motion, k; the other governs a .urbulence characteristic of different dimensions, namely ε, the energy dissipation rate.

The transport equation for k is:

$$\text{div} \left(\rho V k - (\mu_{eff}/\sigma_k) \, \text{grad} k \right) = S_k \qquad (2.2\text{-}8)$$

The transport equation for ε is:

$$\text{div} \left(\rho V \varepsilon - (\mu_{eff}/\sigma_\varepsilon) \, \text{grad} \varepsilon \right) = S_\varepsilon \qquad (2.2\text{-}9)$$

The source terms, S_k and S_ε, are defined in Table 1.

For turbulent flow the laminar viscosity, μ_l, is replaced by an effective viscosity, μ_{eff}, given by:

$$\mu_{eff} = \mu_t + \mu_l \qquad (2.2\text{-}10)$$

The turbulent viscosity, μ_t, described by the turbulence energy k and its turbulence dissipation rate ε, is given by:

$$\mu_t = \frac{C_3 \rho k^2}{\varepsilon} \qquad (2.2\text{-}11)$$

The five empirical constants used are:

$C_1 = 1.44$; $C_2 = 1.92$; $C_3 = 0.09$; $\sigma_k = 1.0$; $\sigma_\varepsilon = 1.3$

These constants were first recommended by Launder and Spalding (1974) for free turbulent flows but since then they have been used satisfactory for strongly buoyant flows [Markatos and Cox (1982)].

Boundary Conditions

In order to complete the mathematical model initial and boundary conditions need to be specified which take into account the effects of walls and free boundaries.

The Wall Conditions

For all walls of the compartments considered, the no-slip condition is applied to the velocity. In that way all velocity components except the velocities parallel to the wall are set to zero.

However, as the flow field created by a fire is turbulent, the viscous effects generated near the walls need to be accounted for. These flow properties vary greatly in the near-wall region. Launder and Spalding (1972) derived an algebraic logarithmic *law of the wall* which is able to take into account the variations of the flow and the turbulence quantities across the wall layer. This method provides an

algebraic relation for the grid points near the wall though sufficiently distant from the neighbouring walls so that they lie within the logarithmic layer. For this region the velocity variations are given by:

$$u = u_\tau/\kappa \ln(Ey^+) \qquad (2.2\text{-}12)$$

where κ is the von Karman constant taken as 0.42, and E is the function of the wall roughness, taken to be 9.0 to assume smooth walls. y^+ is the dimensionless distance from the wall, given by:

$$y^+ = \rho u_\tau \delta / \mu \qquad (2.2\text{-}13)$$

If y^+ is less than 11.5 we are within the laminar sub-layer where the log-law is not applicable.

δ is the normal distance from the wall and u_τ is the *friction velocity* defined as:

$$u_\tau = (\tau_w/\rho)^{1/2} \qquad (2.2\text{-}14)$$

τ_w is the wall shear stress, which is given by:

$$\tau_w = C_3^{3/4} \rho \quad k \qquad (2.2.15)$$

The dissipation rate, ε, in the near wall layer is obtained from:

$$\varepsilon = C_3^{3/4} k^{3/2} / \kappa \delta \qquad (2.2.16)$$

The skin-friction factor is deduced from the implicit log-law:

$$\begin{aligned} s &= (0.435/\ln(1.01 + 9.0*Re*s^{1/2}))^2 \qquad Re > 132.5 \\ s &= 1.0 / Re \qquad\qquad\qquad\qquad\qquad\quad Re \leq 132.5 \end{aligned} \qquad (2.2\text{-}17)$$

For the enthalpy calculations near the wall the friction factor, (Stanton number) is deduced from Couette-flow analysis which gives:

$$St = s/(Pr_t(1.0 + P*s^{1/2})) \qquad (2.2\text{-}18)$$

where Pr_t is the turbulent Prandtl number and P is given by:

$$P = 9.0*(Pr_{lam}/Pr_t - 1.0)*(Pr/Pr_{lam})^{1/4} \qquad (2.2\text{-}19)$$

The above evaluation of the Stanton number is valid for Re>132.5. In the cases when Re≤132.5 the Stanton number is given by:

$$St = s/Pr_{lam} \qquad (2.2\text{-}20)$$

The Free Boundary Conditions

From experience obtained from previous fire simulations [Markatos et al(1982), Cox and Kumar (1987), Galea and Markatos (1987,i)] the flow domains are extended outside the compartments of interest for computational purposes only. On the resulting *free boundaries* a fixed pressure boundary condition was imposed in order that the flow may enter or leave the domain depending on the pressure field.

2.3 The Time-Dependent Fire Model

2.3.1 Introduction

A model for the case of a time-dependent fire situation is presented in the following sub-sections, whereby frequent references will be made to the previous section to avoid unnecessary repetition.

2.3.2 The Dependent and Independent Variables

The dependent variables sol.ed for are the same as described in section 2.2.2. The independent variables used are the width, height and length; x, y and z of a cartesian coordinate system, as well as the time, t.

2.3.3 The Differential Equations

The partial differential equations used for the time-dependent study are of the same form as used for the steady-state analysis, see sections 2.2.3 to 2.2.6, except for the addition of the appropriate transient term. In that way the common form of the generalised conservation equation is:

$$\frac{\partial}{\partial t}(\rho\Phi) + \mathrm{div}(\rho V\Phi - \Gamma_{\Phi}\mathrm{grad}\Phi) = S_{\Phi} \qquad (2.3\text{-}1)$$

↑ transient ↑ convection ↑ diffusion ↑ source

2.3.4 The Auxiliary Relations

In order to complete the mathematical time-dependent model the above set of equations need to be solved for in conjunction with algebraic correlations. These expressions deal with the rate of heat released by a fire source, the modelling of turbulence created by the buoyant flow created by a fire, as well as the heat losses through the walls.

Fire Source

As in the case of the steady-state simulation the fire source was modelled using a volumetric heat release rate. However, as the fire *grows* with time the heat release rate was adjusted accordingly with respect to time. The exact time-dependent heat release rates used can be found in more detail in section 3.3.

Turbulence Modelling

The two-equation k-ε turbulence model described in the auxiliary section 2.2.7 for steady-state fire simulation was modified to take into account the time-dependent effect.

The time-dependent transport equation for k is:

$$\frac{\partial}{\partial t}(\rho k) + \mathrm{div}\,(\rho V k - (\mu_{eff}/\sigma_k)\,\mathrm{grad}k) = S_k \qquad (2.3\text{-}2)$$

The time-dependent transport equation for ε is:

$$\frac{\partial}{\partial t}(\rho\varepsilon) + \text{div}\,(\rho V\varepsilon - (\mu_{eff}/\sigma_\varepsilon)\,\text{grad}\varepsilon) = S_\varepsilon \qquad (2.3\text{-}3)$$

For turbulent flow the laminar viscosity, μ_l, is replaced by an effective viscosity, μ_{eff}, given by equation (2.2-10). The turbulent viscosity, μ_t, is given by equation (2.2-11). The five empirical constants used remain the same as for the steady-state. The source terms are defined in Table 1.

Wall Heat Transfer

For the enthalpy equation a fixed temperature is assumed at the outside surface of the walls enclosing the compartment. The momentum flux to the walls obeys the wall function relationship of Launder and Spalding (1974). A similar approach for the flux of heat to the walls has been found to under-estimate heat loss in fires [Kumar et al (1986,i,ii)]. Experience has indicated that satisfactory solutions may be obtained by combining the heat loss effects together in a local empirical transfer coefficient. This method was suggested within the Harvard Zone Model [Mitler (1978)], and applied within several fire models [Hoffmann and Markatos (1988), Kumar et al(1986,i,ii)]. It is based on the assumption that the heat transfer coefficient, a_c varies linearly with temperature between the ambient temperature, T_0 and $(T_0 + 100)$, and has fixed values outside this range. The relation used was:

$$a_c = \begin{cases} (a_c)_{min} & T = T_0 \\ (a_c)_{min} + \dfrac{((a_c)_{max} - (a_c)_{min})(T - T_0)}{100.0} & T_0 \le T \le T_0+100 \\ (a_c)_{max} & T > (T_0 + 100) \end{cases} \qquad (2.3\text{-}4)$$

The minimum and maximum heat transfer coefficient used in the above relation were 5.0 and 40.0 respectively. The heat losses are then calculated from the balance of this gas phase thermal impedance and the steady-state conduction equation for the compartment boundaries.

2.4 The Numerical Solution Procedure

2.4.1 Introduction

In the previous section, the partial-differential equations which govern steady-state and time-dependent fire phenomena were presented. The numerical integration scheme used to solve the set of differential equations is presented in this section.

The numerical method to be described within this chapter is based on the control-volume formulation. The compartments used to investigate the fire and sprinkler interactions have been discretised into a finite number of control-cells, each of which can be regarded as a control-volume, see section 2.4.2. The discretisation equations derived within this chapter are obtained by integrating the governing differential equations over a small region called the control-volume. For completeness the time-dependent discretisations for the general, momentum and continuity equations are shown in detail, in sections 2.4.3, 2.4.5 and 2.4.6 with the steady-state equations quoted in sections 2.4.4, and 2.4.7. The setting of the boundary conditions is discussed in section 2.4.8.

The resulting set of simultaneous equations are solved for using the iterative

procedure SIMPLEST, illustrated in Appendix 3. A brief outline of the computer package PHOENICS, which has the algorithms built in, is given in section 2.5.1.

2.4.2 The Finite-Difference Grid

The calculation domain of interest is sub-divided into a number of control-volumes (or control-cells) in all three cartesian directions; x, y, and z. The grid points are surrounded by non-overlapping *control-volumes* which together fill the domain of interest completely.

These grid cells were not uniformly spaced within the computational domain in order to be able to place more emphasis in areas where steeper gradients of flow are expected, such as near-walls, fire source or sprinkler regions.

Each control-volume is associated with a discrete point denoted by the node point P at which the dependent variables such as pressure and temperature are to be calculated and stored; see figure 2.1. For clarity figure 2.2 shows a typical control-volume head-on in the x-y direction with its neighbouring cells.

The x-direction neighbours are the points E and W (denoting East and West). While N and S (denoting North and South) are the y-direction neighbours. In order to extend the grid into the third dimension, the z-direction, the neighbours are denoted as H and L (High and Low).

The velocity components are calculated at the interface of control-volumes. Figure 2.3 shows a portion of a three-dimensional grid in the x-y plane where the interfaces are

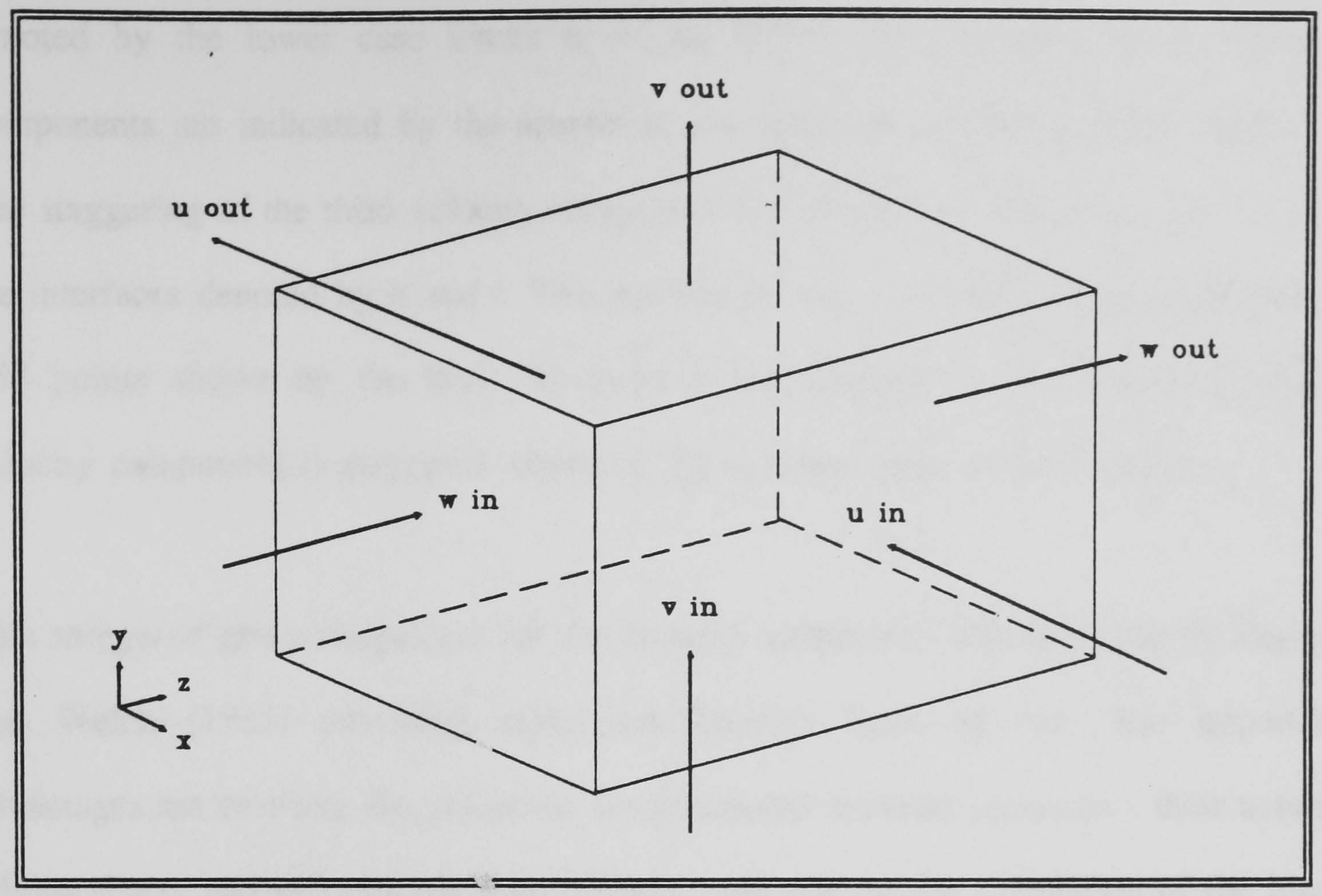

Figure 2.1 A typical Control-Volume

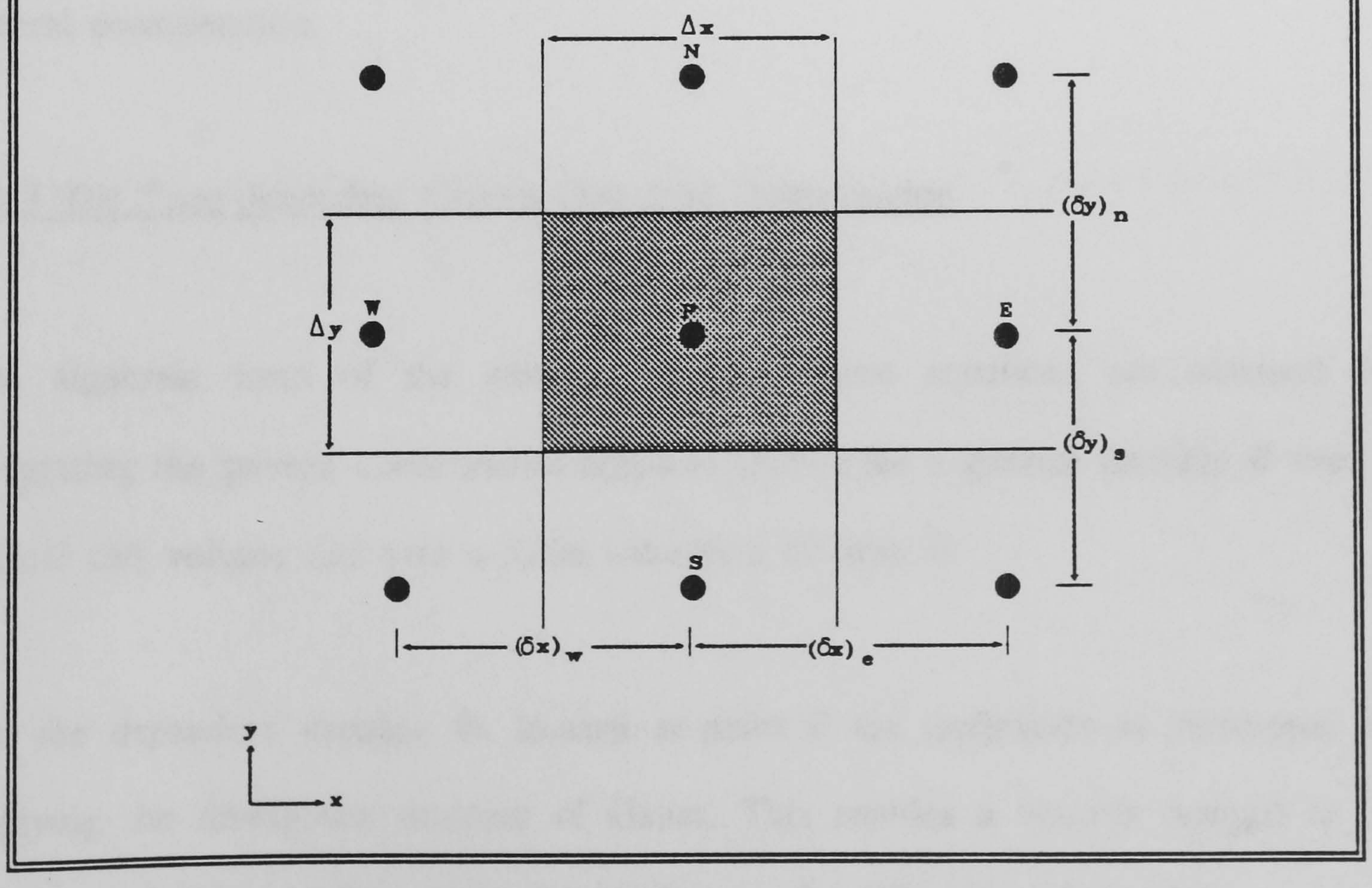

Figure 2.2 Side View of a Control-Volume and its neighbours

denoted by the lower case letters e, w, n, and s. The locations of the velocity components are indicated by the arrows in the direction of the velocity component. The staggering of the third velocity component is performed in a similar manner, with the interfaces denoted by h and l. The location for the dependent variables are at the grid points shown by the dots. As a result the control-volume surrounding each velocity component is staggered ahead of the relevant main control-volume.

This *staggered* grid arrangement for the velocity components was first used by Harlow and Welch (1965) providing significant benefits from its use. The important advantages are twofold; the velocities are positioned between pressures - their natural driving force, and the velocities are directly available for the calculation of the mass flow rates across the boundaries of the control-volume for each node.

A considerable disadvantage is that the control-volumes used to calculate velocities are displaced from those used to calculate the other variables and therefore need special consideration.

2.4.3 The Time-dependent General Equation Discretisation

The algebraic form of the general finite-difference equations are obtained by integrating the general conservation equation (2.3-1) for a general variable Φ over a typical cell volume and over a finite increment of time δt.

For the dependent variable Φ, located at point P the integration is performed by applying the divergence theorem of Gauss. This enables a volume integral to be transformed into a surface integral according to the following relationship:

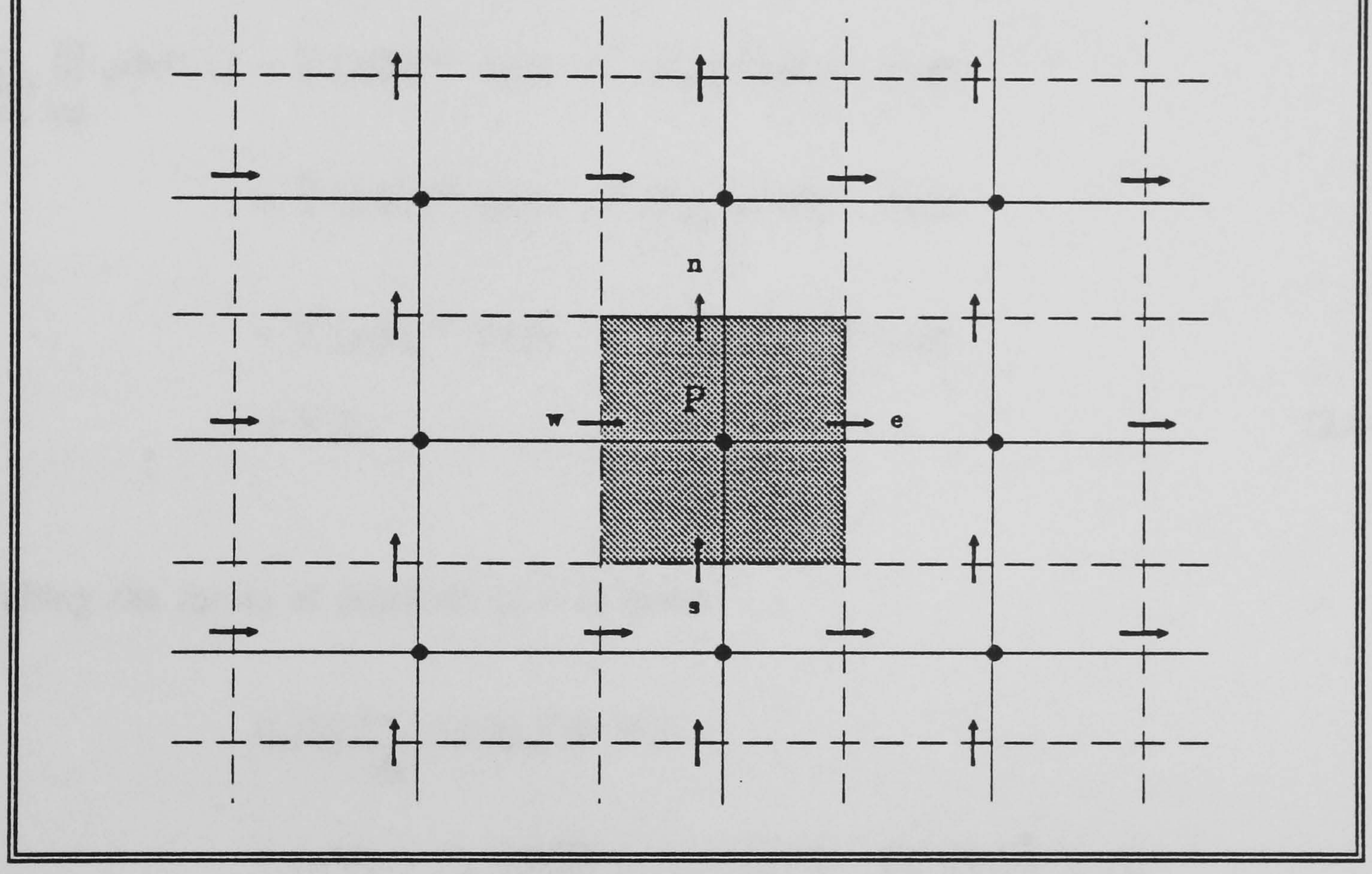

Figure 2.3 Staggered Grid for Velocity Components

$$\iiint_{Vol} \text{div}(\rho V\Phi - \Gamma_\Phi \text{grad}\Phi) \, dVol = \iiint_{s} n.(\rho V\Phi - \Gamma_\Phi \text{grad}\Phi) \, ds \qquad (2.4\text{-}1)$$

where n is the unit normal vector outwardly directed, and s denotes the surface area.

Applying this theorem to the general conservation equation (2.4-1), integrating with respect to time and expanding the result gives:

$$\begin{aligned} &\frac{\partial}{\partial t} \iiint_{Vol} \rho\Phi dVol + \iint [\rho\Phi]_x^{x+\Delta x} \, dydz - \iint [\Gamma_\Phi \text{grad}\Phi]_x^{x+\Delta x} \, dydz \\ &\quad + \iint [\rho\Phi]_y^{y+\Delta y} \, dxdz - \iint [\Gamma_\Phi \text{grad}\Phi]_y^{y+\Delta y} \, dxdz \\ &\quad + \iint [\rho\Phi]_z^{z+\Delta z} \, dxdy - \iint [\Gamma_\Phi \text{grad}\Phi]_z^{z+\Delta z} \, dxdy \\ &\quad = V_\Phi S_p \end{aligned} \qquad (2.4\text{-}2)$$

Taking the limits of equation (2.4-2) gives:

$$\begin{aligned} &\frac{[(\rho\Phi)_p^{new} - (\rho\Phi)_p^{old}]p \; Vol}{\delta t} \\ &+ (\rho V\Phi - \Gamma_\Phi \, \partial\Phi/\partial x)_e \, A_e - (\rho V\Phi - \Gamma_\Phi \, \partial\Phi/\partial x)_w \, A_w \\ &+ (\rho V\Phi - \Gamma_\Phi \, \partial\Phi/\partial y)_n \, A_n - (\rho V\Phi - \Gamma_\Phi \, \partial\Phi/\partial y)_s \, A_s \\ &+ (\rho V\Phi - \Gamma_\Phi \, \partial\Phi/\partial z)_h \, A_h - (\rho V\Phi - \Gamma_\Phi \, \partial\Phi/\partial z)_l \, A_l \\ &= V_\Phi S_p \end{aligned} \qquad (2.4\text{-}3)$$

where the As represent the areas of the various control-volume faces.

Expanding the partial derivatives gives:

$$\frac{[(\rho\Phi)_p^{new} - (\rho\Phi)_p^{old}]_p \text{ Vol}}{\delta t}$$

$$+ (\rho V\Phi)_e A_e - \Gamma_\Phi\frac{(\Phi_E - \Phi_P)}{\delta x_e} A_e - (\rho V\Phi)_w A_w - \Gamma_\Phi\frac{(\Phi_P - \Phi_W)}{\delta x_w} A_w$$

$$+ (\rho V\Phi)_n A_n - \Gamma_\Phi\frac{(\Phi_N - \Phi_P)}{\delta y_n} A_n - (\rho V\Phi)_s A_s - \Gamma_\Phi\frac{(\Phi_P - \Phi_S)}{\delta y_s} A_s$$

$$+ (\rho V\Phi)_h A_h - \Gamma_\Phi\frac{(\Phi_H - \Phi_P)}{\delta z_h} A_h - (\rho V\Phi)_l A_l - \Gamma_\Phi\frac{(\Phi_P - \Phi_L)}{\delta z_l} A_l$$

$$= V_\Phi S_{\Phi p} \qquad (2.4\text{-}4)$$

Let $F = \rho VA$ and $D = \frac{\Gamma_\Phi A}{\delta^*}$

where F represents the mass flow rate and D represents the diffusion flux across a face of the control-volume. D always remains positive whilst F can be both positive or negative, depending on the direction of the flow [Patankar (1980)].

Equation (2.4-4) can be re-written as:

$$\frac{[(\rho\Phi)_p^{new} - (\rho\Phi)_p^{old}]p \text{ Vol}}{\delta t}$$

$$+ F_e\Phi_e - F_w\Phi_w + F_n\Phi_n - F_s\Phi_s + F_h\Phi_h - F_l\Phi_l$$

$$- D_e(\Phi_E - \Phi_P) + D_w(\Phi_P - \Phi_W) - D_n(\Phi_N - \Phi_P)$$

$$- D_s(\Phi_P - \Phi_S) + D_h(\Phi_H - \Phi_P) - D_l(\Phi_P - \Phi_L) = V_\Phi S_{\Phi p} \qquad (2.4\text{-}5)$$

In order to avoid unrealistic oscillatory tendencies within the solution the upwind difference principle is employed.

This method leaves the diffusion term unchanged but the convection term is calculated from the assumption that:

The value of Φ *at an interface is equal to the value of* Φ *at the grid point on the 'upwind' side of the face* [Patankar (1980)].

In that way the values of $(\rho\Phi)$ are taken at $(\rho\Phi)_P$ if the direction of the velocity is outward from the control-volume. If the velocity is inward it uses $(\rho\Phi)_N$ for the north face, $(\rho\Phi)_S$ for the south face etc [Spalding (1980)].

The control-face values of Φ can now be written as:

$$F_e \Phi_e = \Phi_P \{ \max(F_e,0) \} - \Phi_E \{ \max(-F_e,0) \}$$

$$F_w \Phi_w = \Phi_w \{ \max(F_w,0, \} - \Phi_P \{ \max(-F_w,0) \}$$

$$F_n \Phi_n = \Phi_n \{ \max(F_n,0) \} - \Phi_P \{ \max(-F_n,0) \}$$

$$F_s \Phi_s = \Phi_s \{ \max(F_s,0) \} - \Phi_P \{ \max(-F_s,0) \}$$

$$F_h \Phi_h = \Phi_h \{ \max(F_h,0) \} - \Phi_P \{ \max(-F_h,0) \}$$

$$F_l \Phi_l = \Phi_l \{ \max(F_l,0) \} - \Phi_P \{ \max(-F_l,0) \} \qquad (2.4\text{-}6)$$

The volumetric integration of the source term S_Φ has been expressed as:

$$\iiint_{Vol} S_\Phi \, dVol = V_c \, S_{\Phi p} \qquad (2.4\text{-}7)$$

As the source term is often dependent on the variables Φ and in order to keep the resulting discretisation equations linear the source term S is expressed as a linear function of Φ_P. Thus the source term can be expressed in the *linearised* form, see Patankar (1980) as:

$$\frac{\partial}{\partial t}\int_{t}^{t+\delta t}\iiint_{Vol} S_\Phi \, dVol \, dt = S^C_{\Phi p} + S^P_{\Phi p}\,\Phi_P^{new} \qquad (2.4\text{-}8)$$

where $S_C = (S_\Phi)^* - \dfrac{(\partial S)^*}{(\partial \Phi)}\,\Phi_P^*$ and $S_P = \dfrac{(\partial S)^*}{(\partial \Phi)}$

with '*' values denoting the guessed values or values from a previous iteration of Φ_P.

Providing S^P is negative the equation is more diagonally dominant and so numerical stability is ensured [Patankar (1980)].

Substituting equations (2.4-6) and (2.4-8) into (2.4-5) gives the discretised equation of the general differential equation (2.3-1).

$$(A_P - S^P_{\Phi p}\,V_C)\,\Phi_P^{new} = A_E\Phi_E + A_W\Phi_W + A_N\Phi_N + A_S\Phi_S + A_H\Phi_H + A_L\Phi_L + A_P^{old}\Phi_P^{old} + S^C_{\Phi p}V_C \qquad (2.4\text{-}9)$$

where

$$A_E = D_e + \max(-F_e,0) \qquad A_W = D_w + \max(-F_w,0)$$

$$A_N = D_n + \max(-F_n,0) \qquad A_S = D_s + \max(-F_s,0)$$

$$A_H = D_h + \max(-F_h,0) \qquad A_L = D_l + \max(-F_l,0)$$

$$A_P = A_E + A_W + A_N + A_S + A_H + A_L + A_P^{old}$$

$$A_P^{old} = \frac{\Phi_P^{old} + V_P^{old}}{\delta t}$$

Due to the arrangement of the control-volumes it is often necessary to interpolate in order to evaluate quantities at the required location.

The diffusion coefficients at the cell faces are computed using an arithmetic average

of the nodal values. The expression used is:

$$(\Gamma_\Phi)_e = ((\Gamma_\Phi)_E + (\Gamma_\Phi)_P)/2.0 \qquad (2.4\text{-}10)$$

Densities at the faces are calculated by upwinding. As the velocities are stored at the cell faces no interpolation is necessary, highlighting the advantage of staggered grids.

2.4.4 The Steady-State General Equation Discretisation

The above equation (2.4-9) is the discretised equation for the general three-dimensional transient finite-difference equation (2.3-1). For the steady-state situation the discretised form of equation (2.2-1) is:

$$(A_P - S_{\Phi P}^P V_C)\, \Phi_P^{new} = A_E\Phi_E + A_W\Phi_W + A_N\Phi_N + A_S\Phi_S + A_H\Phi_H + A_L\Phi_L + S_{\Phi P}^C V_C \qquad (2.4\text{-}11)$$

where $$A_P = A_E + A_W + A_N + A_S + A_H + A_L$$

and A_E, A_W, A_N, A_S, A_H, and A_L remain unchanged.

2.4.5 The Momentum Equation Discretisation

Equation (2.4-9) is valid for all dependent variables. However, due to the staggered control-volumes for the velocity components, figure 2.3, the calculation of the diffusion coefficient and mass flow rate at the faces require interpolation. Therefore, the coefficients in equation (2.4-9) require alteration.

Also, due to the integration of the momentum equation an extra term describing the pressure gradient appears. Thus a term needs to be added to the right hand side of the integrated transport equation. This new term is:

$$\iiint_{Vol} \text{grad } p \; dVol \qquad (2.4\text{-}12)$$

Thus the corresponding finite-difference equations for the velocities are:

$$\begin{aligned}
(A_P - S^P_{uP})\,(u)_e &= \Sigma\, A_j\,(u)_j + S^C_{uP}\,V_C + (p_P - p_E)\,A_e \\
(A_P - S^P_{vP})\,(v)_n &= \Sigma\, A_j\,(v)_j + S^C_{vP}\,V_C + (p_P - p_N)\,A_n \\
(A_P - S^P_{wP})\,(w)_h &= \Sigma\, A_j\,(w)_j + S^C_{wP}\,V_C + (p_P - p_H)\,A_h
\end{aligned} \qquad (2.4\text{-}13)$$

where j takes the value E, W, N, S, H or L to identify the neighbouring staggered velocities. S_{uP}, S_{vP}, S_{wP} are the sources/sinks of momentum.

2.4.6 The Time-Dependent Continuity Equation Discretisation

As the flow field in equation (2.3-1) must satisfy the continuity equation (2.3-2) the flow rates through the faces of the control-volume need to satisfy the discretised form of the continuity equation. Therefore, the continuity equation needs to be integrated over the control-volume in the same fashion as the general differential equation.

Integrating equation (2.3-1) over a typical control-volume and over a finite step in time gives:

$$\iiint \frac{\partial}{\partial t}(\rho\Phi) + \text{div}(\rho\Phi - \Gamma_\Phi \text{grad}\Phi_i)\; dVol = 0 \qquad (2.4\text{-}14)$$

which discretises into the form:

$$(\rho_P - \rho_P^{old}) * V + (\rho ur)_e A_e - (\rho ur)_w A_w + (\rho vr)_n A_n - (\rho vr)_s A_s + (\rho wr)_h A_h - (\rho wr)_l A_l = 0 \qquad (2.4\text{-}15)$$

2.4.7 The Steady-State Continuity Equation Discretisation

Performing the same reasoning and steps on equation (2.2-1) results in the discretised form for the steady-state continuity equation. This equation is:

$$(\rho ur)_e A_e - (\rho ur)_w A_w + (\rho vr)_n A_n - (\rho vr)_s A_s + (\rho wr)_h A_h - (\rho wr)_l A_l = 0 \qquad (2.4\text{-}16)$$

2.4.8 The Boundary Conditions

The above discretisations assume that the nodes lie *internal* within the grid. However, corresponding equations exist for the cases when the nodes are *boundary* nodes. These are incorporated into the numerical calculations as source terms, which are represented by linear expressions of the form:

$$S_\Phi = S_{\Phi P}^P \Phi_P + S_{\Phi P}^C = C_\Phi(V_\Phi - \Phi_P) \qquad (2.4\text{-}17)$$

where C_Φ, the coefficient, is given by:

$$C_\Phi = - S_{\Phi P}^P$$

and V_Φ, the value term for the variable Φ, is given by:

$$V_\Phi = - S_{\Phi P}^C / S_{\Phi P}^P$$

2.5 The Solution of the Equations

The control-volume equations form a set of simultaneous equations which are solved for using the iterative procedure SIMPLEST (SIMPLE ShorTened) [Spalding (1980)]. SIMPLEST is an improved version of the SIMPLE algorithm which is well documented by Patankar (1980). A brief outline of the algorithm can be found in Appendix 3.

2.5.1 The Computer Package

In recent years a number of fluid-.low packages have been developed. FLOW-3D [Burns et al(1989)], FLUENT [Swithenbank et al(1987)] and PHOENICS [Spalding (1981), Rosten and Spalding (1986)] are only three such packages dedicated to the solution of fluid-flow and heat/mass transfer processes.

However, due to a number of reasons, such as prior knowledge and availability at the outset of the project the general fluid-flow package PHOENICS was utilised. Furthermore, the algorithm SIMPLEST forms an integral part of its solution procedure.

PHOENICS is a general computer-code system capable of simulating a wide range of fluid-flow, heat/mass-transfer, and chemical reaction problems found in industry and the environment. It is designed to simulate flow processes which are up to three-dimensional, steady-state or turbulent, single- or two-phase, laminar or turbulent, within a framework of either cartesian, polar or body-fitted co-ordinates.

These phenomena are described in terms of distributions in space and time of temperatures, pressures, velocities and other physically relevant quantities using the finite-domain equations outlined above.

The resulting set of algebraic equations are solved for using the iterative processes SIMPLEST (see Appendix 3) or IPSA, which is specific to two-phase simulations (see chapter 3 for IPSA algorithm). The resulting solution process is very complicated involving several stages of adjustments. The most noteworthy concepts referred to are *slabs*, *sweeps* and *whole-field solution.*

Slabs are arrays of cells or slices within the z-plane. A *sweep* is a set of slabwise operations conducted in sequence from the lowest to the highest slab.

Unlike for the slab-by-slab approach, the *whole-field* method takes into account the z-direction links simultaneously with the x- and y-direction links. Hence, in cases when the z-direction links dominate, such as a fire in a room, the whole-field method is more effective, particularly for pressure. However, though it reduces the number of sweeps necessary to eliminate the imbalances in the equations, the amount of computer storage needed is increased.

Another vital part of simulating fluid-flow processes is that converged solutions cannot always be guaranteed due to their very nature and the non-linearity of the equations necessary to be solved. Hence, special settings or relaxation parameters are used to ensure convergence. However, it should be noted that the results obtained should not be dependent on these settings but are merely used to ensure convergence within a reasonable number of sweeps.

2.6 Summary

This chapter has outlined the physical relationships and correlations necessary to mathematically simulate the environment created by a compartment fire for steady-state and time-dependent situations using the field modelling approach.

The derivation of the finite-domain equations from the general transport equations have been described. The iterative solution algorithm SIMPLEST, embedded within the computer code PHOENICS has been outlined.

Φ	Γ_Φ	S_Φ
1	0	0 (continuity)
u	μ_{eff}	$-\frac{\partial p}{\partial x} + \frac{\partial}{\partial x}(\mu_{eff}\frac{\partial u}{\partial x}) + \frac{\partial}{\partial y}(\mu_{eff}\frac{\partial v}{\partial x}) + \frac{\partial}{\partial z}(\mu_{eff}\frac{\partial w}{\partial x})$
v	μ_{eff}	$-\frac{\partial p}{\partial y} + \frac{\partial}{\partial x}(\mu_{eff}\frac{\partial u}{\partial y}) + \frac{\partial}{\partial y}(\mu_{eff}\frac{\partial v}{\partial y}) + \frac{\partial}{\partial z}(\mu_{eff}\frac{\partial w}{\partial y})$ $-g(\rho-\rho_{ref})$
w	μ_{eff}	$-\frac{\partial p}{\partial z} + \frac{\partial}{\partial x}(\mu_{eff}\frac{\partial u}{\partial z}) + \frac{\partial}{\partial y}(\mu_{eff}\frac{\partial v}{\partial z}) + \frac{\partial}{\partial z}(\mu_{eff}\frac{\partial w}{\partial z})$
H	$\mu_{lam}/Pr_{lam} + \mu_t/Pr_t$	$\dot{q}$
k	μ_{eff}/Pr_k	$G_K - \rho\varepsilon + G_B$
ε	μ_{eff}/Pr_ε	$(\varepsilon/k)\ [(G_K+G_B)C_1 - C_2\rho\varepsilon]$

where

$$G_K = \mu_t \{ 2 [(\partial u/\partial x)^2 + (\partial v/\partial y)^2 + (\partial w/\partial z)^2] + [(\partial u/\partial z) + (\partial w/\partial x)]^2 + [(\partial w/\partial y) + (\partial v/\partial z)]^2 + [(\partial u/\partial y) + (\partial v/\partial x)]^2 \}$$

$$G_B = \frac{\mu_t\ g}{\rho}\frac{\partial \rho}{\partial y}$$

Table 1 : The Diffusion coefficients and Source Terms of the one-phase conservation equations.

Chapter 3

Validation and Results for Single-Phase Fire Simulations

Chapter 3 Validation and Results of Single-Phase Fire Simulations

3.1 Introduction

One of the difficulties in validating field fire models is the considerable quantity of detailed information predicted and the very difficult task of obtaining experimental data for comparison purposes.

Fortunately, experimental results were obtained for two distinct fire and sprinkler experiments. These were chosen for final validation purposes. The first experiment was carried out within an office sized compartment containing a wastepaper basket fire [Cooper and Stroup (1987)]. The sprinkler was positioned remote from the fire source. The effect of a sprinkler nearly above the fire source was investigated in the second experiment. The data used was obtained by Smith (1987) during a series of eight fire tests within a hospital room. The experiments were carried out to discover whether a sprinkler could control a typical bed-fire early enough to prevent life-hazardous conditions from occurring. These two cases were used for the transient simulations as described in their respective reports. However, as no experimental data was available for the steady-state situation the office fire scenario was modified and used as a basis for a feasibility study for the proposed modelling technique.

Prior to validation of the two-phase interaction model, outlined in chapter 4, the resulting three compartment environments created by a fire were obtained. The predictions made for these simulations are used as the initial conditions of the gas phase for the fire-sprinkler simulations described in chapter 5. Hence the results presented below are in preparation for the second part of the study, whereby planes

through the compartments and scales for the velocity vectors are chosen to be uniform for ease of comparison.

3.2 Steady-State Simulation

The steady-state simulation was performed using the office lay-out. The compartment represents an office of dimensions 2.44m by 3.66m in plan and 2.44m in height. A doorway of dimensions 0.76m in width and 2.03m in height was situated on the far end of the room and was open throughout the scenario[1]. However, as this particular study was mainly a feasibility study and experimental results for a steady-state situation did not exist the actual location of the fire was slightly altered. The fire source, which was to represent a wastepaper basket, was moved from the corner of the room into the middle of the far wall producing a symmetry along the centre line of the room, shown schematically in figure 3.1. Hence only half the room was modelled. A steady total fire intensity of 30kW was assumed and released over a hypothetical wastepaper basket volume of dimensions 0.3mx0.3mx0.3m.

A single sprinkler was located along the line of symmetry, near the centre of the room, about 1.8m away from the fire source and 0.1m below the ceiling.

As no details concerning the wall materials were given in the report an isothermal wall condition was assumed. The wall temperature was fixed at the ambient temperature of 24°C.

---

[1]This compartment configuration will become a standard and will be referred to as the ASTM (American Standards for Testing Materials) room [Cox (1990)].

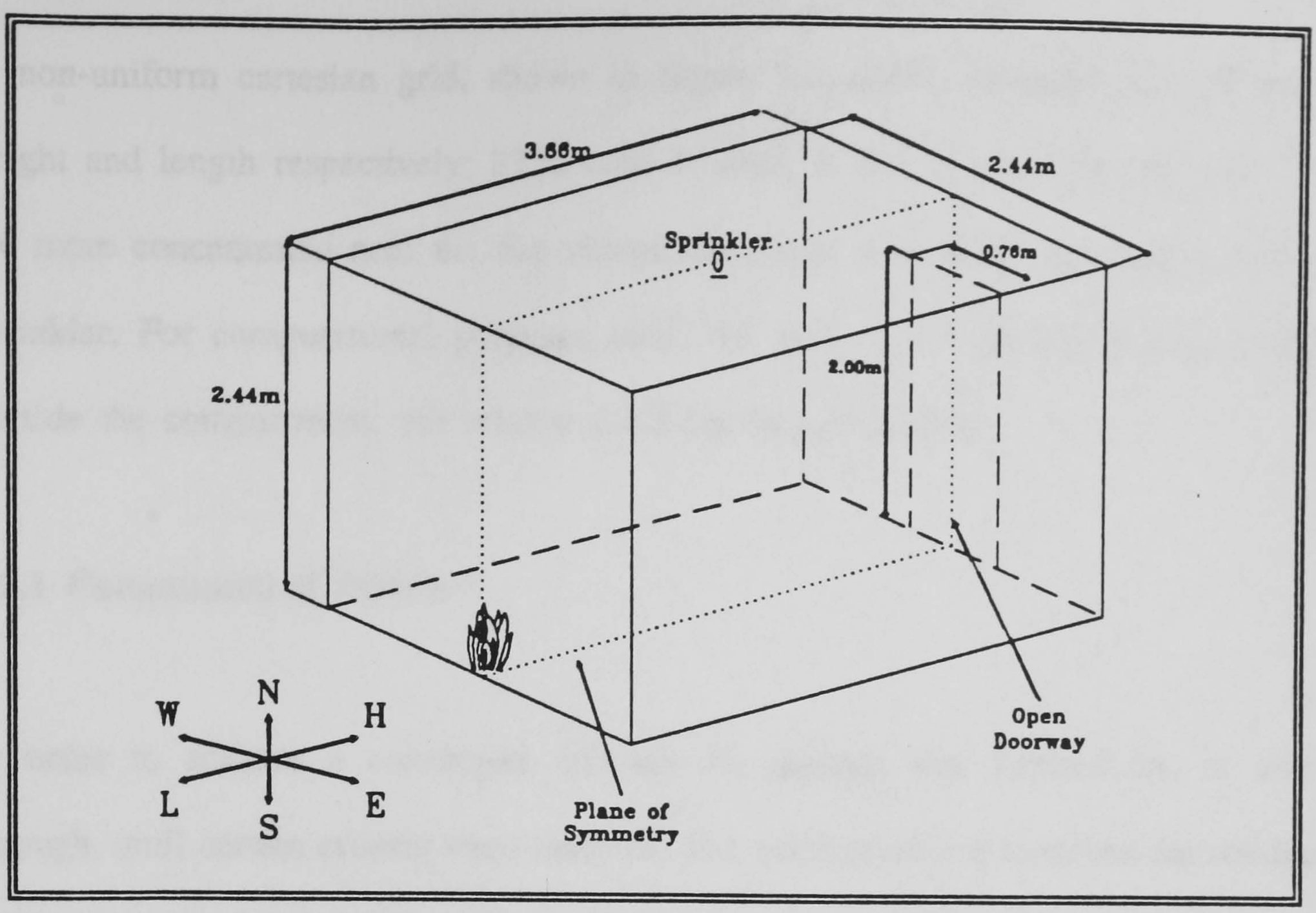

Figure 3.1 Symmetric Office Schematic

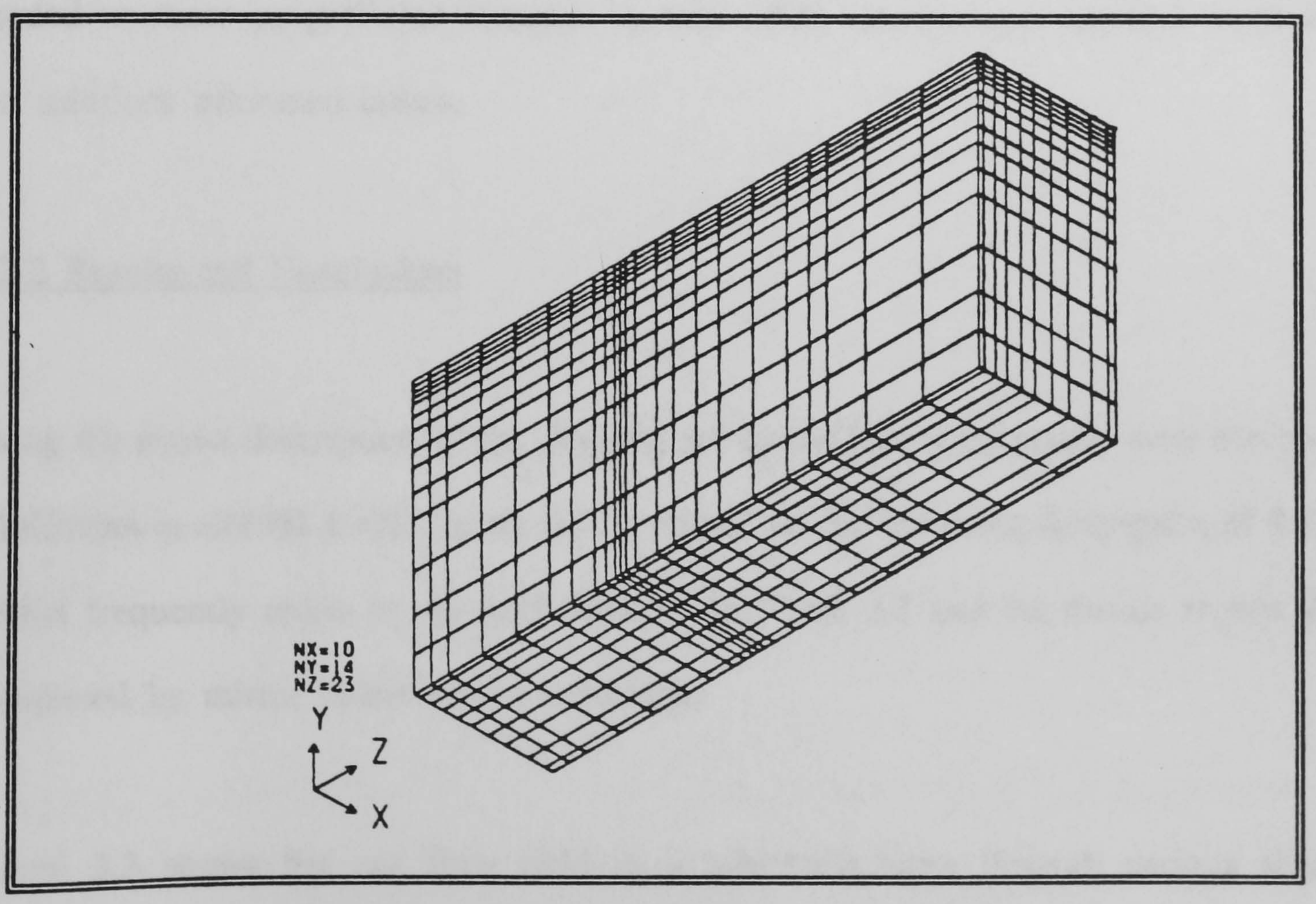

Figure 3.2 Finite-Difference Grid used for symmetric office study

A non-uniform cartesian grid, shown in figure 3.2, used 10x14x23 cells in width, height and length respectively; 3220 cells in total. It can be seen that the grid lines are more concentrated near the fire source, the walls, especially the ceiling, and the sprinkler. For computational purposes only, the grid was extended by three z-slabs outside the compartment; see section 2.2.7 for further details.

3.2.1 Computational Details

In order to achieve a converged solution the domain was iterated on, or swept through, until certain criteria were satisfied. The main condition involved the residuals in the balance equations. These had to fall to below $1.0x10^{-4}$ whereby the values were normalised with respect to some typical values of the fluxes within the flow field. Further criteria include limits on the pressure correction and mass balances values to be of the order of $1.0x10^{-4}$. Furthermore comparisons of spot-values between sweeps needed to show insignificant changes. In total 2600 sweeps were required to obtain the solutions presented below.

3.2.2 Results and Conclusions

Using the above description of the physical set-up the following results were obtained [Hoffmann et al(1988,1989)]. It should be noted that the following description of these results frequently refers to the grid depicted in figure 3.2 and the results shown are completed by mirror image where necessary.

Figure 3.3 shows the gas flow field in a schematic form through various slices through the office, whereby figure 3.3-a shows two slices through the fire source

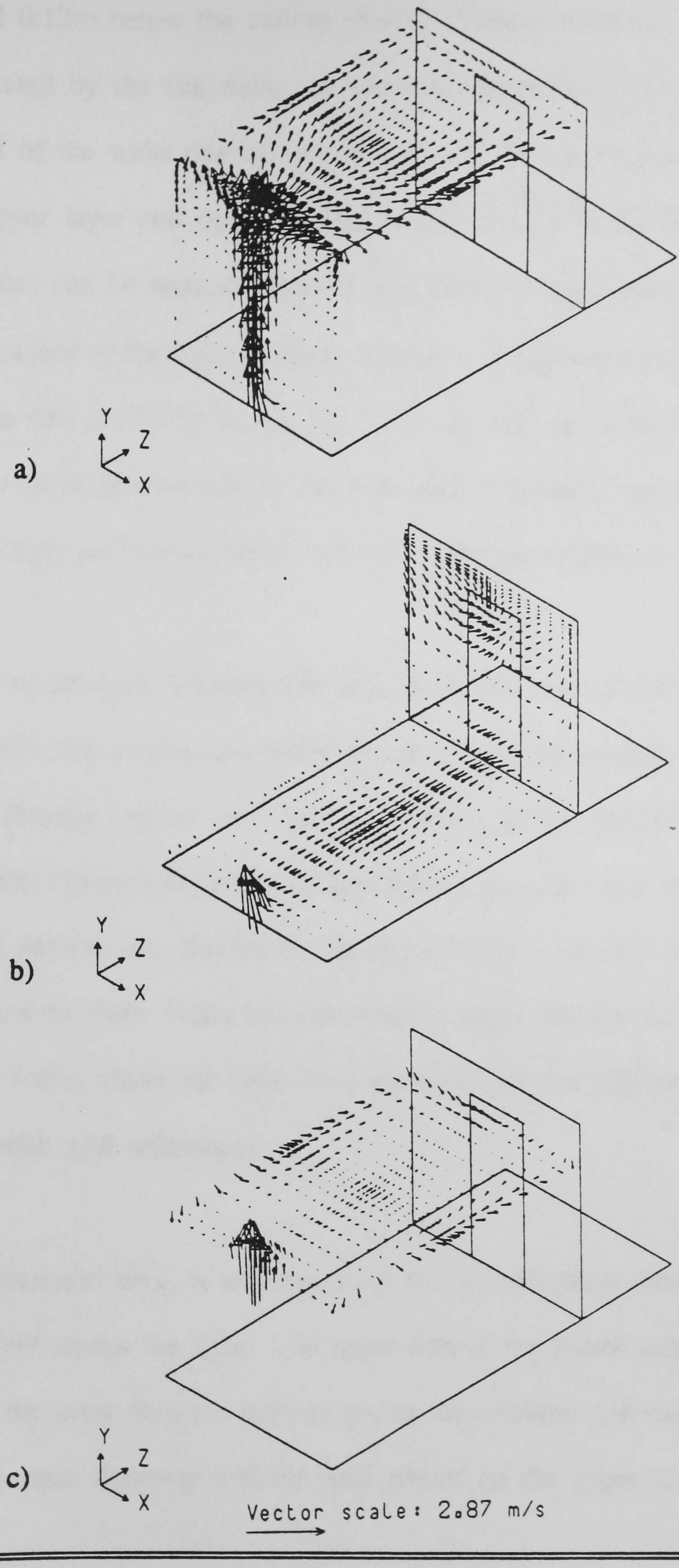

Figure 3.3 Schematic Views of the predicted gas velocity vectors
a) through the fire source and below the ceiling
b) along the floor and near the doorway
c) slice 1.96m above the floor

(Z=1) and 0.12m below the ceiling (Y=12). These indicate the very strong buoyant plume created by the fire rising up and then spreading outwards along the ceiling. The effect of the walls can be seen in the way the vectors *curve* downwards along the hot upper layer and move parallel to the vertical walls. The flow field of two further slices can be seen in figure 3.3-b. Here the entrainment of cold air through the lower region of the open doorway into the compartment and subsequently into the base of the fire is clearly shown (Y=2). It can also be noted, by the way in which the vectors point downwards on the east and west walls, and the hotter gases from the upper layer are pushed down and mix with the entrained colder air.

The effect of the open doorway can also be clearly seen (Z=10). The hot upper layer hits the soffit and surrounding walls and is re-directed towards the upper part of the doorway through which the hot and subsequently lighter air can leave the compartment. Colder and denser air is entrained into the room through the lower part. These two sections are divided by the neutral plane, which is predicted to be about 1.15m above the floor. From measurements [Cooper and Stroup (1987)] this interface was about 1.45m above the floor. It is expected that the half meter difference can be improved with grid refinement.

The last schematic view, is in preparation for the two-phase study and shows a plane 2.095m (Y=9) above the floor. The upper part of the plume can clearly be identified as well as the other features such as plume entrainment, the escape of the hot gases through the open doorway and the wall effects on the upper layer's flow.

Flow fields through vertical slices, from the low to the high wall, and different distances from the fire are shown in figure 3.4. A slice through the centre of the fire

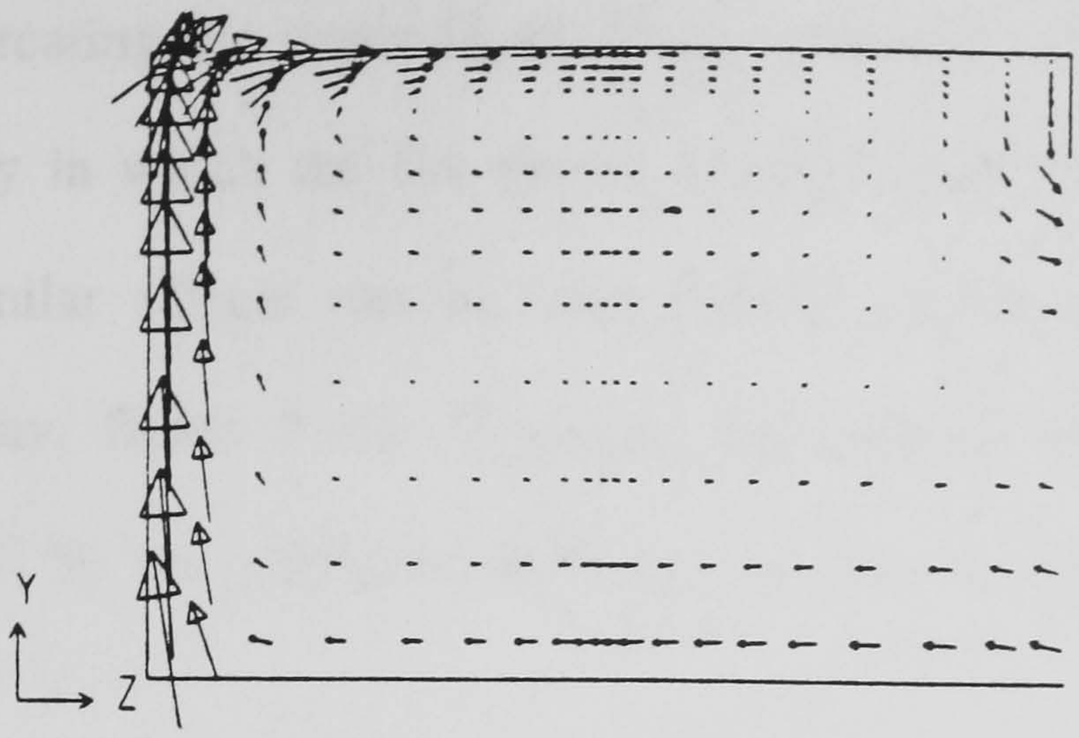

a) x=1 Vector scale: 2.87 m/s

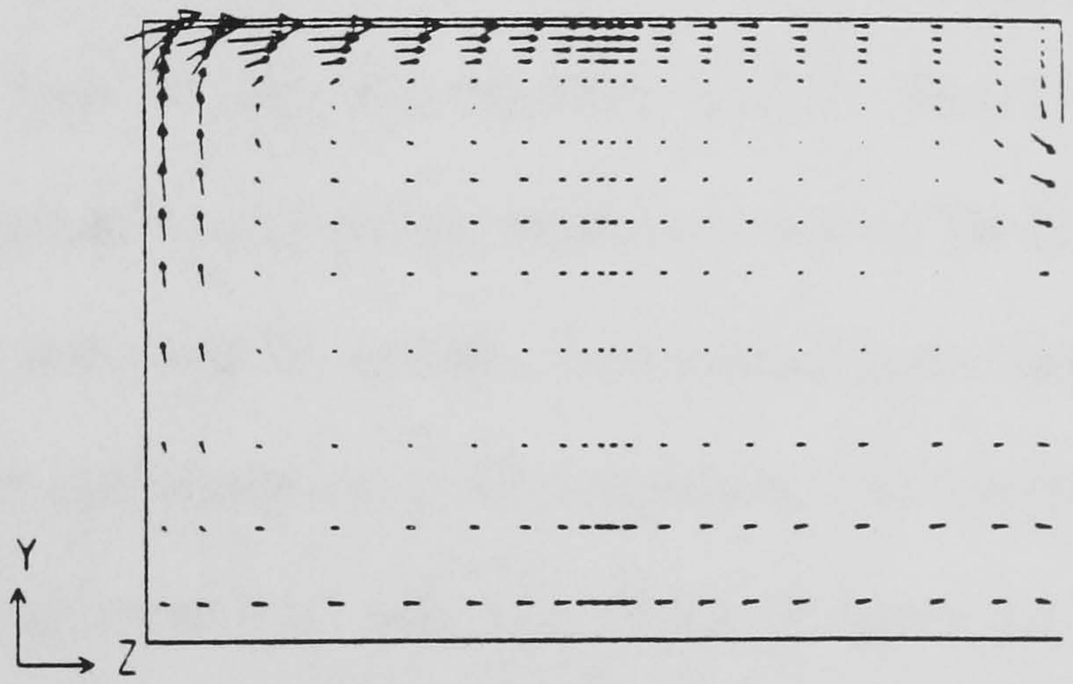

b) x=4 Vector scale: 2.87 m/s

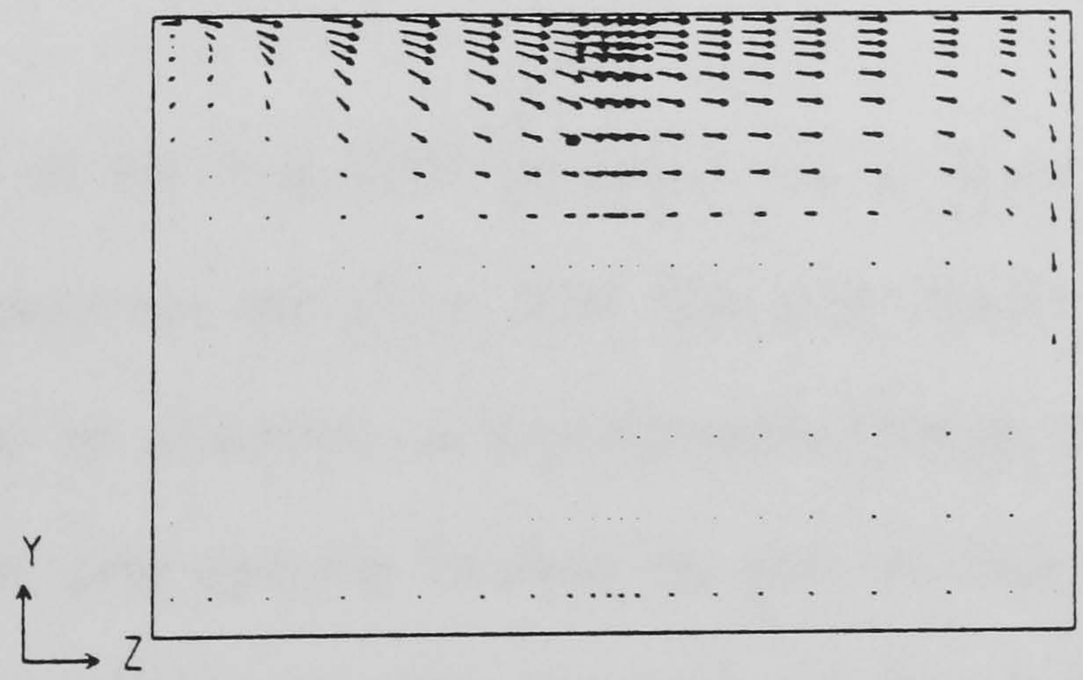

c) x=9 Vector scale: 2.87 m/s

Figure 3.4 Side view of office: predicted gas velocity vectors along the room
a) through the fire source
b) 0.165m away from the fire
c) 1.075m away from the fire/ 0.145m from the wall

plane, figure 3.4-a, shows the strong rising fire plume, which after hitting the ceiling is forced along, creating the upper layer. These gases are able to escape through the doorway. The way in which the fire plume entrains gases both hot and cold is also demonstrated. Similar effects can be seen 0.165m (X=4) away from the fire still within the doorway, figure 3.4-b. However, the way in which the upper layer is pushed downwards by the east/west walls can be seen in figure 3.4-c (X=9).

Some of the temperature distributions obtained can be seen in figure 3.5. These are presented in degrees centigrade following a conversion from enthalpy assuming variable specific heat of air; see equation (2.2-7). Previous studies had indicated significant temperature discrepancies, especially within the lower temperature regimes between constant and variable specific heat calculations. Hence, all the temperatures shown herein were calculated using this approach. The two slices shown in figure 3.5 should be compared to the first two flow fields of figure 3.4; 3.4-a and 3.4-b. In both figures the stratification of temperatures remote from the fire can be observed, along with the extent of the hot upper layer.

Bird's eye views of the flow field are illustrated in figure 3.6, where three slices through the compartment are given. The first slice, 0.45m above the floor (Y=2) shows what could be described as expanding/contracting flow. After being forced through the narrow door opening the flow expands out into the room. However, due to the strong entrainment at the base of the fire the flow is forced to constrict again. The way in which the walls constrict the flow and direct it along the boundaries can be seen in figure 3.6-b, where a slice 2.095m (Y=9) above the floor is taken. A central circulation as well as two smaller circulations in the left hand corners can also be observed. These are due to the downward movement of the upper layer and the

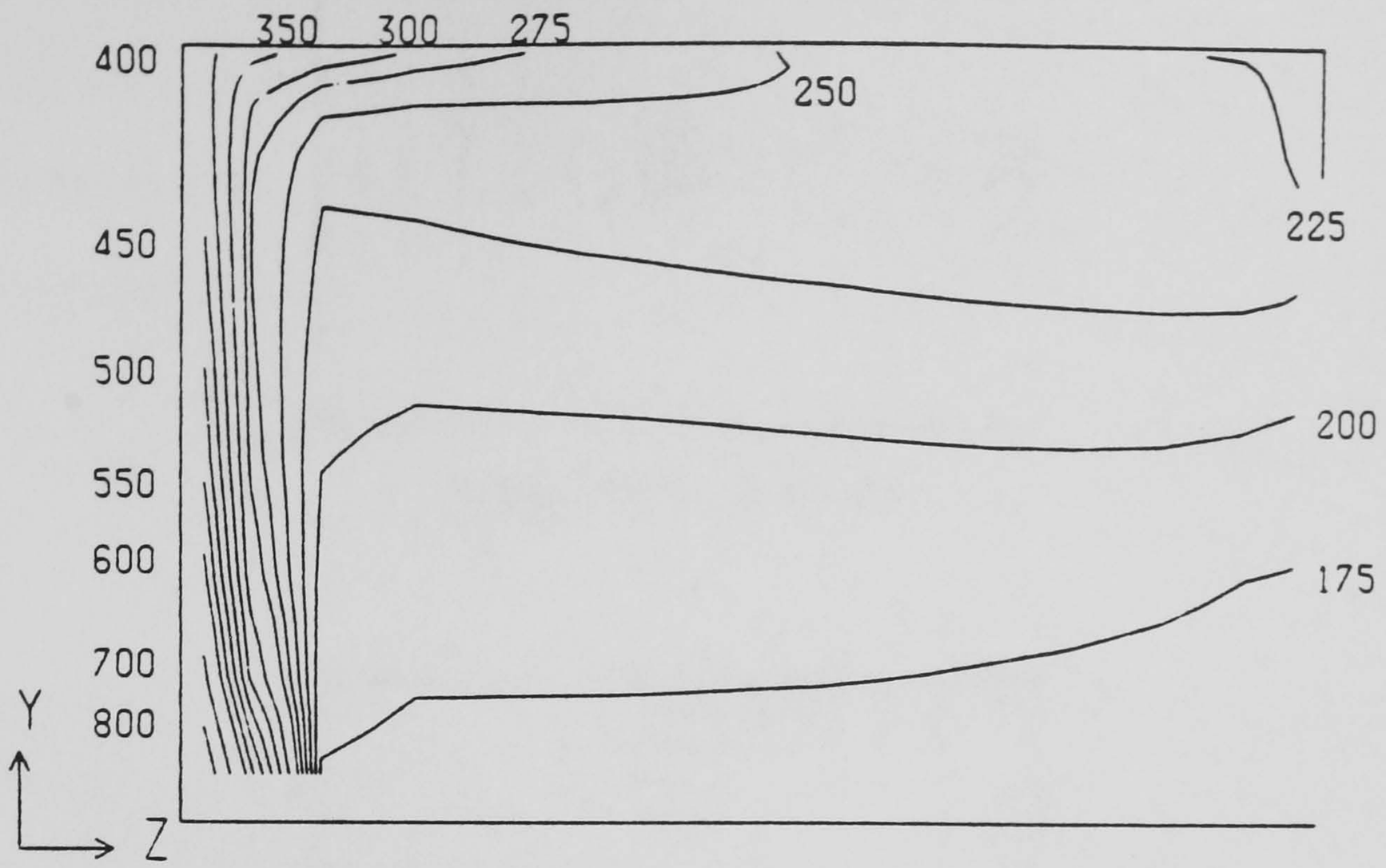

a) X=1

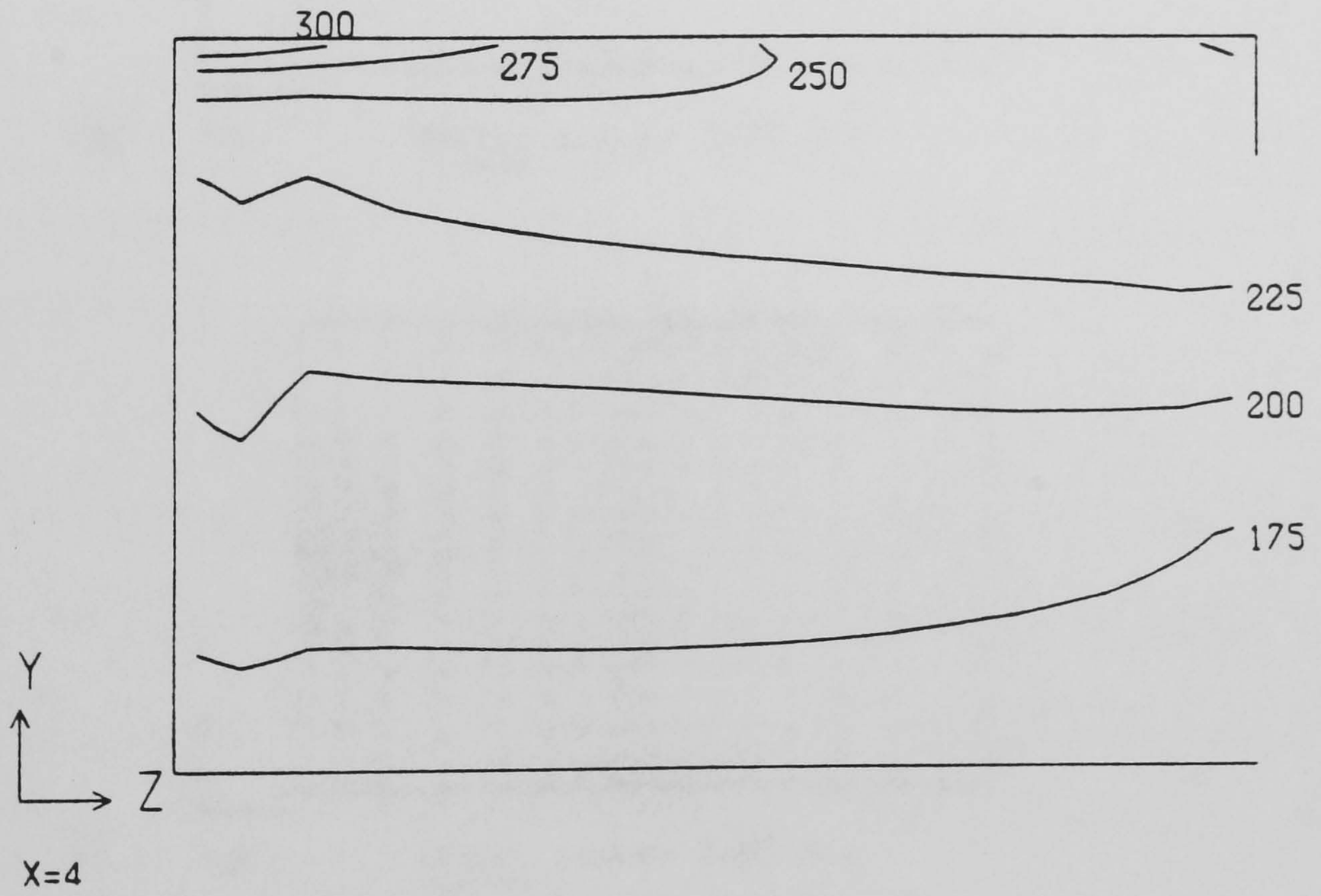

b) X=4

Figure 3.5 Side view of office: predicted gas temperature contours along the room
a) through the fire source
b) 0.165m away from the fire

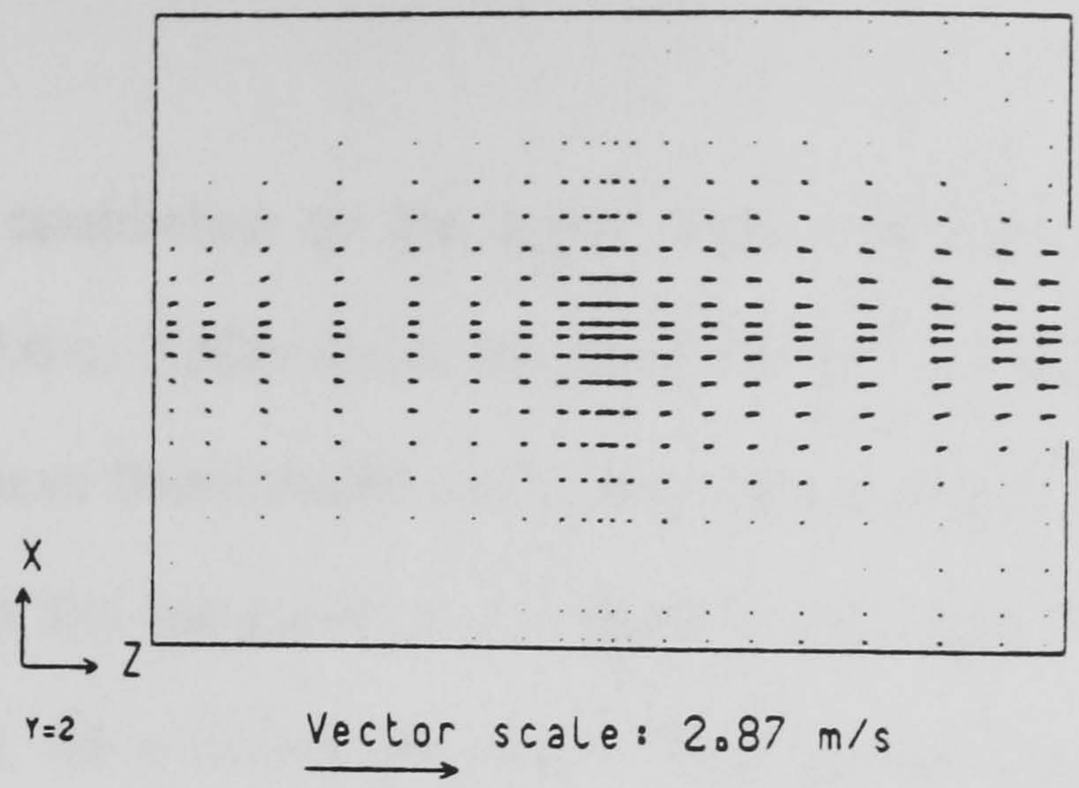

Figure 3.6 Plan view of office: predicted gas velocity vectors
a) 0.45m above the floor
b) 2.095m above the floor
c) 2.32m above the floor/ 0.12m below the ceiling

entrainment by the fire plume.

The strong flow established by the upper layer, spreading out along the ceiling is shown in figure 3.6-c, 2.32m above the floor (Y=12). As in the previous figure, two stagnant regions have been created in the left hand corners. The downward movement along the walls by the hot gases can be more clearly seen in the next set of figures, figure 3.10, where slices across the room (from east to west) are shown.

The strong upward movement by the plume, re-direction by the walls and creation of circulation fields in the top corners of the room are shown in figure 3.7-a. Figures 3.7-b and 3.7-c, slices 0.7m (Z=4) and ..805m (Z=10) away from the fire, show similar circulation patterns and indicate a two-dimensional effect remote from the fire. The flow field occurring on the side of the room near the doorway (Z=20) is shown in figure 3.7-d, whereby it should be remembered that the gases are leaving the office through the upper section and the cooler air is entrained through the lower section of the doorway.

Though no experimental data was available for this specific fire situation the above results are nevertheless acceptable considering the main aim of this feasibility study. The purpose was not to make exact predictions, which were unlikely to have been obtained due to the lack of necessary experimental data but to predict flow behaviours and temperature distributions which are generally observed.

From comparisons with a previous study [Markatos et al(1982)] the above results indicate that the criteria have been met. Hence these results were used as the initial field for the gas phase of the two-phase feasibility study, discussed in chapter 5.

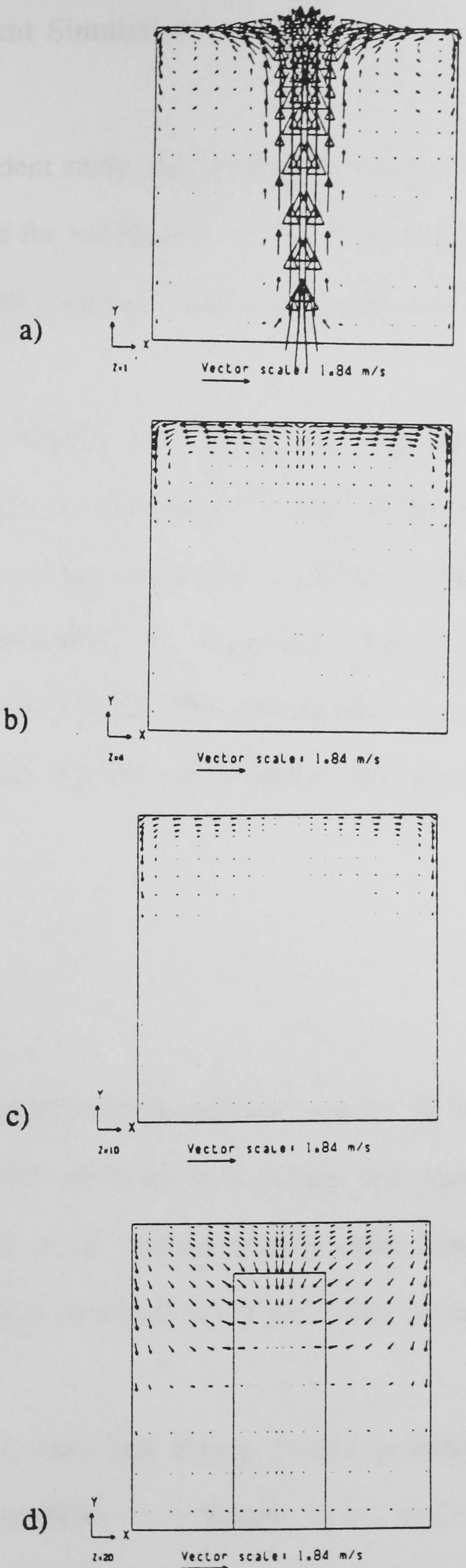

Figure 3.7 Cross view of office: predicted gas velocity vectors across the room
a) through the fire source b) 0.7m away from the fire
c) 1.805m away from the fire d) through the doorway

3.3 Time Dependent Simulations

For the time dependent study, the experimental data for both the office and a hospital room fire were used for validation purposes. Within this section these simulations will be outlined and their respective results presented and discussed.

As one aim of fire modelling is to determine temperature rise and general conditions within a compartment, their subsequent impact on life should also be considered. One criteria for determining life threatening conditions is the level of the gas temperature, whereby it is recommended that temperature should not exceed 50° C below 1.5m from the floor [Smith (1987)]. The development and spread of this hot layer is of interest to evacuation and life safety studies and can be monitored during transient simulations.

3.3.1 Office Fire

The office's dimensions were the same as used for the steady-state simulation; section 3.2. However, for this study the heat source, still representing a wastepaper basket fire, was positioned in its original corner, using exactly the same dimensions as detailed in section 3.2. A schematic of the office lay-out can be seen in figure 3.8.

As the report by Cooper and Stroup (1987) provided no details concerning the materials of the boundaries, heat transfer to the walls was not taken into account. Instead an isothermal wall condition, with a temperature of 24°C, as assumed in the steady-state study, was used.

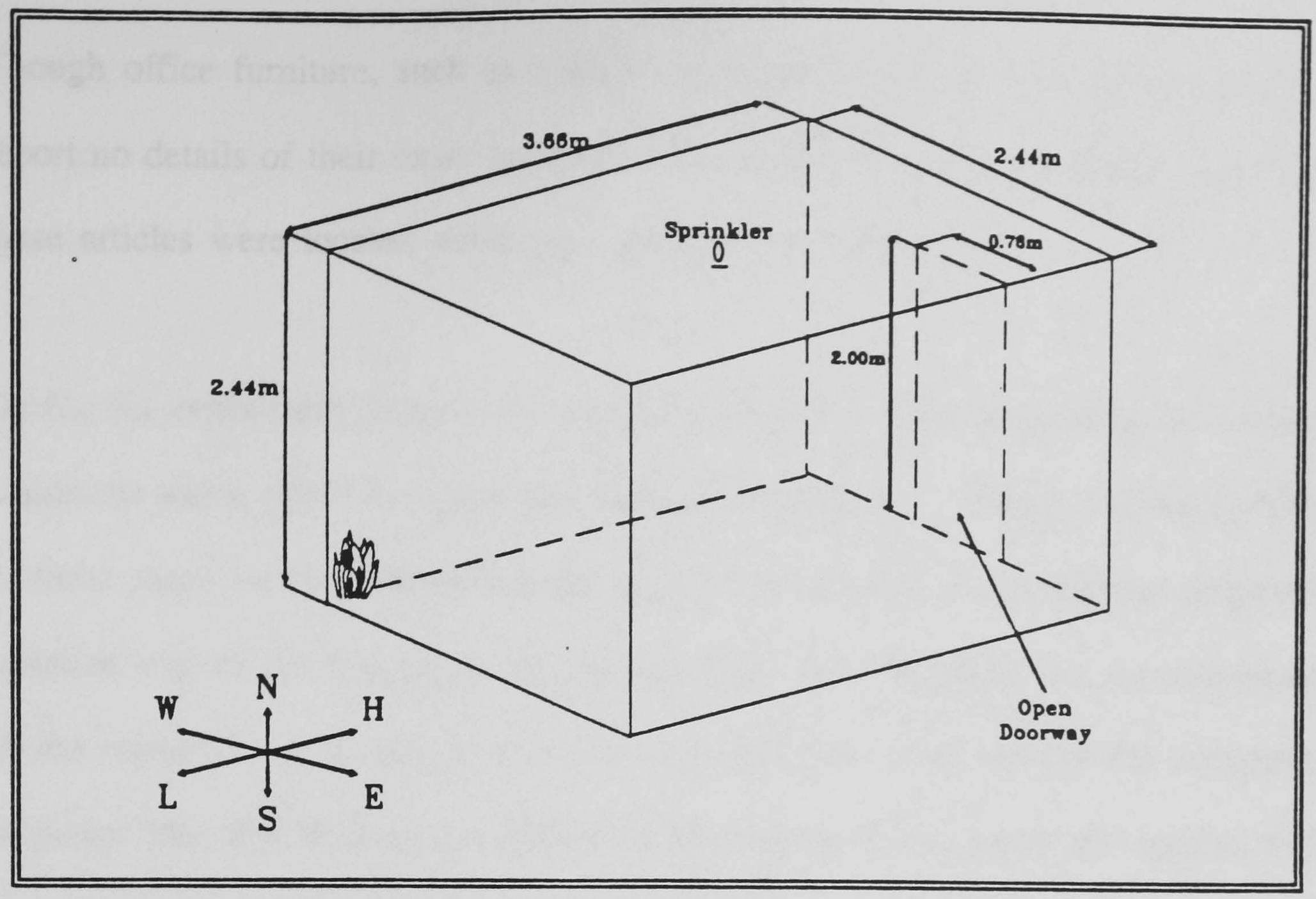

Figure 3.8 Office Schematic

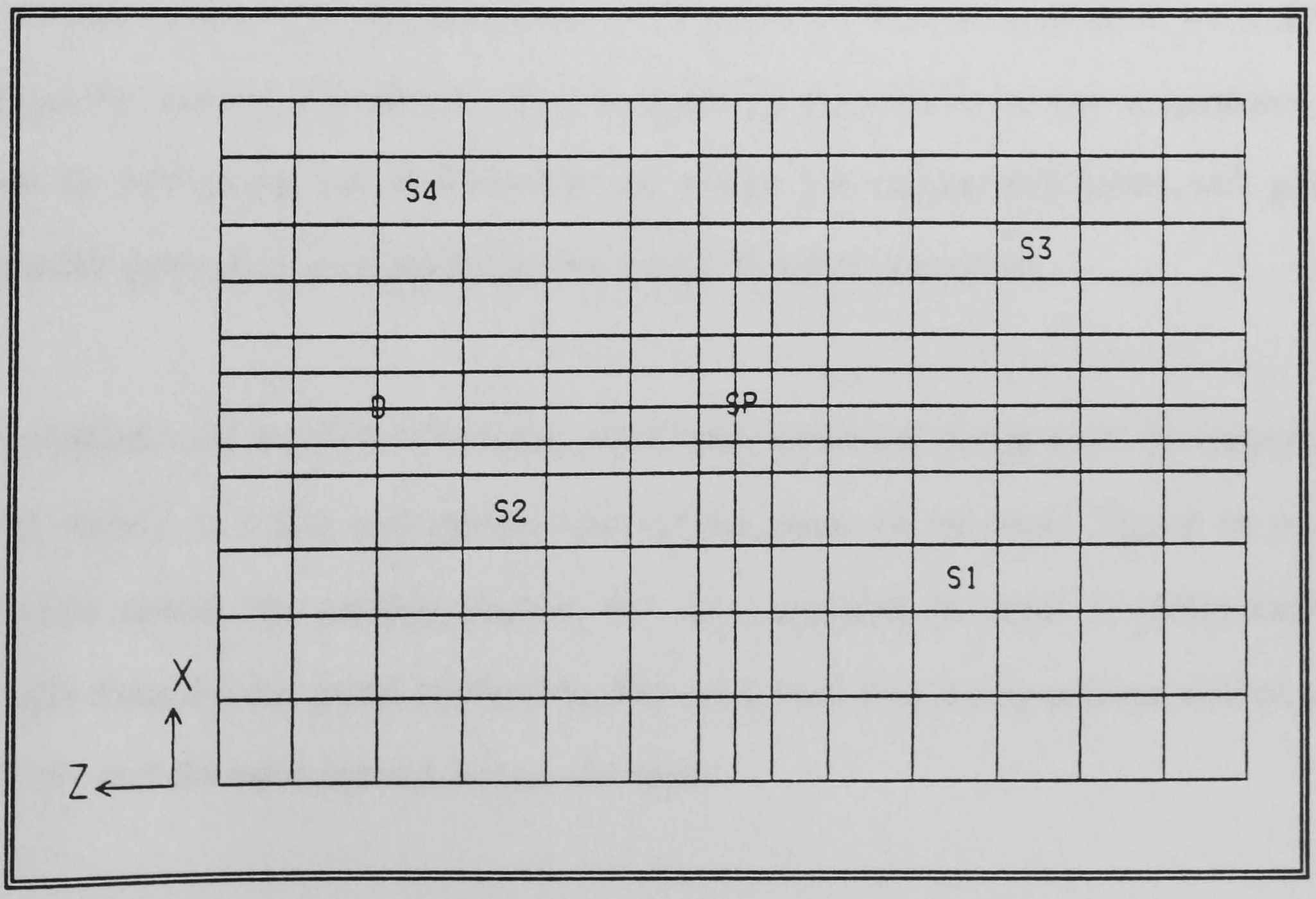

Figure 3.9 Details of the Measuring Locations

Though office furniture, such as a desk, chair and bookcase were mentioned in the report no details of their exact locations were given. Hence no blockages to represent these articles were located within the computational domain.

During the experiment temperature measurements were taken at two distinct locations within the room; near the centre and halfway between the sprinkler and the doorway. At these locations small thermocouple stacks were situated measuring the temperature variation with height just below the ceiling. From these locations and the arrangement of the numerical grid used two coinciding positions were chosen for comparison purposes. The first location just above the sprinkler is 0.05m below the ceiling, whilst the other near the doorway is 0.24m below the ceiling. The positions of these locations are marked in figure 3.9 as 'SP' and 'D', for the sprinkler and doorway positions respectively.

A further temperature comparison was made at the sprinkler head position itself, 0.1m below the ceiling. Though this only involves the comparison of gas temperatures it aids in monitoring the temperatures just below the ceiling and hence will guide possible extensions into predicting the actual sprinkler activation.

In addition one thermocouple stack which monitored the temperature developments with respect to height was situated towards the centre of the room. Due to no exact location details the position marked 'SP' was assumed. In order to obtain further details from the numerical predictions, four additional monitoring regions marked S1, S2, S3 and S4 were located within the room.

In order to obtain the rate of time-dependent heat release from the fire the smoke

flowing out through the doorway was collected and analysed. However, three different fire growth rates were postulated in order to *represent experimentally the observed fire growth* [Cooper and Stroup (1987)]. The actual fire growth rate used within this time dependent simulation can be seen in figure 3.10, alongside the three growth rates the report presented.

As can be observed, the heat release rate used during the simulation does not exactly follow any of the three suggested curves. The reason for this adjustment was that implementations of the three suggested growth rates either greatly over- or under-predicted the transient temperature development. However, as one condition for this fire simulation was to obtain a *realistic* flow field within the compartment to use as initial conditions for the sprinkler simulation, it was felt necessary to utilise the alternative growth rate, as illustrated. The basis for this alternate rate is an initial exponential growth generally observed [Lie (1972)], whereby the growth was between the three suggested rates. After 120 seconds the characteristic variation as suggested by the three given growth rates was accounted for. However, it should be noted that heat transfer calculations to the walls were not performed due to the lack of boundary conditions provided. Hence, an adjustment was made to account for this effect, and the combustion efficiency of the fuel in the actual rate of heat released. Thus, the heat release rate used within the model was 50% of the graph shown.

The above adjustments indicate how sensitive this type of fire prediction can be to experimental data and also suggests the necessity for modellers to be provided with accurate heat release rates.

The numerical grid fitted to the above specifications can be seen in figure 3.11. It can

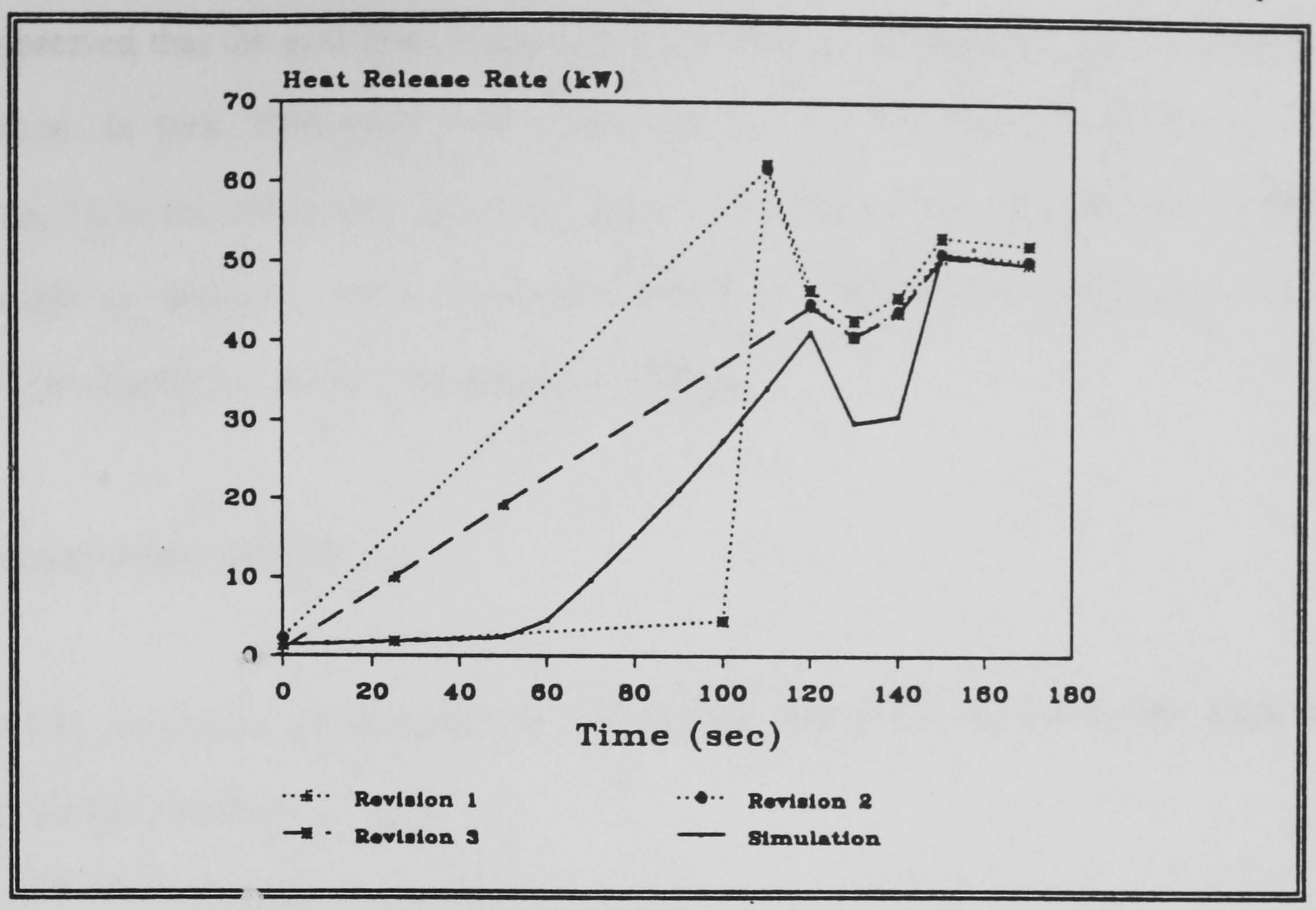

Figure 3.10 Heat Release Rates

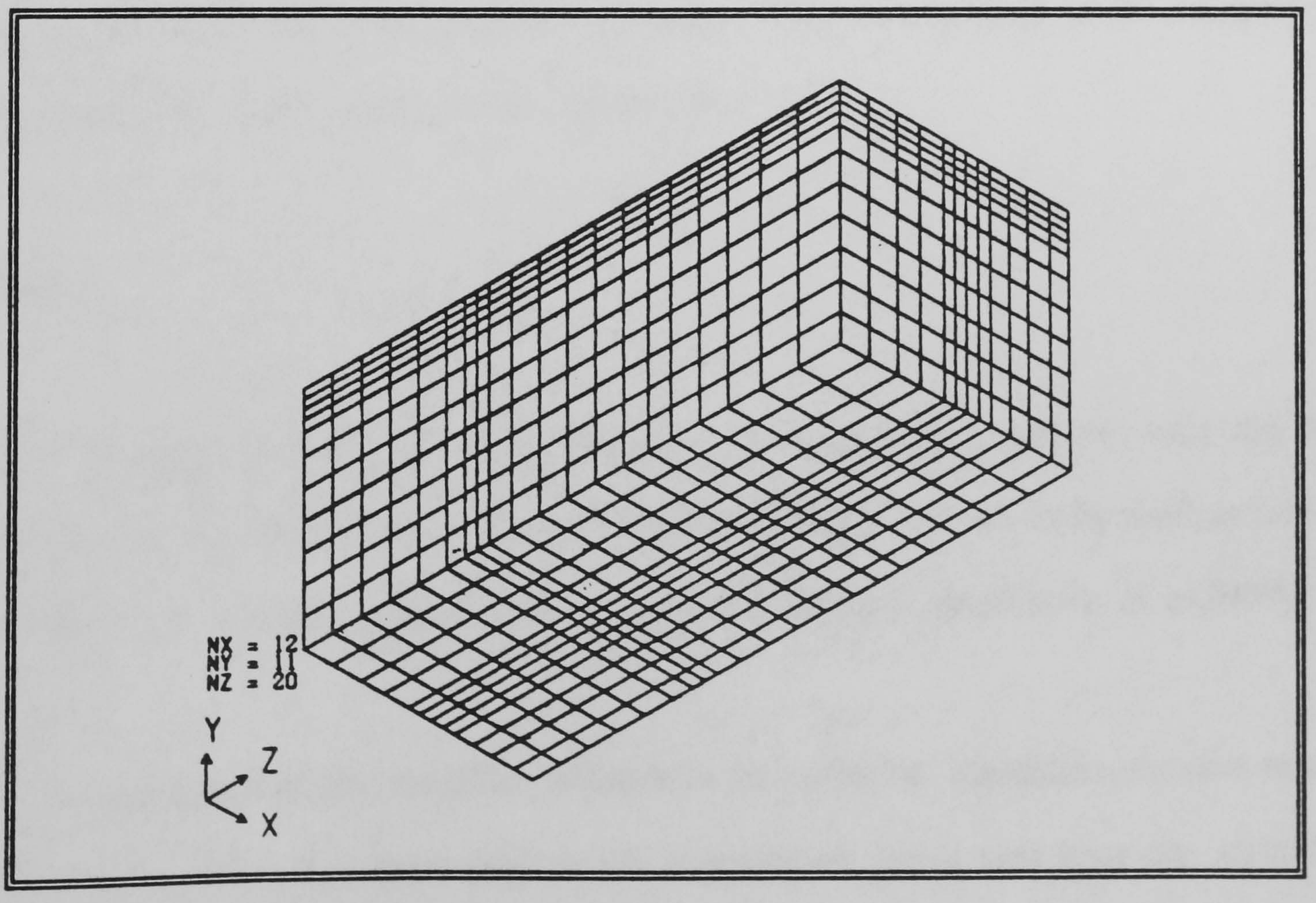

Figure 3.11 Numerical grid used

be observed that the grid lines become narrower near the boundaries and the sprinkler location. In total 2640 cells were used, whereby 12 cells were distributed in the width, 11 in the height and 20 in the length of the office. Note that the last number includes six divisions which were taken outside the compartment (see section 2.2.7 and the discussion of the free boundary setting).

Computational Details

The fire simulation which lasted for 175 seconds was performed using time steps of one second duration.

In order to obtain converged solutions, it was necessary to alter the number of sweeps performed during each time step, whereby criteria such as those mentioned in section 3.2.1 needed to be satisfied. Hence during the initial stages of the simulation a one second time step calculation required 50 sweeps. This was lowered to 40 sweeps per step during the latter stages of the simulation.

Results

As in the case of the steady-state simulation the results presented not only aid the validation of the fire model discussed within this chapter but are to be used as initial conditions for the next stage of this two-phase simulation [Hoffmann et al(1990)].

As the activation of the sprinkler element is currently an important research topic, particular attention has been paid to the temperature predictions near the sprinkler location. Figure 3.12 shows comparisons of the predicted and experimental time

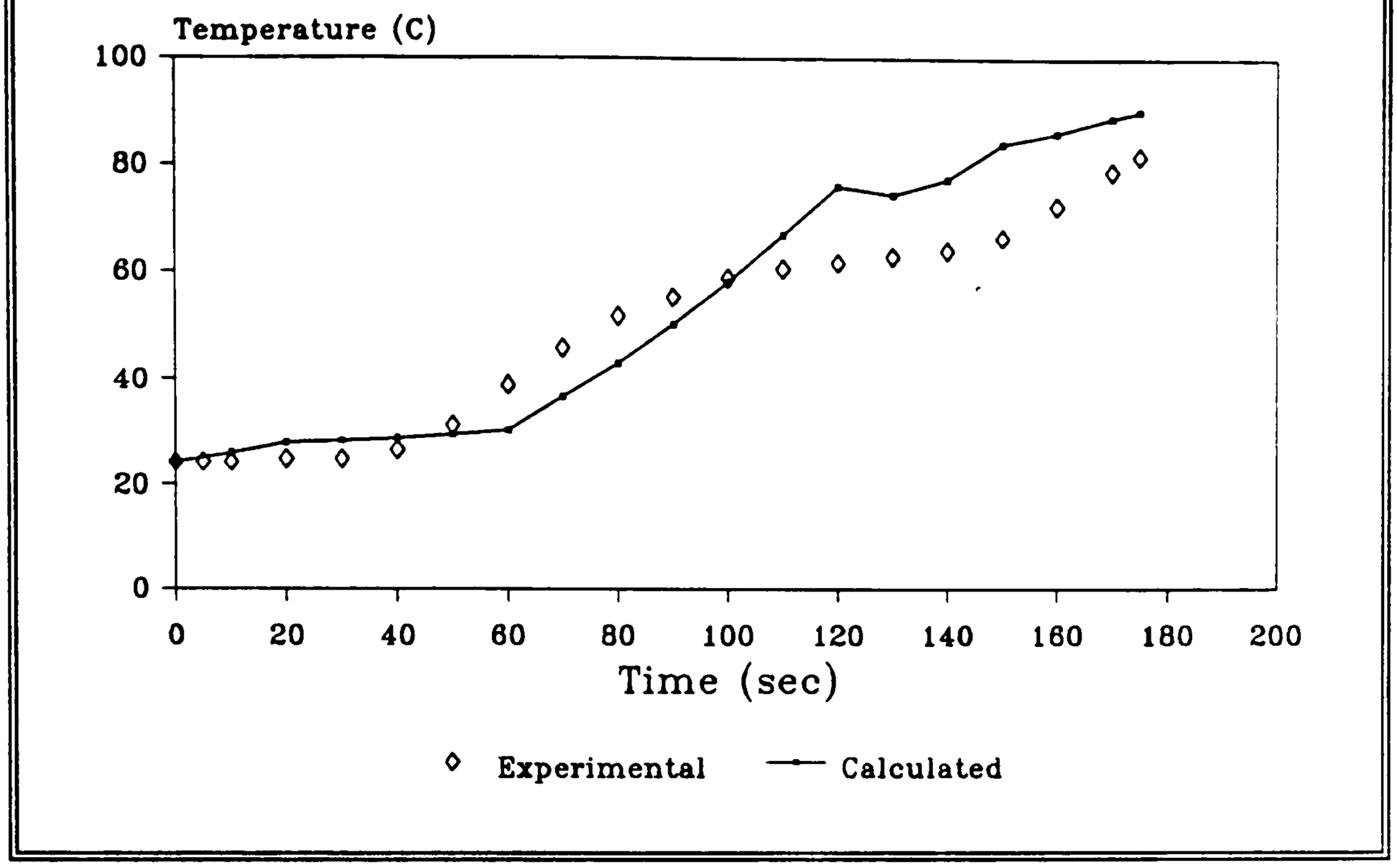

a) Temperatures 0.05m below the ceiling

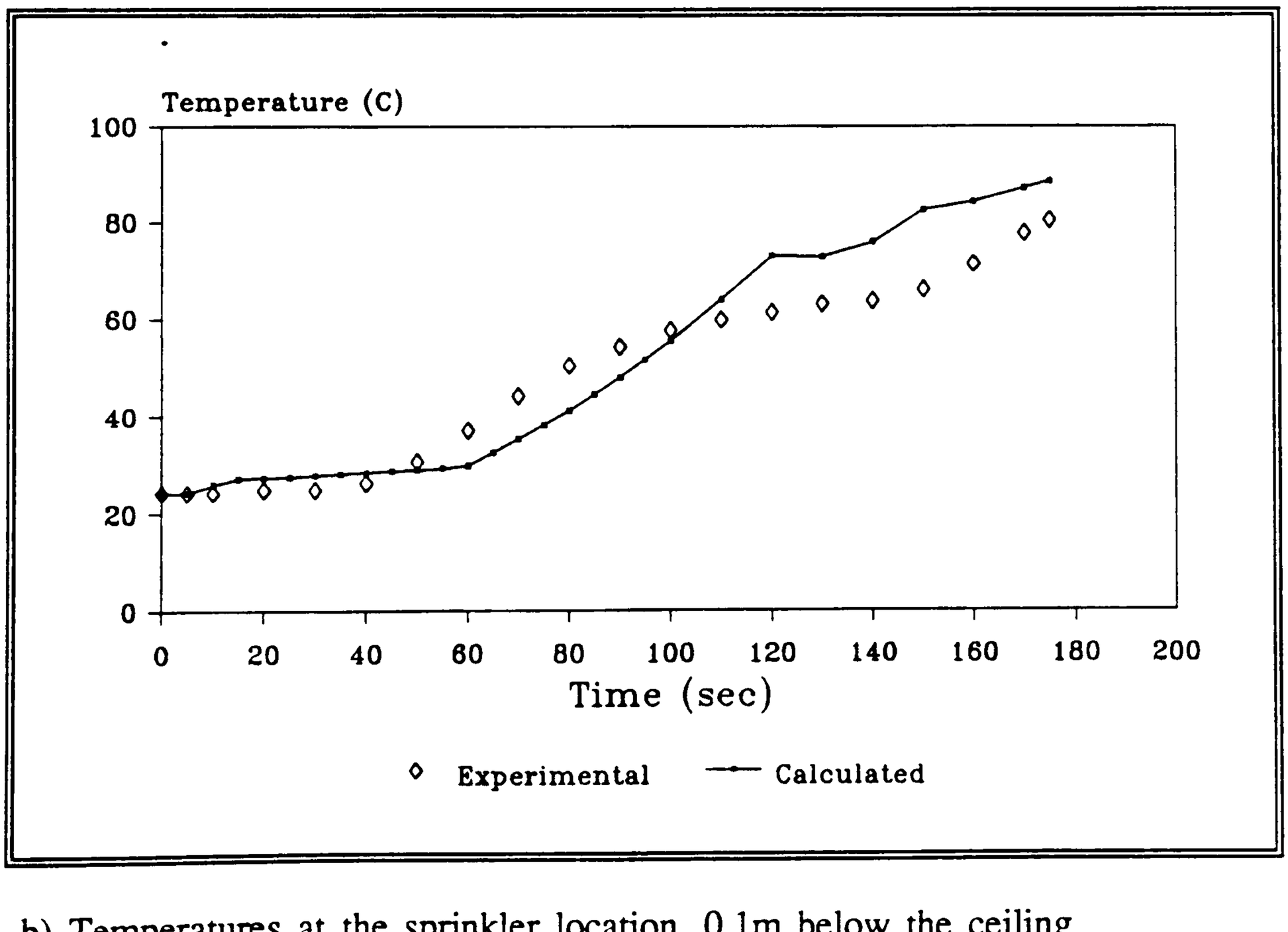

b) Temperatures at the sprinkler location, 0.1m below the ceiling

Figure 3.12 Predicted and measured gas temperatures towards the centre of the room

histories of gas temperatures near the sprinkler location. From these it can be seen that utilising the suggested fire growth rate as discussed above, the correct trends in the temperature increase within the upper layer has been captured. However, the degree of accuracy obtained during certain stages of the scenario still need attention and further consideration. This in turn reflects on the number of assumptions involved, such as the heat release rate and size of the fire source along with the adiabatic wall condition.

Taking these into account it can nevertheless be seen in figure 3.12-a at a position 0.05m below the ceiling that the predictions made are between 3% and 27% of the measured data.

The gas temperature comparisons made in figure 3.12-b are at the sprinkler location, 0.1m below the ceiling. These are illustrative of the scope for development that this mathematical model has to offer. Knowledge of gas temperatures occurring around a sprinkler head are necessary to perform heat transfer calculations to the sprinkler's trigger mechanism. Hence, subsequent versions of the model would no longer rely on measured data and timings of sprinkler activation, but instead would be able to determine this time itself. However, as this location is only five centimetres below the previous position the predictions made closely follow those trends.

Similar trends in predictions of gas temperatures can be observed in figure 3.13. This location is near the doorway (marked 'D' in figure 3.9) and is 0.24m below the ceiling. The results are between 2% to 30% of the experimental data. Though these results are very similar to the centre of the room comparisons, the added effect of the outside conditions could very well provide further explanation to the amount of

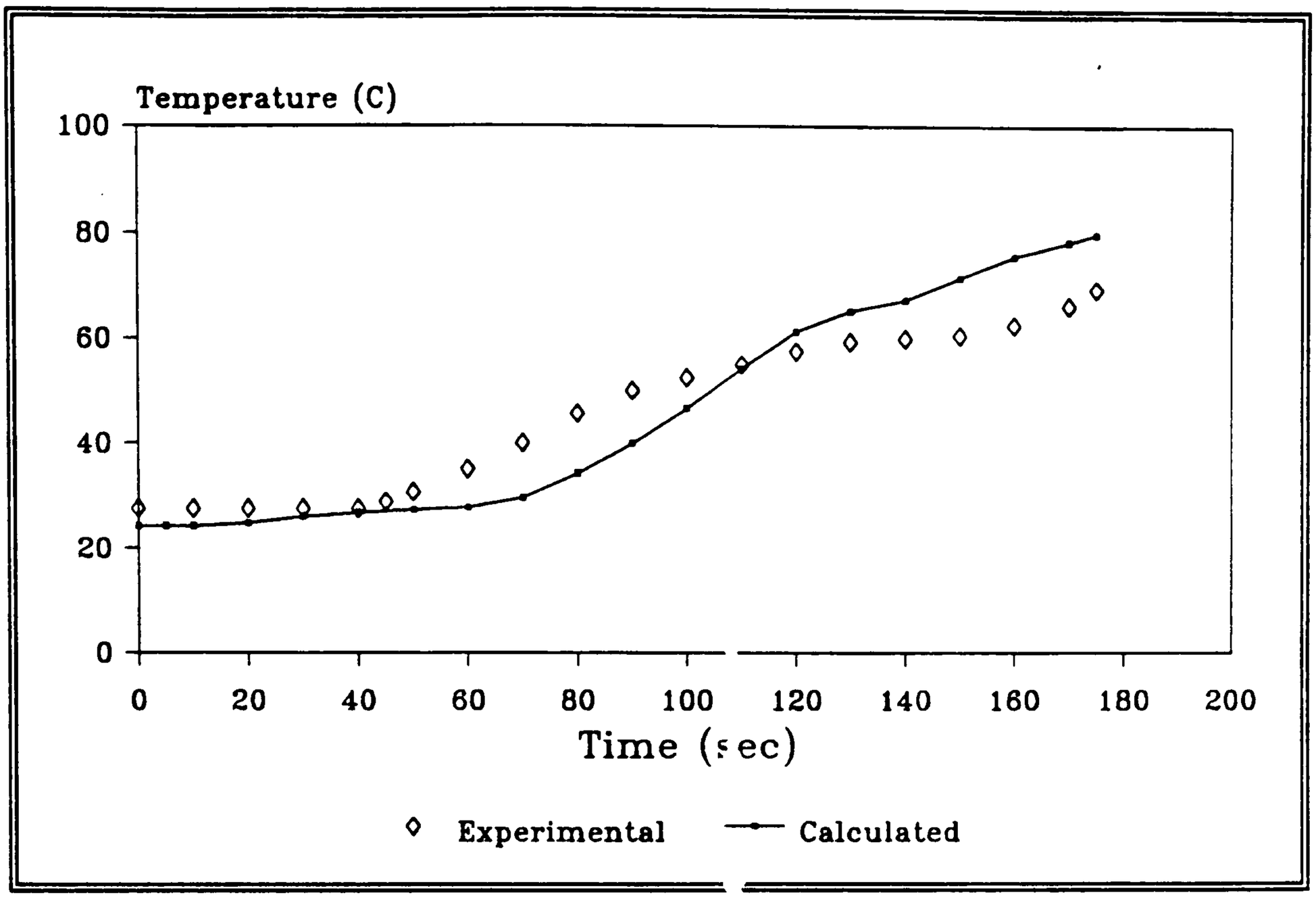

Figure 3.13 Predicted and measured gas temperatures: near the doorway, 0.24m below the ceiling

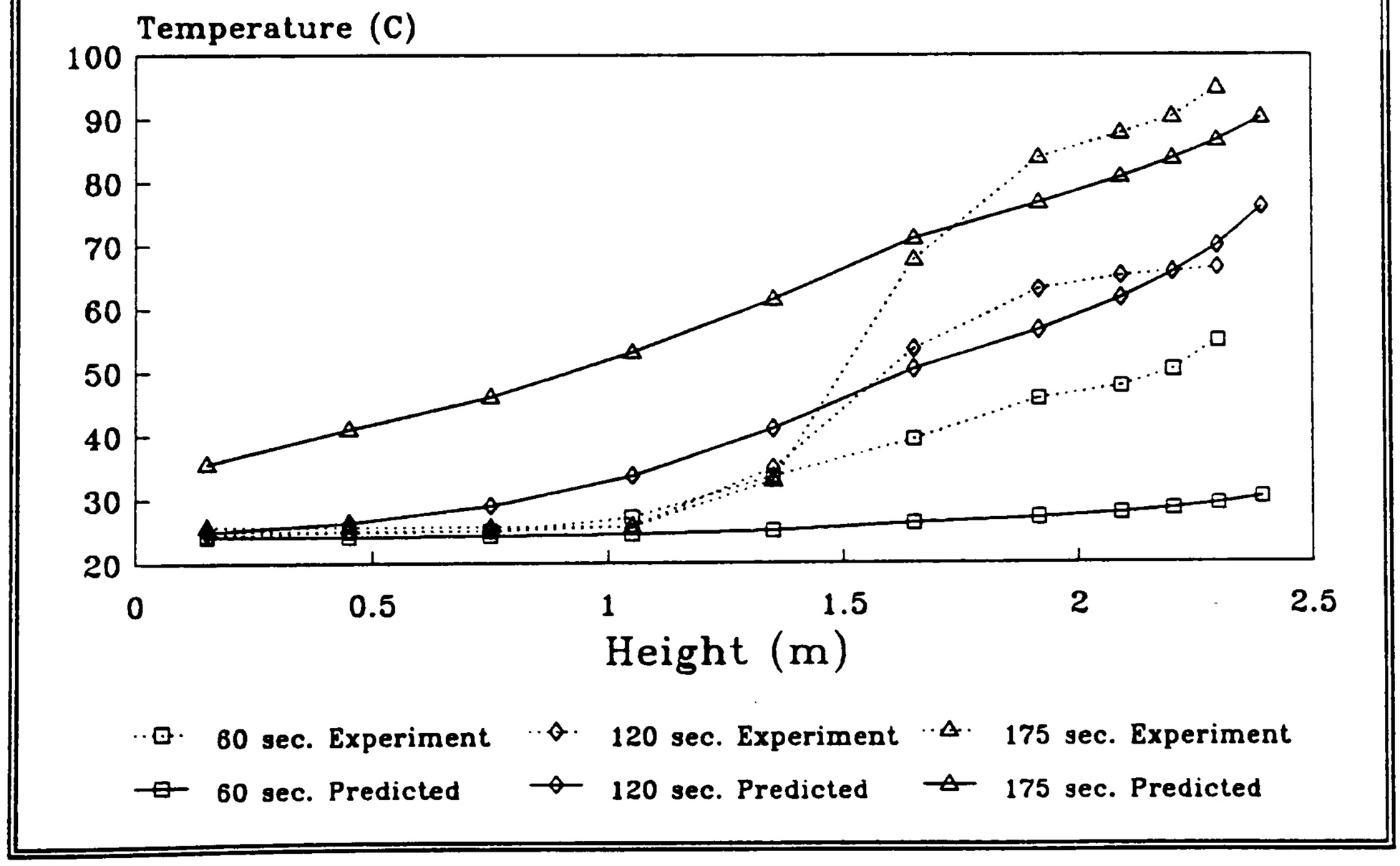

Figure 3.14 Predicted gas temperature variations with height towards the centre of the office

deviation between the predictions and experimental data.

The variation of temperature with respect to height can be seen in figure 3.14, whereby the vertical temperature predictions made at the stack 'SP' are compared to measured data after 60, 120 and 175 seconds.

From these it can clearly be seen that the temperatures were significantly under-predicted after the first 60 seconds. This in turn casts doubt on the accuracy of the heat release rate used, which appears to have been low for too long a period.

After 120 seconds the predictions are much closer to measurements. However, it is clear that the predicted interface between the hot and cold layer is not as sharp as that measured in the experiment. Several reasons for this exist. Firstly the grid-size distribution could have been too large and hence the interface could not be distinguished precisely enough. The smearing of the interface also suggests mixing of the two layers. This in turn leads to the conditions prevailing outside the compartment. During the simulation the hot air was able to escape out of the compartment, whilst cooler air was entrained. However, no details concerning the conditions prevailing outside the compartment during the experiment were given. This shows the influence of outside conditions and hence the importance of very detailed experimental data.

By the end of the experiment a similar picture emerges; predictions near the ceiling are fairly close, however the interface is smeared and the lower layer is considerably warmer than measured. What appears to happen according to the measurements is that the hot upper layer escapes out of the compartment without any kind of mixing. In

fact some of the lower temperatures have cooled down during the fire scenario! This highlights the importance of detailed measurements both inside and outside the fire compartment.

In order to monitor more closely the effect of the fire with respect to height, temperatures at four additional monitoring locations within the room were examined. Figure 3.15 shows the variation in temperature with height at the locations for 30, 60 120 and 175 seconds into the fire scenario. As can be seen temperatures have only increased slightly within 60 seconds. The most change can be observed, as expected, at the first location closest to the fire. After 120 seconds, the development of temperature stratification can be seen across the room, whereby some areas produce more developed layers than others.

Location S1, which is the closest to the fire has as expected a much higher temperature near the ceiling as well as a thinner upper layer than that at S4, which is in the opposite corner of the room. However, at location S4 the hot upper layer is much deeper and more uniform due to the accumulation of hot gases within this corner. Meanwhile the other two locations show more gradual rises in temperatures due to mixing of gases in their respective regions.

Considering the life safety criteria of temperatures less than 50°C below 1.5m, and disregarding the effect of thermal radiation, it can be seen that after 120 seconds the locations of S1, S2 and S3 have not met this criteria and in fact S4, the place furthest away from the fire, is a more dangerous place. However, by the end of the scenario the safest place has become the outside of the compartment, as temperatures have continued to increase following the same temperature stratifications as observed during the previous interval.

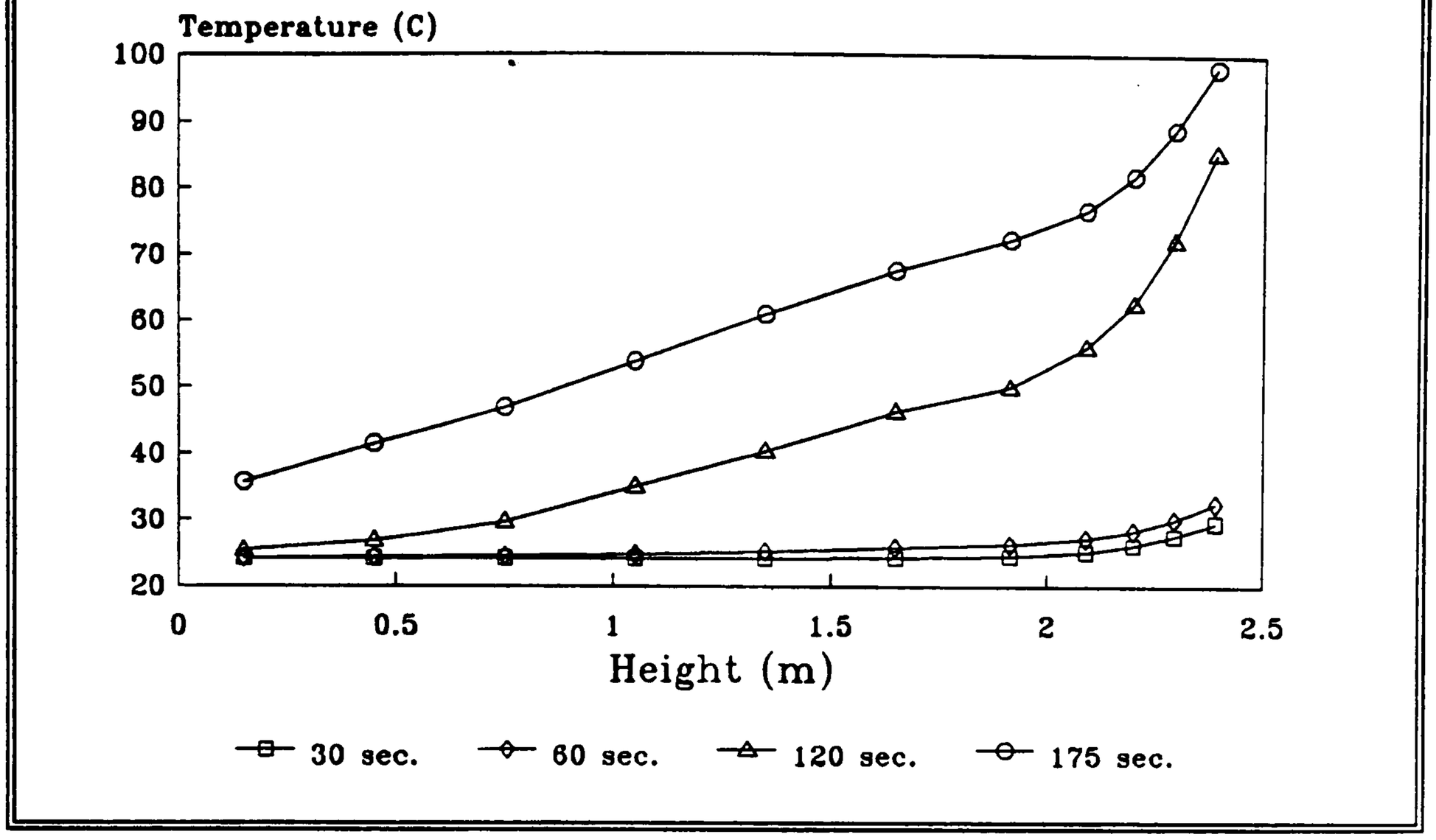

a) Location S1

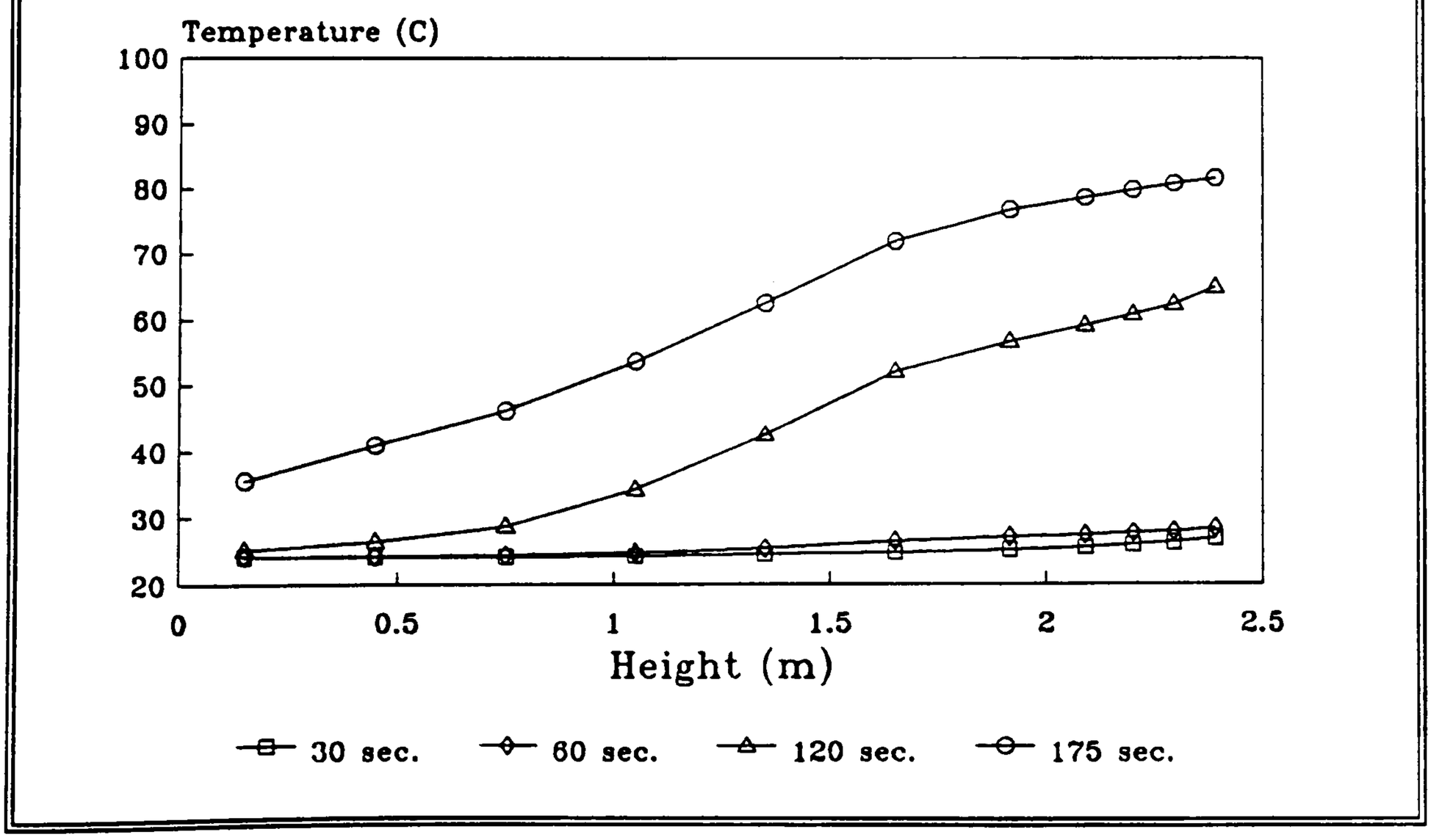

b) Location S2

Figure 3.15 Predicted gas temperature variations with height

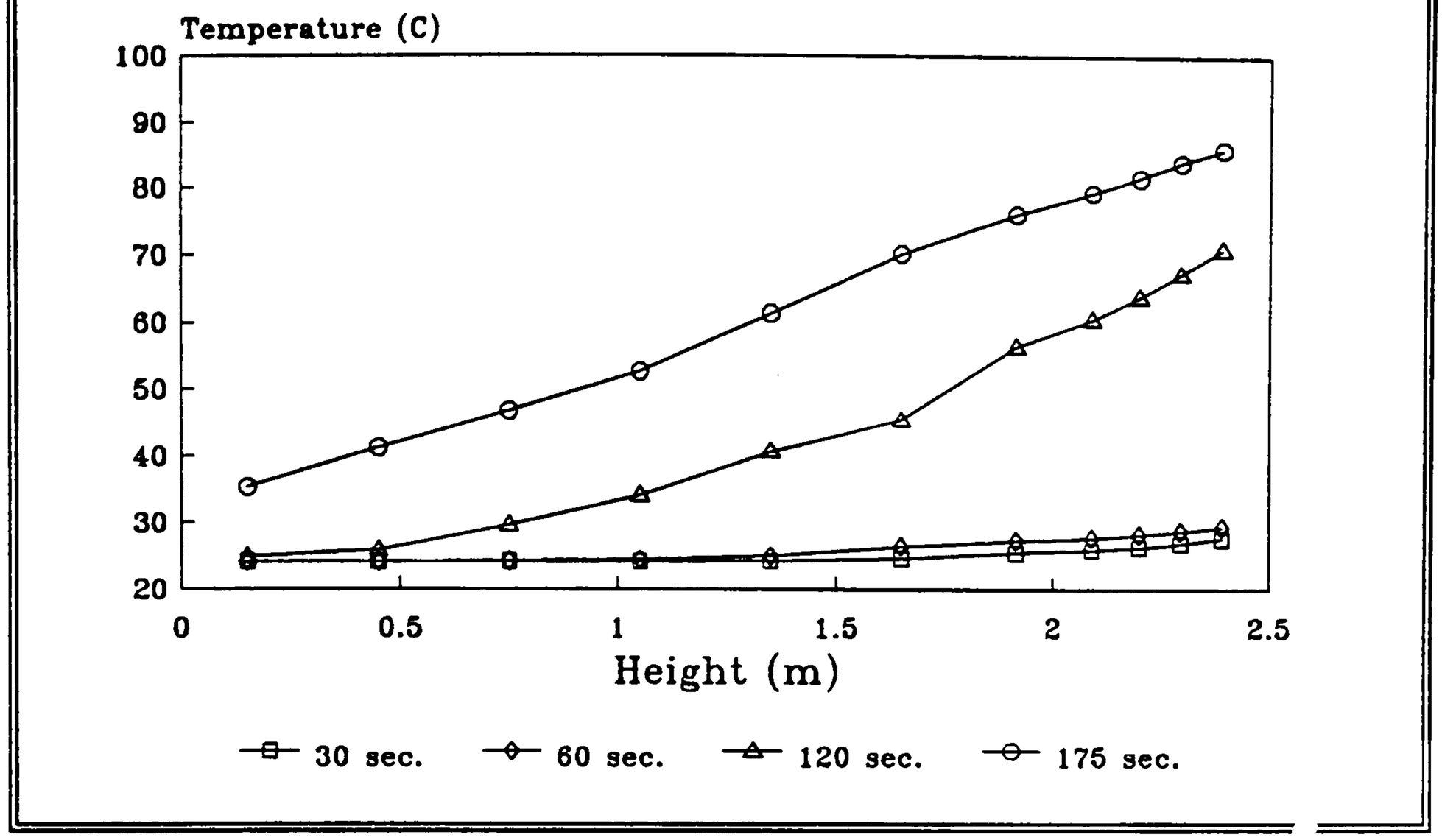

c) Location S3

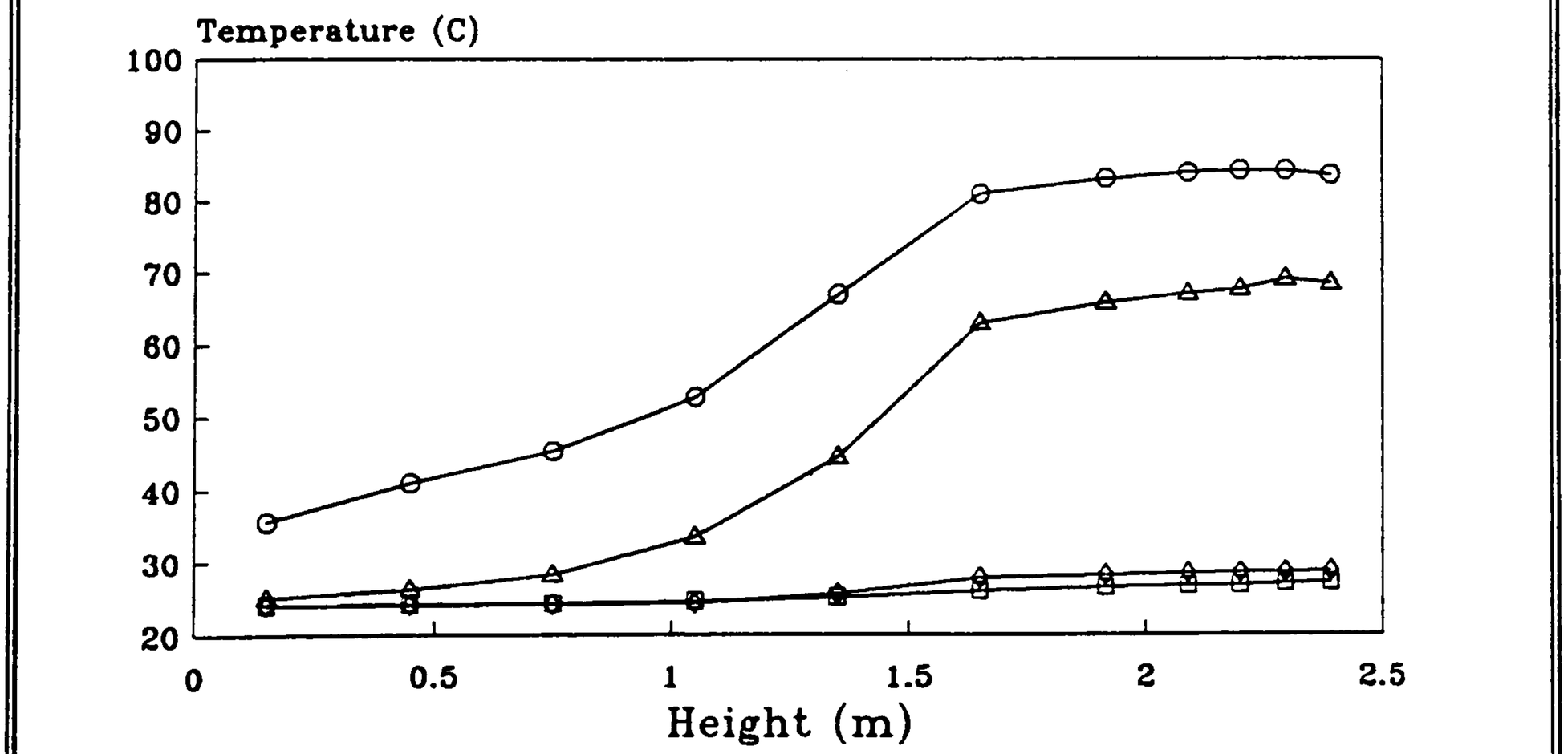

d) Location S4

Figure 3.15 Predicted gas temperature variations with height (continued)

Further details and explanations concerning the above mentioned characteristics are highlighted in greater detail in subsequent figures, such as figures 3.23 and 3.24.

A summary of the final temperatures with height after 175 seconds can be seen in figure 3.16. Here it can be seen more clearly that temperatures at all four locations are virtually the same up to a height of 1.1m. Above that height three distinct temperature stratifications can be observed. Locations S1 and S4 provide a very thin and thick hot layer respectively, whilst more gradual rises in temperatures are observed at S2 and S3 due to the mixing.

Due to the lack of experimental data, the inform ation in figures 3.17 to 3.30 cannot be validated, however, they serve to illustrate the general conditions within the compartment and the way in which they vary in time. Temperature contours, such as the 50°C contour, and gas velocity vectors are presented after 60, 120 and 175 seconds of fire ignition at distinct planes within the room. These provide an insight into the development of the hot upper layer and the circulation patterns created. For clarification of the location of the planes shown, a small diagram with the plane of interest highlighted is situated in the top right hand corner of each figure.

The first two diagrams, see figures 3.17 and 3.18, show the temperature development and flow field in time at the plane along the east wall through the fire source (X=1), which is positioned on the left hand side. Here it can clearly be seen how the hot upper layer is created and is initially pushed outwards along the ceiling. However, due to the circulation patterns, generated within the compartment, the air is heated up producing a distinct layering effect remote from the fire source.

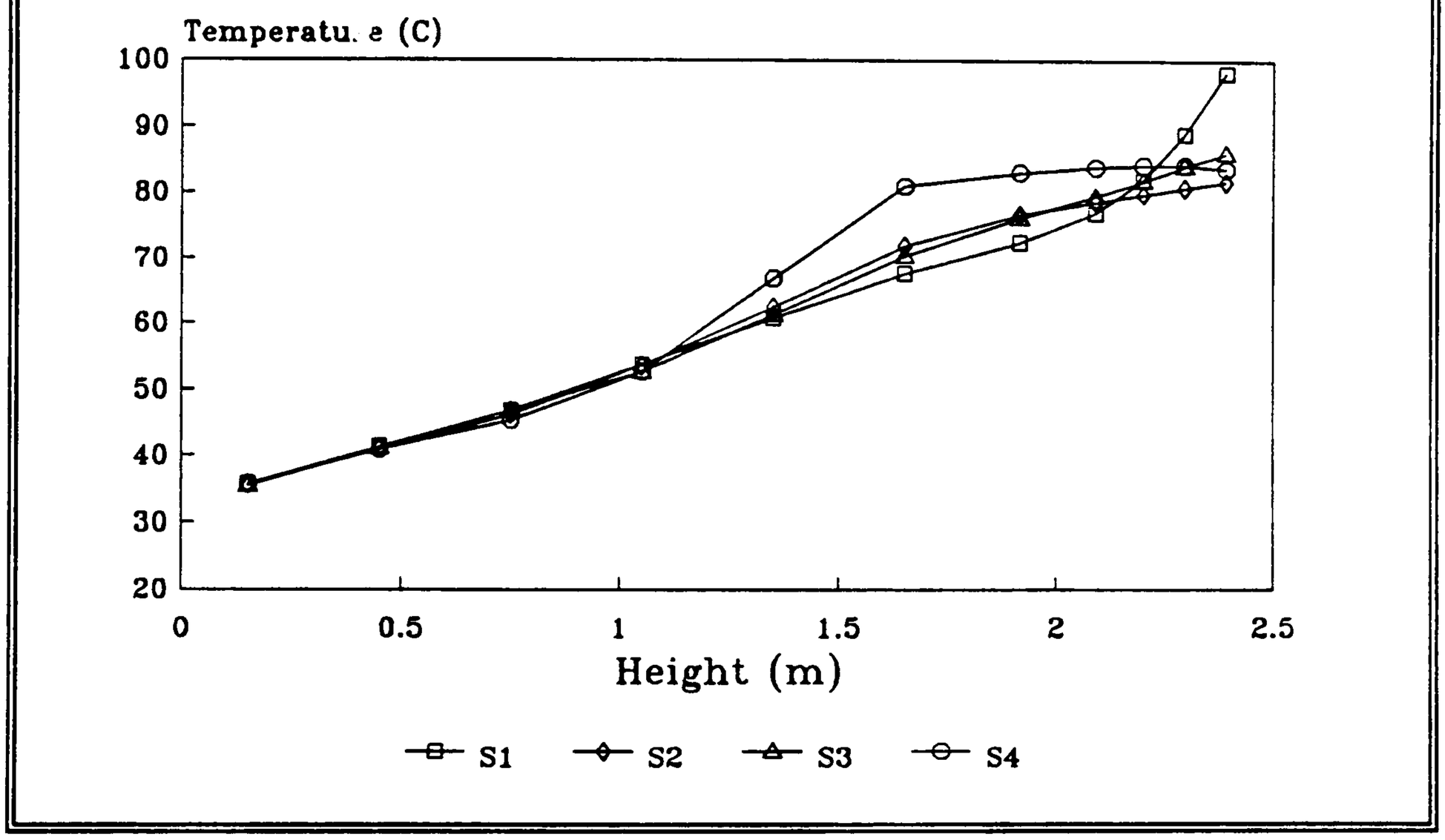

Figure 3.16 Temperature predictions with height after 175 seconds at the four monitoring locations

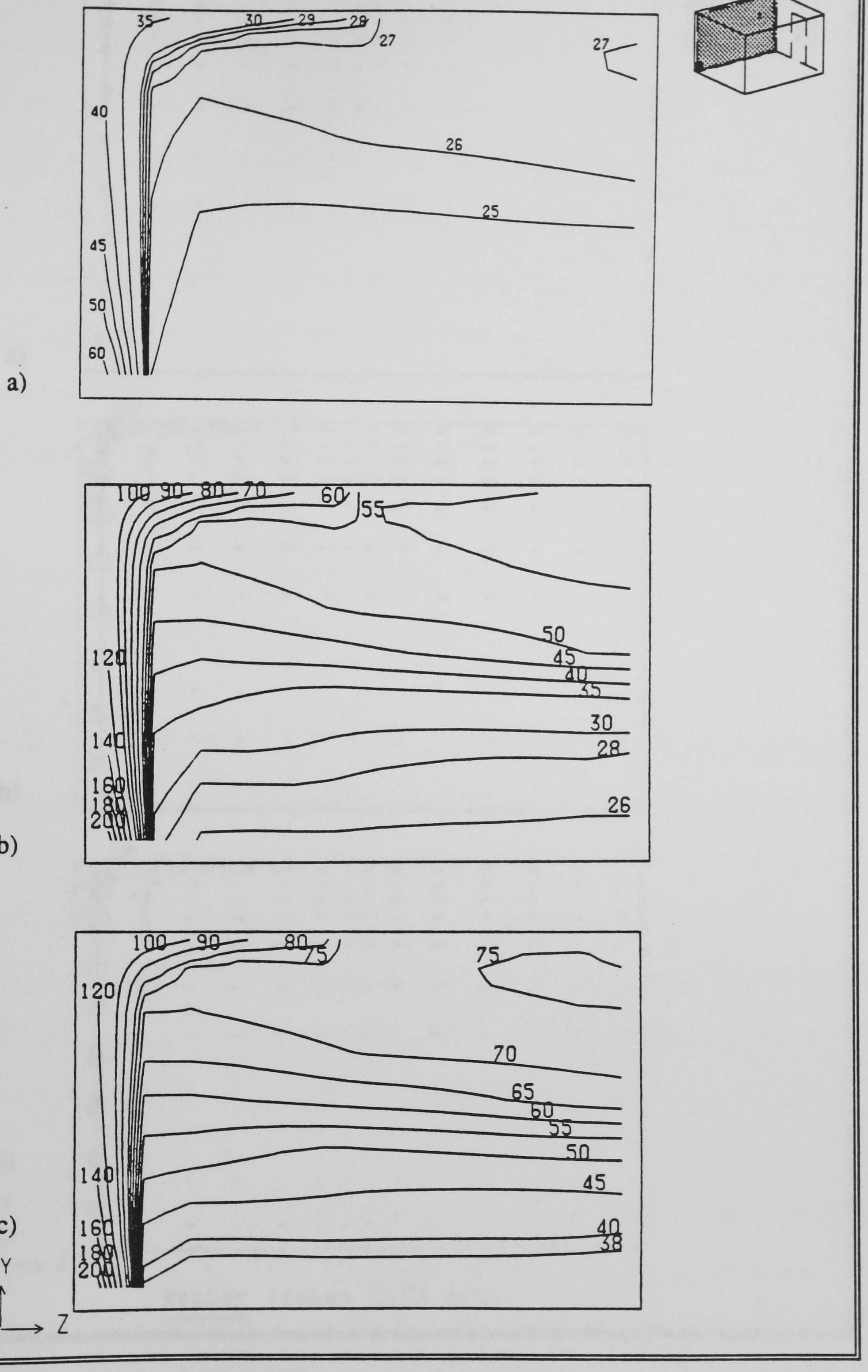

Figure 3.17 Side view of office: predicted gas temperature contours along the west wall through the fire source (X=1)
a) 60 sec. b) 120 sec. c) 175 sec.

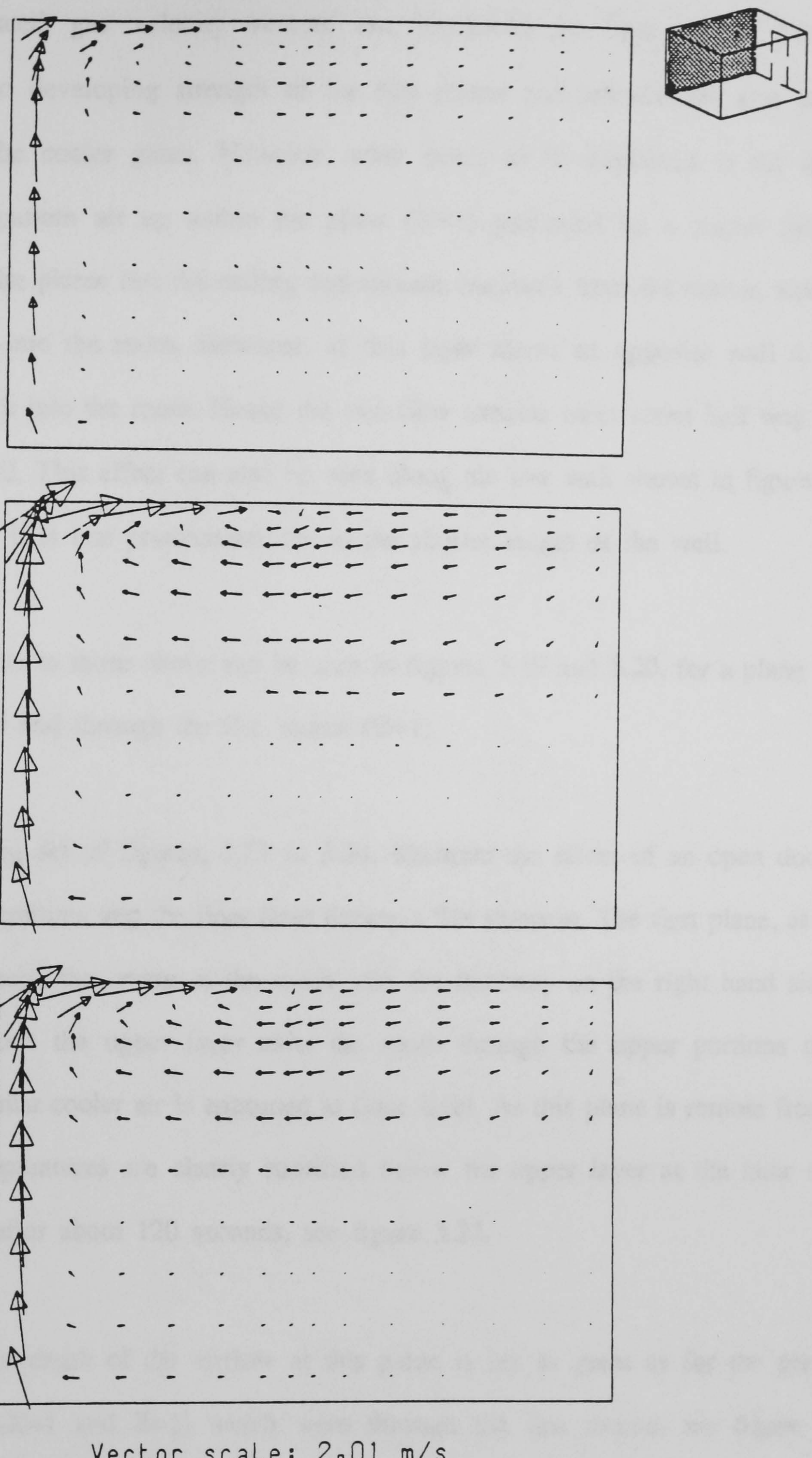

Figure 3.18 Side view of office: predicted gas velocity vector fields along the west wall through the fire source (X=1)
a) 60 sec. b) 120 sec. c) 175 sec.

The associated gas velocity vectors are illustrated in figure 3.18. Note the characteristic developing strength of the fire plume and entrainment into the fire source of the cooler gases. However, what needs to be explained is the distinct circulation pattern set up within the plane (X=1) generated by a corner fire. The associated fire plume hits the ceiling and spreads outwards from the corner, along the ceiling and into the room. However, as this layer meets an opposite wall it is re-directed back into the room. Hence the two flow streams meet about half way along the west wall. This effect can also be seen along the low wall shown in figure 3.20, though here it is less pronounced due to the shorter length of the wall.

Similar results to those above can be seen in figures 3.19 and 3.20, for a plane along the low wall and through the fire source (Z=1).

The following set of figures, 3.21 to 3.24, illustrate the effect of an open doorway on the temperatures and the flow field during a fire scenario. The first plane, at X=6, is taken through the centre of the room with the doorway on the right hand side. In these situations the upper layer exits the room through the upper portions of the doorway, whilst cooler air is entrained at floor level. As this plane is remote from the fire, the temperatures are clearly stratified below the upper layer at the later stages of the fire; after about 120 seconds, see figure 3.21.

The overall strength of the airflow at this plane is not as great as for the previous two planes (X=1 and Z=1) which were through the fire source, see figure 3.22. Instead the strength of the hot upper layer and the way in which it leaves the room is well pronounced. It can also be observed how the cooler air is entrained from the outside.

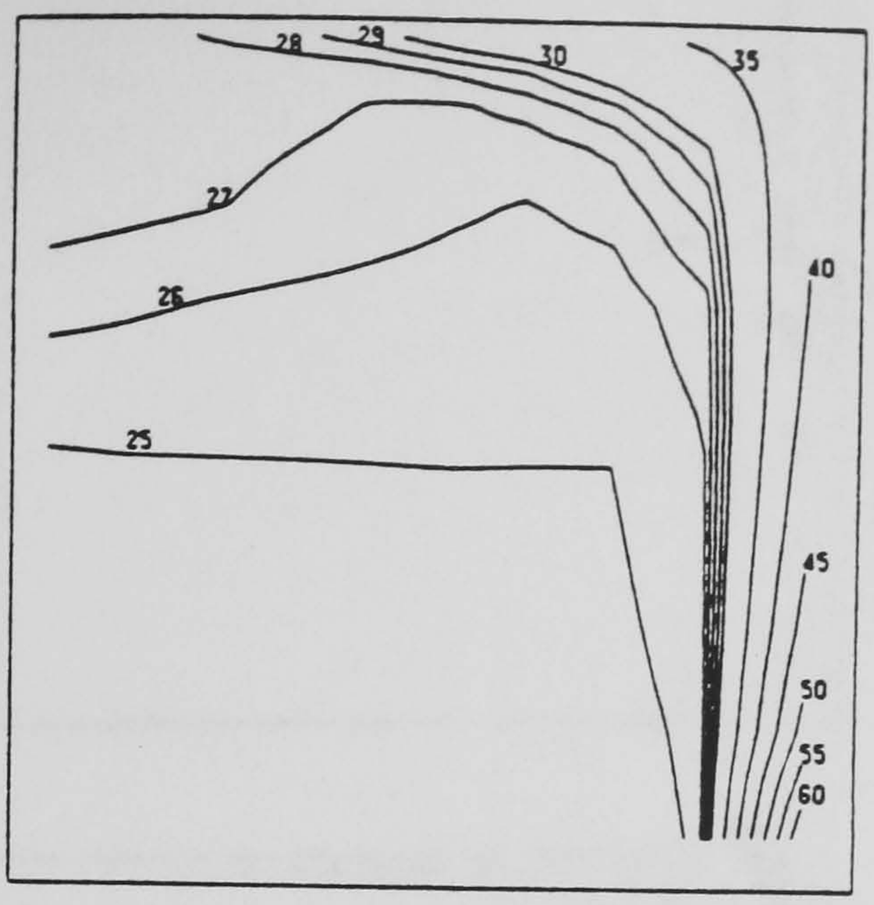

a)

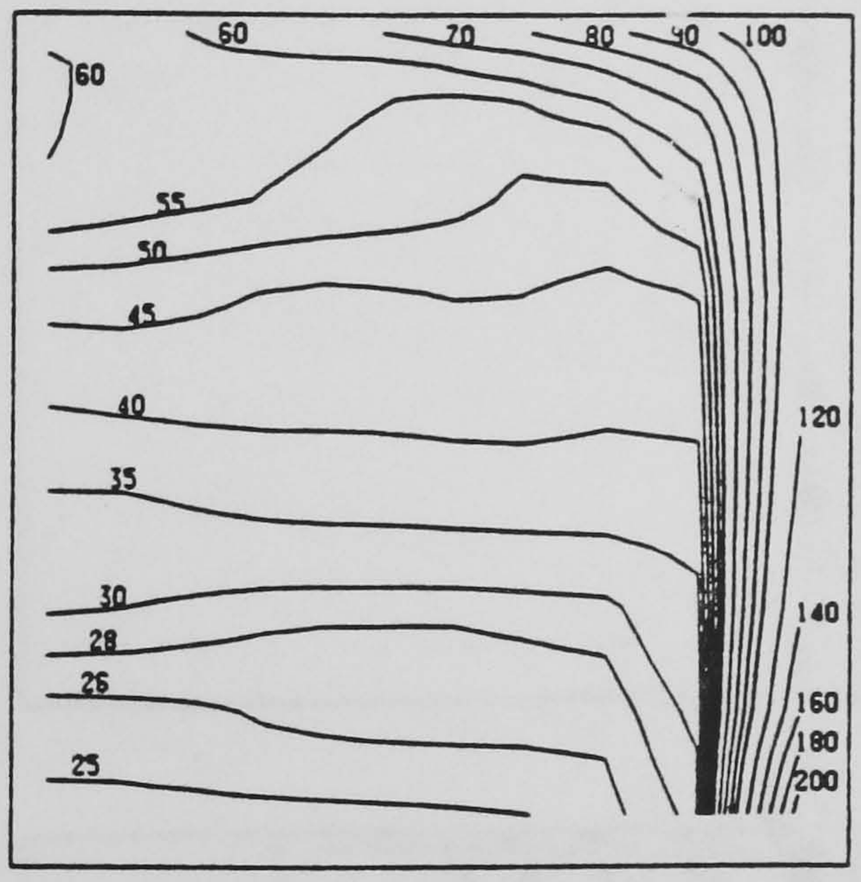

b)

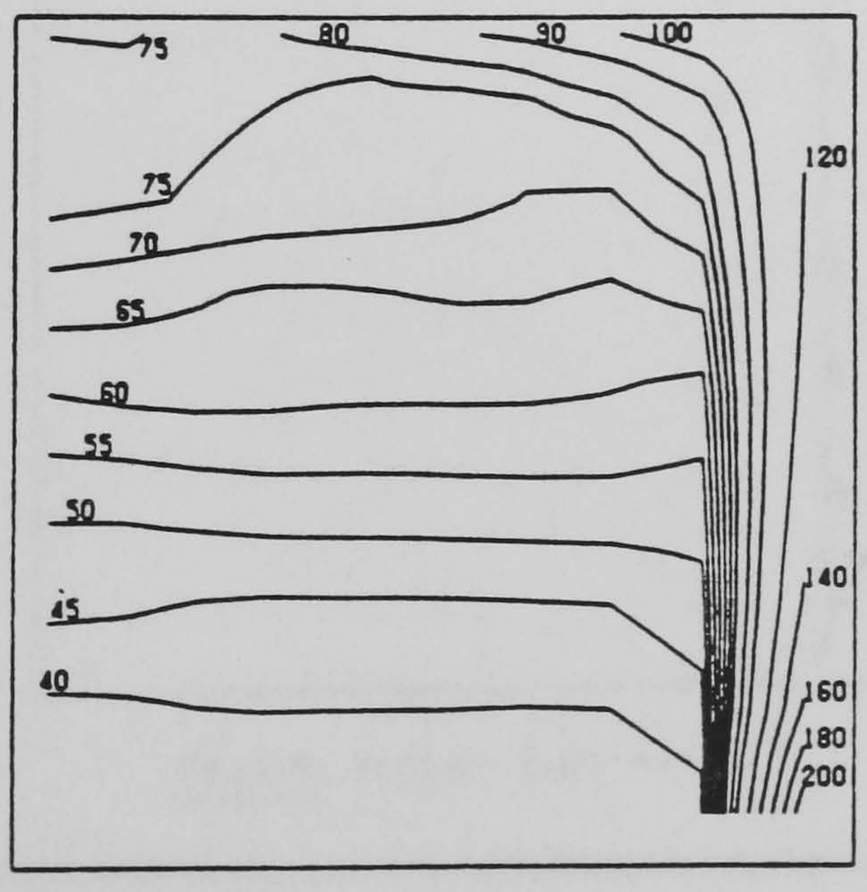

c)

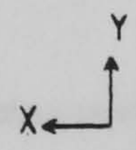

Figure 3.19 Cross view of office: predicted gas temperature contours along the low wall through the fire source (Z=1)
a) 60 sec. b) 120 sec. c) 175 sec.

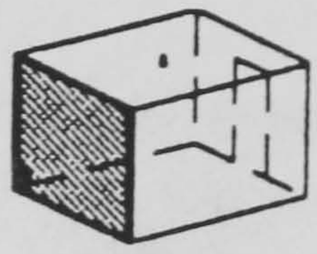

a)

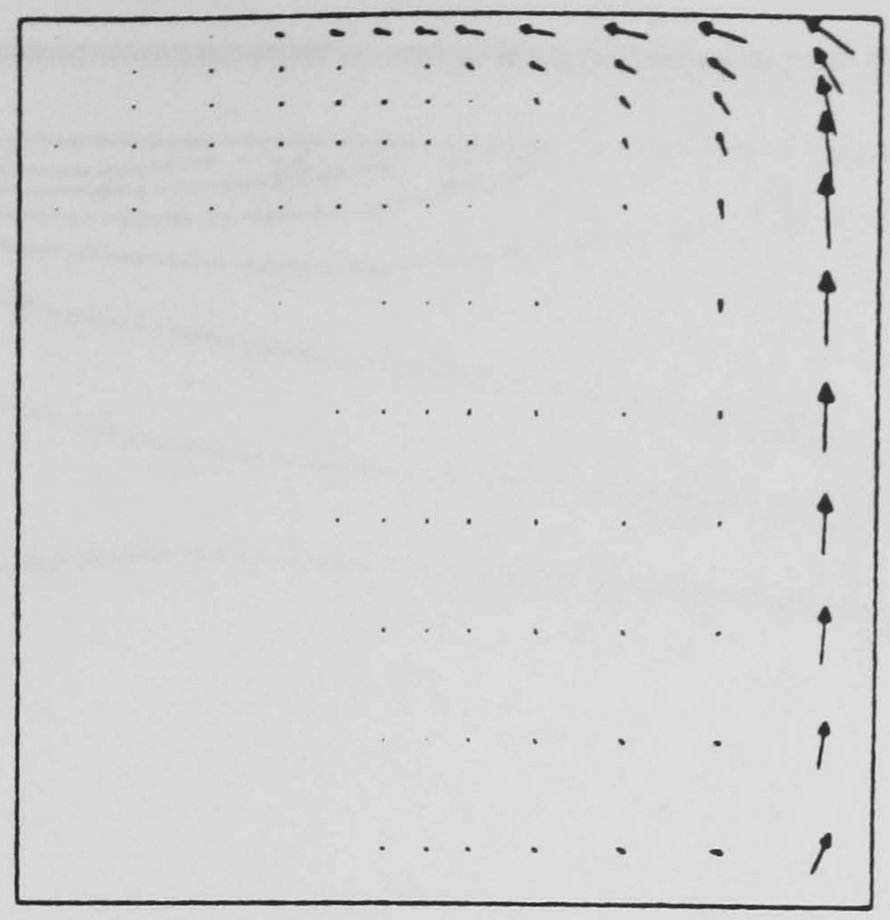

b)

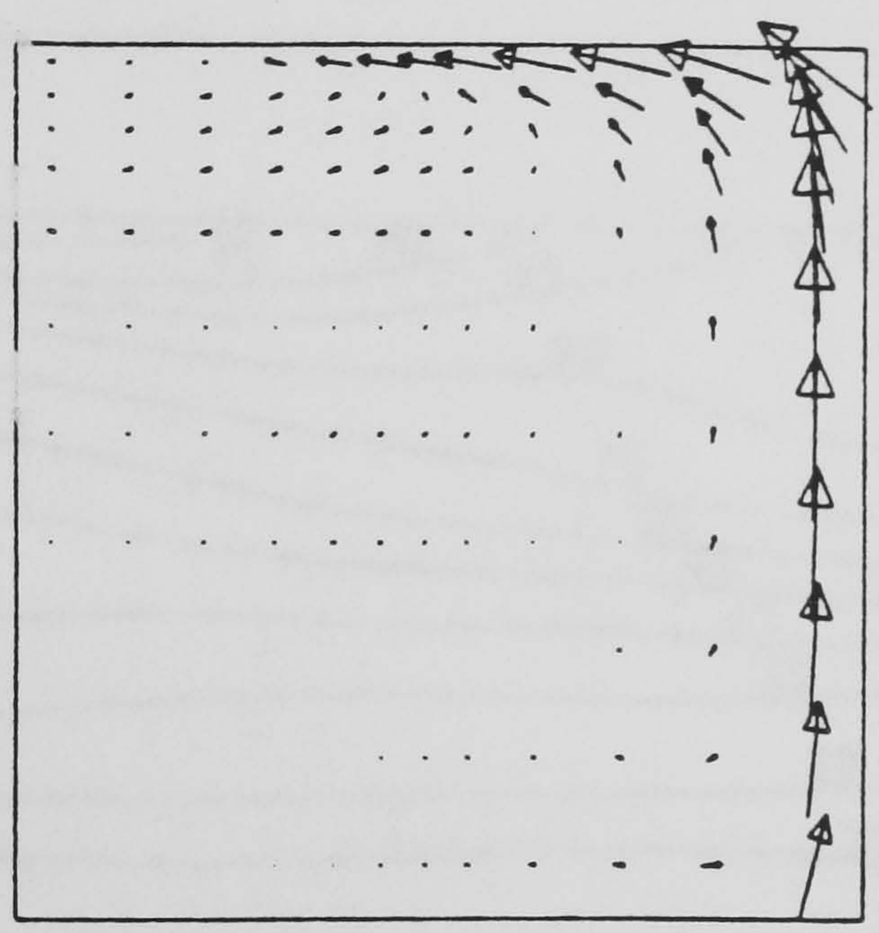

c)

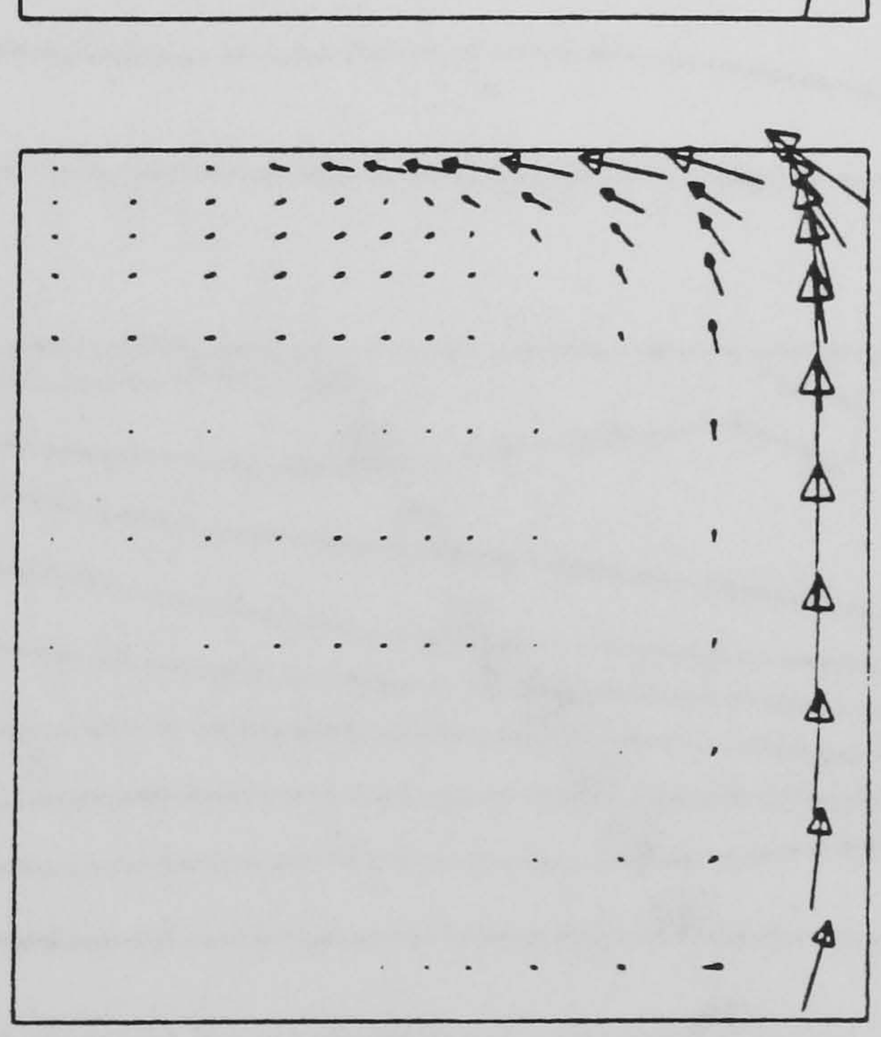

Vector scale: 2.01 m/s

Figure 3.20 Cross view of office: predicted gas velocity vector fields along the low wall through the fire source (Z=1)
a) 60 sec. b) 120 sec. c) 175 sec.

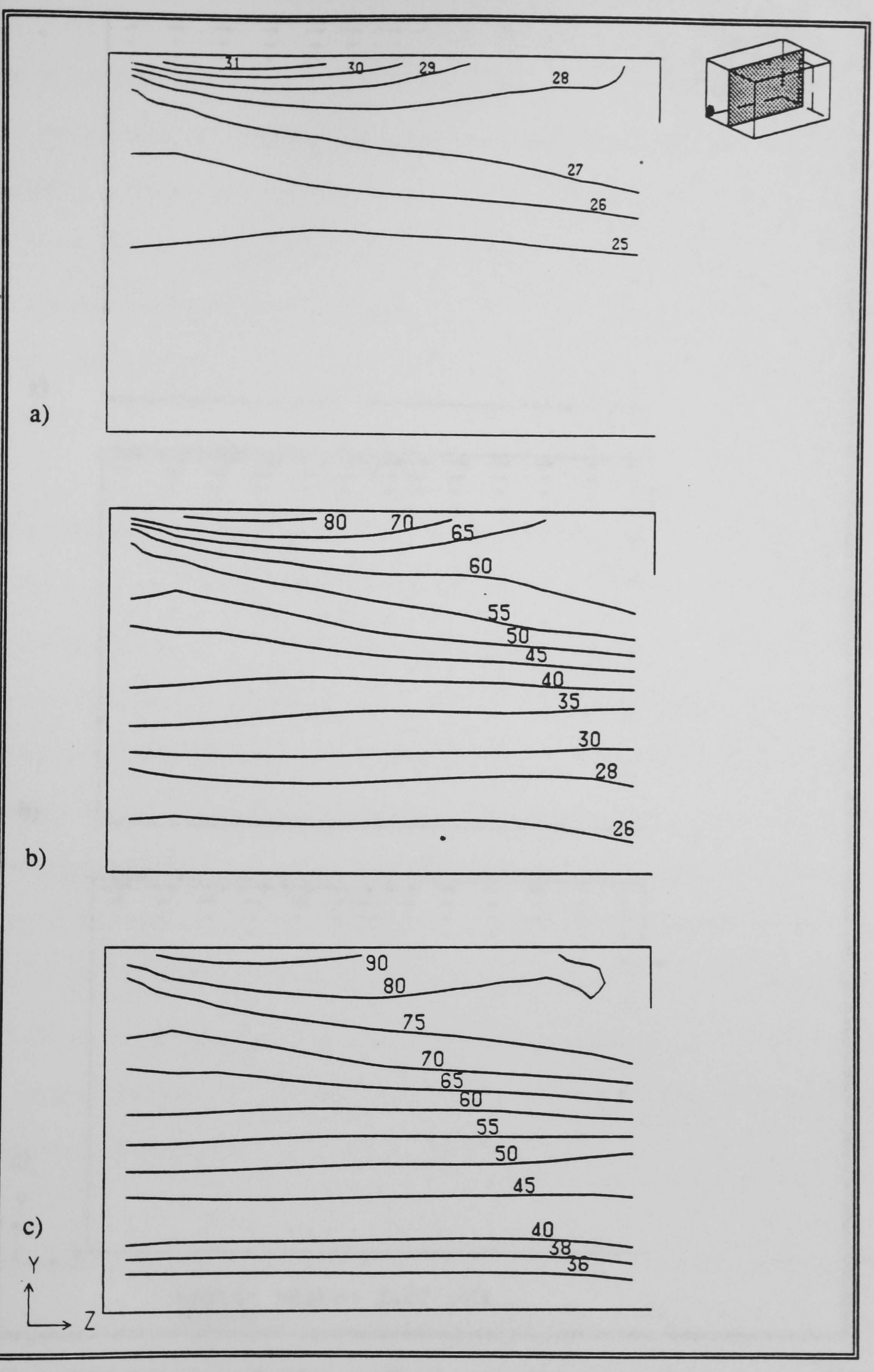

Figure 3.21 Side view of office: predicted gas temperature contours through the centre of the room, sprinkler location and doorway (X=6)
a) 60 sec. b) 120 sec. c) 175 sec.

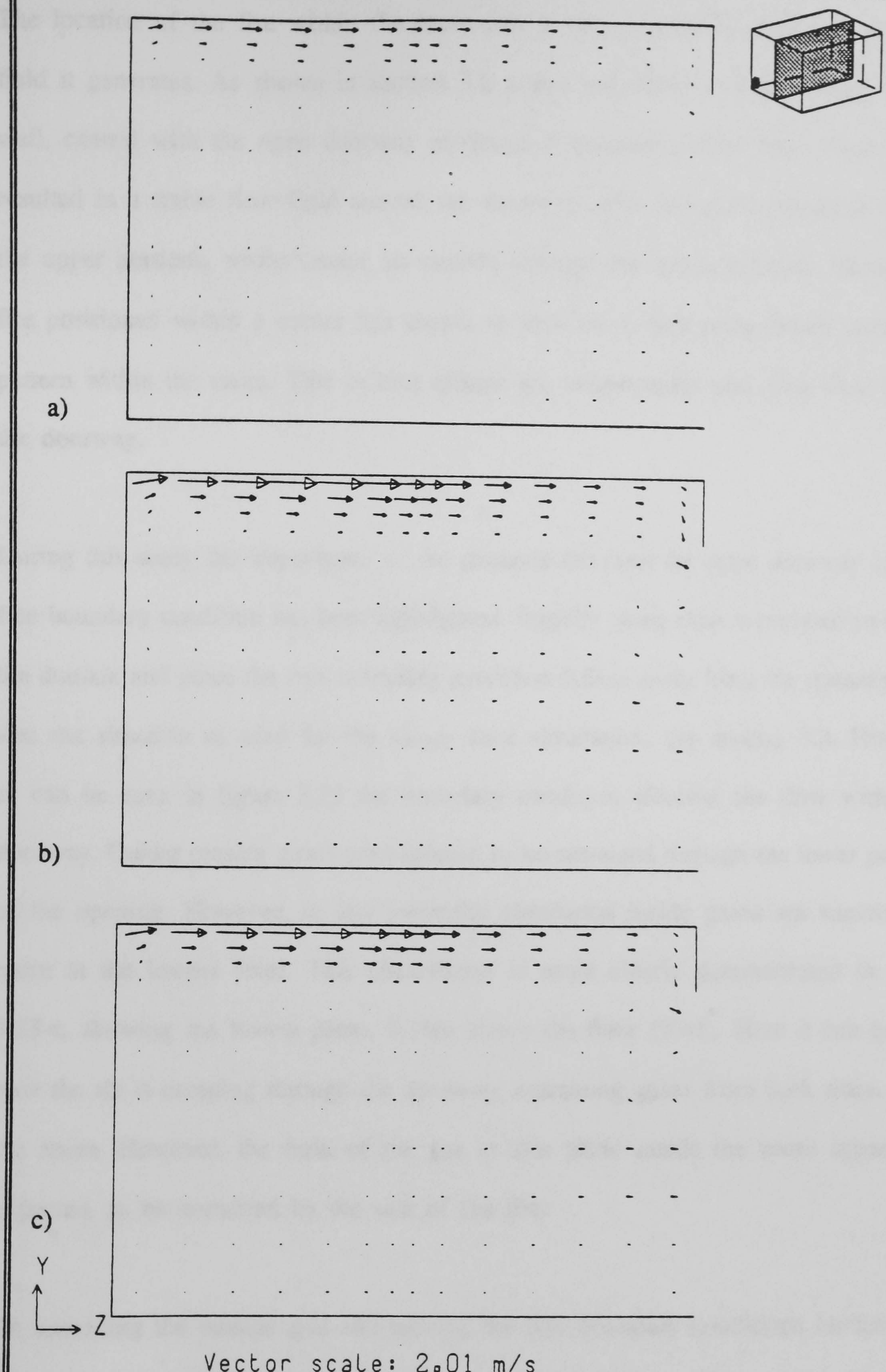

Figure 3.22 Side view of office: predicted gas velocity vector fields through the centre of the room, sprinkler location and doorway (X=6)
a) 60 sec. b) 120 sec. c) 175 sec.

The location of the fire within the room has a very significant effect on the flow field it generates. As shown in section 3.2 a fire positioned halfway along the low wall, central with the open doorway produced a symmetric flow field. This in turn resulted in a stable flow field around the doorway, with hot gases escaping through the upper portions, whilst cooler air entered through the lower sections. However, a fire positioned within a corner has shown to produce a very complicated circulation pattern within the room. This in turn affects the temperatures and flow field around the doorway.

During this study the importance of the distance between the open doorway and the free boundary condition has been highlighted. Initially three slabs were used to extend the domain and place the free boundary condition 0.84m away from the opening. This was the situation as used for the steady-state simulation, see section 3.2. However, as can be seen in figure 3.23 the boundary condition affected the flow within the doorway. Colder outside gases are expected to be entrained through the lower portions of the opening. However, in this particular simulation inside gases are vacating the room at the lowest level. This observation is more clearly demonstrated in figure 3.23-c, showing the lowest plane, 0.15m above the floor (Y=1). Here it can be seen how the air is escaping through the doorway, entraining gases from both sides within the room. However, the bulk of the gas at this plane inside the room appears, as expected, to be entrained by the seat of the fire.

On extending the outside grid and moving the free boundary conditions further away from the doorway this erroneous effect can be eliminated. Figure 3.24 shows the results of extending the domain by six cells and hence increasing the distance between the doorway and the free boundary to 2.04m. As can be seen in figure 3.24-c gases

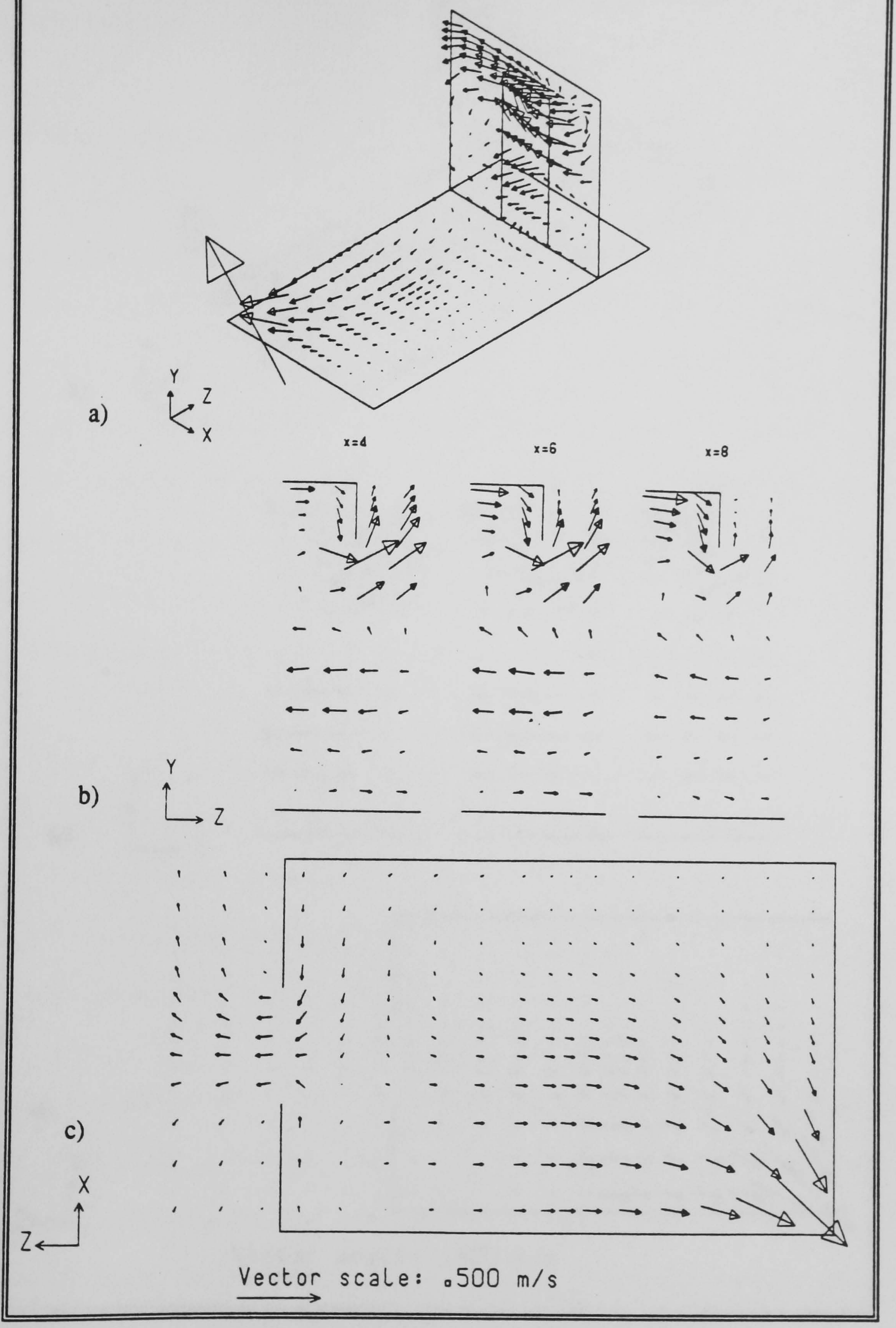

Figure 3.23 Predicted gas velocity vectors after 175 sec. with 3 slabs outside
a) schematic view (Y=1 and Z=14)
b) through the doorway
c) 0.15m above the floor (Y=1)

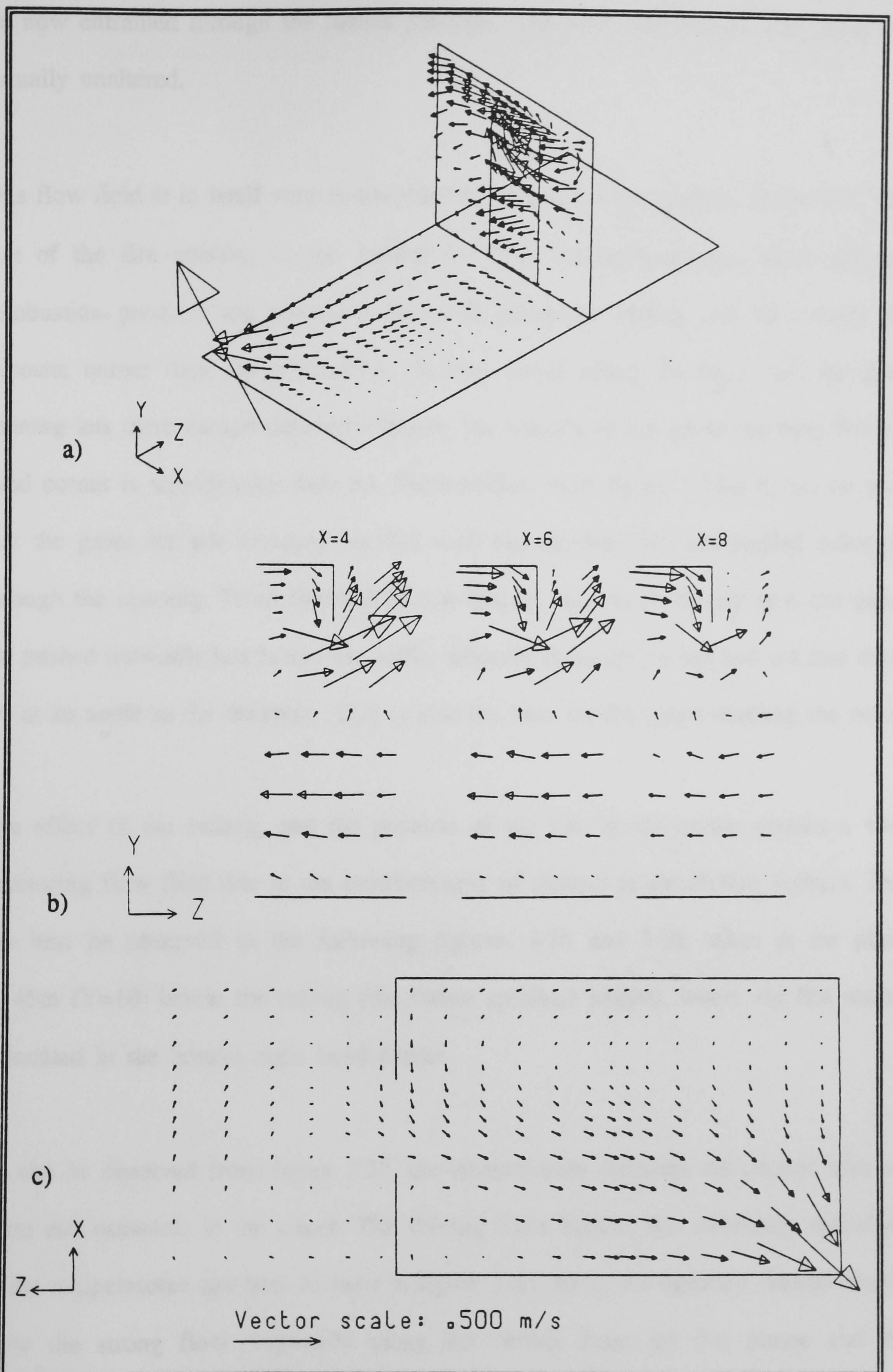

Figure 3.24 Predicted gas velocity vectors after 175 sec. with 6 slabs outside
a) schematic view (Y=1 and Z=14)
b) through the doorway
c) 0.15m above the floor (Y=1)

are now entrained through the lowest portions. The flow fields above that plane are virtually unaltered.

This flow field is in itself very noteworthy due to the corner position of the fire. The seat of the fire entrains cooler, fresher air from its surroundings, whilst the hot combustion products are travelling outwards along the ceiling. As they reach the opposite corner they are re-directed. As they move along the high wall the door opening lets them escape outwards. Hence, the amount of hot gases reaching the left hand corner is significantly reduced. Furthermore, from figure 3.24-a it can be seen that the gases are not escaping parallel with the doorway but are pushed sideways through the opening. From figure 3.24-b it can be seen more clearly how the gases are pushed outwards just below the soffit, whereby it should be pointed out that these are at an angle to the doorway. This is also the case for the gases entering the room.

The effect of the ceiling, and the position of the fire in the corner creates a very interesting flow field due to the establishment of distinct re-circulation regions. This can best be observed in the following figures, 3.25 and 3.26, taken at the plane 0.145m (Y=10) below the ceiling (the future sprinkler height), where the fire source is located in the bottom right hand corner.

As can be observed from figure 3.25, the temperatures contours are *pushed* into the room and outwards to the edges. The driving force behind this outwardly spreading of the temperatures can best be seen in figure 3.26. Here, the velocity vectors clearly show the strong flow diagonally along the ceiling from the fire plume and the subsequent circulation patterns generated in the corners, hence re-circulating the hot gases. Note how this ceiling flow is increasing in strength and the entrainment of the

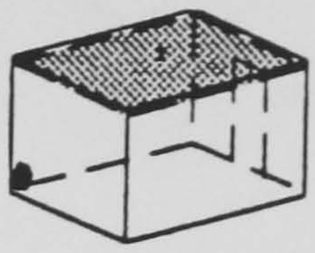

a)

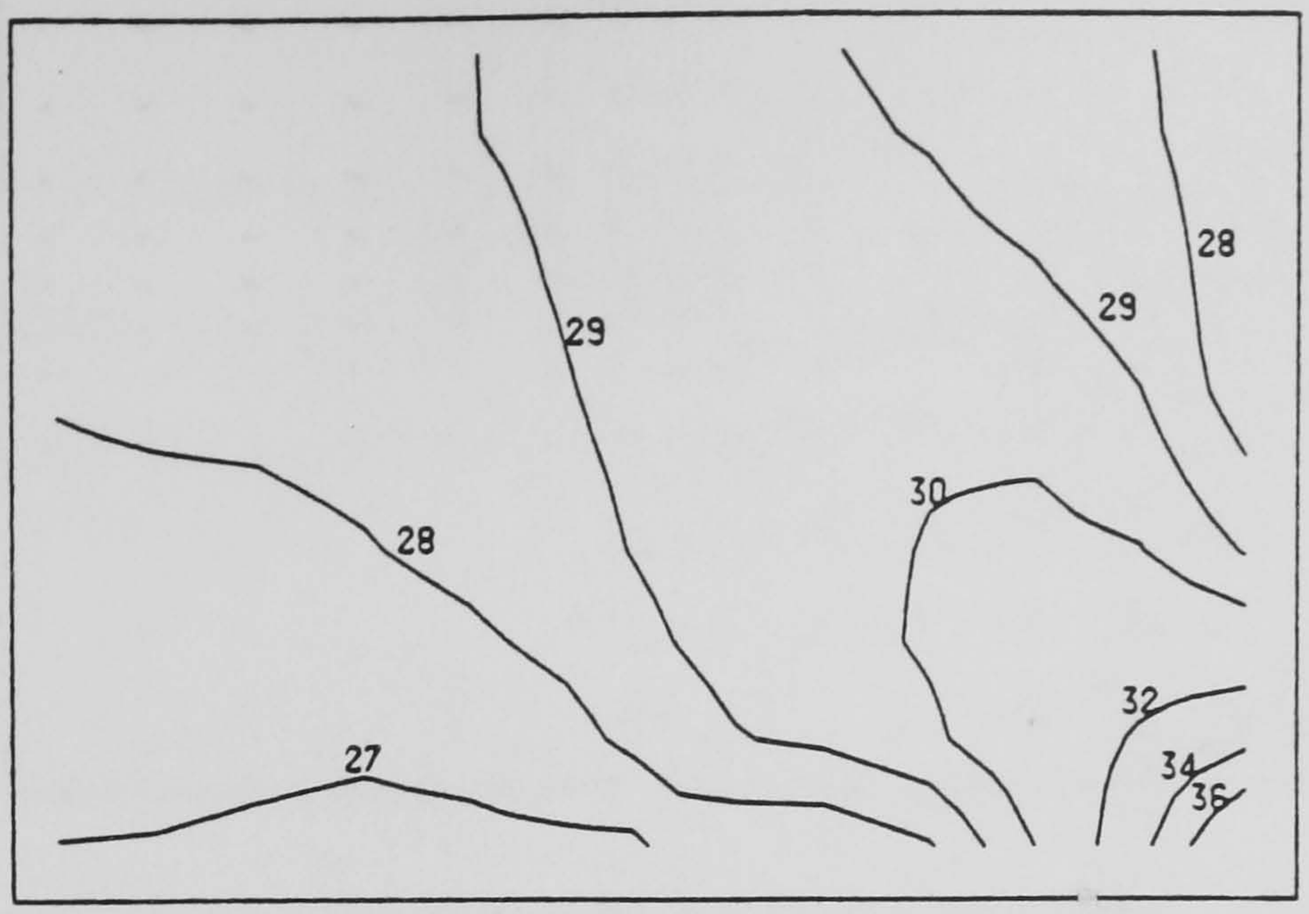

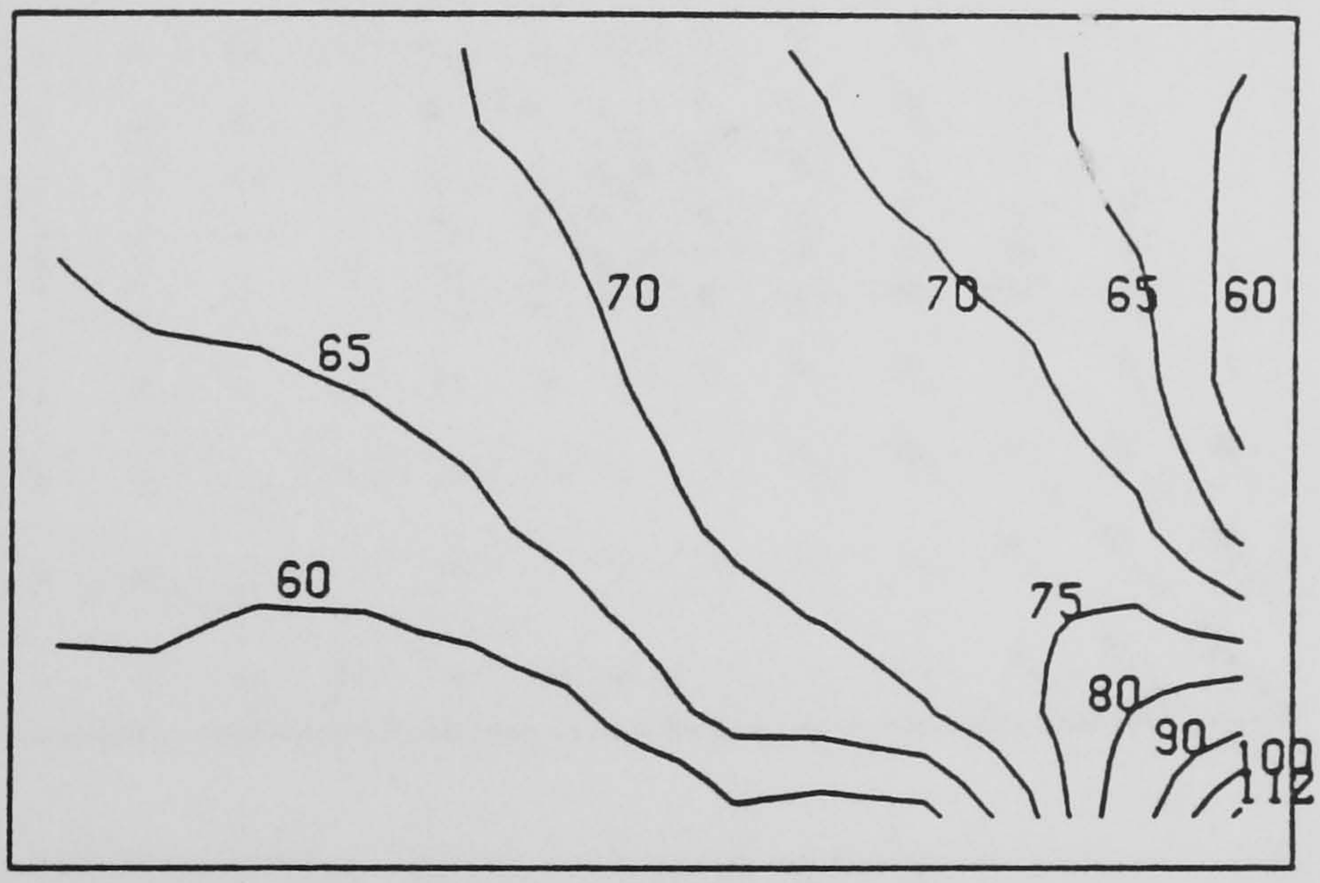

b)

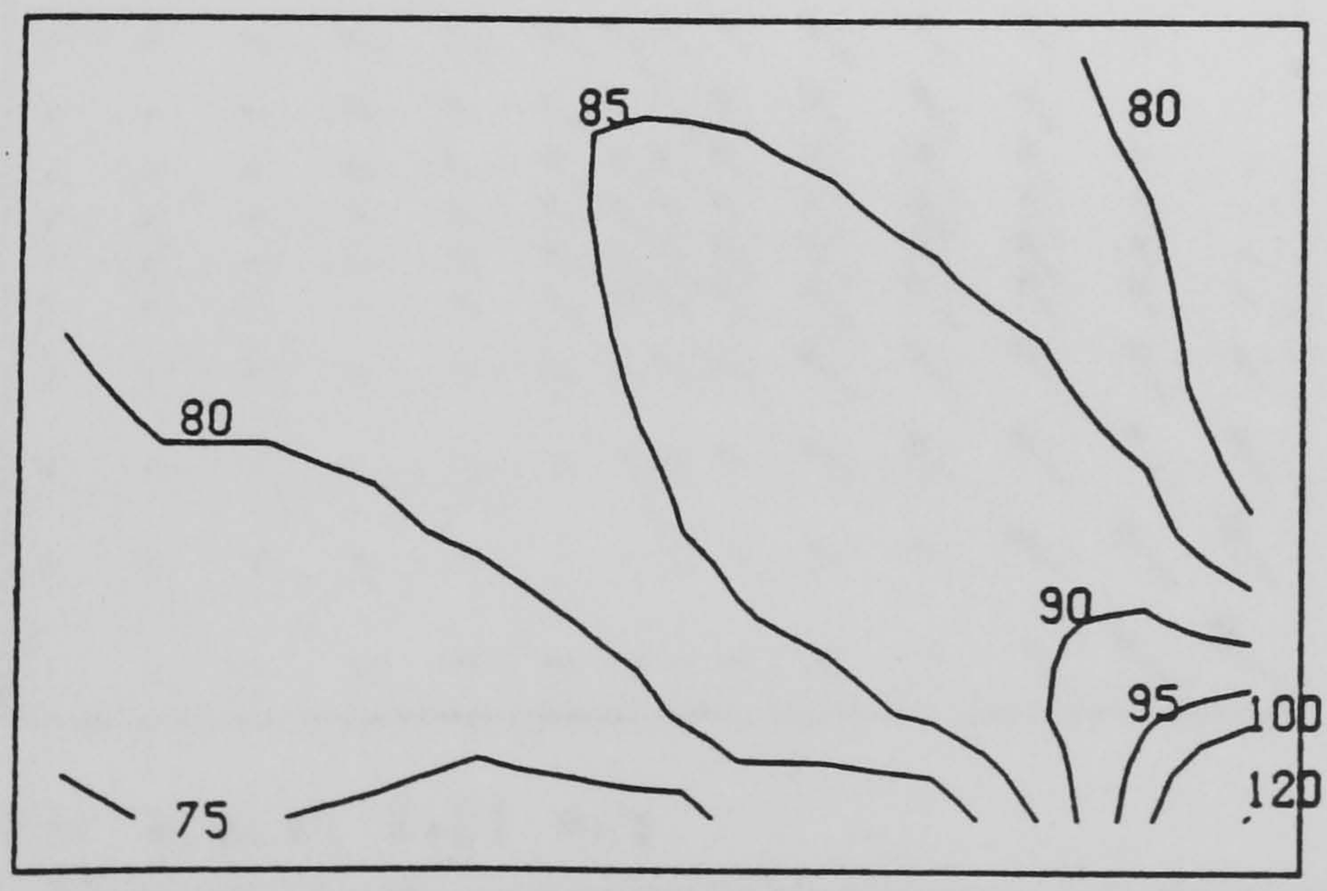

c)

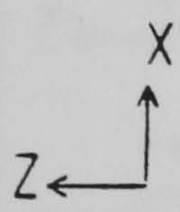

Figure 3.25 Plan view of office: predicted gas temperature contours through a horizontal plane, 0.145m below the ceiling (Y=10)
a) 60 sec. b) 120 sec. c) 175 sec.

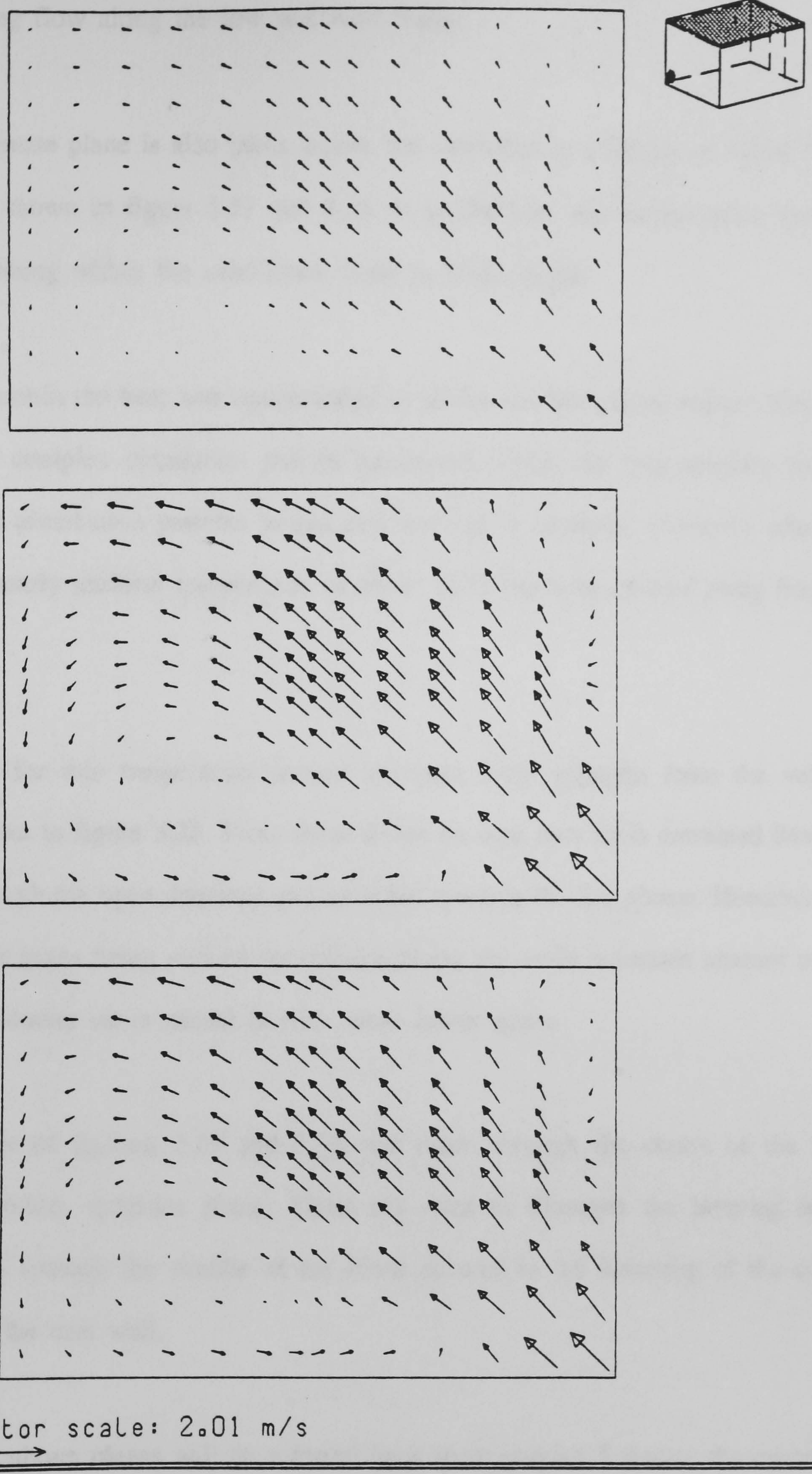

Figure 3.26 Plan view of office: predicted gas velocity vector fields through a horizontal plane, 0.145m below the ceiling (Y=10)
a) 60 sec. b) 120 sec. c) 175 sec.

re-circulating flow along the low and west walls.

The penultimate plane is also taken across the room but at a height of 1.05m (Y=4). This view, shown in figure 3.27 and 3.28, is to illustrate the temperatures and flow regimes existing within the cold lower layer at body-height.

After 60 seconds the heat was concentrated to within the fire plume region. However, due to the complex circulation pattern generated within the compartment unusual temperature distribution patterns within this layer have occurred. However, after 175 seconds a nearly uniform temperature of about 52°C has been created away from the fire plume.

The reason for this temperature pattern becomes more apparent from the velocity vectors shown in figure 3.28. From these it can be seen that air is entrained from the outside through the open doorway and attracted towards the fire plume. However, due to the hotter gases being pushed downwards along the walls a certain amount of this fresher and cooler air is mixed in with these hotter gases.

The final set of figures, 3.29 and 3.30, are taken through the centre of the room (Z=8); the future sprinkler plane. These are used to illustrate the layering of the temperatures towards the middle of the room as well as the lowering of the ceiling layer along the east wall.

Most of the above planes will be referred back to in chapter 5 during the discussion of the two-phase fire-sprinkler simulation results.

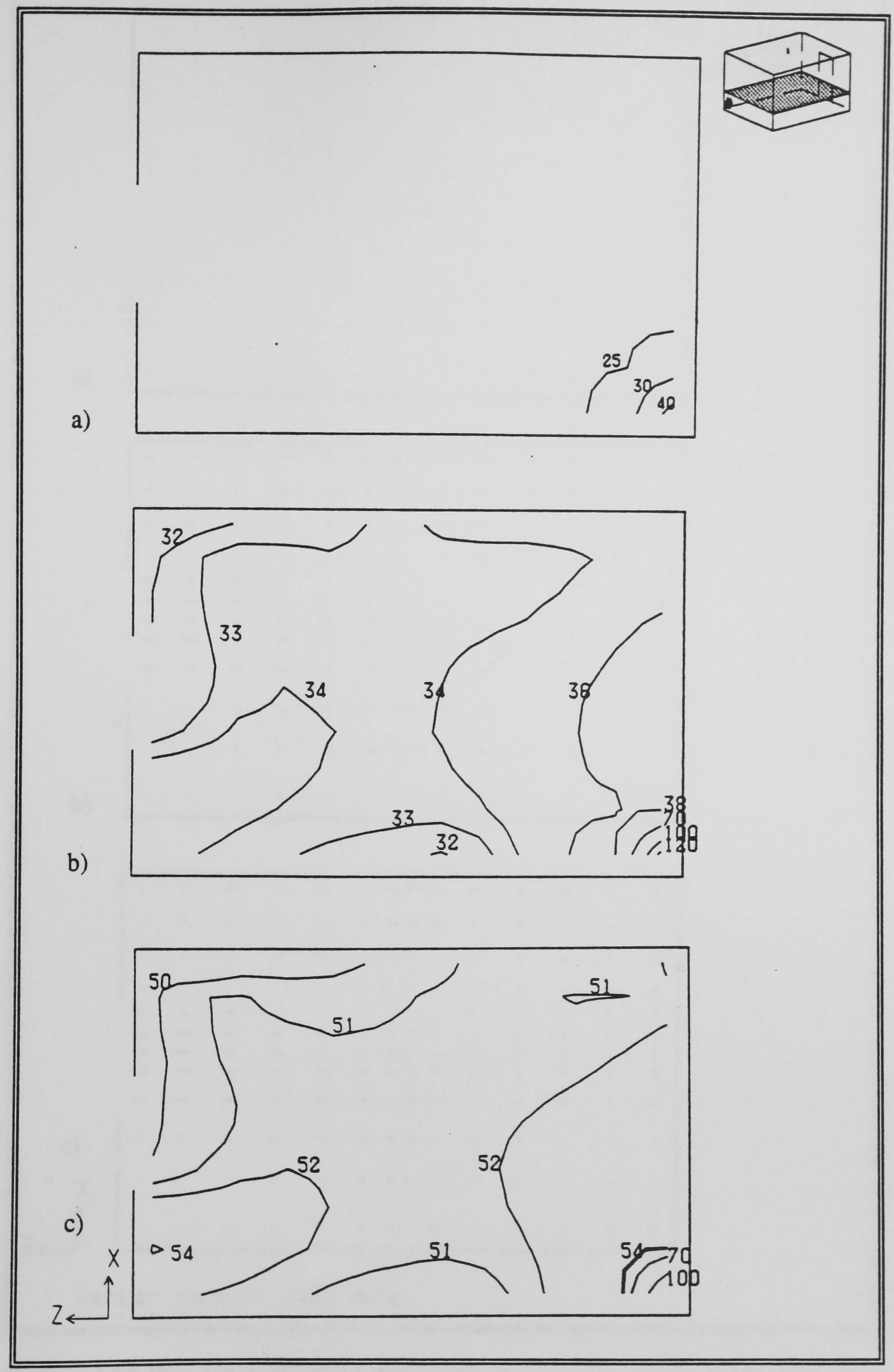

Figure 3.27 Plan view of office: predicted gas temperature contours through a horizontal plane, 1.05m above the floor (Y=4)
a) 60 sec. b) 120 sec. c) 175 sec.

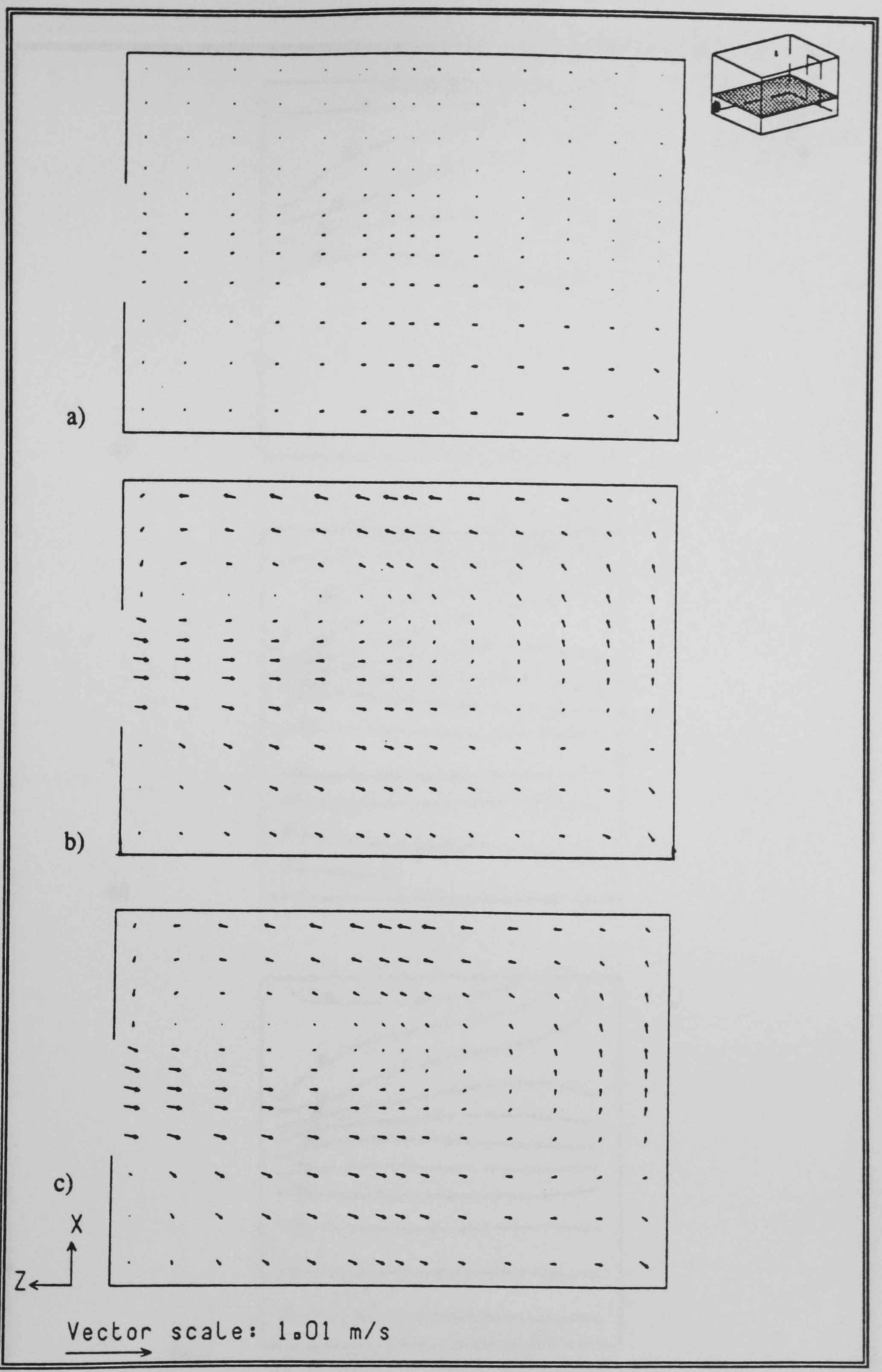

Figure 3.28 Plan view of office: predicted gas velocity vector fields through a horizontal plane, 1.05m above the floor (Y=4)
a) 60 sec. b) 120 sec. c) 175 sec.

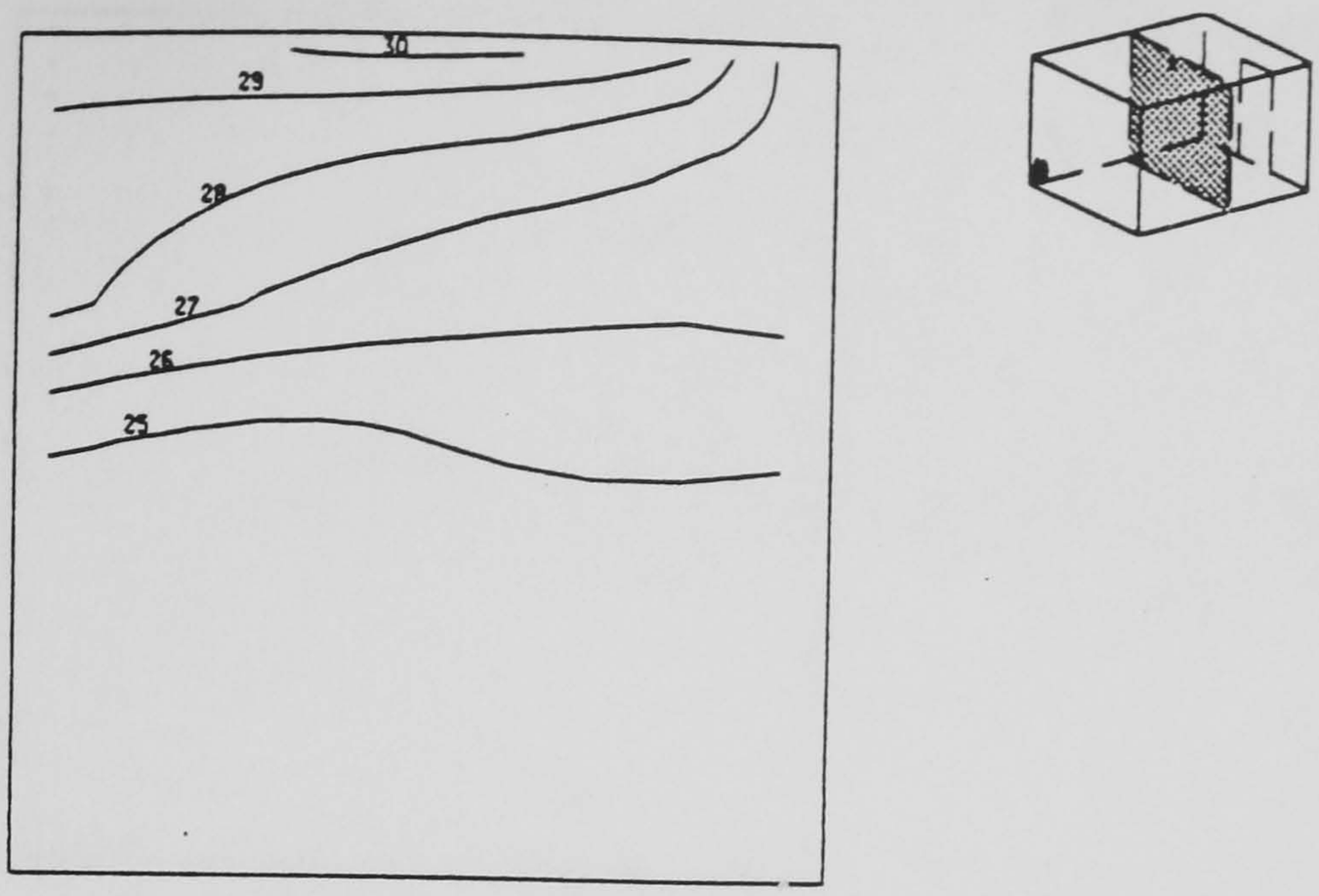

a)

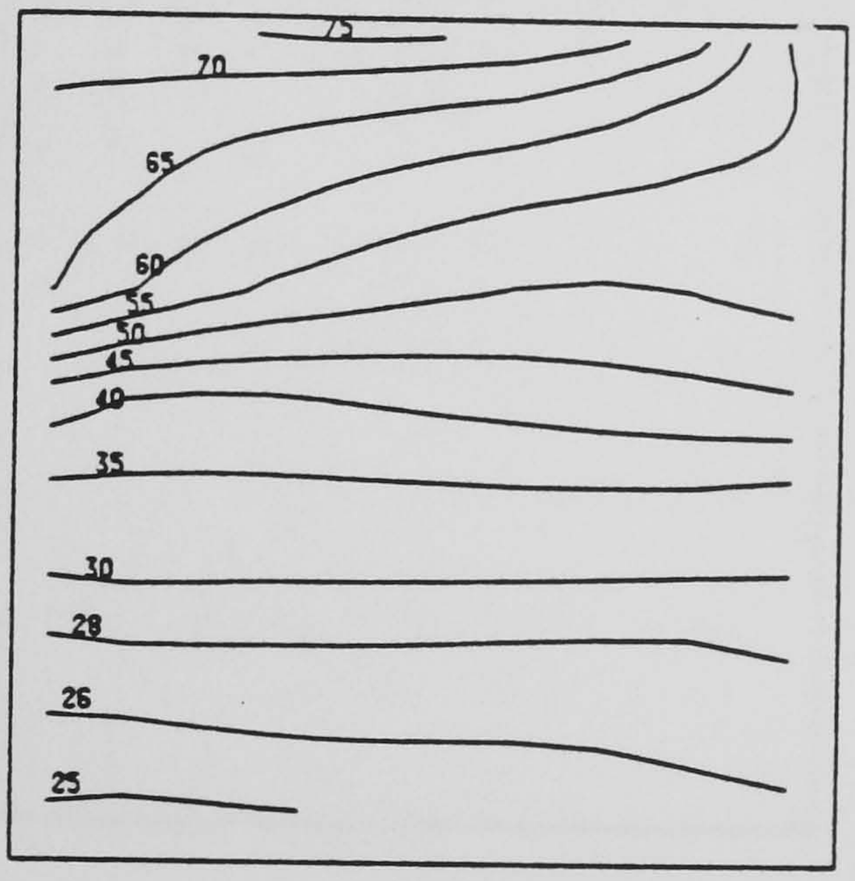

b)

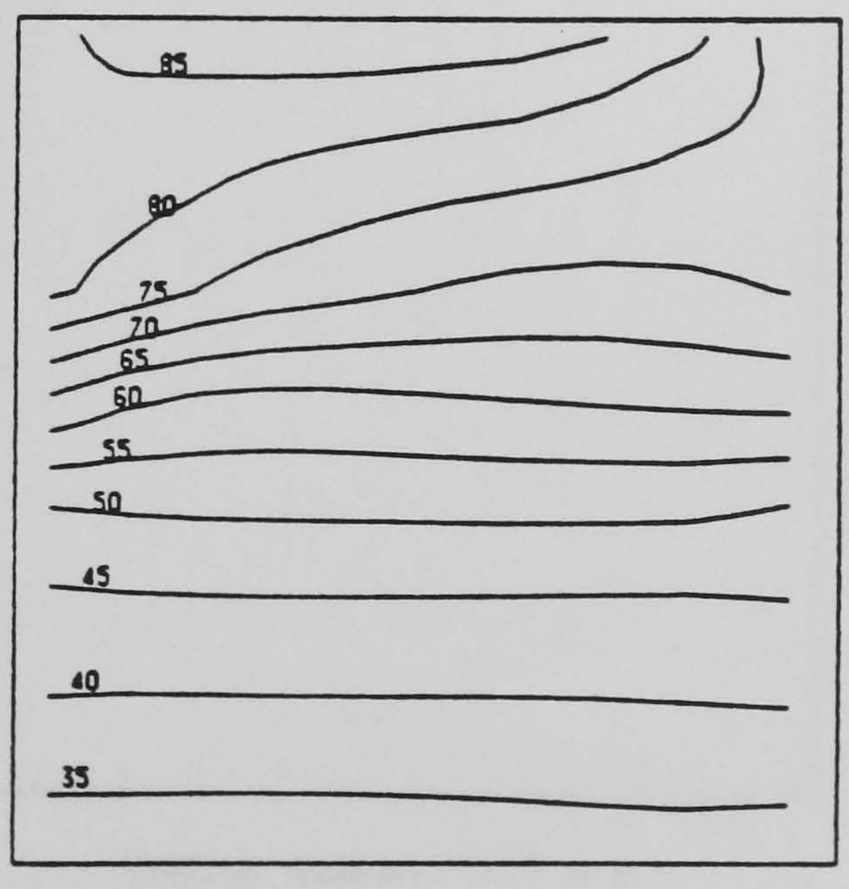

c)

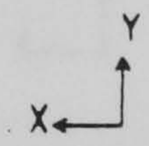

Figure 3.29 Cross view of office: predicted gas temperature contours through the centre of the room (Z=8)
a) 60 sec. b) 120 sec. c) 175 sec.

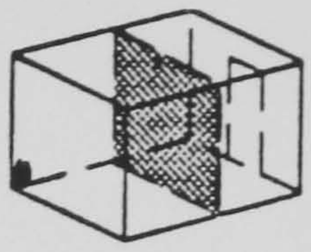

a)

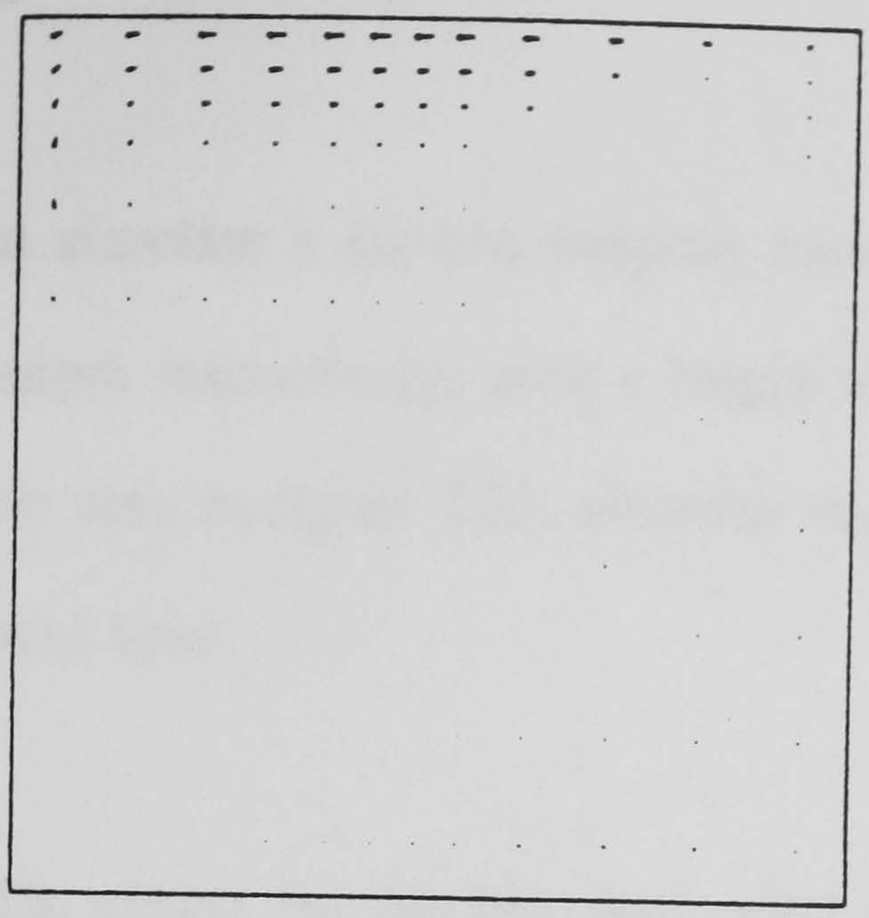

b)

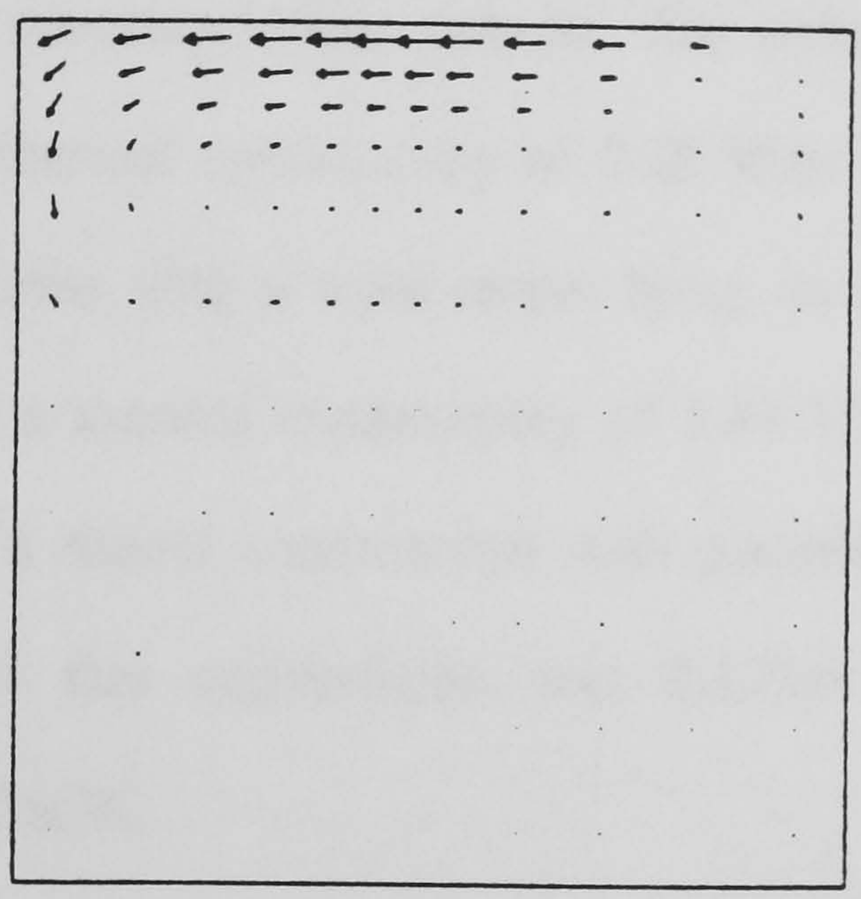

c)

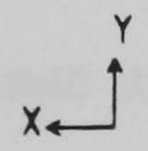

Vector scale: 2.01 m/s

Figure 3.30 Cross view of office: predicted gas velocity vector fields through the centre of the room (Z=8)
a) 60 sec. b) 120 sec. c) 175 sec.

3.3.2 Hospital Ward Fire

The compartment used to simulate a six-bed hospital room had dimensions 7.325m by 7.85m in width and length respectively, with a height of 2.7m. A schematic view of the compartment can be seen in figure 3.31, whereby the closed doors on the high wall are indicated by dotted lines.

The main supporting walls, except for the low wall, were considered to be made of thick plasterboard with concrete blocks behind. The overall thickness of the walls were 0.2286m giving a thermal conductivity of 0.25 W/m°K. The floor was assumed to consist of gravel concrete with a wool carpet lying on top. In total a thickness of 1.0m was assumed with a thermal conductivity of 1.44 W/m°K. The ceiling and the low wall were made of a timber construction with plasterboard on the inside of the room. The thickness of this construction was 0.127m in total with a thermal conductivity of 0.237 W/m°K.

A window which was situated in the low wall was not considered during the studies [Kumar (1985)]. The six 1kW oil filled radiators situated underneath the window were represented by one floor-standing 6kW heater, 7.85m long, 0.3m in width and 0.5m high.

The bed on which the fire was situated was in the centre of the east wall. During the simulation the base area of the bed was approximated to be 1.35m wide and 1.75m in length, and was situated 0.5m above the floor.

The sprinkler was located 0.353m below the ceiling and 0.895m away from the east

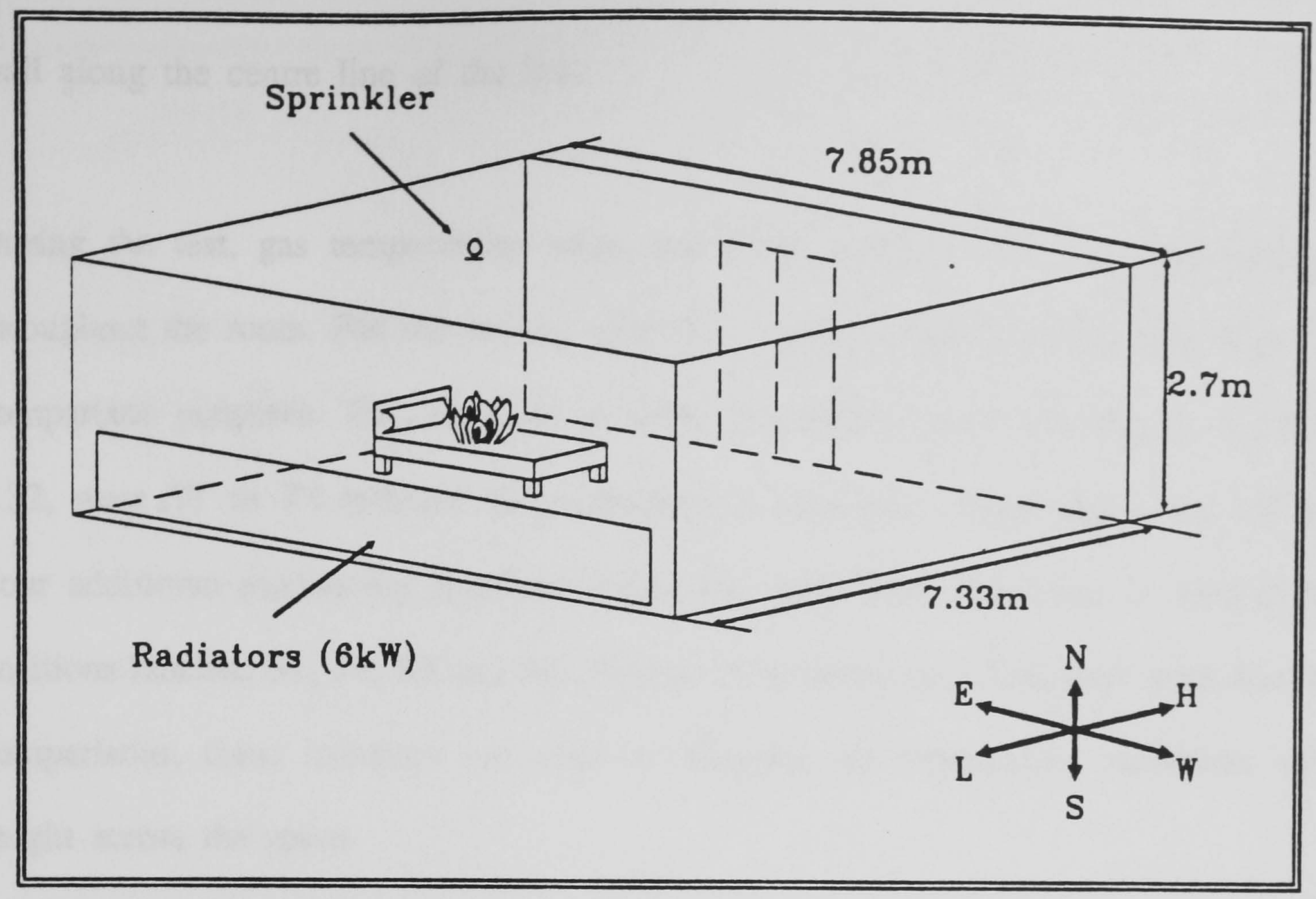

Figure 3.31 Hospital Room Schematic

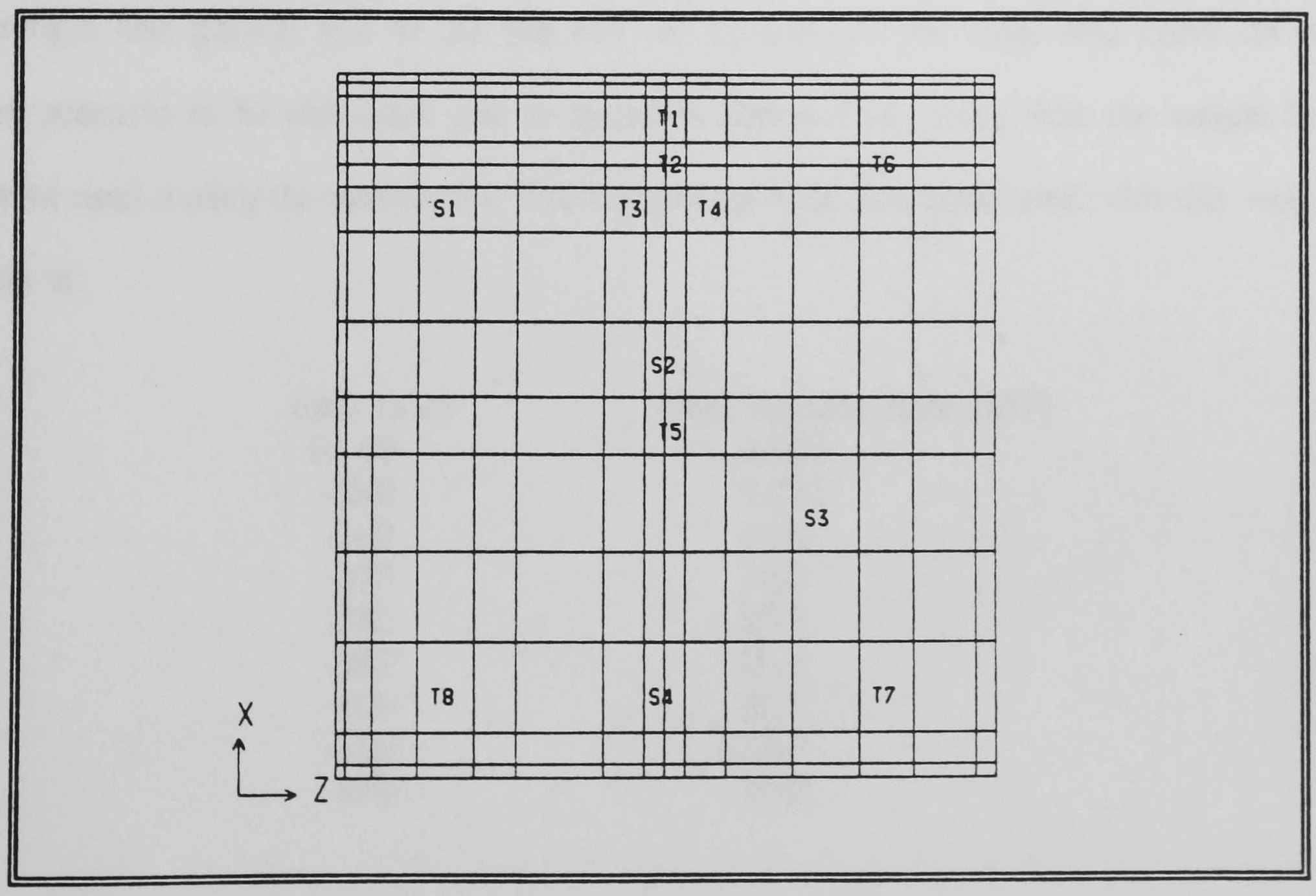

Figure 3.32 Details of the Measuring Locations

wall along the centre line of the bed.

During the test, gas temperatures were monitored at various heights and locations throughout the room. For the current validation studies eight locations were used for comparison purposes. The locations of these monitoring points are shown in figure 3.32, were T1 to T8 indicate the thermocouple locations 75mm below the ceiling. Four additional monitoring locations within the room were examined, located at the positions labelled S1, S2, S3 and S4. Though no experimental data were available for comparisons, these locations are used to illustrate the temperature variations with height across the room.

Another important value measured during the fire experiment was the weight of the bed. It is from this weight loss and knowledge of the material being burned that the strength and growth rate of the fire can be determined. The mass loss curve for the fire scenario to be simulated can be found in figure 3.33, along with the weight loss curve used during the simulation. The fire heat release rate associated with this weight loss is:

time (sec)	Heat Release Rate (kW)
0- 60	4.695
-240	7.223
-360	10.0
-370	15.0
-380	20.0
-390	25.0
-400	30.0
-410	35.0
-420	40.0

During the calculations of these values it was assumed that polyurethane (PU) foam was a major component. The actual fuel however was far more complex; consisting

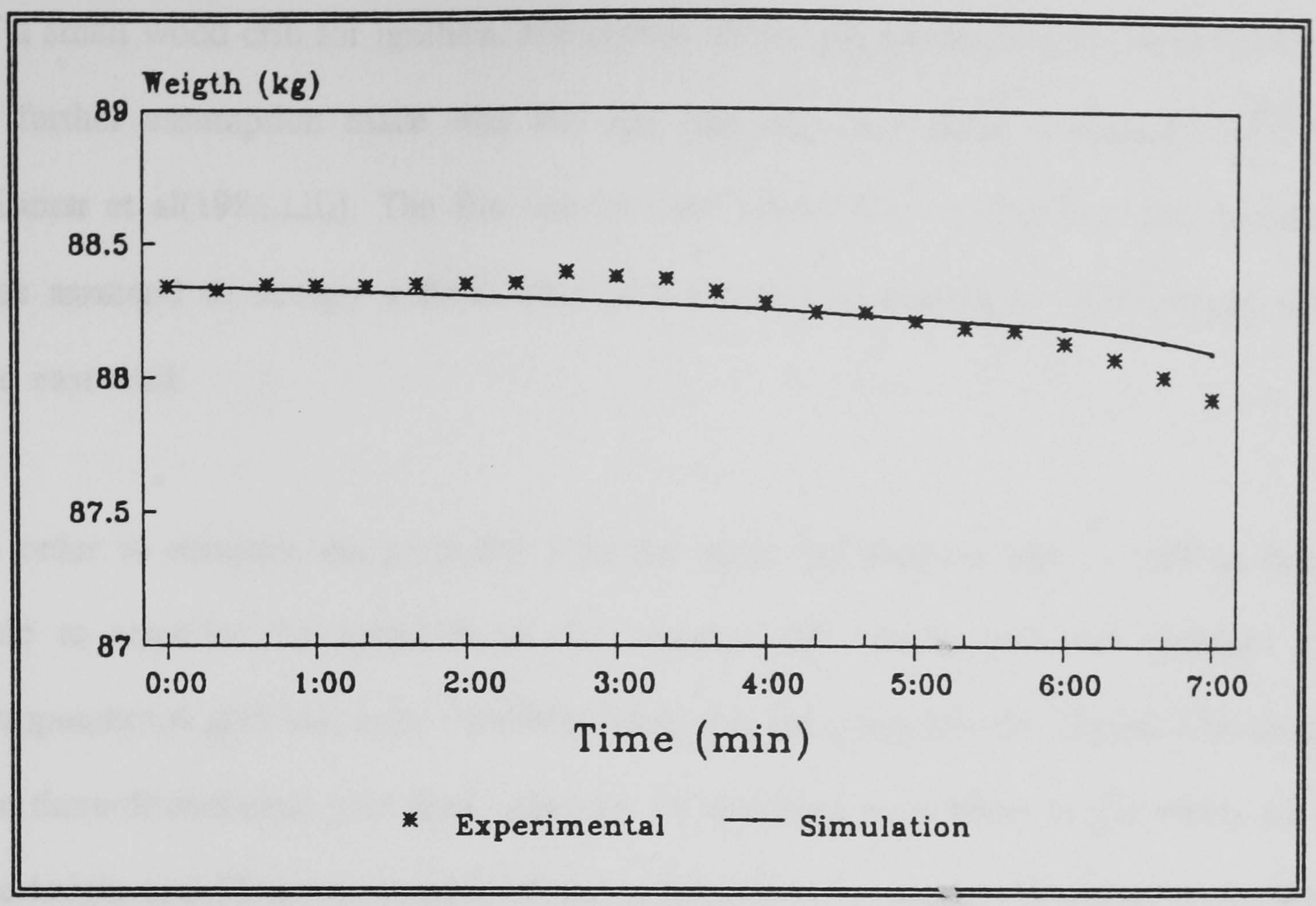

Figure 3.33 Mass Loss of Bed

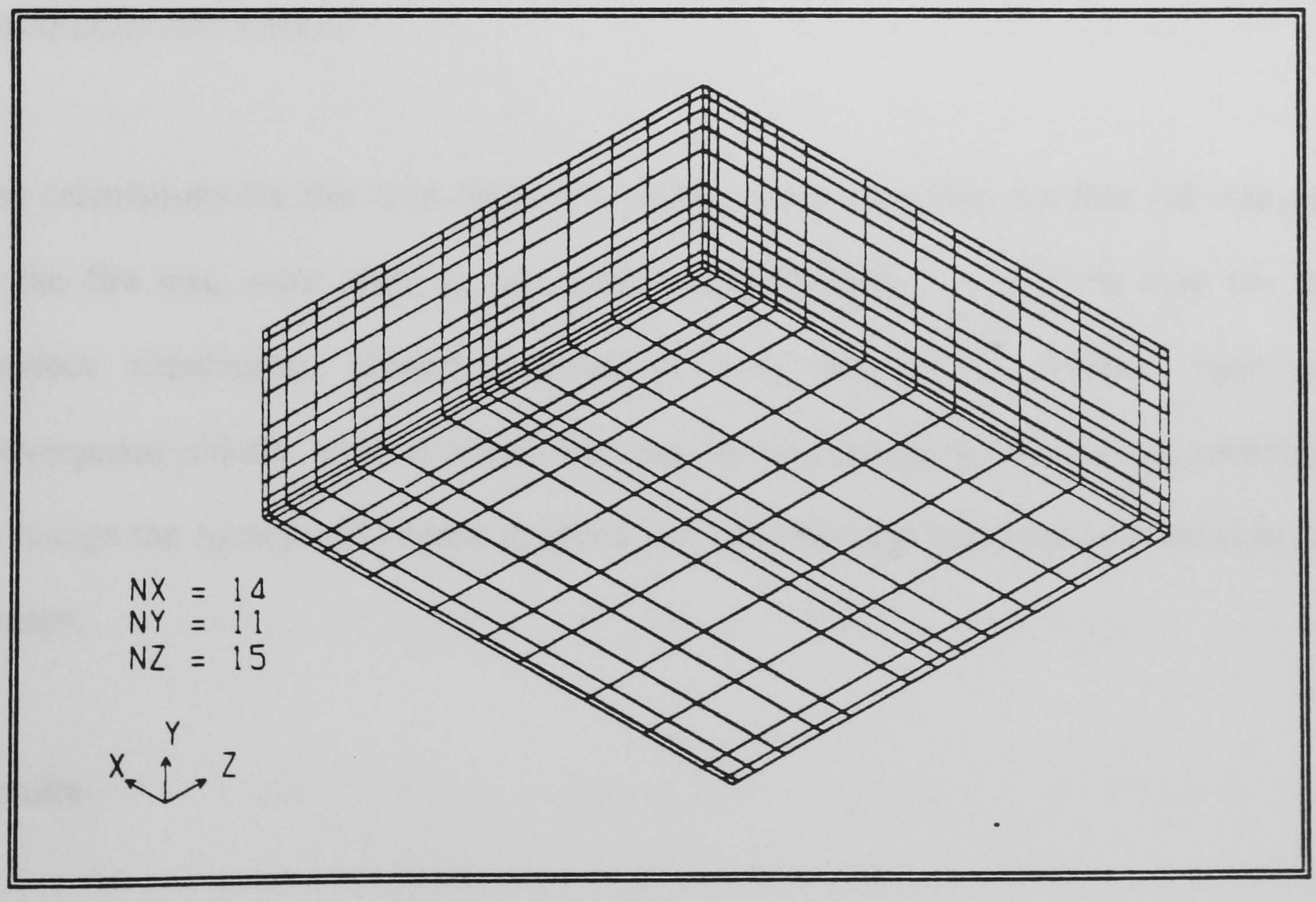

Figure 3.34 The numerical grid used

of a small wood crib for ignition, and cotton, nylon and polyester as bedding material. A further assumption made was that the fuel was only 65% combustion efficient [Kumar et al(1986,i,ii)]. The fire source, over which this varying heat was released, was assumed to occupy a fixed area of 0.45m*0.5m, positioned 0.25m away from the east wall.

In order to compare the predicted with the measured temperatures as well as being able to consider the locations of the heaters, fire source, bed and sprinkler the computational grid had to be carefully fitted into the compartment. Figure 3.34 shows the three-dimensional grid used, whereby 14 divisions were taken in the width, 11 in the height and 15 in the breadth of the compartment. In total 2310 control-cells were used. It should be noted that figure 3.32 also shows the grid in plan view.

Computational Details

The calculations for this time-dependent study, which simulated the first 420 seconds of the fire test, were made at one second time-intervals. As was the case for the previous simulations, converged solutions were said to be obtained once the convergence criteria were satisfied. For this set of simulations it was not necessary to change the number of sweeps required per time step but remained at a constant 50 sweeps.

Results

As in the case of the office fire scenario the results presented below were used as initial conditions for the fire-sprinkler situation; discussed in chapter 5. Even in such

a thoroughly instrumented experimental rig as the hospital ward, it is only possible to compare predictions and measurements at comparatively few points.

During this simulation the accuracy of the predicted temperatures at the eight thermocouple locations, T1 to T8, were assessed by comparing them to the measured data. The transient development of these temperatures are shown in figure 3.35.

It is evident from these comparisons that the correct *trends* have been obtained throughout the compartment; for all eight monitoring locations. In fact the predictions for the first six locations; T1 to T6, are between 7% to 16% of the measured data. However, the rate of temperature increase *felt* further afield from the fire, at locations T7 and T8, appear to have been larger than measured.

This poses questions concerning the grid-size and -distribution used during the simulation, as well as the accuracy of the assumptions made and their effect remote from the fire source. To answer some of these queries a modest grid-refinement study was made. The results and conclusions are presented in section 3.3.4.

However, the important fact which emerges from these results is that the predictions near the fire and the sprinkler head are very close to measured data. Hence further work concerning the modelling of sprinkler head activation is encouraged.

The variation of the temperature at specific times with respect to height can be seen in the following figure 3.36. For these predictions, made at locations S1 to S4 (see figure 3.32) no experimental values were available for comparisons, but instead are used to show the temperature distribution and layering generally observed in a

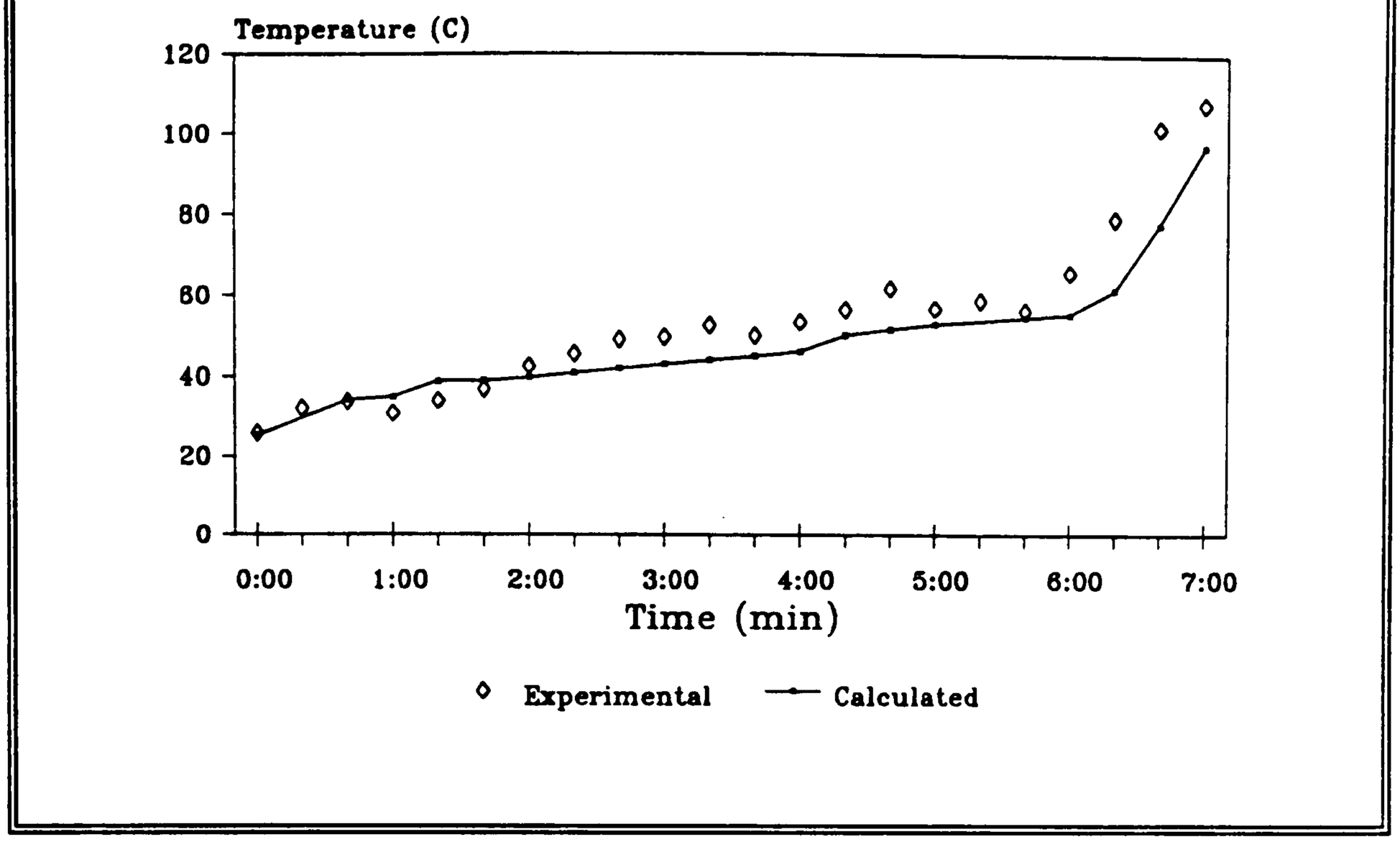

a) T1 location

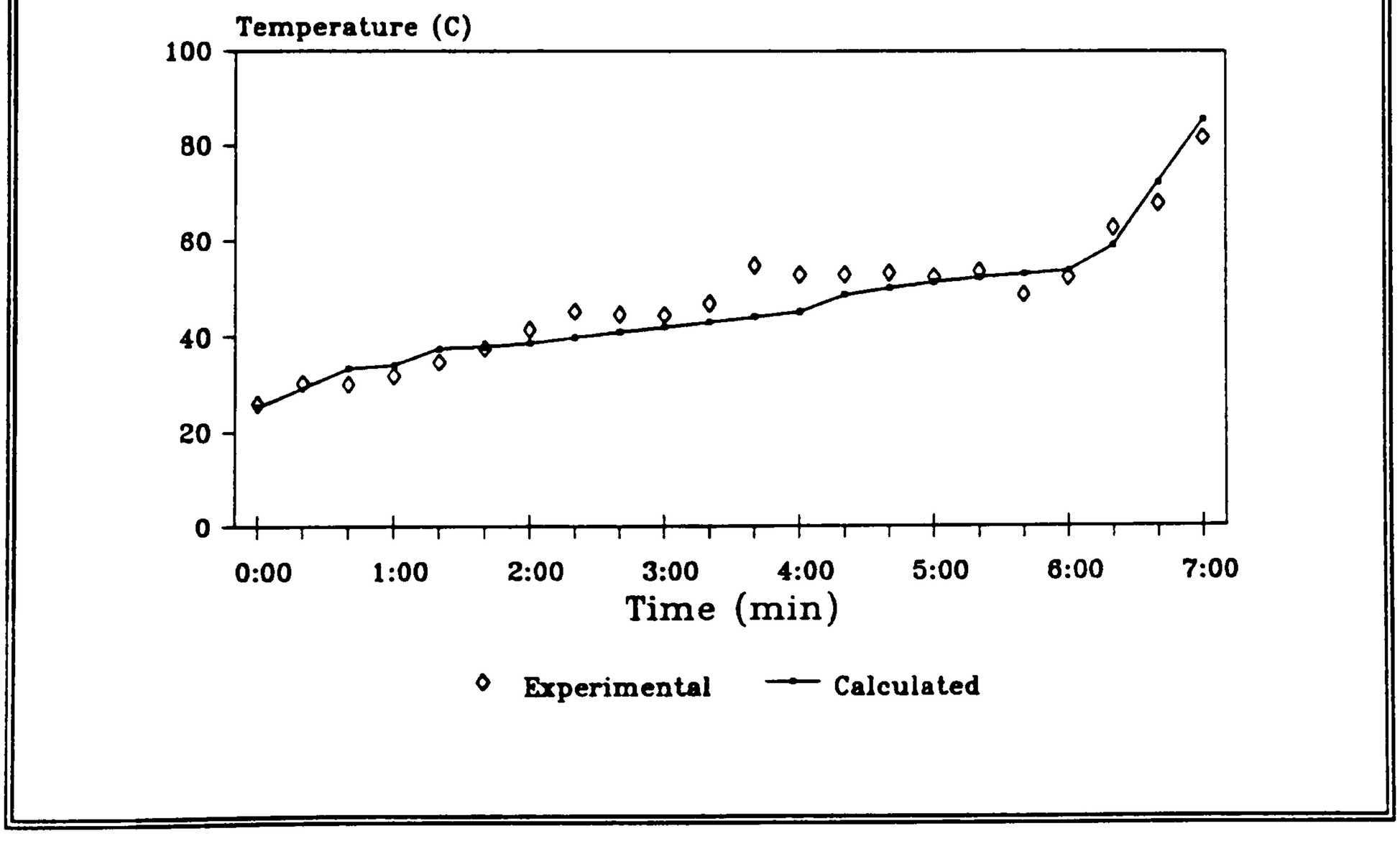

b) T2 location

Figure 3.35 Predicted and measured gas temperatures at eight thermocouple locations, 0.075m below the ceiling

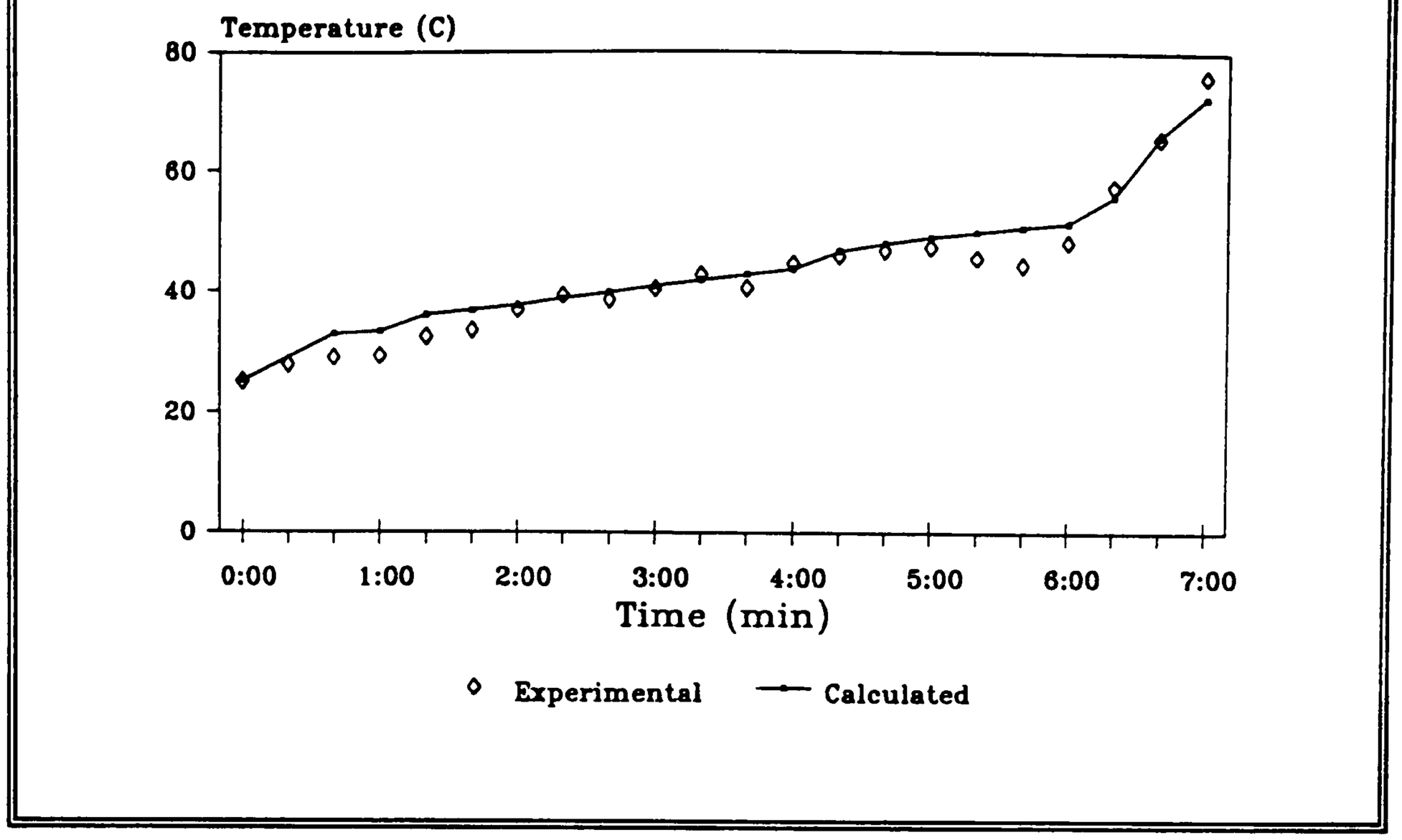

c) T3 location

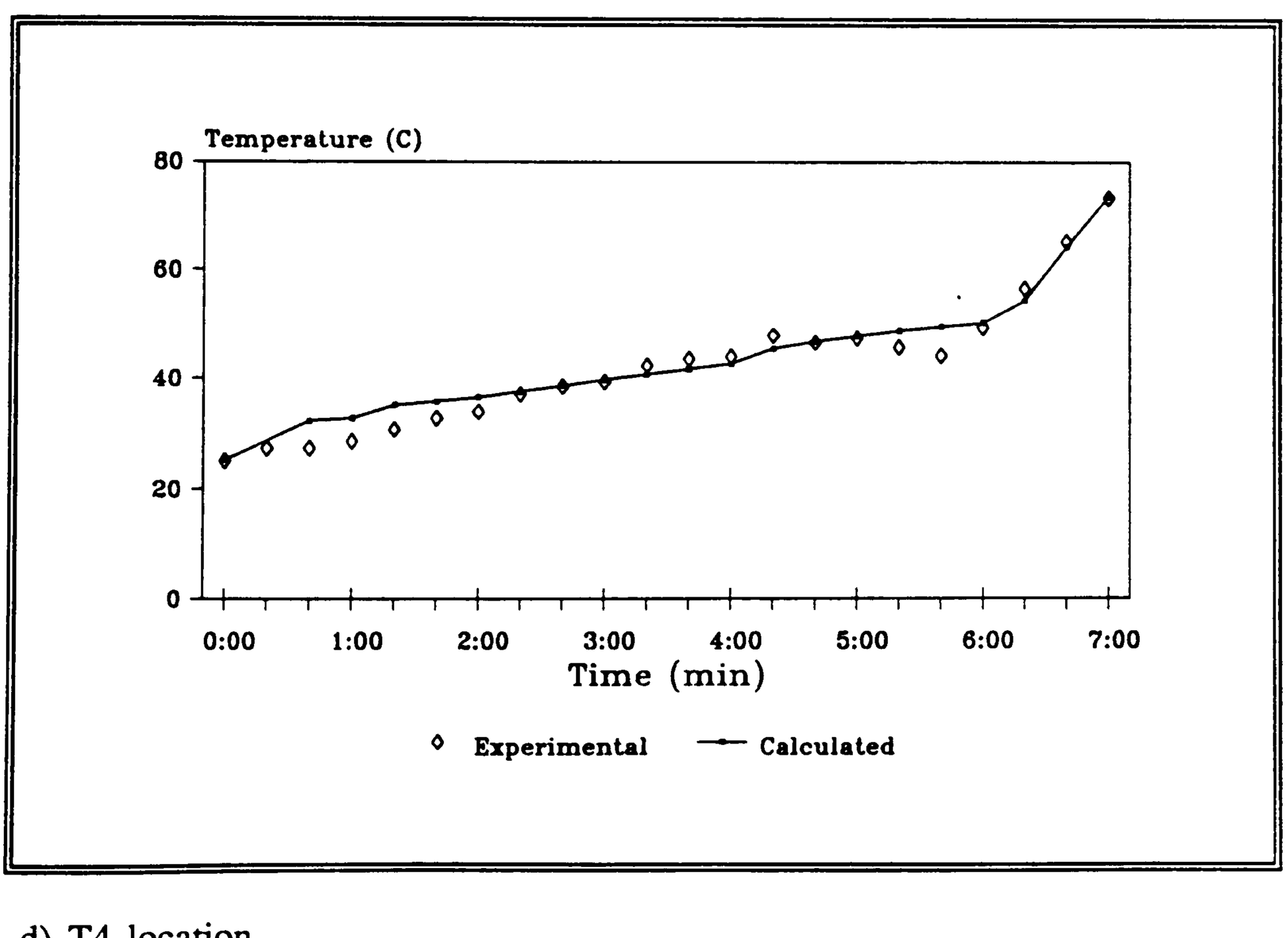

d) T4 location

Figure 3.35 Predicted and measured gas temperatures (continued)

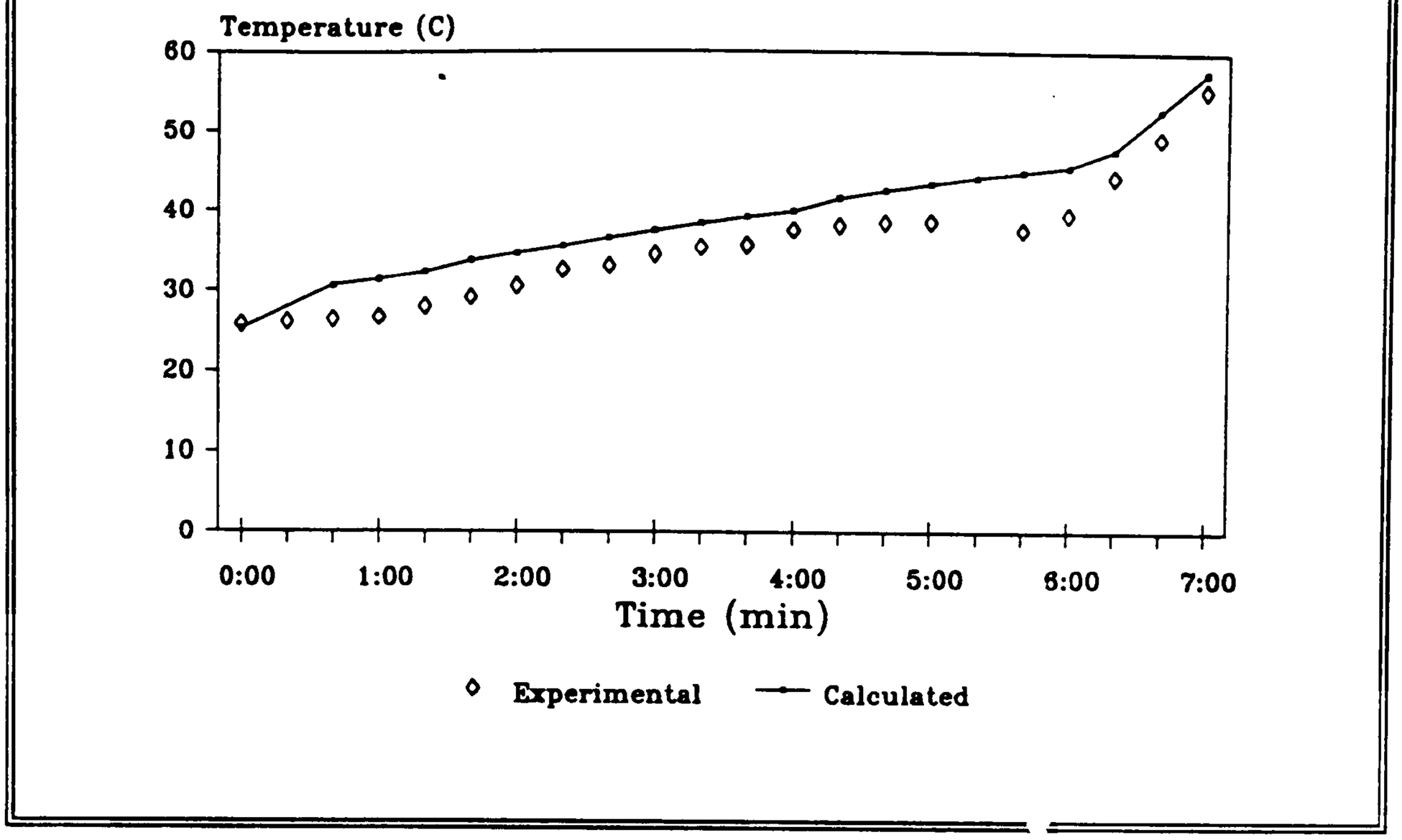

e) T5 location

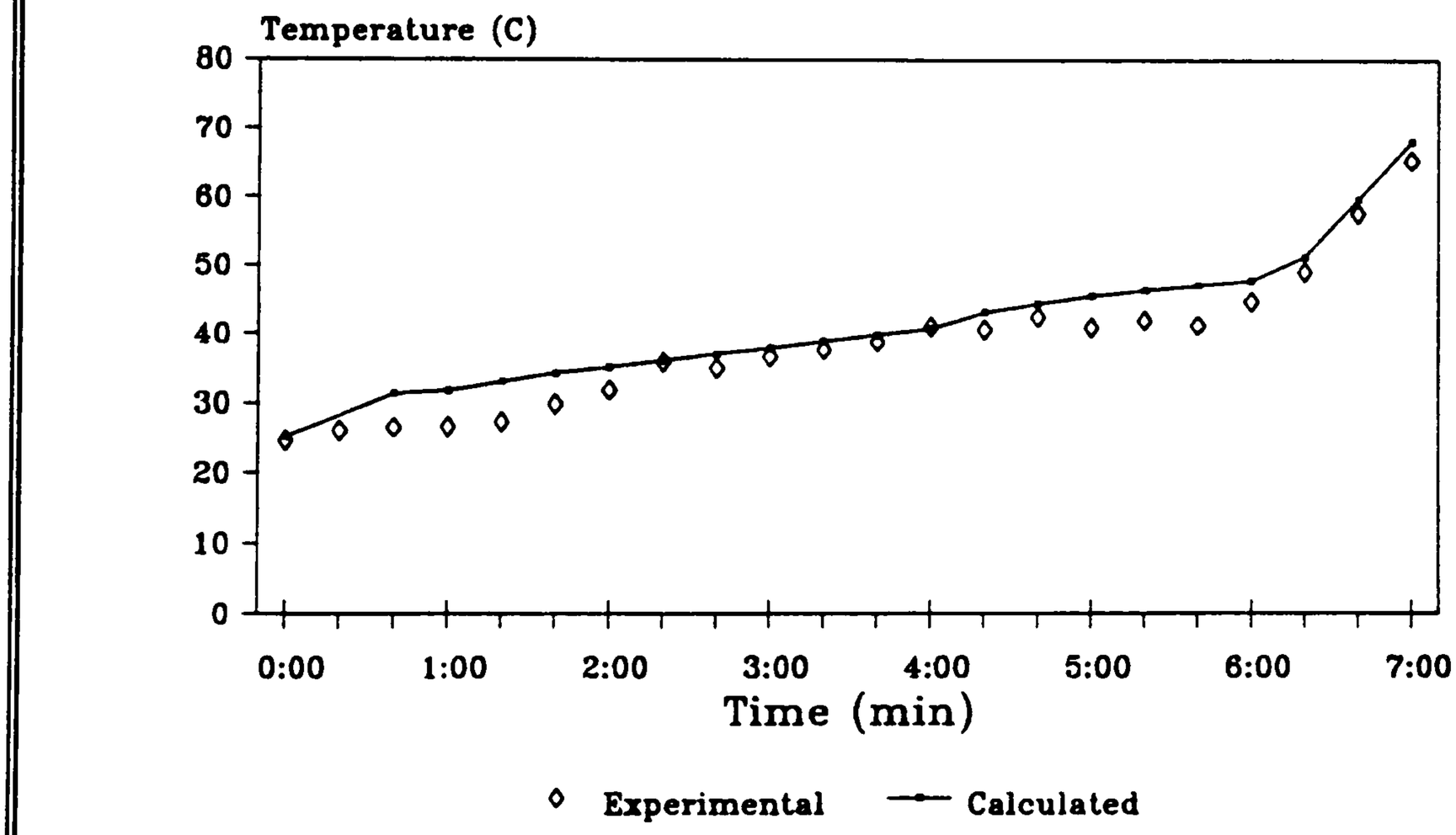

f) T6 location

Figure 3.35 Predicted and measured gas temperatures (continued)

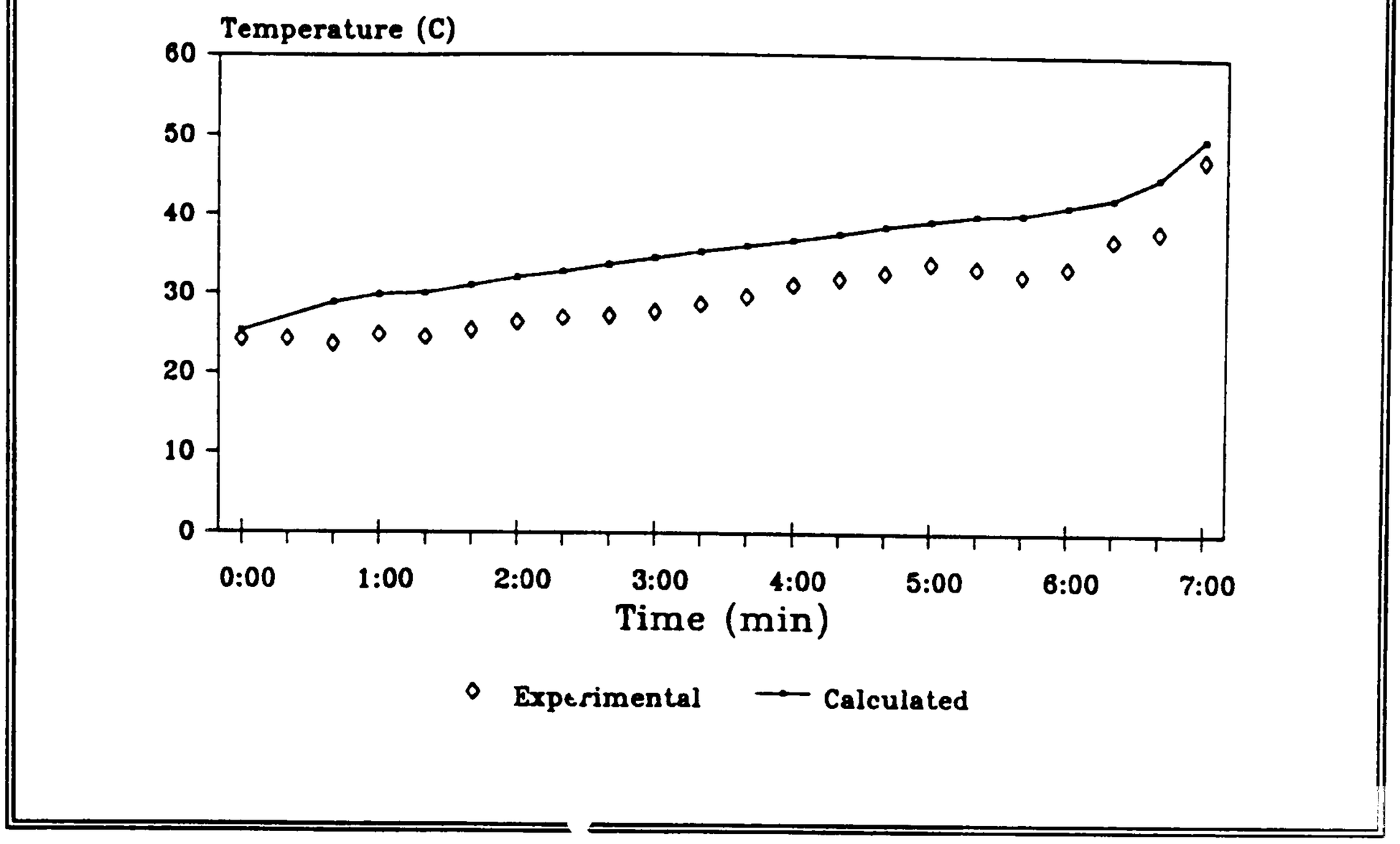

g) T7 location

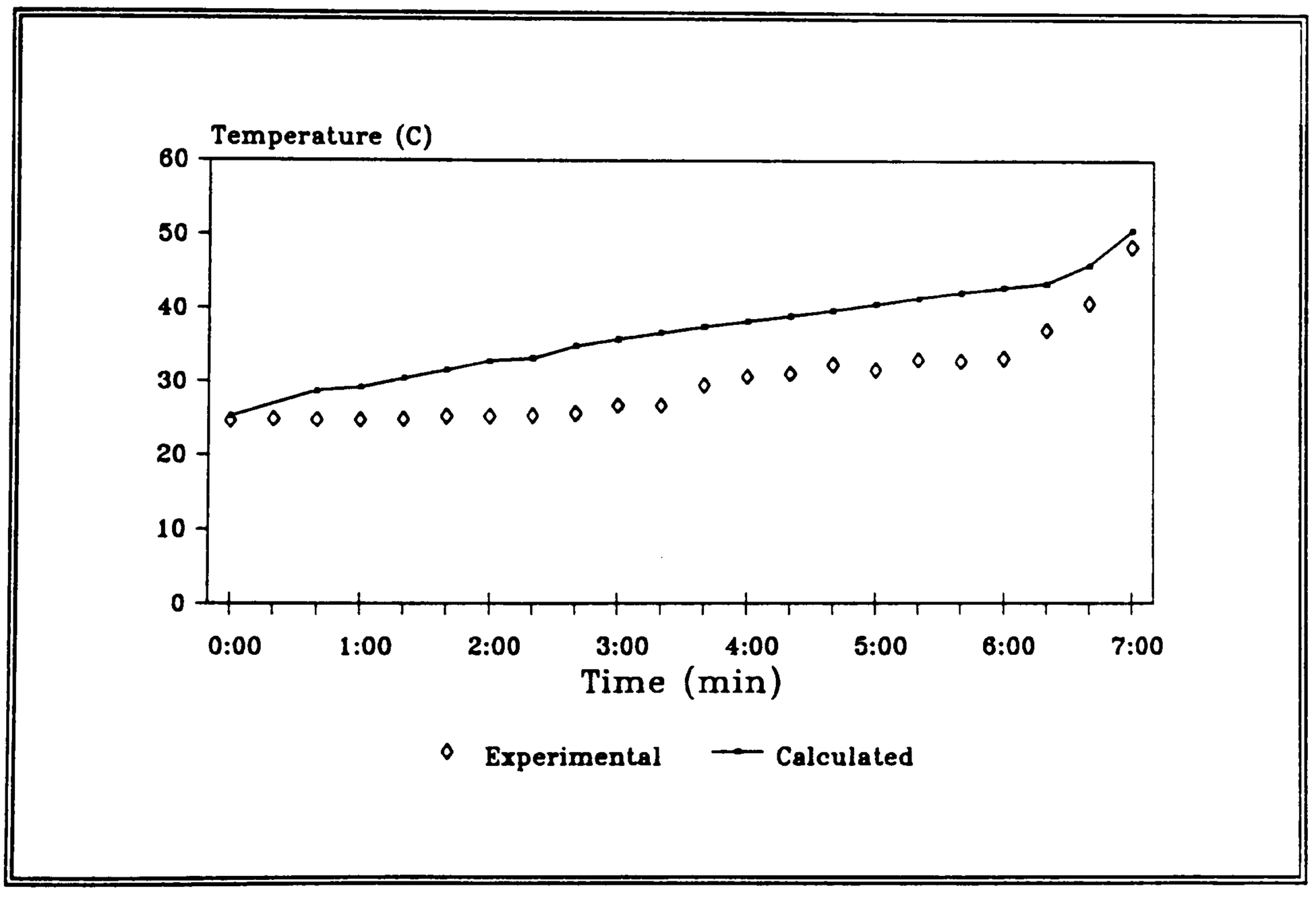

h) T8 location

Figure 3.35 Predicted and measured gas temperatures (continued)

compartment fire.

From all four locations it can be observed that the initial temperature variation with height after 60 seconds is minimal; only about a 2.2 to 3.9°C temperature rise. With time this temperature variation between the floor and the ceiling becomes more pronounced as the hot upper layer is created and pushed outwards below the ceiling from the fire source. The spreading of this upper layer can also be observed from these four diagrams. The locations which are closest to the fire, such as S1 and S2, *feel* the hot and cold layering effect much sooner and it is more pronounced. Hence after 420 seconds the characteristic 'S' type curve can be seen at locations S1 and S2, and to some extent at S3, though less pronounced. At S4, which is the furthest from the fire source this effect has not as yet been noticed.

However, what should also be pointed out is that whilst the air is circulated within the closed hospital room it is also heated up. Hence the temperatures near the floor are warmed up more than in the case of an open compartment like the office fire scenario, where cooler air is entrained at floor level, lowering the temperatures. Thus a distinct temperature layering is not as clearly defined in this situation.

A summary of these conditions after 420 seconds can be found in figure 3.37. Here it can be seen that the temperatures up to a height of 1.5m are at all four locations very much the same; between 40°C and 50°C, and hence below the life threatening gas temperature criteria. However, the effect of the upper layer and its spread through the room is more pronounced above this height, as the temperatures predicted start to deviate considerably. The expected relationship between temperature and distance from the fire source can clearly be observed.

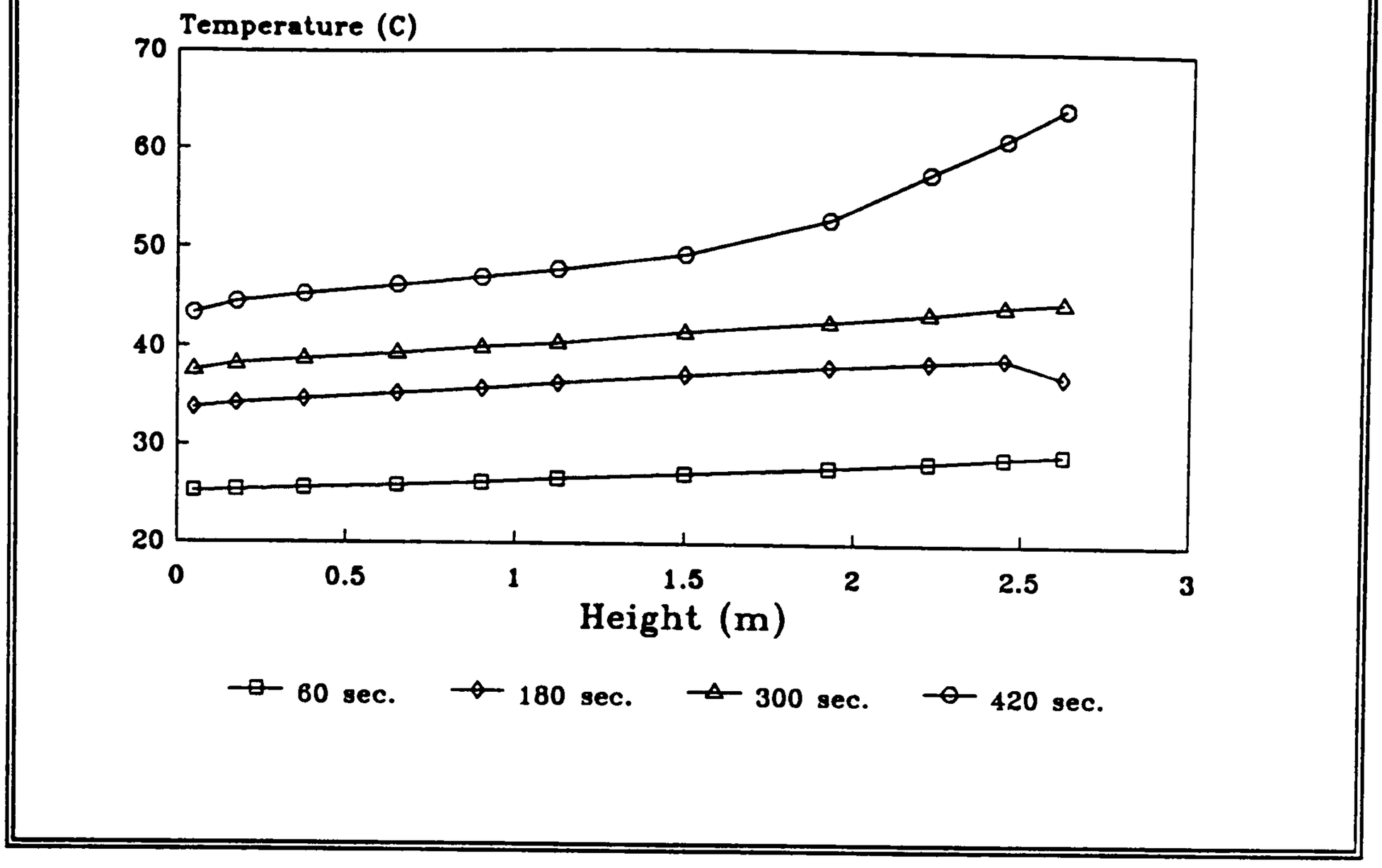

a) Location S1

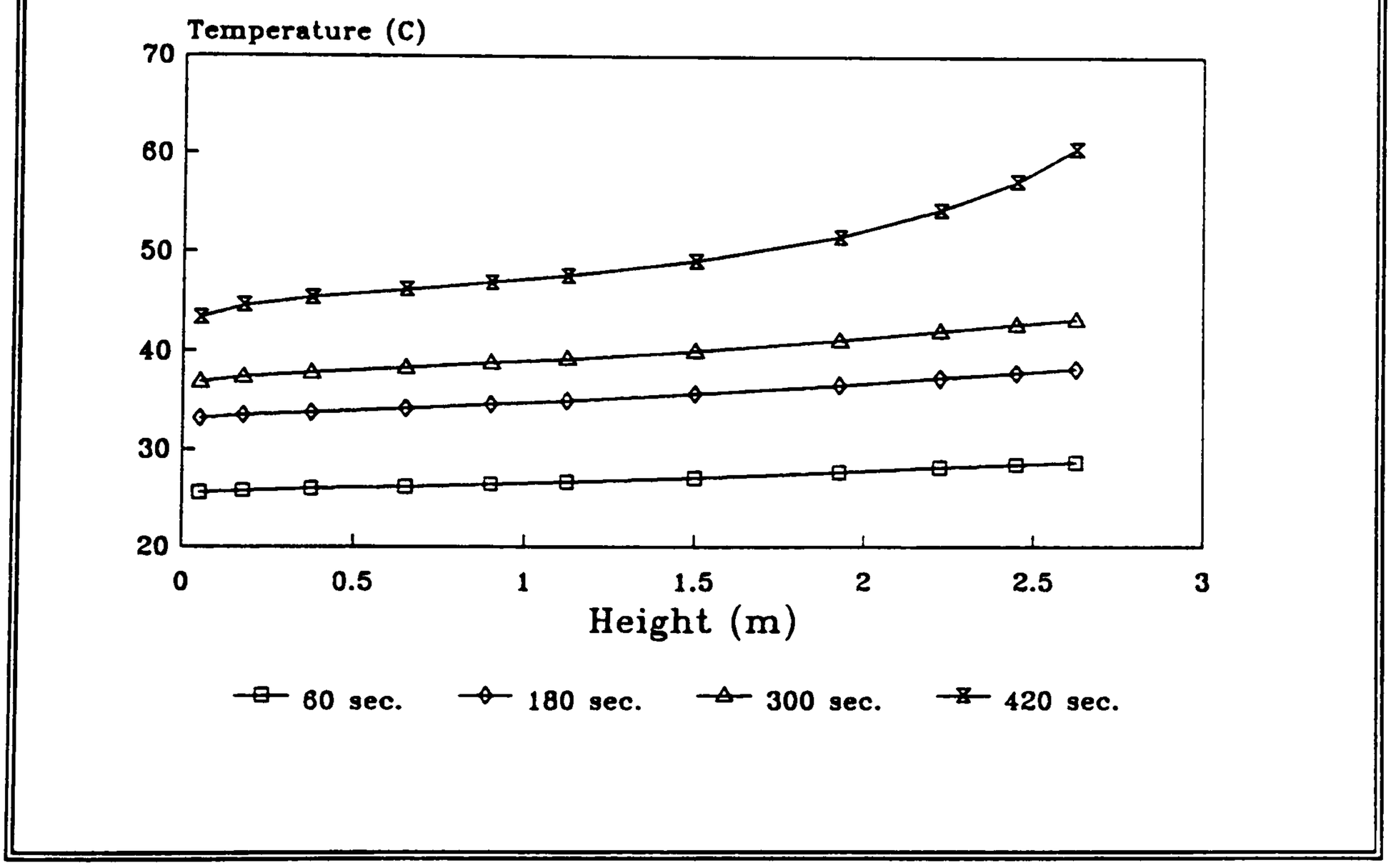

b) Location S2

Figure 3.36 Predicted gas temperature variations with height

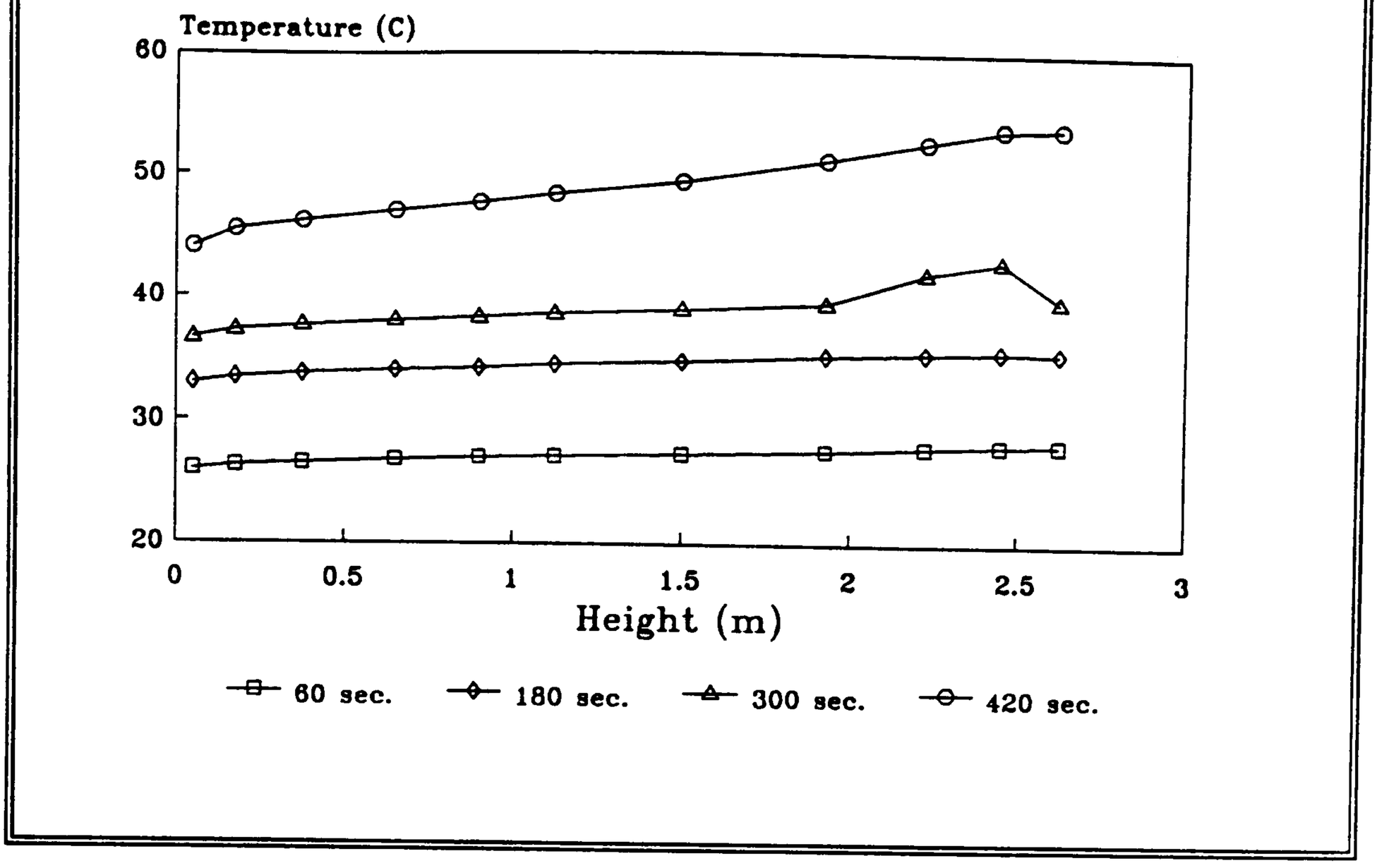

c) Location S3

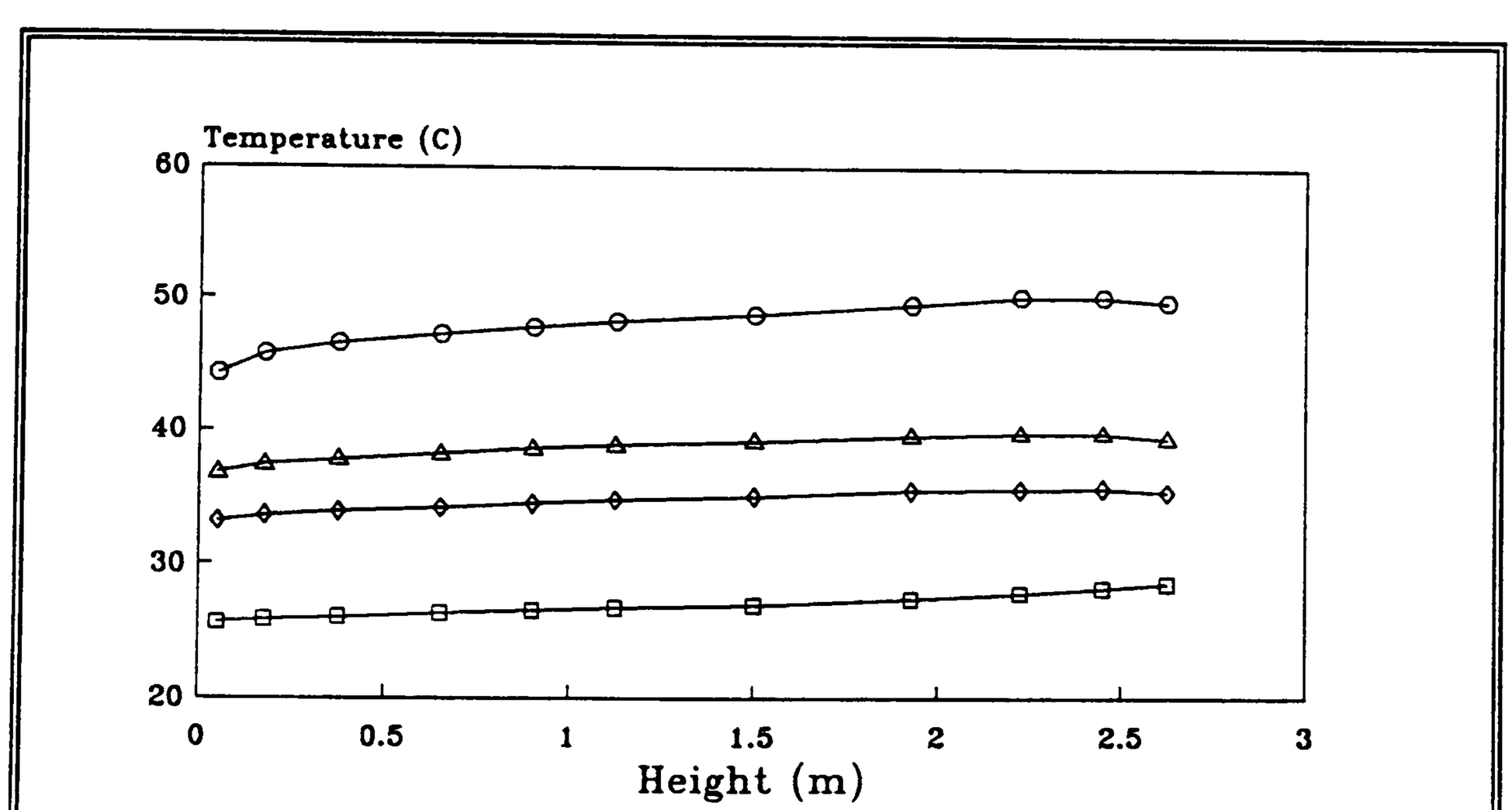

d) Location S4

Figure 3.36 Predicted gas temperature variations with height (continued)

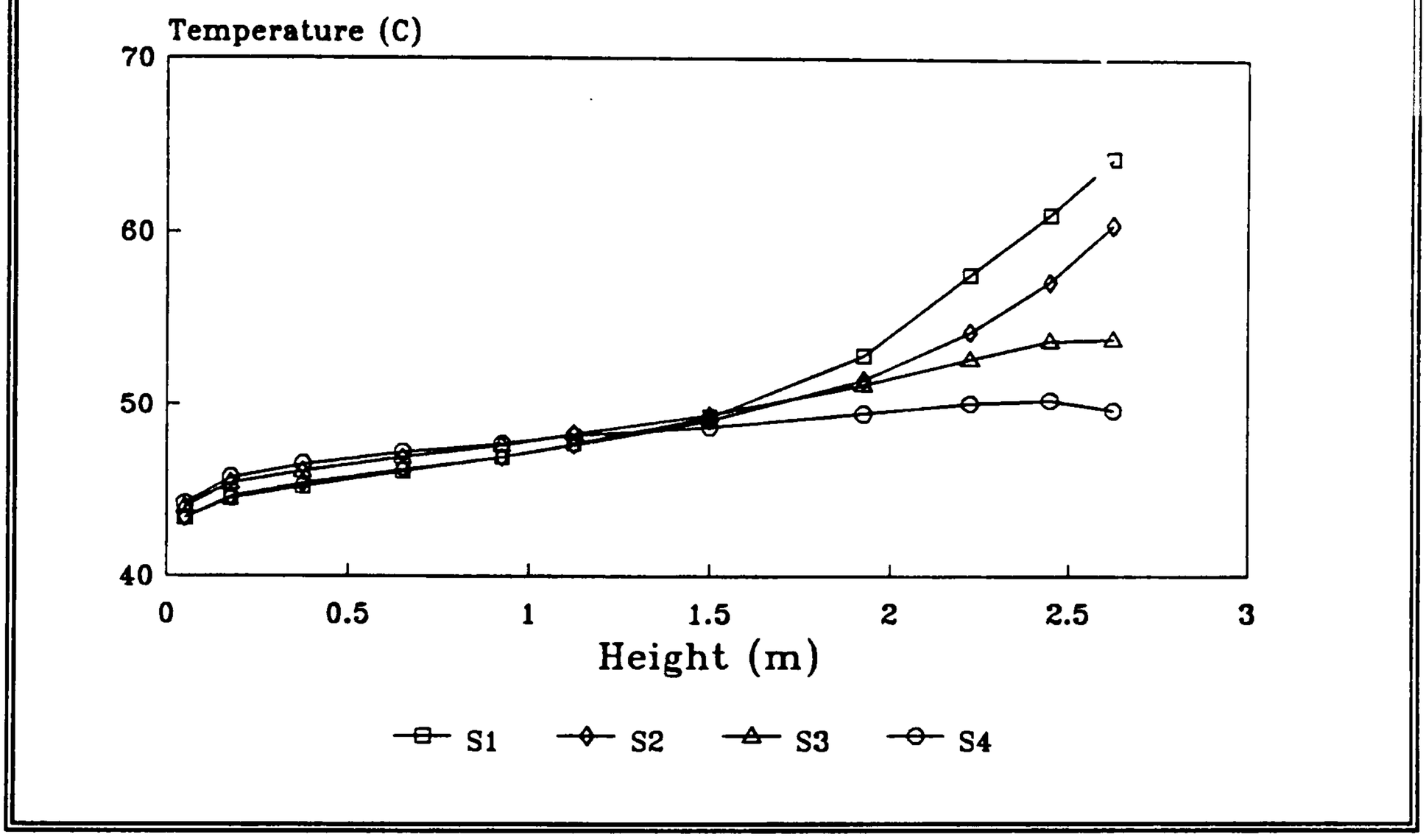

Figure 3.37 Predicted gas temperature variation with height after 420 seconds at the four monitoring locations

As only a limited number of effects can be measured during a full-scale fire experiment a more effective way of observing the growth of the simulated fire can be seen in the following figures. These illustrate the effects which can generally be observed visually, such as the temperature layering described above and the generated flow fields. The results presented below are taken at distinct points in time and at discrete slices through the compartment, whereby reference can be made to the original grid plan shown in figure 3.34. Please note the small diagram in the top right hand corner of each figure, which shows the relevant slice shaded.

The first planes, shown in figure 3.38 and 3.39 are across the room with the heaters on the left and the fire source in the centre elevated off the floor (X=12). Here it can be seen how initially the heaters were the dominant heat source within the room. With time, as the strength of the fire was increasing, the heat generated by the fire becomes more intense. By the end of the simulation an *onion* shaped temperature distribution near the fire source is generated with fairly constant layering of temperatures around it.

The associated velocity vectors, shown in figure 3.39 underline these facts. They also indicate the general circulation patterns and strength of the flow created. Note how during the early stages, figure 3.39-a, the heater's plume is forced upwards and is turned around by the ceiling. In time, as the hot upper layer generated by the fire becomes more pronounced, it is substituted as a new lower *ceiling level* for the heater's plume. Hence two small circulations are generated, as the heater's rising plume meets the upper layer which is forced downwards along the walls.

The effect of the increasing strength of the fire source can also be noticed in the

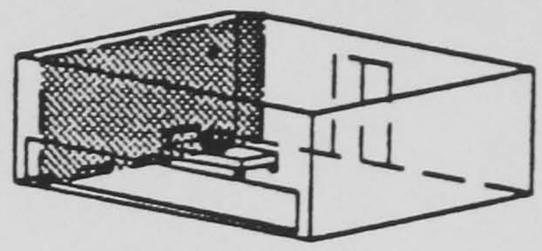

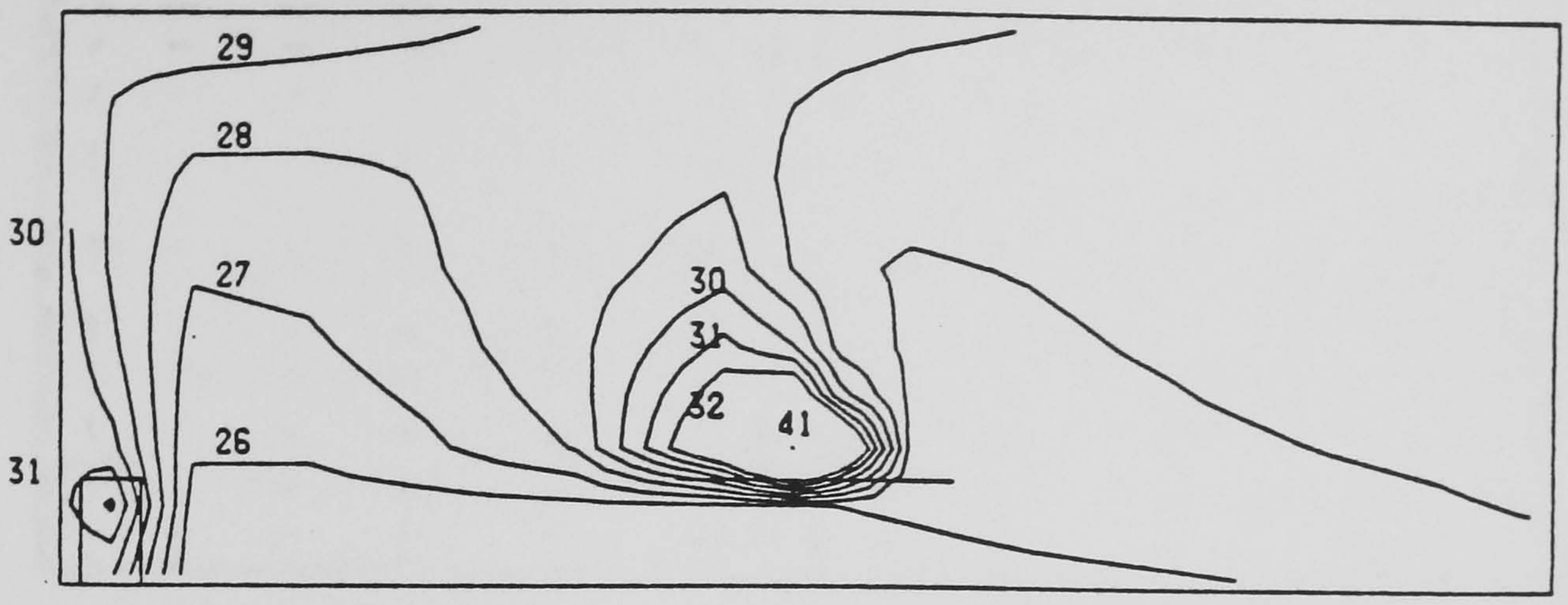

a)

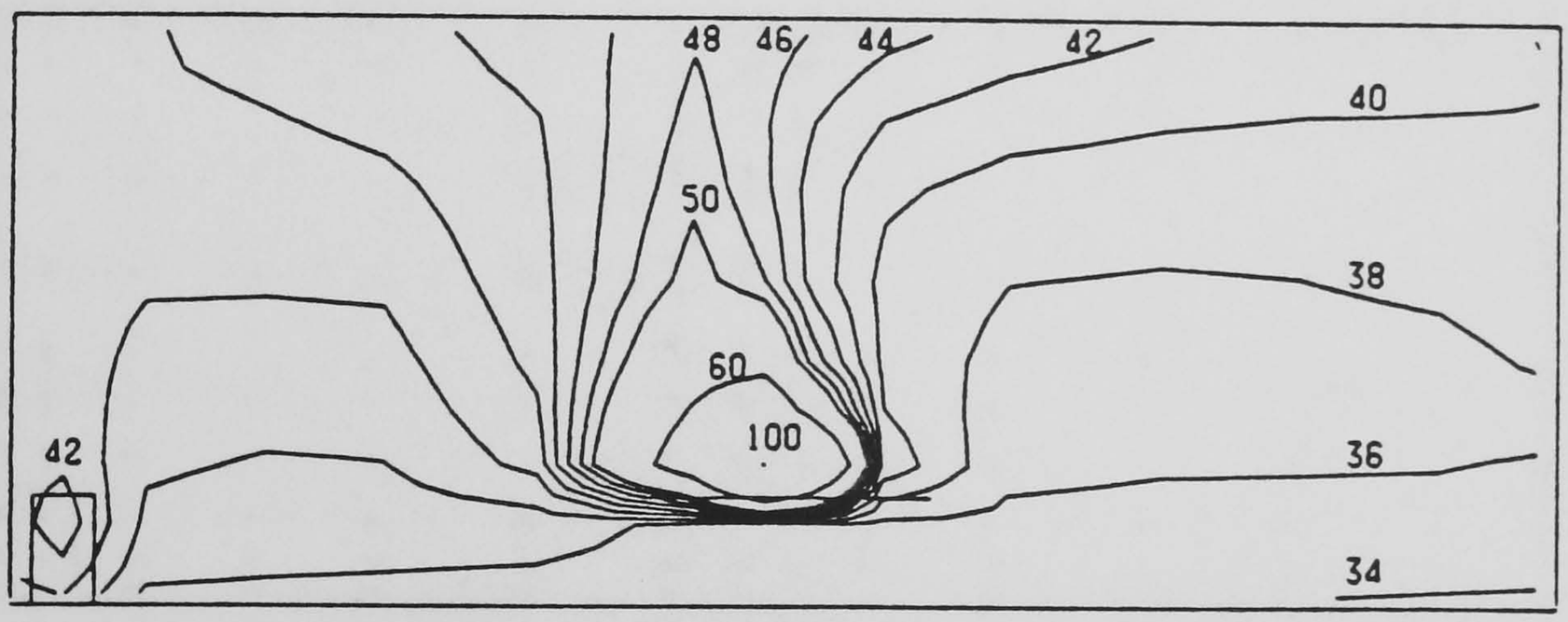

b)

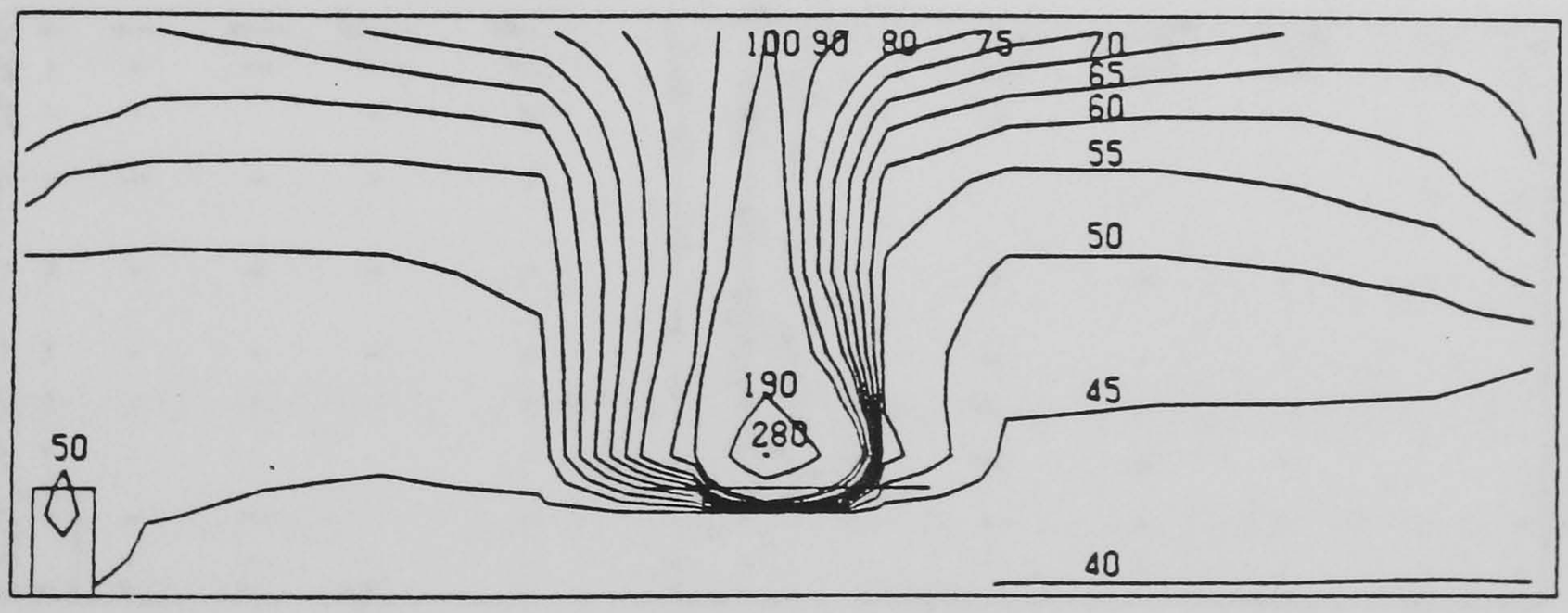

c)

Figure 3.38 Side view of Hospital ward: predicted gas temperature contours along the west wall through the fire source (X=12)
a) 60 sec. b) 240 sec. c) 420 sec.

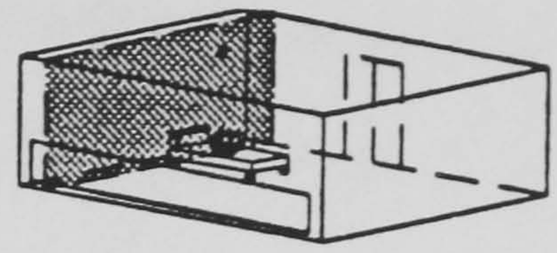

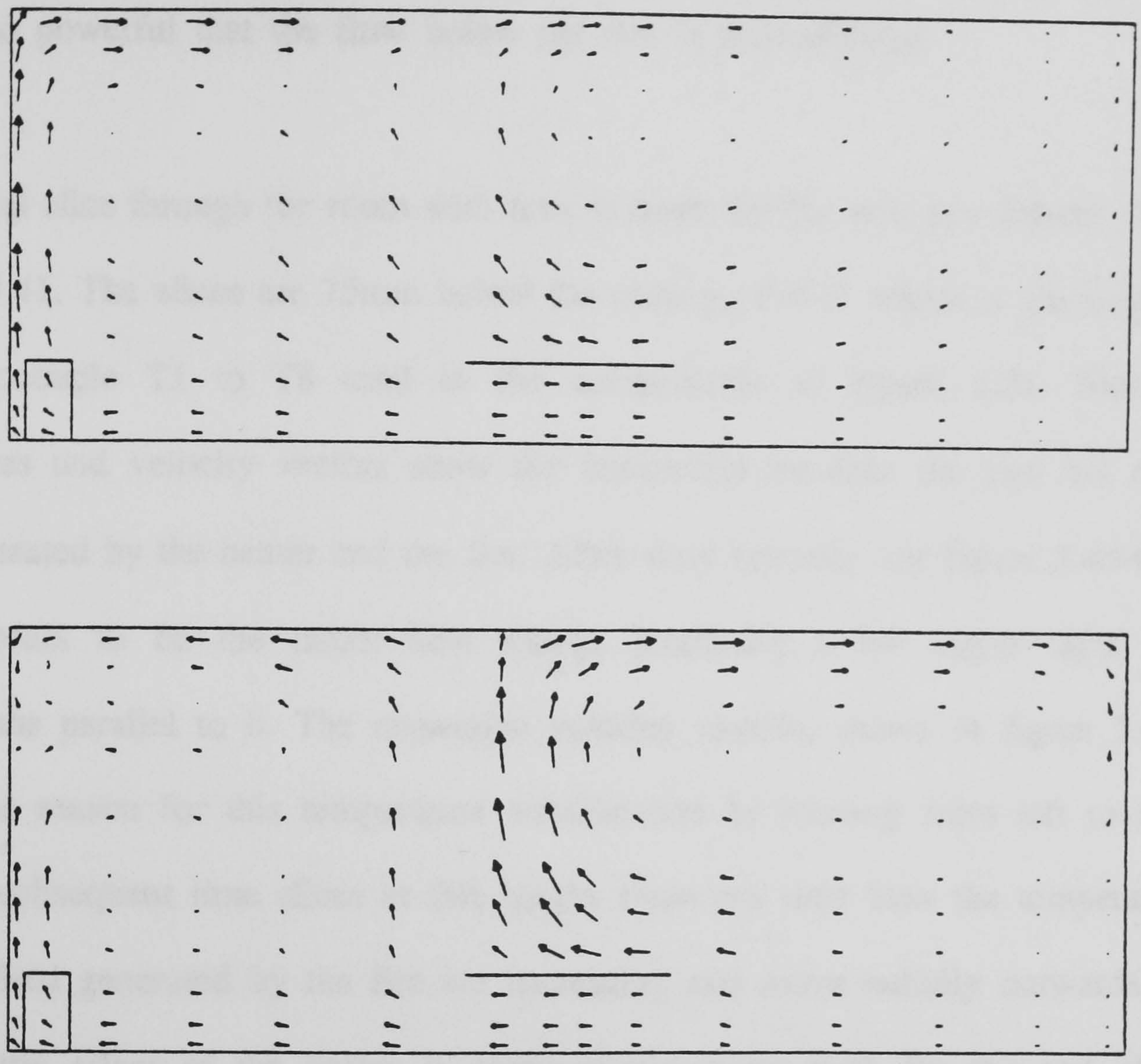

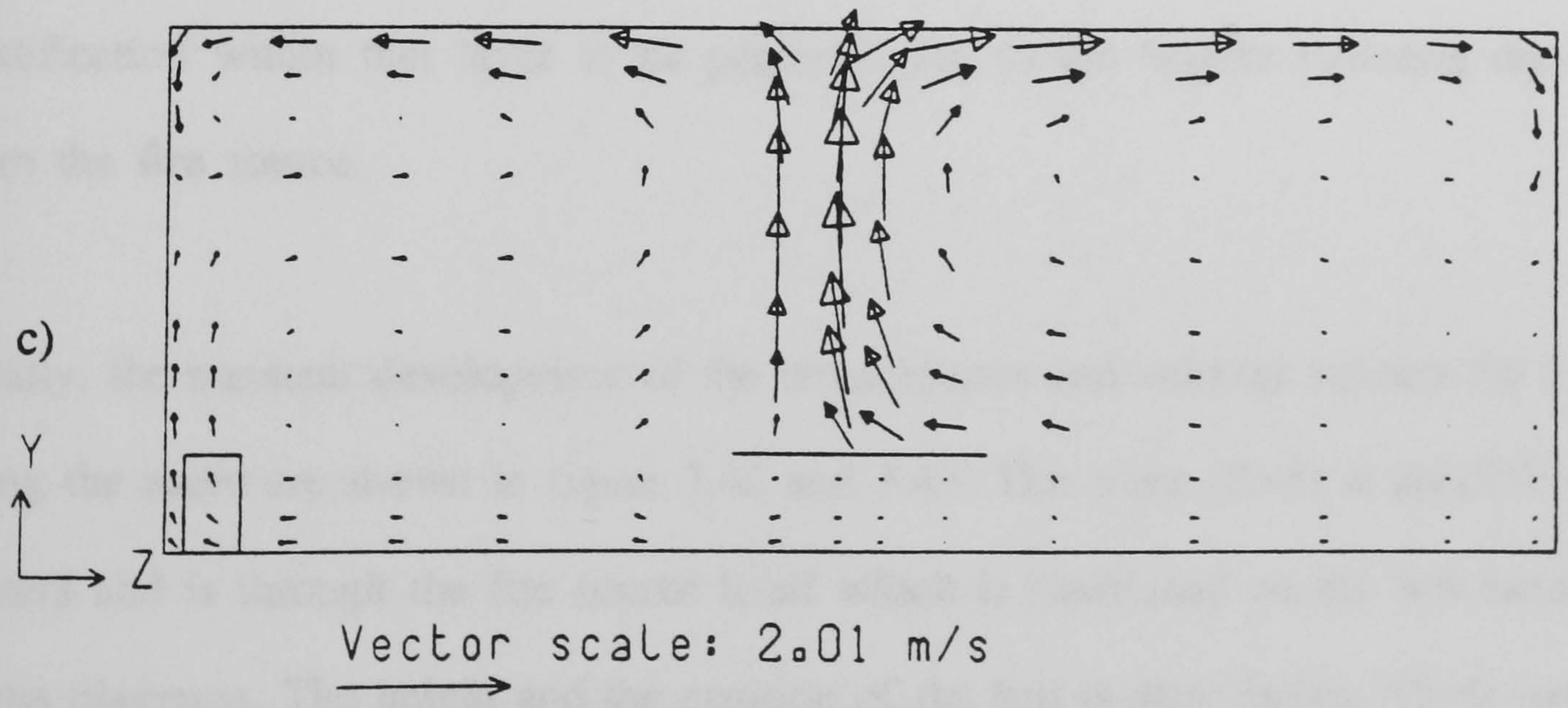

Figure 3.39 Side view of Hospital ward: predicted gas velocity vector fields along the west wall through the fire source (X=12)
a) 60 sec. b) 240 sec. c) 420 sec.

entrainment patterns around the base of the fire source. During the early stages the entrainment comes mainly from the right side. However, towards the end of the fire simulation, entrainment occurs from both sides of the fire base. This *attraction* becomes so powerful that the flow below the bed is also affected.

A horizontal slice through the room with time is taken for the next two figures, figure 3.40 and 3.41. The slices are 75mm below the ceiling (Y=11) which is the height of the thermocouple T1 to T8 used in the comparisons of figure 3.35. Here the temperatures and velocity vectors show the interaction between the two hot upper layers generated by the heater and the fire. After sixty seconds, see figure 3.40-a, the heater appears to be the major heat source producing a hot upper layer with stratifications parallel to it. The respective velocity vectors, shown in figure 3.41-a, indicate the reason for this temperature stratification by moving from left to right. However, subsequent time slices at this height show not only how the temperatures and flow field generated by the fire are increasing and move radially outwards, but also how the effect of the heater is consequently suppressed. By the end of the simulation the fire has become the dominant force, resulting in the temperature stratification within that layer to be perpendicular to the heaters radiating outwards from the fire source.

Finally, the transient development of the temperatures and velocity vectors for a slice along the room are shown in figure 3.42 and 3.43. This view (Z=8) is parallel to the heaters and is through the fire source itself which is positioned on the left hand side of the diagrams. The height and the position of the bed is also shown. These indicate how the fire as well as the hot upper layer is growing with time. However, once again the effect of the heaters can be observed in figure 3.42-a, where a distinct

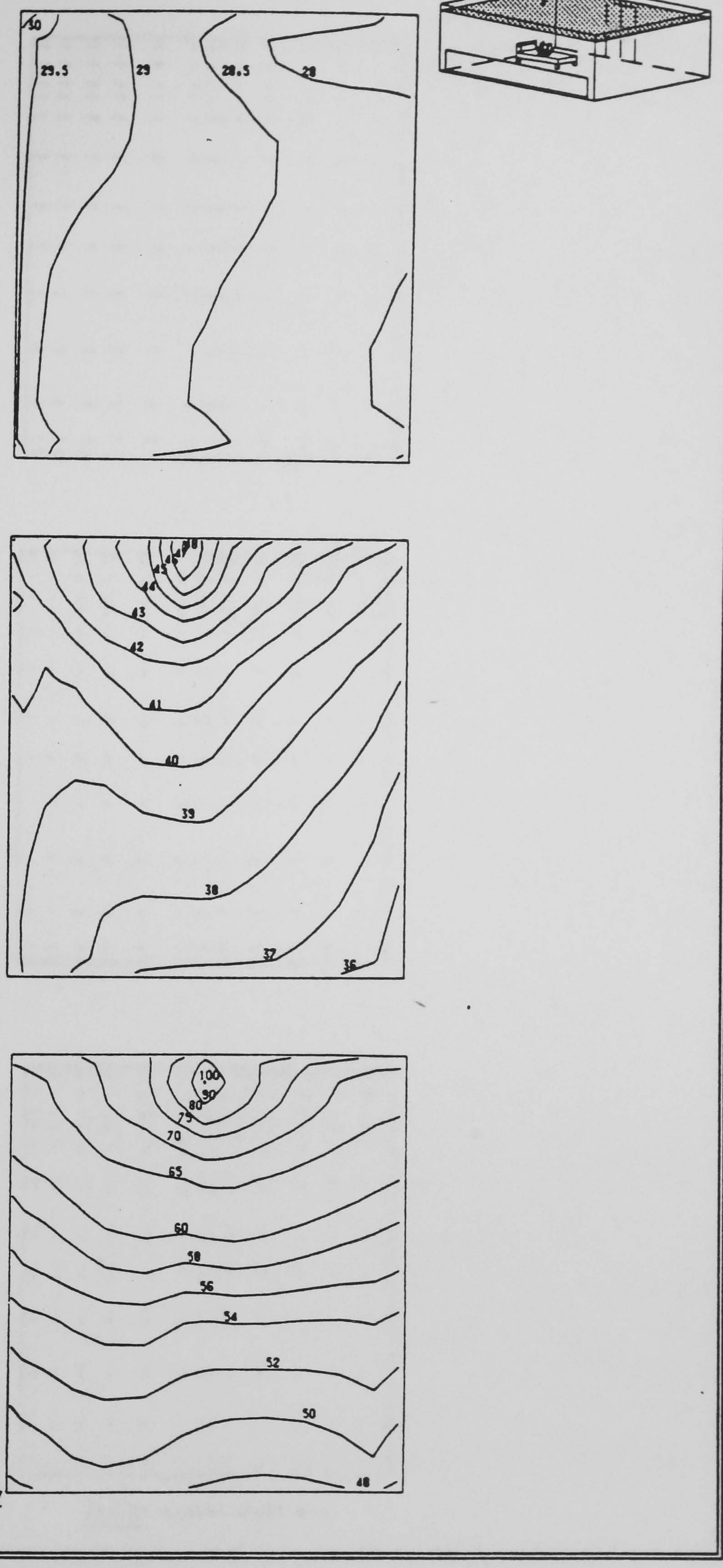

Figure 3.40 Plan view of Hospital ward: predicted gas temperature contours, 0.075m below the ceiling (Y=11)
a) 60 sec. b) 240 sec. c) 420 sec.

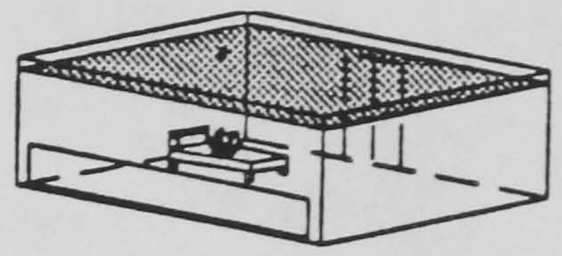

a)

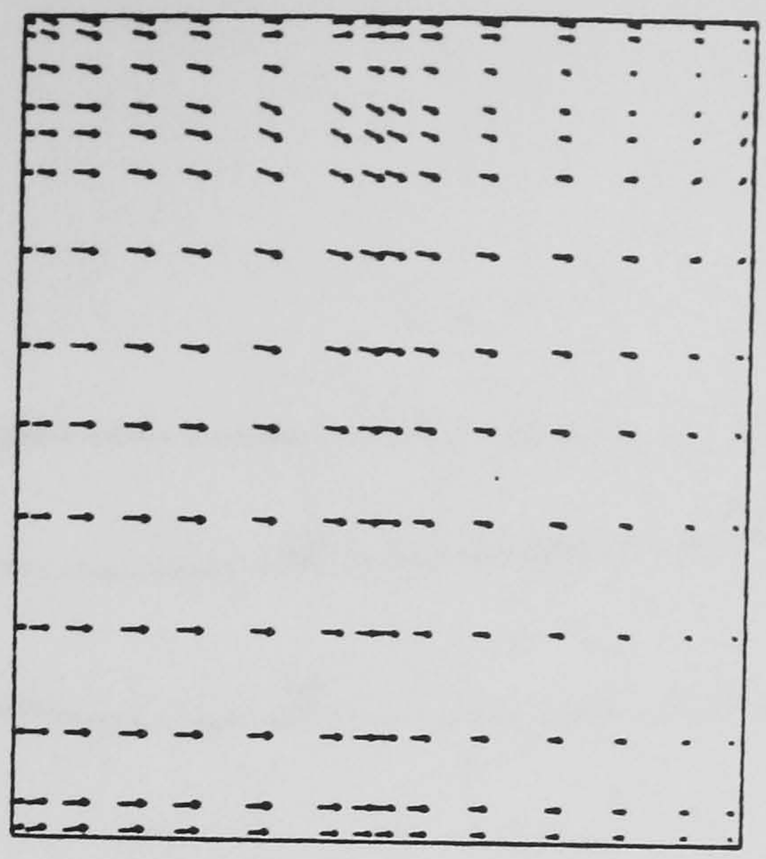

b)

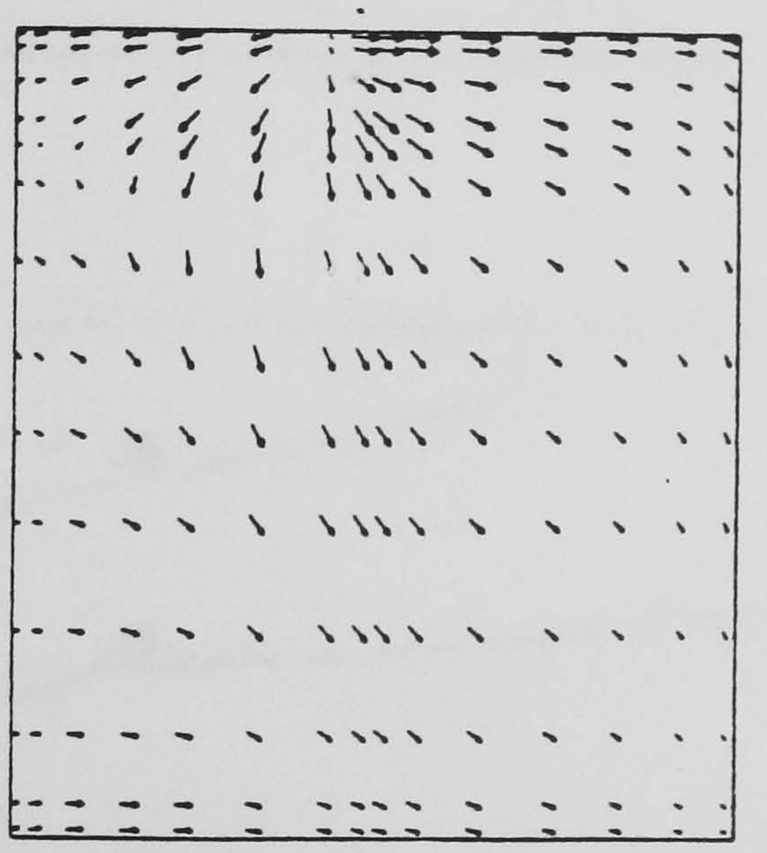

c)

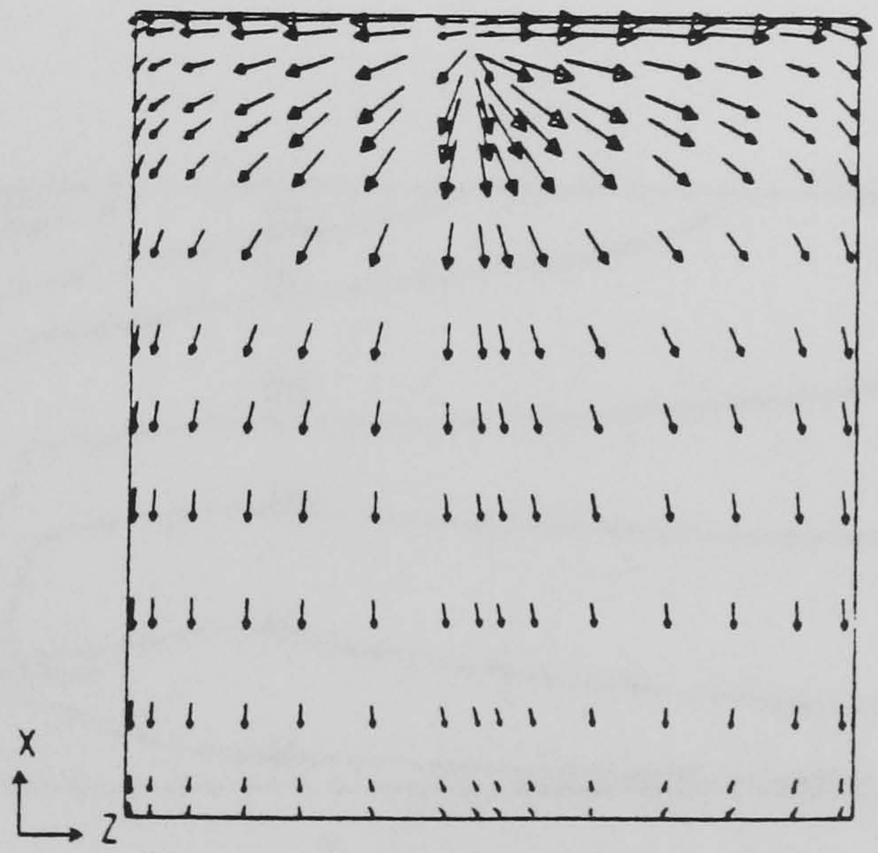

Vector scale: 2.01 m/s

Figure 3.41 Plan view of Hospital ward: predicted gas velocity vector fields, 0.075m below the ceiling (Y=11)
a) 60 sec. b) 240 sec. c) 420 sec.

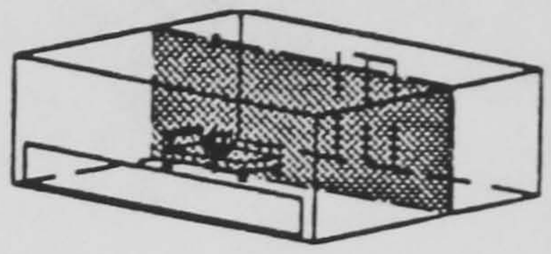

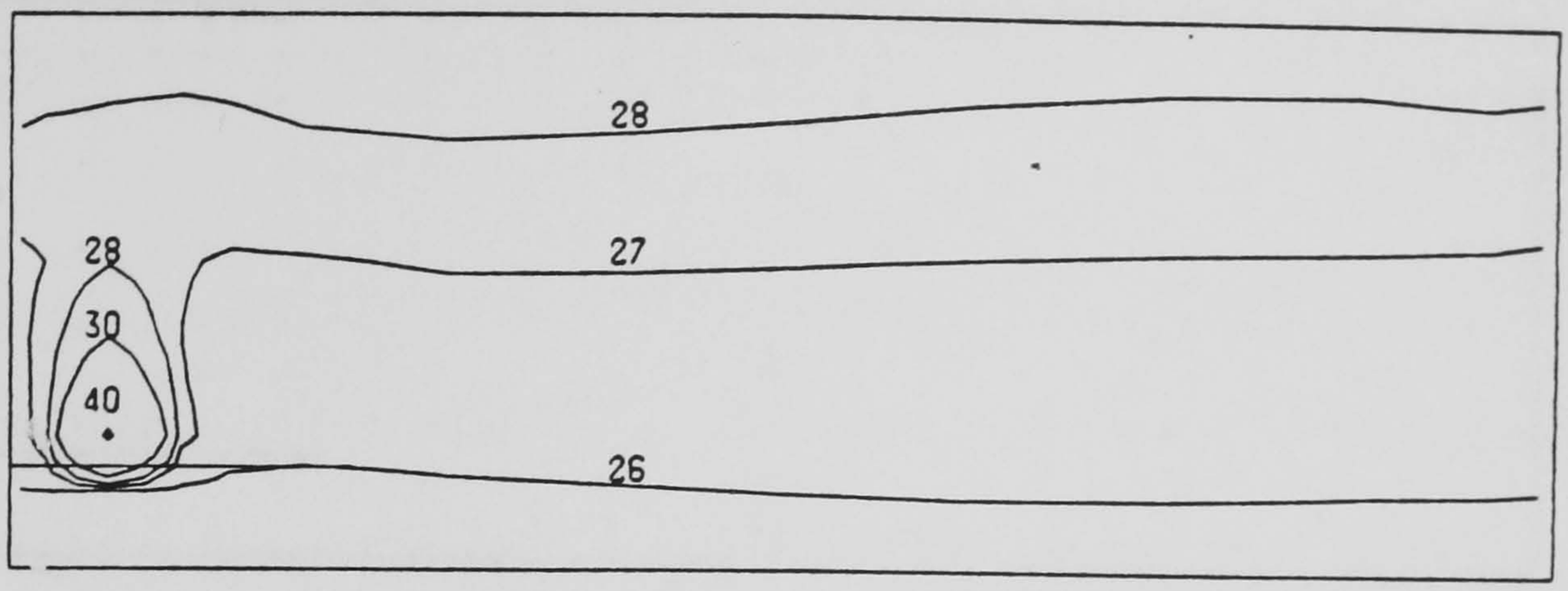

a)

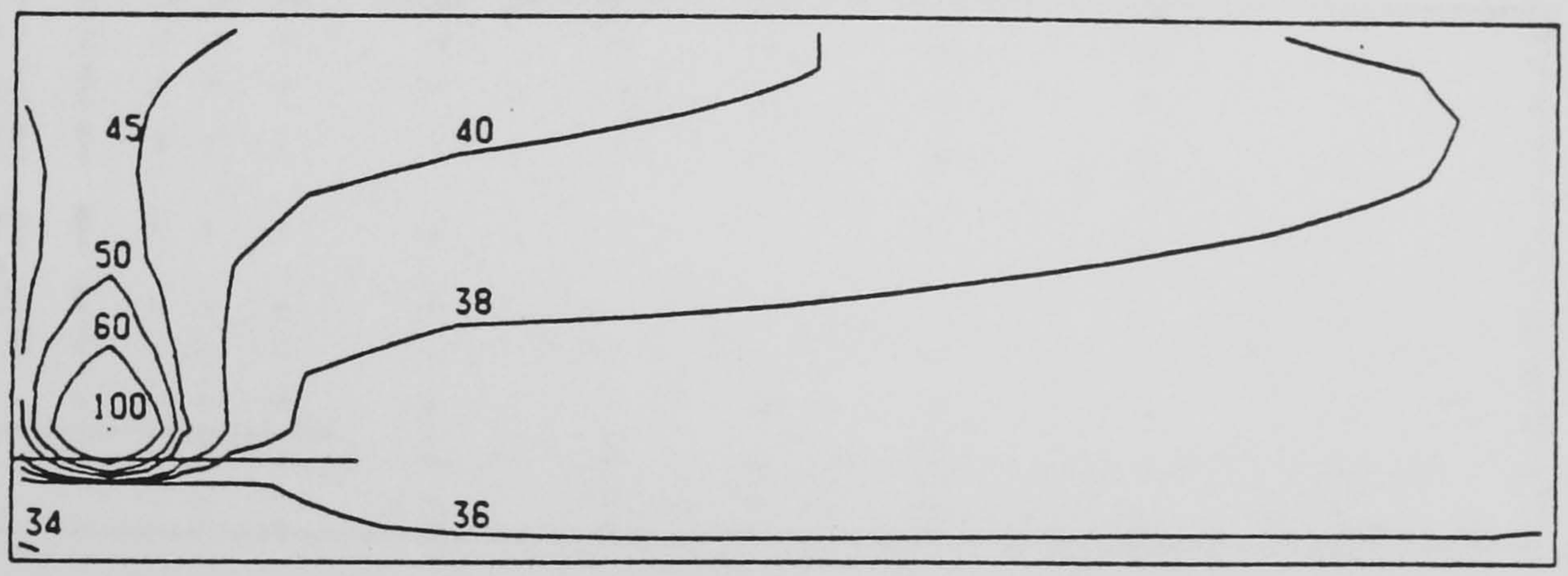

b)

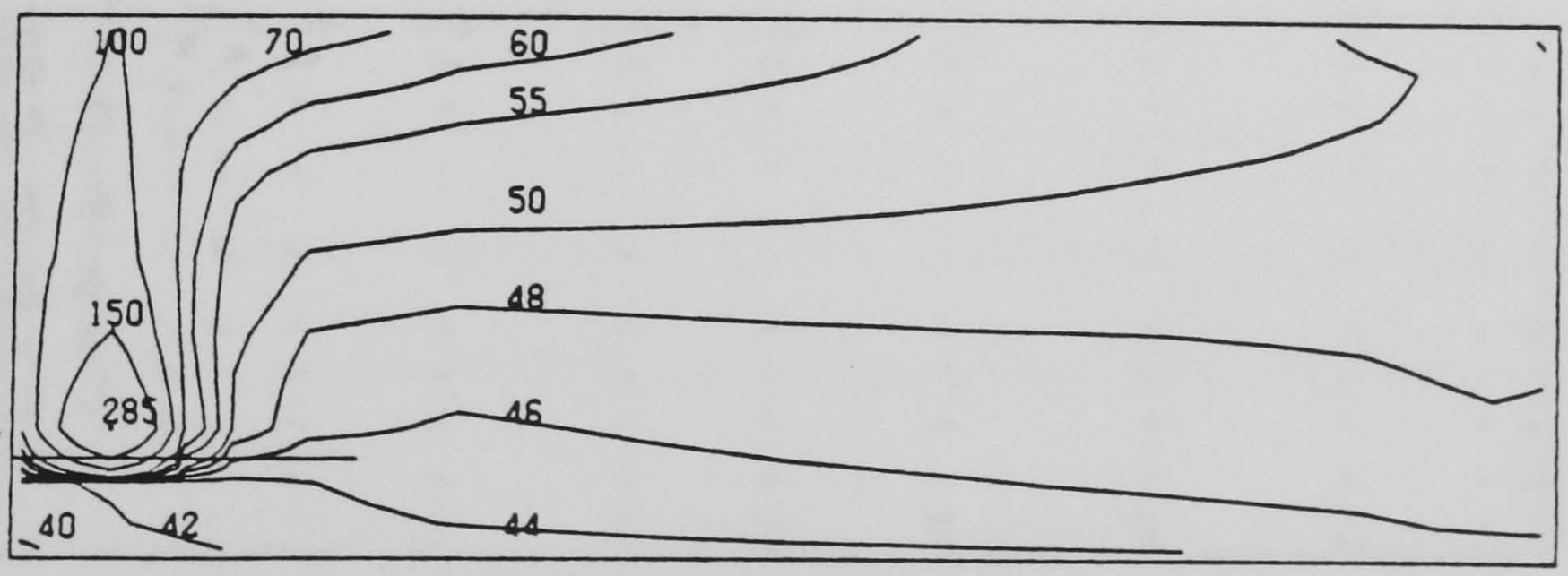

c)

Figure 3.42 Cross view of Hospital ward: predicted gas temperature contours through the centre of the room (Z=8)
a) 60 sec. b) 240 sec. c) 420 sec.

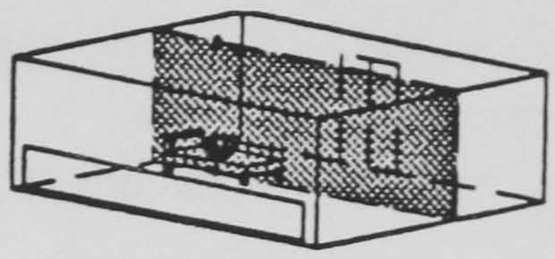

a)

b)

c)

Y

X

Vector scale: 2.01 m/s

Figure 3.43 Cross view of Hospital ward: predicted gas velocity vector fields through the centre of the room (Z=8)
a) 60 sec. b) 240 sec. c) 420 sec.

stratification of temperatures remote from the fire can be seen. This effect though becomes negligible with time as the fire is increasing in strength, subsequently heating up the compartment including the area beneath the base of the bed.

3.3.3 Timings

One aspect which is crucial in the development of mathematical models is the amount of CPU time used to obtain the results. However, it should not be forgotten that a considerable number of preliminary *trial-runs* need to be performed prior to having obtained a *working* model with which predictions can be made. Hence this following data should be used as a rough guideline for future developments of the model or simulations on different computer architectures.

The above time-dependent simulations were carried out on two Norsk Data ND-5900 computers at Thames Polytechnic between 1986 and 1989, consisting of three and four processors respectively. Based on Linpack tests the performance of each of the processors is 0.6 Mflops (Million floating point operations per second) and 6.5 Mips (Million instructions per second) [Leggett (1990)]. During the above studies it was possible to *dedicate*[2] a single processor on each machine to perform the calculations. During the simulations the total amount of CPU time used by the processors were recorded. From these results the following average timings were obtained:

Case	No. of cells	CPU time
Office	2640 cells	12.5 seconds
Hospital Room	2310 cells	13 seconds

[2]Note that in this context *dedicated* means that the job was restricted to one processor, rather than given the opportunity to share all available processors.

whereby the above timings are per step per sweep for a one second time-step simulation.

Using this data the following CPU times for the complete simulations, including the number of steps and sweeps utilised, were calculated as:

Case	Simulated Time	Total CPU time
Office	175 sec.	1 day 6 hours 23 mins
Hospital Room	420 sec.	3 days 3 hours 13 mins

These figures clearly show that to perform a full fire scenario the time taken is measured in terms of days of CPU time compared to only minutes for a zone model. However, the plethora of predictions obtained at the end make this well worth the effort especially when considering that they can aid the design of room configurations and fire safety measures.

Further factors to consider are that these figures were specific to one computer architecture during one period in time. With the advent of more widespread availability of faster computer architectures and software these run-times will be drastically reduced; from days down to hours/minutes [Cross et al(1989)]. This will be necessary if the field model is to become a design rather than a research tool.

3.3.4 Grid Refinement

The technique of finite-volumes is based on the idea of sub-dividing the compartment under consideration into a number of small individual control-cells or -volumes. Hence

the numerical accuracy of the results obtained will depend on the number of cells used, their aspect ratio and subsequently their size. A very apt description of the effect of grid-size can be found in the PHOENICS manual [Rosten and Spalding (1986)]:

If a complex phenomena has been simulated by a grid containing only few computational cells, the effect will be like that of photographing an intricate object on a coarse-grained film - rather blurred.

In order to check that the predictions made are close approximations, the number of grid nodes should be large enough for any further increases in their number to produce only insignificant changes in their values of predicted quantities.

The only reliable method to determine the optimum number of grid nodes used is to vary the grid-sizes in successive repetitions and to check for significant changes. This generally would involve successively doubling the number of cells used within each direction. However, this would imply an increase in the amount of CPU time used by at least a factor of eight. Hence, due to the limitations of CPU time three smaller scale grid-refinement studies were performed.

These studies were carried out using the hospital ward fire scenario as a basis as more detailed measurements across the room were available and thus the effect of the grid-size could be monitored more effectively. Hence a separate grid-refinement study for the office fire scenario was not carried out due to the similarity in compartment dimensions and grid-discretisations used. The three studies performed used the following number of cells:

Refinement Number	NXxNYxNZ	number of cells
Original	14x11x15	2310
1	16x11x18	3168
2	14x19x15	3990
3	16x19x18	5472

Figure 3.44 shows the temperature predictions made with the above three grid-refinements at four distinct positions; T1, T3, T5 and T7, for 100 second simulations. The results of the original predictions are supplied for comparison purposes.

From these figures it can be seen that the predictions made during the three refinement studies were not significantly different from the originals. In fact, the most noteworthy changes were seen during the second refinement when further cells were added to the height discretisations. However, even then only a maximum temperature difference of about 1°C was achieved.

Though the change in predictions is an important point to consider, a further consideration to be made during a refinement study is the considerable increase in the overall number of cells. Adding only eight cells to the height discretisation, see refinement number 2, the number of cells has increased by a factor of 1.73 which in turn increases the amount of CPU time needed to perform the simulations. Hence, the question that needs to be raised is; does the improvement in accuracy obtained justify the added expense of computation involved?

With respect to the simulations and refinements studies presented the answer was no, as yet a further factor needed to be accounted for; the addition of the second phase.

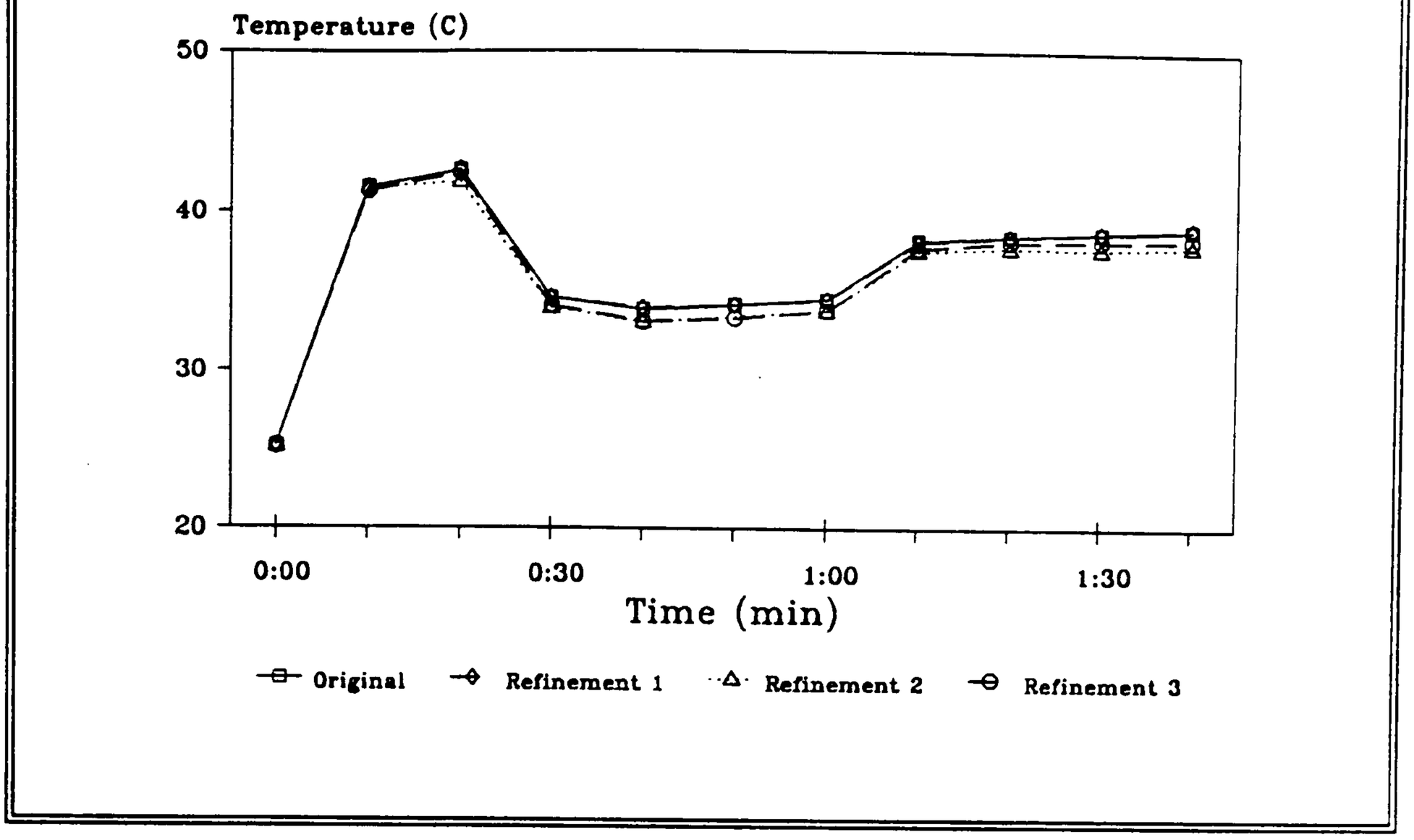

a) T1 location

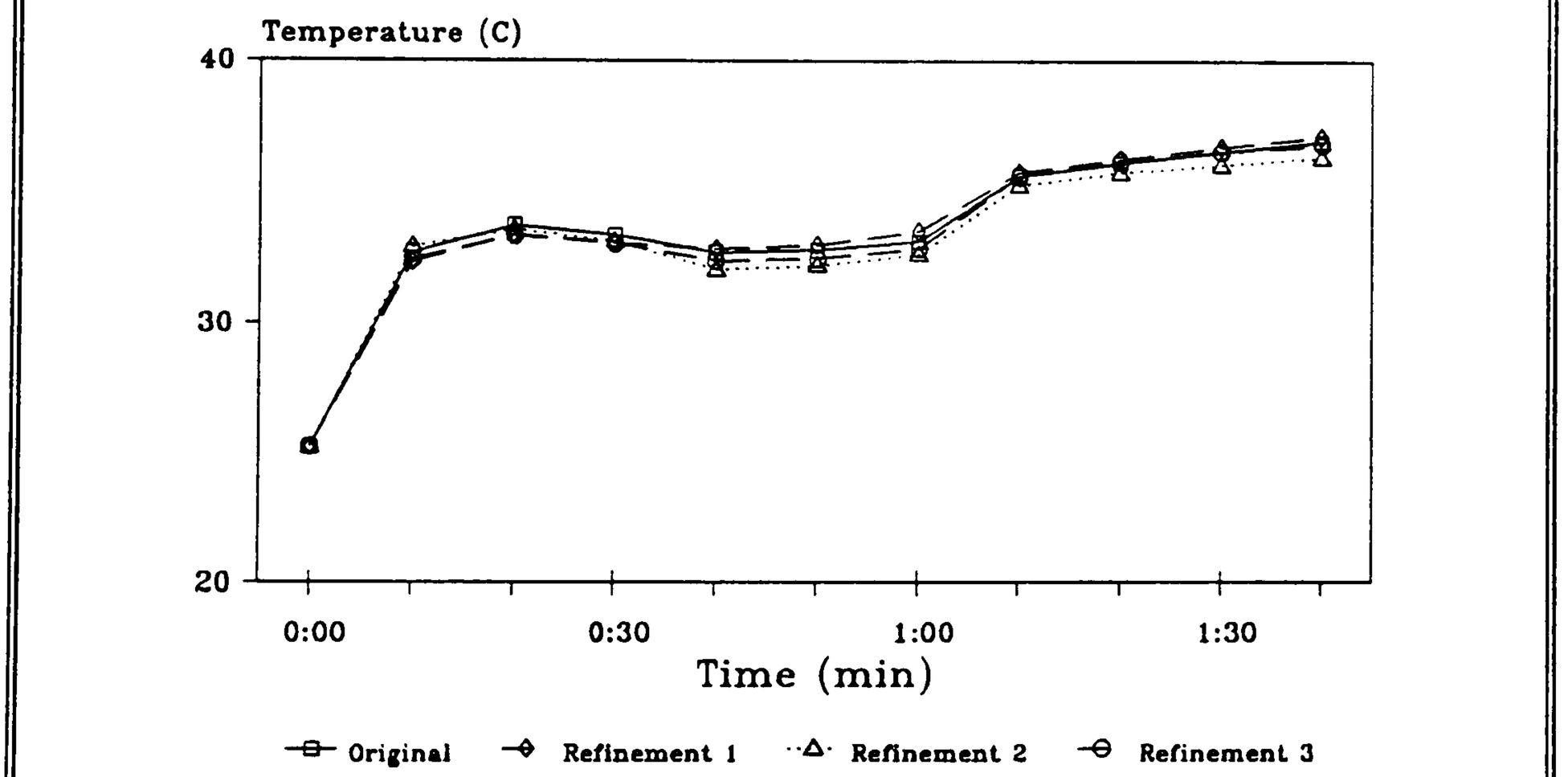

b) T3 location

Figure 3.44 The effect on gas temperature predictions within the Hospital ward using different grid-sizes

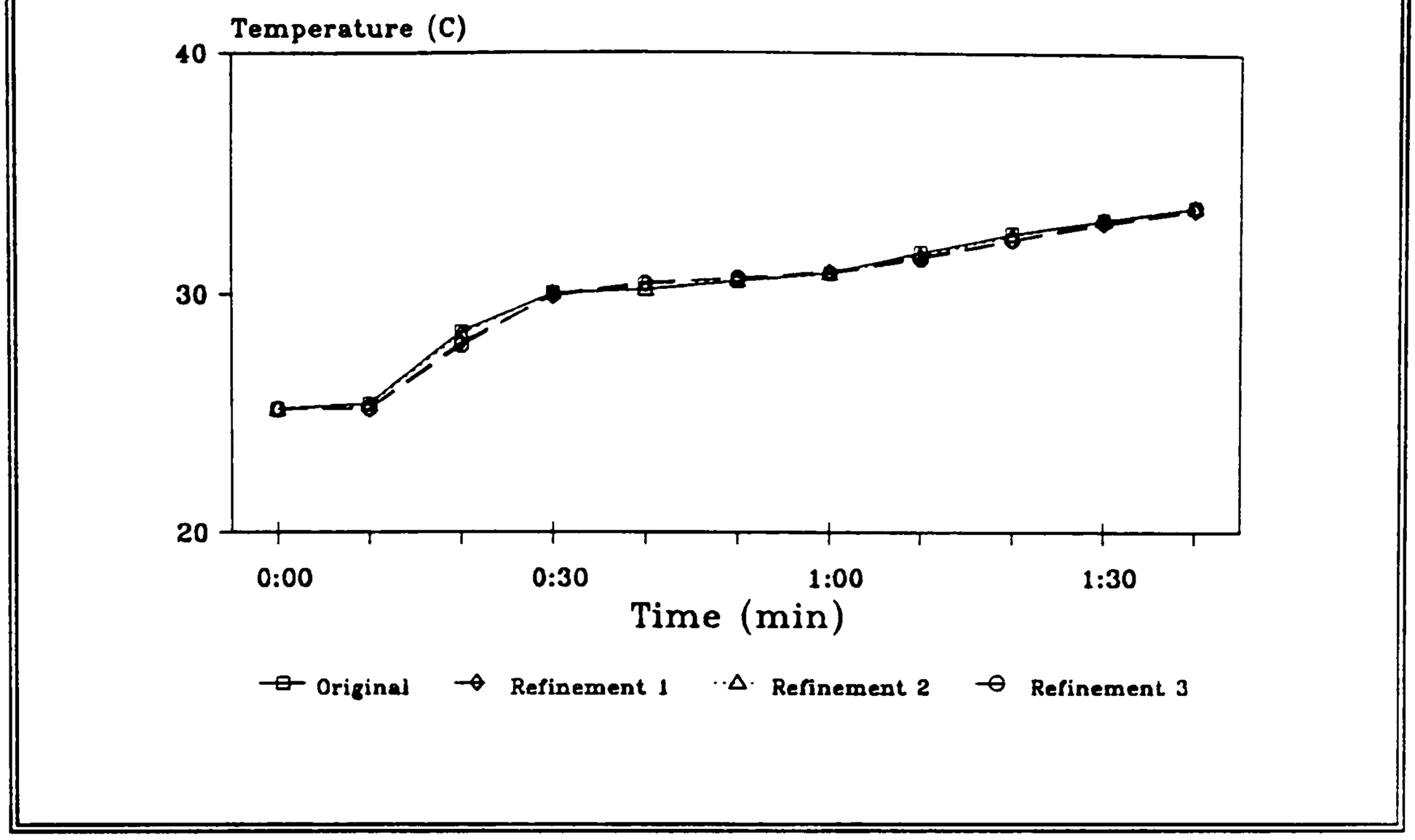

c) T5 location

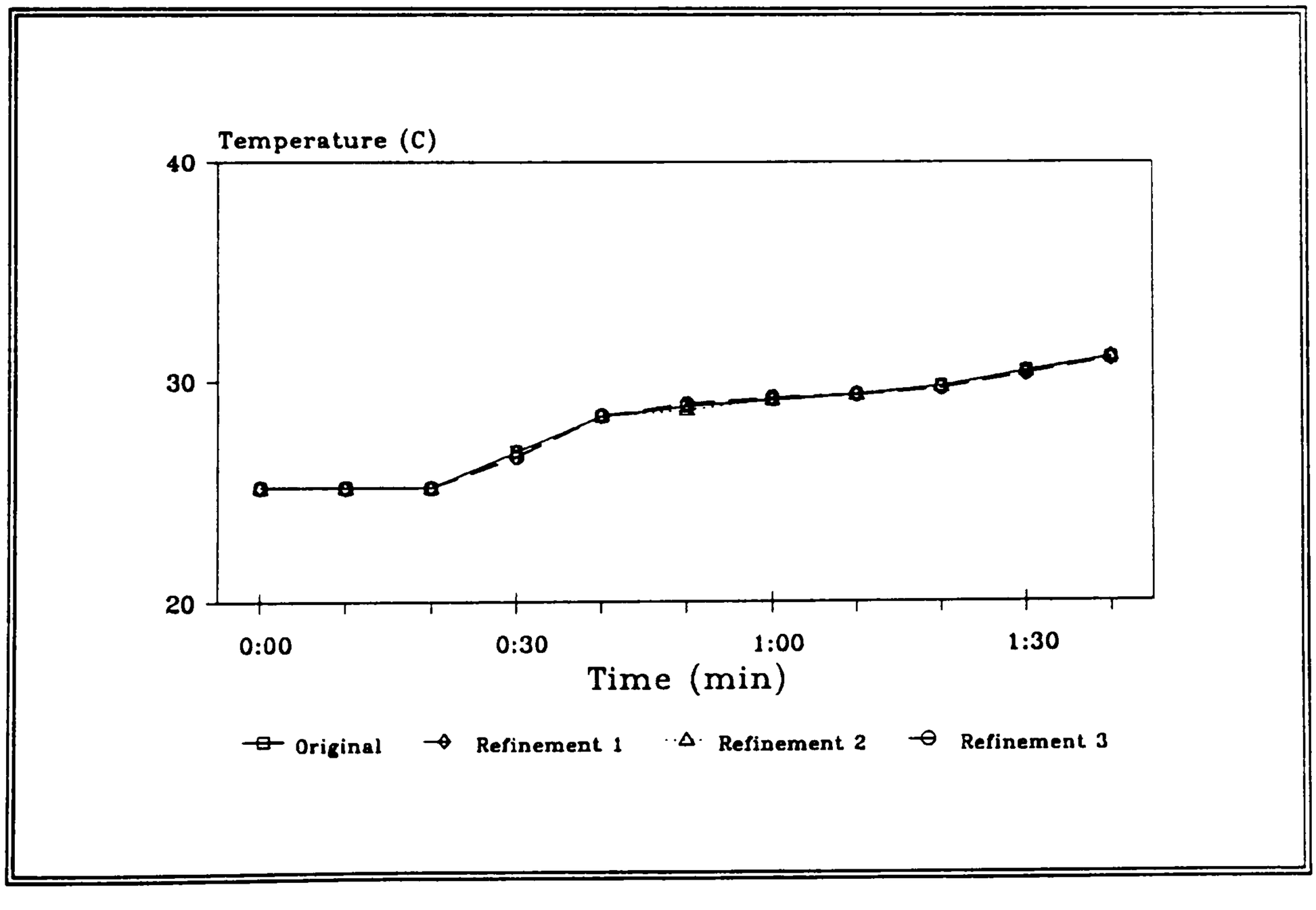

d) T7 location

Figure 3.44 Gas temperature predictions with different grid-sizes (continued)

As can be seen in chapter 5 the addition of the water phase already presented a considerable strain on the amount of CPU time needed to carry out the simulations. Hence, in view of the amount of CPU time required per time step and based on the results of the modest grid-refinement study, a grid of 2310 cells provides a suitable basis for model development.

3.3.5 Conclusions

The above two distinct fire simulations clearly highlight the complexity of the fire phenomena and effect of fire orientations and compartment conditions.

Due to these factors the importance of detailed experimental results are made more apparent and urgent. This can clearly be seen in the above two cases. The office fire was sparsely instrumented in terms of necessary thermocouple locations. Even the measurements of the combustion products were questionable as several adjustments were needed to fit predictions to measured temperatures.

The hospital ward fire simulation provided a more solid base for model validation due to the number of thermocouple locations positioned within the room and details of the room characteristics provided. Even the initial experimental error in the weight loss measurements can not detract from the fairly good degree of accuracy achieved for the temperature predictions.

From a brief overall review of the predictions made for the two distinct fire scenarios it can clearly be seen that with the details provided the results are qualitatively correct. In fact it could be argued that quantitative results were obtained in the case

of the hospital ward fire. However, further improvements are necessary whereby these are dependent on detailed experimental information.

A further consideration to be taken into account is the grid-size used. Though the modest grid-refinement study for the hospital ward fire indicated that temperature predictions were not significantly affected by the grid-distribution further investigation is desirable.

3.4 Summary

This chapter presented the simulation results for the steady-state and transient fire scenarios.

The steady-state model which formed part of an initial feasibility study was tested using a modified office fire configuration. However, the transient model was validated using two distinct fire scenarios. The first scenario involved the office fire compartment with an open doorway which enabled the hot combustion products to escape. The second compartment was closed and based on a hospital ward configuration.

The results for all three scenarios were presented and discussed. Whenever possible predictions were compared with experimental measurements. These indicated that qualitatively correct results were obtained for the office fire scenarios. Significantly better results were obtained for the hospital ward fire. These in turn highlighted the need for detailed and accurate measurements. Furthermore, discussions with respect

to grid-refinement studies and necessary processing times were made.

Chapter 4

Two-Phase Modelling

Chapter 4 Two-Phase Modelling

4.1 Introduction

Having developed a one-phase fire model capable of predicting temperature distributions within compartments especially with respect to a sprinkler element, the next stage is to activate the sprinkler.

It is the purpose of this chapter to outline the models developed to simulate sprinkler activation in steady-state as well as in transient situations. For both events the established flow fields and temperature distributions obtained from the fire simulations in chapter 2 were used as the initial conditions for the gas phase. As in the previous chapter, the starting point of the simulation is the development of the partial differential equations.

For a fire-sprinkler interaction model these equations need to be able to deal with the flow of two distinct fluids; gas and liquid, together with the general physical laws that describe the associated interphase friction resistance and heat/mass transfer between the two phases. These differential and empirical relations are presented both for steady-state and transient conditions in this chapter.

For completeness and clarity the remainder of this chapter has been divided into six main sections. Sections 4.2 and 4.3 are devoted to the steady-state and time-dependent equations and relations that deal with a fire and sprinkler interaction model. Within each of these sections the dependent and independent variables are highlighted; along with their respective conservation equations of mass, momentum, and energy which

are presented in the general form. The auxiliary equations necessary for completeness of the model are also presented. The discretisation of the sets of equations into a set of algebraic finite-difference equations is shown in section 4.4. The numerical solution procedure IPSA used to solve for the algebraic set of equations is outlined in section 4.5, along with a brief desciption on using the computer package PHOENICS for two-phase flow calculations. A summary of this chapter is given in section 4.6.

4.2 The Steady-State Fire-Sprinkler Model

4.2.1 Introduction

This section is devoted to detailing the equations, both partial differential and auxiliary, necessary for developing a steady-state two-phase mathematical model of a fire-sprinkler situation. Whenever necessary further background information for individual topics covered will be given. It should be noted that as the following section is an extension to the single-phase fire model presented in chapter 2, frequent references to the chapter will be made to avoid unnecessary replication.

4.2.2 The Dependent and Independent Variables

The independent variables used are the width, height and length; x, y and z of a cartesian co-ordinate system.

The dependent variables solved for are the velocities of the gas and liquid phases in the three space directions u_g, u_l, v_g, v_l, w_g and w_l; along with the pressure p, which

is assumed to be the same for both phases. The gas enthalpy H_g, the concentration of water vapour within the gas phase, c, as well as the gas and liquid volume fractions r_g and r_l are solved for including the effect of evaporation. The *shadow* volume fraction r_s is the volume fraction in the absence of evaporation. The two turbulence parameters, the kinetic energy, k, and its dissipation rate for the gaseous phase, ε, are also evaluated.

4.2.3 The General Differential Equations

The generalised conservation equation for the steady-state, two-phase model is of the same form as the steady-state, single-phase model (see chapter 2), except that the volume fractions of each phase needs to be taken into consideration. In that way the equation can be written as:

$$\underset{\uparrow}{\text{div}}\left(r_i\rho_i V_i\Phi_i - \underset{\uparrow}{r_i\Gamma_{\Phi i}\text{grad}\Phi_i} \right) = \underset{\uparrow}{r_i S_{\Phi i}} \qquad (4.2\text{-}1)$$

convection diffusion source

where r is the volume fraction and the subscript i refers to the phase in question; gas (g) or liquid (l).

In that way the continuity equation of the flow field is given by:

$$\text{div}\left(\rho_i V_i \right) = 0 \qquad (4.2\text{-}2)$$

4.2.4 The Conservation of Mass Equations

In order to satisfy the mass-conservation principle, the volume fractions, densities and velocities of the two-phases obey the following equation:

$$\mathrm{div}(r_i \rho_i V_i) = r_i S_i \qquad (4.2\text{-}3)$$

where r_g and r_l are the volume fractions of the gas and liquid phases respectively. These are related by the *space sharing* condition:

$$r_g + r_l = 1.0 \qquad (4.2\text{-}4)$$

The source terms S_g and S_l take into account the mass transferred between the two phases due to the evaporation of the particles.

4.2.5 The Conservation of Momentum Equations

The conservation equation of momentum for the gas and liquid phases is given by:

$$\mathrm{div}(r_i \rho_i V_i \Phi_i - r_i \Gamma_\Phi \mathrm{grad}\Phi) = S_\Phi \qquad (4.2\text{-}5)$$

where the subscript i refers to the phase in question; gas or liquid. Φ stands for u_g, u_l, v_g, v_l, w_g and w_l. Γ_Φ is the diffusion coefficient. The source terms for S_Φ are given in Table 2.

4.2.6 The Conservation of Energy Equations

Let H_g stand for the gas enthalpy per unit mass. Then the conservation of energy equation for the gas phase is given by:

$$\text{div} \left(r_g \rho_g V_g H_g - r_g (\lambda_g / Cp_g) \text{ grad } H_g \right) = S \qquad (4.2\text{-}6)$$

The term on the right hand side is the source term which prescribes the rate of heat transferred from one phase to another.

4.2.7 The Auxiliary Relations

The above set of equations specify the necessary conservation laws. In order to complete the mathematical formulation certain correlations need to be specified to close the problem. These relations deal with the interphase heat and mass transfers and the friction between the gas and the particles. The assumptions made are that the gas and the particles are dispersed within a control-volume and that the droplets are spherical. These are initial assumptions made to simplify the nature of the equations.

Fire Source

The method used to describe the location and strength of the fire was not altered for the two-phase calculation; see sections 2.2.7 and 5.2 for further details.

Turbulence Modelling

Turbulence not only plays a vital role in single-phase flows, but can also be found in many two-phase flow situations. In the case of a particulate phase this leads to the production of vortices behind the particle. The scale of these would be relative to the particle in question. However, little is known about the quantitative effects of particle size and concentration on the turbulence parameters [Crowe et al(1975)]. Hence, no method as yet exists to deal with turbulence in a two-phase situation [Lumley (1978)]. Therefore, the two-equation k-ε turbulence model formulated for the single-phase steady-state fire model, equations (2.2-8) and (2.2-9) was not altered to take into account the dispersed liquid phase. Instead it was only applied to the gas phase calculations assuming that the turbulence created by the particles are negligible.

The Interphase-Friction Coefficient

The ability to predict the interphase drag or the relative velocity between phases is of considerable importance for modelling a two-phase system, as the use of a reliable interphase drag correlation can significantly affect the results.

Studies of the magnitude of the drag force on spheres in a steady motion of a fluid began with Newton's experiment in 1710 where it was shown that at high velocities the forces exerted on the sphere were mainly due to the inertia effect [Soo(1967)]. Stokes suggested in 1850 that at low relative velocities the inertial effect was so small that it could be neglected from the Navier-Stokes equations. This asymptotic approximation gives a symmetric flow field about a sphere. The drag force can be related with a drag coefficient, C_D, to the particle Reynolds number. The interface

friction force for flow around a sphere is related to the drag coefficient as shown by the equation [Bird et al (1960)]:

$$F = 0.5 * C_D * \rho_g * A_p * V^2_{slip} \qquad (4.2\text{-}7)$$

where ρ_g is the density of the gas phase, A_p is the total projected area of the liquid phase present within a control-volume given by the equation:

$$A_p = \frac{1.5 * r_l * Vol}{d} \qquad (4.2\text{-}8)$$

where Vol is the volume of the cell and d the droplet diameter.

V_{slip} is the slip velocity between the phases calculated by the function:

$$V_{slip} = \sqrt{\{ (u_g - u_l)^2 + (v_g - v_l)^2 + (w_g - w_l)^2 \}} \qquad (4.2\text{-}9)$$

Subsequent experiments resulted in the *standard drag coefficient curve*, see figure 4.1, which is applicable to a single solid sphere moving at constant velocity in a still, isothermal, incompressible fluid, which is infinite in extent. A considerable amount of research has been carried out to obtain a clearer idea of the effects of different types of flow fields on a single particle. Clift and Gauvin (1971) reviewed these studies which show that the drag experienced by a solid particle moving through a fluid is dependent on a number of factors such as turbulence and particle shape. In this review they present their own equation, equation (4.2-10) shown below, which represents the standard drag curve throughout the transitional and Newton regimes, ie. it is applicable for $Re<10^5$.

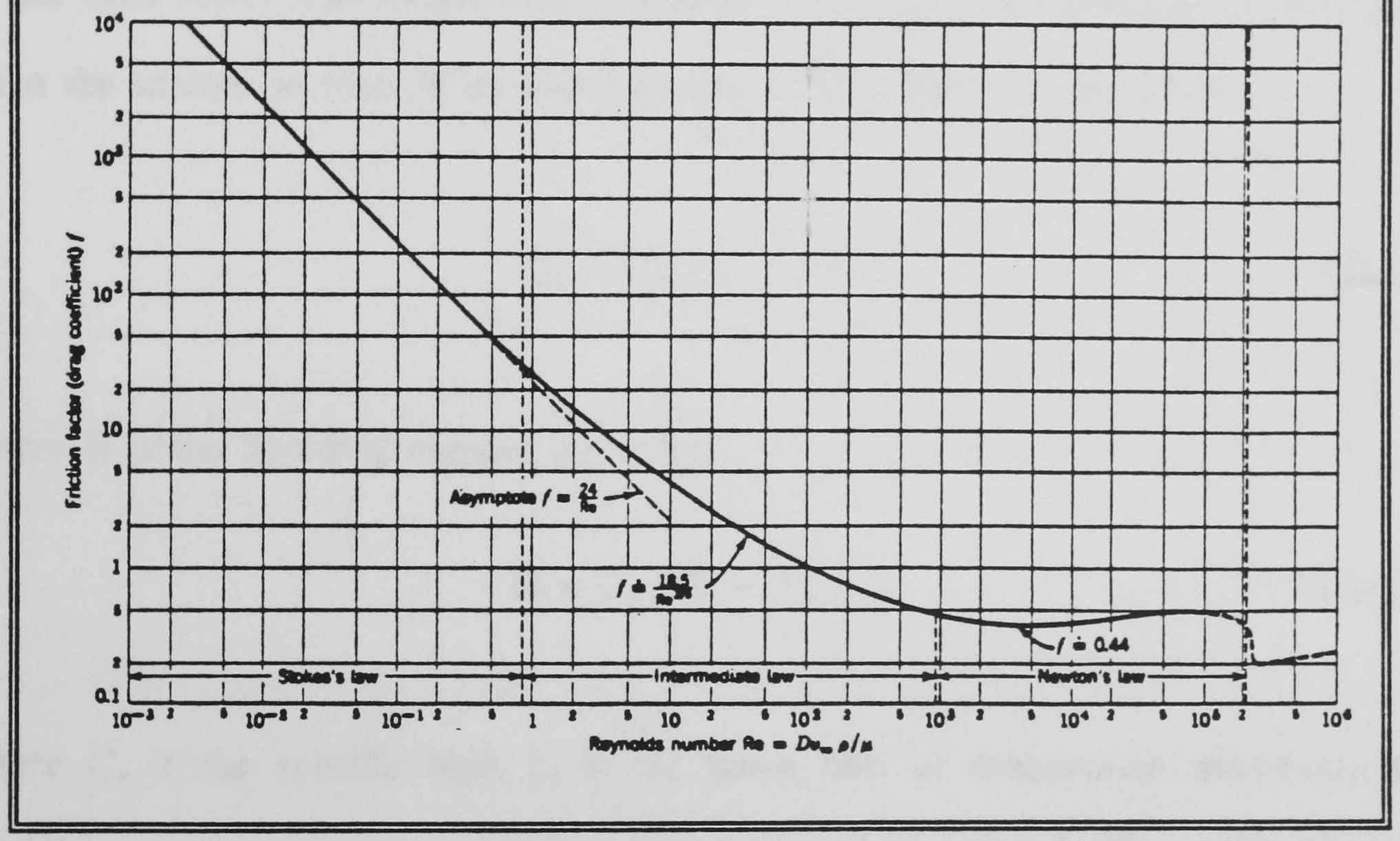

Figure 4.1 Drag Coefficient for spheres moving relative to a fluid [Bird et al(1961]

$$C_D = \frac{24}{Re} * (1+0.15*Re^{0.687}) + \frac{0.42}{1.0+4.25*10^4*Re^{-1.16}} \qquad (4.2\text{-}10)$$

where Re is the particle Reynolds number given by:

$$Re = d * V_{slip} / \nu \qquad (4.2\text{-}11)$$

where ν is the laminar kinematic viscosity.

It has been shown that evaporation can reduce the drag coefficient due to mass flux from the surface so tl at [Wise and Agoston (1958), Crowe et al(1975)]:

$$C_D = C_D / (1 + B) \qquad (4.2\text{-}12)$$

where B is the Spalding number given by:

$$B = C_p * (T_g - T_l) / L \qquad (4.2\text{-}13)$$

where C_p is the specific heat, L is the latent heat of evaporation. However, the Spalding number is only significant for burning fuel droplets [Wise and Agoston (1958), Crowe et al(1975)]. For small evaporating water droplets Yuen and Chen (1976) showed that the mass efflux has little effect on the drag.

Prior to implementation, equation (4.2-10) which has already been used by other workers such as Kircaldy and Markatos (1982), Kostamis (1987) and Markatos and Kircaldy (1983) was compared with other equations for the drag coefficient [Crowe et al(1975), Ishii and Zuber (1979)]. These showed insignificant differences. Hence, equation (4.2-10) was used without adjustment.

The Interphase-Heat Transfer Coefficient

When a particle at a given temperature is submerged in a flowing fluid at a different temperature, heat will be transferred. The conservation of energy equation (4.2-6) takes this phenomena into consideration and solves for the gas phase enthalpy H_g. However, it is convenient to think in terms of temperatures T_g by introducing the specific heat Cp. The enthalpy and temperature are related by the following relationship:

$$H_g = Cp * T_g \qquad (4.2\text{-}14)$$

The specific heat, Cp used in the above equations (4.2-6) and (4.2-14) is a function with respect to its associated temperature, T_g, whereby Cp was calculated using the function given in equations (2.2-7).

Central to the following treatment is the concept of an interface between two phases, with temperature T_s. Using this third temperature, the rate of heat transferred from the gas to the interface is given by Kircaldy and Markatos (1982):

$$\dot{q}_l = -\dot{m} [Cp (T_g - T_s) + L] \qquad (4.2\text{-}15)$$

The Interphase-Mass Transfer Coefficient

As droplets are falling through hot air they are not only heated up but also lose a certain amount of mass due to convection. Once they have been heated up to

evaporation temperature this mass loss is increased due to the effect of the evaporation. For this particular model, as suggested by Spalding (1979) and applied by Kircaldy and Markatos (1982), it is assumed that the mass transferred from the liquid phase to the gas phase is due to the evaporation process.

The relationship suggested by Spalding (1979) is:

$$\dot{m} = \frac{A * \lambda}{Cp * d} \ln \left[1 + \frac{Cp}{L} (T_g - T_s) \right] \qquad (4.2\text{-}16)$$

where λ is the thermal conductivity of the water droplets, Cp is the specific heat, which is assumed constant for both phases, L is the latent heat of evaporation. T_g is the temperature of the gas phase and T_s the temperature at the surface or interface between the particle and the gas. A is the interface surface area per cell given by:

$$A = \frac{6.0 * r_i * Vol}{d} \qquad (4.2\text{-}17)$$

Particle Size Calculation

During the development of this model, several assumptions concerning the particles were made. From early experiments into droplet size distributions several functions were obtained using statistical analysis which were able to fit the data. Mugele and Evans (1951) reviewed these functions, such as the empirical Rossin-Rammler and the log-normal distribution functions, alongside their own proposed equation. However, further studies carried out by Dundas (1974) specifically for sprinkler devices using more advanced measuring techniques found that the gross droplet size distribution obtained could not be fitted entirely by either a log-normal or the Rossin-Rammler distribution. Instead he proposed a composite of these two functions whereby the log-

normal equation is applied to the small droplets and the Rossin-Rammler distribution to the larger droplets, typically above the median droplet size for the spray. With this combination he obtained a better agreement for water droplet size distributions. However, as a first approximation during the development of the model, it was decided to assume a uniform droplet size of 1mm.

The shape of the droplets was the second area where an assumption needed to be made. Droplets remain nearly spherical for a Re<500 if the surface tension is sufficiently strong. In fact water droplets which are smaller than a critical size are stable and do not break up. In order for the drops to retain their spherical shape when falling within a gas certain conditions need to be satisfied. An equation by Gardner and Lane (1959) calculates a critical value taking into account the droplet's diameter, surface tension and the density difference between the droplet and the gas. The equation by Gordon (1959) calculates the critical droplet size taking into account the slip velocity between the gas and the droplet as well as the surface tension and gas density. If any of these criteria was broken the droplet would shatter [Lane (1951)].

The last assumption is concerned with the interaction of the particles themselves. During this study it was assumed that particles are sufficiently distant so as not to be able to interact. In that way it was assumed that they were not able to hit or coalesce with each other, hence diminishing or enlarging their diameter. Furthermore, bouncing off boundaries or collecting on walls or ceiling were not taken into consideration at this point. However, water was able to collect on the floor.

For this model the distribution of the average particle size throughout the domain and the number of particles present within a control-volume was evaluated. The *shadow*

volume fraction method developed by Spalding (1982) (see chapter 1) specifically for finite-difference calculations was employed.

From the shadow volume calculations described in chapter 1, the average diameter of the particles within each control-volume can be determined using the relation:

$$d = d_0 \left(r_l / r_s \right)^{1/3} \qquad (4.2\text{-}18)$$

where d_0 is the initial average diameter of the particles, which are assumed uniform across the sprinkler orifice.

The number of water particles per cell can be cal ulated from:

$$n = \frac{6.0 * r_l * Vol}{\pi * d^3} \qquad (4.2\text{-}19)$$

Surface Temperature

The heat transfer equation (4.2-15) was described in terms of gas phase and interphase temperatures, T_g and T_s respectively. The interphase or particle surface temperature is obtained from an energy balance over a control-volume enclosing the interface. The balance yields [Kostamis (1987)]:

$$T_s = \frac{a_g T_g + a_l T_l + \dot{m} * Cp * T_l}{a_g + a_l + \dot{m} * Cp} \qquad (4.2\text{-}20)$$

where a_g and a_l are the heat transfer coefficients between the gas and the interface, and the interface and the liquid respectively, and T_l represents the liquid temperature.

The heat transfer coefficients, a_g and a_l are evaluated using the following relationships.

The heat transfer coefficient from the gas to the interface, a_g is estimated by assuming a uniform Nusselt number, namely:

$$a_g = 2.0 \tag{4.2-21}$$

The heat transfer coefficient, a_l is evaluated assuming a cubic temperature distribution within the particle [Markatos and Kircaldy (1983)]. Which leads to:

$$a_l = \frac{3\lambda_l}{d/2} \tag{4.2-22}$$

where λ_l is the thermal conductivity of water.

Boundary Conditions

The boundary conditions specified at the walls and free boundaries for the gas phase were those as used in chapter 2 for the single-phase simulations. For the second phase of the Eulerian-Eulerian approach no method exists as yet to incorporate such phenomena such as bouncing on the boundaries. Hence, the conditions used for the gas phase of no-slip on the walls and fixed pressure on the free boundaries were applied to the liquid phase.

4.3 The Time-Dependent Fire-Sprinkler Model

4.3.1 Introduction

The following sub-sections outline an extension for the time-dependence to the steady-state fire-sprinkler model described above. Hence, references will be made to the previous section and if necessary the previous chapter.

4.3.2 The Dependent and Independent Variables

The dependent variables solved for are the same as described in section 4.2.2 for the steady-state simulation, along with the addition of the liquid enthalpy, H_l. The independent variables used are the width, height and length; x, y and z of a cartesian coordinate system, as well as the time, t.

4.3.3 The Differential Equations

A physical situation involving fluid flow and heat and mass transfer is governed by the conservation principles of mass, momentum, energy etc. These principles can be expressed in terms of differential equations which posses a common form. The form of the generalised conservation equation is:

$$\frac{\partial}{\partial t}(r_i\rho_i\Phi_i) + \mathrm{div}(r_i\rho_i V_i\Phi_i - r_i\Gamma_\Phi \mathrm{grad}\Phi) = r_i S_{\Phi i} \qquad (4.3\text{-}1)$$

↑ transient ↑ convection ↑ diffusion ↑ source

4.3.4 The Auxiliary Relations

This sub-section describes the modified auxiliary equations obtained for treating the interphase conditions and general flow conditions for a time-dependent situation.

Fire Source

The fire source was prescribed using the same technique as was outlined for the single-phase time-dependent situations described in section 2.3.4 with further details provided in section 5.3.

Turbulence Modelling

For the same reasons as were detailed for the case of steady-state turbulence modelling, the turbulence model formulated for single-phase time-dependent flow, equation (2.3-2) and (2.3-3) was not altered to take into account the effect of the second phase. Instead it was only applied to the gas phase.

Wall Heat Transfer

The model applied in the one phase time-dependent model, equation (2.3-4) was utilised but was only applicable to the gas phase enthalpy calculations.

The Interphase-Friction Coefficient

The expressions used for the transient interphase-friction force and the drag coefficient

are the same as were used for the steady-state calculations; equation (4.2-7) and (4.2-10) respectively. However, in the time-dependent studies account was made for the effect on the drag coefficients if the particles enter the flame. In this case the drag coefficient is calculated by [Rasbash (1962)]:

$$C_D = 18.5 * Re^{-0.6} \qquad (4.3\text{-}2)$$

In order to know exactly when a droplet enters the flame, the length of the flame, l, needs to be known. This length is calculated from the relationship for enclosure fires [Drysdale (1985)]:

$$l = 0.23 * (Q/1000)^{0.4} - 1.02 * D \qquad (4.3\text{-}3)$$

where Q is the total heat release of the fire and D is the diameter of the fire source.

The Interphase-Heat Transfer Coefficient

The conservation of energy equation solves for the gas enthalpy H_g and the liquid enthalpy H_l. However, it is convenient to think in terms of temperatures T_g and T_l by introducing the specific heats Cp_g and Cp_l for the two phases respectively. The enthalpies and temperatures are related by the following relationships:

For the gas phase:

$$H_g = Cp_g * T_g \qquad (4.3\text{-}4)$$

For the liquid phase:

$$H_l = \begin{cases} Cp_l * T_l & \text{for } \dot{m} = 0 \\ Cp_l * T_l - L & \text{for } \dot{m} \neq 0 \end{cases} \quad (4.3\text{-}5)$$

where L is the specific latent heat of evaporation.

The specific heats, Cp_g and Cp_l, used in the above equations (4.3-4) and (4.3-5) are functions with respect to their associated temperatures, T_g and T_l. The function used for the specific heat of the gas was the same as applied to the one phase simulation, see equation (4.2-15). The specific heat for the liquid was obtained from statistical analysis performed on the data from Rogers and Mayhew (1985). The function is:

$$Cp_l = 5508.0 - 1.9963E\text{-}3 * H_l + 7.4966E\text{-}10 * H_l^2 \quad (4.3\text{-}6)$$

Central to the following treatment is the concept of an interface between two phases, with temperature T_s. Then, using this third temperature, the rate of heat transferred from the gas to the interface, $\dot{q}_g$, and from the interface to the particle interior is evaluated using the relations, $\dot{q}_l$:

$$\dot{q}_g = a_g * A(T_g - T_s) \quad (4.3\text{-}7)$$

$$\dot{q}_l = a_l * A(T_s - T_l) \quad (4.3\text{-}8)$$

where a_g and a_l are the heat transfer coefficients between the gas and the interface, and the interface and the liquid respectively.

It may be noted here, that the above heat transfer relations; (4.3-7) and (4.3-8), are

based only on convection. Following studies by Hoffmann and Gauvin (1961) and Rasbash (1962) to evaluate the importance of radiation on particles they concluded that for droplets of about one millimetre in diameter, the magnitude of radiation absorbed is negligible small.

The heat transfer coefficients, a_g and a_l are evaluated using the following relationships.

The heat transfer coefficient from the gas to the interface, a_g is:

$$a_g = Nu * \lambda_g/d \qquad (4.3\text{-}9)$$

where Nu is the Nusselt number. In the case of laminar flow conditions, only conduction is taken into consideration so that:

$$Nu = 2.0 \qquad (4.3\text{-}10)$$

However, due to the relative motion of the fluid the local heat transfer coefficient depends on the velocity and the temperature profile. From experiments a number of correlations have been obtained for different flow conditions and different geometries of the objects suspended within the fluid.

The correlation used within this model was obtained by Ranz and Marshall (1952,i) for evaporating water droplets. To calculate the heat transfer between the gas and the drops the function is [Bird et al (1960), Whalley (1987)]:

$$Nu = 2.0 + 0.6\ Re^{1/2}\ Pr^{1/3} \qquad (4.3\text{-}11)$$

where Pr is the Prandtl number of the gas phase given by:

$$Pr = 0.790282 - 4.28334E\text{-}4 * T + 5.18038E\text{-}7 * T^2 - 1.7871354E\text{-}10 * T^3 \quad (4.3\text{-}12)$$

The above equation was obtained by statistically fitting a polynomial to the data given by Rogers and Mayhew (1985).

The heat transfer coefficient, a_t is evaluated assuming a cubic temperature distribution within the particle, see equation (4.2-22) [Markatos and Kircaldy (1983)].

The Interphase-Mass Transfer Coefficient

Mass transfer involves the transportation of a mixture from a region of higher to an area of lower concentration. If this transport is due to the motion of a fluid it is said to be convected. In this particular study the rate of mass transfer, the evaporation of small water droplets within a hot gas atmosphere is due to the concentration difference between the hot dry air produced by the fire and the saturated concentration level of the droplets. The equation governing the rate of mass transfer is analogous to the interphase heat transfer coefficients discussed in the previous section. Hence, the interphase mass transfer equation is given by:

$$\dot{m} = b*A(c_i - c_g) \quad (4.3\text{-}13)$$

where b is the mass transfer coefficient and c_i and c_g are the concentration of water vapour at the interface and in the gas respectively [Kreith and Black (1980)].

The mass transfer coefficient, b, is evaluated using:

$$b = \frac{Sh * D}{d} \qquad (4.3\text{-}14)$$

where D is the mass diffusivity of water in gas, and d is the average droplet diameter. Sh is the Sherwood number which is analogous to the Prandtl number used within the heat transfer calculations.

As in the case of heat transfer, the evaporation from a spherical droplet into still air is given by Sh = 2.0. In the more general cases of forced convection, Frössling proposed the following expression for evaluating the Sherwood number for a variety of flow situations. The expression is:

$$Sh = 2.0 + \eta\ Re^{\alpha}\ Sc^{\beta} \qquad (4.3\text{-}15)$$

where α, β and η are constants which vary depending on the Reynolds number and the particle diameter investigated. In a review by Ahmadzadeh and Harker (1974) values for these constants are specified for a number of different cases investigated. This list also includes the correlation obtained by Ranz and Marshall (1952,ii) for evaporating water droplets. The correlation is:

$$Sh = 2.0 + 0.6\ Re^{1/2}\ Sc^{1/3} \qquad (4.3\text{-}16)$$

Following their study, which was initially restricted to Re<200.0, water droplet diameter range between $0.6*10^{-4}$ to $1.1*10^{-3}$ m and air temperatures up to 220°C, they showed that their results could be *extrapolated with remarkable accuracy five times*

beyond their experimental range of Reynolds numbers.

The concentration of water vapour present within the air was calculated using the following equation [Kreith and Black (1980)]:

$$c_g = \frac{M_w * hum * p_{sat}}{R_u * T_g} \qquad (4.3\text{-}17)$$

where M_w is the molecular weight of water, hum is the relative humidity of the gas, p_{sat} is the saturation pressure and R_u is the universal gas constant.

The concentration of water present at the interface was calculated using [Kreith and Black (1980)]:

$$c_i = \frac{M_w * p_{sat}}{R_u * T_l} \qquad (4.3\text{-}18)$$

Particle Size Calculation

The average diameter of the particles present within each control-volume is evaluated using the same method as outlined in the section 4.2.7, dealing with the particle size calculation for the steady-state situation.

Surface Temperature

In the section describing the interphase heat transfer coefficients the details of calculating the amount of heat transferred between the phases was described in terms

of three temperatures; gas phase temperature T_g, liquid phase temperature T_l and interphase temperature T_s.

The interphase or particle surface temperature is obtained from an energy balance over a control-volume enclosing the interface. The balance yields:

$$T_s = \frac{a_g T_g + a_l T_l}{a_g + a_l + \dot{m} (Cp_g - Cp_l)} \qquad (4.3\text{-}19)$$

where a_g is the heat transfer coefficient between the gas and the interface evaluated using equation (4.3-9), and a_l is the heat transfer coefficient between the interface and the centre of the particle evaluated using equation (4.2-22).

Clear details on how the interface temperature calculations are incorporated in the solution scheme can be found in Appendix 3.

Boundary Conditions

The boundary conditions used were those as described in chapter 2, for the gas phase. The boundary conditions for the second phase at the walls and free boundaries were those as specified in section 4.2.7.

4.4 The Numerical Solution Procedure

4.4.1 Introduction

In the previous section the partial-differential equations which govern steady-state and time-dependent fire and sprinkler interactions were presented. The numerical integration scheme used to solve the set of differential equations is presented in this chapter.

The numerical method to be described within this chapter is based on the control-volume formulation. The compartments used to investigate the fire and sprinkler interactions have been discretised into a finite number of control-cells, each of which can be regarded as a control-volume. The discretisation equations derived within this chapter are obtained by integrating the governing differential equations over a small region called the control-volume. The final algebraic form of the general, momentum and continuity equations are shown in sections 4.4.3, 4.4.4 and 4.4.5 respectively.

The resulting set of simultaneous equations are solved for using the algorithms SIMPLEST (see Appendix 3) and IPSA, see section 4.5.2. These are illustrated along with a brief outline of the computer package PHOENICS, in section 4.5.2 which has these algorithms built in.

4.4.2 The Finite-Difference Grid

As this particular study is a continuation to the one-phase fire simulation the division of the compartment into thousands of control-volumes was adhered to. Full description

of this method can be found in chapter 2, section 2.4.2.

4.4.3 The General Equation Discretisation

The algebraic forms of the general finite-difference equations for transient and steady-state are obtained in the same manner as described in sections 2.4.3 and 2.4.4 for the single-phase equations respectively. In fact the form of the final discretised equations are the same as shown in equations (2.4-9) and (2.4-11). Account of the two-phases are made in the flux terms F and D; the mass flow rate and diffusion flux across a control-face respectively. The modified equations for F and D are:

$$F = r_i \rho_i V_i \; A \qquad\qquad D = \frac{r_i \Gamma_\phi A}{\delta^*}$$

4.4.4 The Momentum Equation Discretisation

In the same manner as in the single-phase velocities for the momentum equation discretisation needed adjustments, the two-phase velocities need altering. This is performed in a similar manner as described in section 2.4.5, whereby the two-phases are taken into account in the 'A' terms. Thus, there are now six rather than three velocity equations which must be solved. The corresponding finite-difference equations for the velocities are:

$$(A_P - S_{uP}^{\,P}) \; (u_i)_e = \Sigma \; A_j \; (u_i)_j + S_{uP}^{\,C} \; V_C + (p_P - p_E) \; A_e$$

$$(A_P - S_{vP}^{\,P}) \; (v_i)_e = \Sigma \; A_j \; (v_i)_j + S_{vP}^{\,C} \; V_C + (p_P - p_N) \; A_n$$

$$(A_P - S_{wP}^{\,P}) \; (w_i)_e = \Sigma \; A_j \; (w_i)_j + S_{wP}^{\,C} \; V_C + (p_P - p_H) \; A_h \qquad (4.4\text{-}13)$$

where i refers to the phase in question and j takes the value E, W, N, S, H or L to identify the neighbouring staggered velocities. S_{uP}, S_{vP}, S_{wP} are once again the sources/sinks of momentum.

4.4.5 The Continuity Equation Discretisation

As in the case of single-phase flow the flow field in equation (4.2-1) must satisfy the continuity equation (4.2-2). Hence, the flow rates through the faces of the control-volume need to satisfy the discretised form of the continuity equation. Therefore, the continuity equation needs to be integrated over the control-volume in the same fashion as the general differential equation.

Integrating equation (4.2-2) over a typical control-volume and over a finite step in time gives:

$$\iiint \frac{\partial}{\partial t}(r_i\rho_i\Phi_i) + \mathrm{div}(r_i\rho_{i\Phi}\mathbf{i} - r_i\Gamma_\Phi \mathrm{grad}\Phi_i)\, dVol = 0 \qquad (4.4\text{-}14)$$

which discretises into the form:

$$(\rho_P - \rho_P^{old}) * Vol + (\rho_i u_i r_i)_e A_e - (\rho_i u_i r_i)_w A_w + (\rho_i v_i r_i)_n A_n - (\rho_i v_i r_i)_s A_s + (\rho_i w_i r_i)_h A_h - (\rho_i w_i r_i)_l A_l = 0 \qquad (4.4\text{-}15)$$

For the steady-state situation the discretisation equation is:

$$(\rho_i u_i r_i)_e A_e - (\rho_i u_i r_i)_w A_w + (\rho_i v_i r_i)_n A_n - (\rho_i v_i r_i)_s A_s + (\rho_i w_i r_i)_h A_h - (\rho_i w_i r_i)_l A_l = 0 \qquad (4.4\text{-}16)$$

4.4.6 The Boundary Conditions

The boundary conditions are dealt with in exactly the same manner as described for the one-phase boundary conditions in section 2.4.10.

4.5 The Solution of the Equations

The control-volume equations derived in the previous section form a set of simultaneous equations which are solved using the iterative procedure IPSA (InterPhase Slip Algorithm) [Spalding (1977), (1983)]. IPSA, a variant of SIMPLEST which was described in section 2.5.2, allows the two phases to be treated as interspersed continua competing for the occupance of the same space. As this algorithm is well documented only a brief outline of its implementation is presented here.

4.5.1 The IPSA Algorithm

For multi-phase problems the number of equations which require solution is greatly increased, as is the specification of auxiliary relations and boundary conditions. However, as these equations are of the same kind as for a single-phase problem the degree of difficulty will not increase.

IPSA [Spalding (1983)] is an algorithm for solving the momentum equations of several interspersed and mutually slipping phases which share a single pressure.

As in the case of SIMPLEST special care needs to be taken when solving for the single shared pressure. IPSA satisfies the continuity equation and predicts a pressure field which is satisfactory across the whole domain. Also, if all but one volûme fraction were to diminish, the scheme is able to proceed as if for only a single-phase.

A further consideration to be taken into account is that the two phases present are *linked* together with respect to the interphase friction, heat and mass transfers. This linkage is taken into account in the addition of PEA (Partial Elimination Algorithm) [Spalding (1980)] within IPSA, whereby added source terms are solved for during the iterations.

When solving the equations iteratively, one major constraint is the compliance of the *space sharing* condition equation (1.4-1). In order for this equation to be satisfied a *trick* is employed within IPSA.

Let r_g^* and r_l^* be the results of solving the individual continuity equations. These however, may not necessarily sum to unity as required. In order that they may, the following two equations are used to solve for the actual volume fractions. The equations are:

$$r_g = r_g^* / (r_g^* + r_l^*)$$

$$r_l = r_l^* / (r_g^* + r_l^*) \qquad (4.5\text{-}1)$$

In this way it is assured that r_g and r_l sum to unity as required, whether r_g^* and r_l^* do or not.

The solution cycle takes the form:

1. guess the initial field for all variables
2. solve for the enthalpies
3. solve for the volume fractions using equation (4.5-1)
4. using the guessed pressure, solve for the velocities using the momentum equation
5. using the volume fractions and the velocities solve for the joint continuity equation to obtain the cor tinuity error for each cell
6. differentiate the joint continuity equation with respect to pressure so as to derive the correction equation
7. solve in the same manner as used in SIMPLEST (see Appendix 3)
8. apply appropriate corrections to the pressure and the velocities
9. return to step 2 and repeat until convergence has been achieved

In a single cycle of the iteration the equations are solved for in order of enthalpy, volume fraction, velocity and pressure correction. It should be noted that the calculations of the volume fractions include the interphase mass transfer which is closely connected to the enthalpies and the heat transfer.

4.5.2 The Computer Package

The algorithm IPSA outlined in the above section, section 4.5.1, forms an integral part of the solution procedure employed within the general fluid-flow package PHOENICS [Spalding (1981), Rosten and Spalding (1986)].

4.6 Summary

The situation of an activated sprinkler and its interaction with the hot buoyant combustion products generated by a fire has been addressed within this chapter. Two-phase mathematical models for steady-state and time-dependent situations, employing the Eulerian-Eulerian approach have been presented.

The discretisations of the general transport equations along with the iterative solution procedure IPSA, utilised by PHOENICS, were outlined.

Φ	Γ_Φ	S_Φ
1	0	0 (continuity)
u_g	μ_{eff}	$-\frac{\partial p}{\partial x} r_g + \frac{\partial}{\partial x}(\mu_{eff} \frac{\partial u}{\partial x}) + \frac{\partial}{\partial y}(\mu_{eff} \frac{\partial v}{\partial x}) + \frac{\partial}{\partial z}(\mu_{eff} \frac{\partial w}{\partial x})$ $+ F(u_l - u_g) + \dot{m} u_l$
u_l	0	$-\frac{\partial p}{\partial x} r_l - F(u_l - u_g) - \dot{m} u_l$ + source of particle momentum
v_g	μ_{eff}	$-\frac{\partial p}{\partial y} r_g + \frac{\partial}{\partial x}(\mu_{eff} \frac{\partial u}{\partial y}) + \frac{\partial}{\partial y}(\mu_{eff} \frac{\partial v}{\partial y}) + \frac{\partial}{\partial z}(\mu_{eff} \frac{\partial w}{\partial y})$ $-g(\rho-\rho_{ref}) + F(v_l - v_g) + \dot{m} v_l$
v_l	0	$-\frac{\partial p}{\partial y} r_l - F(v_l - v_g) - \dot{m} v_l$ + source of particle momentum
w_g	μ_{eff}	$-\frac{\partial p}{\partial z} + \frac{\partial}{\partial x}(\mu_{eff} \frac{\partial u}{\partial z}) + \frac{\partial}{\partial y}(\mu_{eff} \frac{\partial v}{\partial z}) + \frac{\partial}{\partial z}(\mu_{eff} \frac{\partial w}{\partial z})$ $+ F(u_l - u_g) + \dot{m} w_l$
w_l	0	$-\frac{\partial p}{\partial z} r_l - F(w_l - w_g) - \dot{m} w_l$ + source of particle momentum
H_g	$\mu_{lam}/Pr_{lam} + \mu_t/Pr_t$	$\dot{q} + [(Cint_g + \max(0,\dot{m}))*(H_{sg} - H_g)]$
H_l	0	$[(Cint_l + \max(0,-\dot{m}))*(H_{sl} - H_l)]$
k	μ_{eff}/Pr_k	$G_K - \rho\varepsilon + G_B$
ε	μ_{eff}/Pr_ε	$(\varepsilon/k) [(G_K+G_B)C_1 - C_2\rho\varepsilon]$

where

G_K and G_B have been defined in Table 1

Table 2 : The Diffusion coefficients and Source Terms of the two-phase conservation equations.

Chapter 5

Validation and Results for Two-Phase Fire-Sprinkler Simulations

Chapter 5 Validation and Results of Two-Phase Fire-Sprinkler Simulations

5.1 Introduction

In order to be able to validate a mathematical model, a plethora of experimental data needs to exist for initial value and comparison purposes. However, as has already been highlighted in chapter 3 the amount of data available from fire experiments is not sufficient to compare even half the predictions the field model makes. This situation becomes more critical in the event of a sprinkler operating. The model then requires a further set of data to take into account the water phase. However, this data is generally not forthcoming due to the difficulty, impossibil :y and expense of making the required measurements. Hence, experimental data involving fire-sprinkler scenarios are not generally available.

Fortunately, the fire scenarios outlined in chapter 3 not only included the activation of a water sprinkler but they were also fairly well instrumented, both before and after the activation. This makes them suitable for initial model validation.

However, prior to developing a transient fire-sprinkler model, the proposed volume-fraction modelling technique was investigated using the steady-state situation. Subsequently, as the results of this study, presented below, showed that the strategy was feasible, a time-dependent model was developed. This two-phase fire-sprinkler model was attempted to be validated using the two transient fire scenarios; an office and a hospital ward fire. These two rooms are not only distinct by the location of their fires and status of the door but also in their location of the sprinkler relative to the fire. In the case of the office scenario, the sprinkler was located about 2.2m away

from the fire, compared to only 0.5m in the case of the hospital scenario. Hence, the following studies can show how well the mathematical model is able to cope with these two contrasting situations. It should be pointed out that during the simulations only the general cooling effect on the gas was considered and not the actual extinguishment of the fire.

The results of the fire scenarios, presented in chapter 3, were used as the initial conditions for the gas phase for the two-phase fire-sprinkler simulations. Unfortunately, not all the required sprinkler details could be measured, making it necessary to draw assumptions, which will be pointed out where necessary.

5.2 Steady-State Simulation

The sprinkler scenario presented below is a continuation of the steady-state fire scenario presented in section 3.2. Hence, the overall description of the office arrangement and the grid used remained unaltered; see figures 3.1 and 3.2 respectively.

The fire was assumed to be still in progress with the same heat release rate of 30kW. The now active sprinkler was situated near the centre of the room, about 1.8m away from the fire source and 0.1m below the ceiling. As no details or measurements concerning steady-state sprinkler activation were available it was assumed that the water was released at a rate of 7kg/sec at an angle of 70° from the line of symmetry. Furthermore, it was assumed that the droplets consisted of a uniform average diameter of 1mm with an initial temperature of 10°C.

5.2.1 Computational Details

As discussed in section 3.2, the results presented below were only accepted once the values of the residuals, pressure correction and mass balances reached $1.0x10^{-4}$. As this current study is two-phase, mass balances for each phase were considered. In order to achieve this criteria around 11000 sweeps were necessary.

5.2.2 Results and Conclusions

Using the above description of the physical set-up and the outlined mathematical model the following results for a steady-state fire-sprinkler simulation were obtained [Hoffmann et al(1988,1989)].

As this scenario is a continuation of the earlier fire simulation, the gas temperatures and flow field for the steady-state simulation were used as an initial field for the gas-phase. Due to this continuity and to illustrate the consequences of an active sprinkler more effectively, the results are displayed through the same locations and positions as for the single-phase fire scenario; see figures 3.3 to 3.7. It should be pointed out, that the following velocity diagrams are of the gas phase as the affects can be seen more clearly.

In figure 5.1-a two planes through the sprinkler (Y=10) and the fire sources (Z=1), illustrate the drastic effect the sprinkler has on the overall gas flow field. The sprinkler forces the air downwards as well as entraining air from its surroundings. The subsequent circulation pattern causes the air to be forced upwards along the walls such as the low wall illustrated. Further note that water collects along the floor, hence reducing the amount of air within the lowest plane (Y=1).

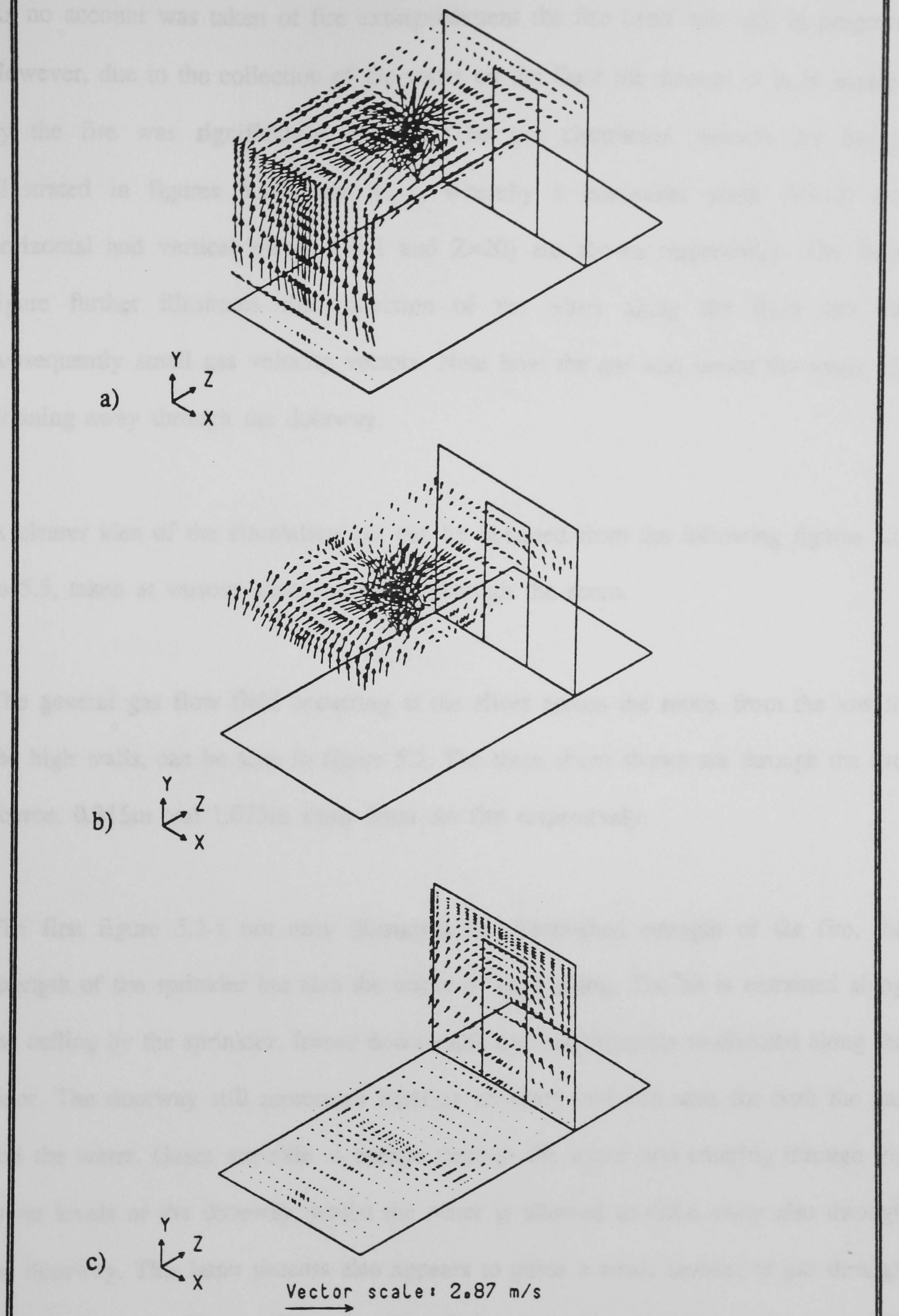

Figure 5.1 Schematic view of office: predicted gas velocity vectors
a) through the fire source and below the ceiling
b) along the floor and near the doorway
c) slice 1.96m above the floor

As no account was taken of fire extinguishment the fire itself was still in progress. However, due to the collection of the water on the floor the amount of heat released by the fire was significantly reduced. The gas circulation patterns are further illustrated in figures 5.1-b and 5.1-c, whereby a horizontal plane (Y=12) and horizontal and vertical planes (Y=1 and Z=20) are shown respectively. The latter figure further illustrates the collection of the water along the floor and the subsequently small gas velocity vectors. Note how the gas and hence the water are draining away through the doorway.

A clearer idea of the circulating gas can be obtained from the following figures 5.2 to 5.5, taken at various slices and slabs through the room.

The general gas flow field occurring at the slices across the room, from the low to the high walls, can be seen in figure 5.2. The three slices shown are through the fire source, 0.315m and 1.075m away from the fire respectively.

The first figure 5.2-a not only illustrates the diminished strength of the fire, the strength of the sprinkler but also the effect of an opening. The air is entrained along the ceiling by the sprinkler, forced downwards and subsequently re-directed along the floor. The doorway still represents itself as an entry and exit area for both the gas and the water. Gases are able to escape through the upper and entering through the lower levels of the doorway, whilst the water is allowed to drain away also through the doorway. This latter process also appears to guide a small amount of gas through the lowest levels. These effects are also observed further along the room, shown in figure 5.2-b, which is 0.315m away from the fire.

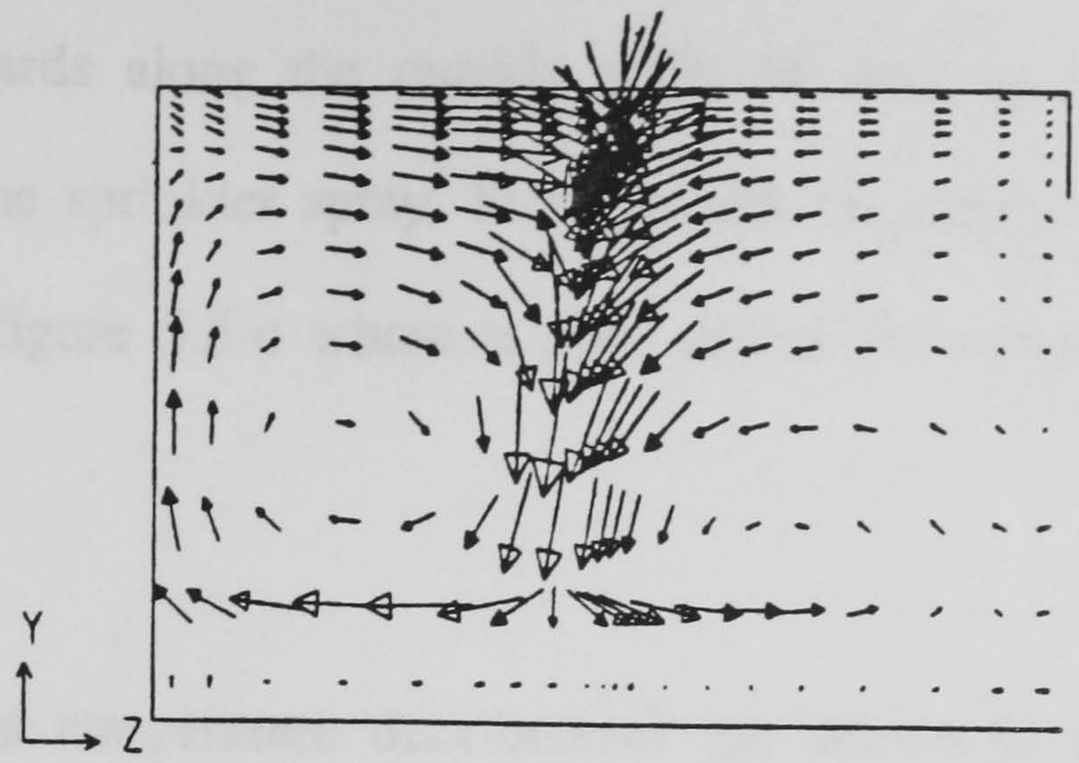

Figure 5.2 Side view of office: predicted gas velocity vectors along the room
a) through the fire source
b) 0.165m away from the fire
c) 1.075m away from the fire/ 0.145m from the wall

The resulting flow field near a wall is illustrated in figure 5.2-c. Note how the gases are pushed upwards along the outside walls as well as forced downwards by the entrainment of the sprinkler spray. More details and explanations for this occurrence can be seen in figure 5.5-c where a slice across the centre of the current plane is shown.

The resulting gas temperature distributions are shown in figure 5.3. These clearly show the drastic reduction in gas temperatures, from around 250°C (see figure 3.5) to about 20°C. As the initially hot gases are rising from the fire source they are entrained by the sprinkler spray, forced downwards and cooled down. In that way the hot gases and the fire source are 'washed out', reducing not only the gas temperatures but also diminishing the strength of the fire source.

Plan views of the office as shown in figure 5.4 clearly demonstrate the new flow field at distinct heights within the office. Near the floor, see figure 5.4-a (Y=2) the gas stream impacts and is re-directed radially outwards from the central sprinkler position until reaching the confining outside walls. Note the entrainment of air through the doorway in the centre of the right hand plane. Entrainment into the sprinkler 'plume' can be observed in figures 5.4-b and 5.4-c, which are 2.0935m and 2.32m above the floor respectively. Note the strengthening entrainment closer to the sprinkler location.

Finally, slices taken across the room are shown in figure 5.5, which illustrate the effect of the walls on the gas circulation. The first plane is through the weakened fire source (Z=1) and depicts the strength of the upward moving air.

The strengthening entrainment and general circulation can be observed in figure 5.5

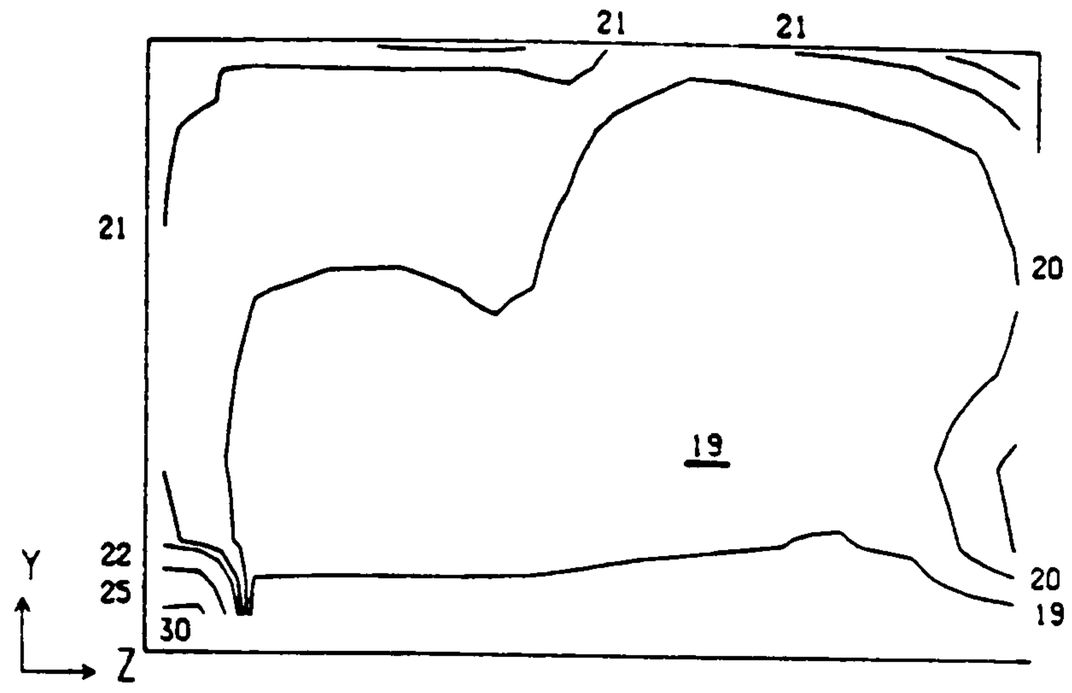

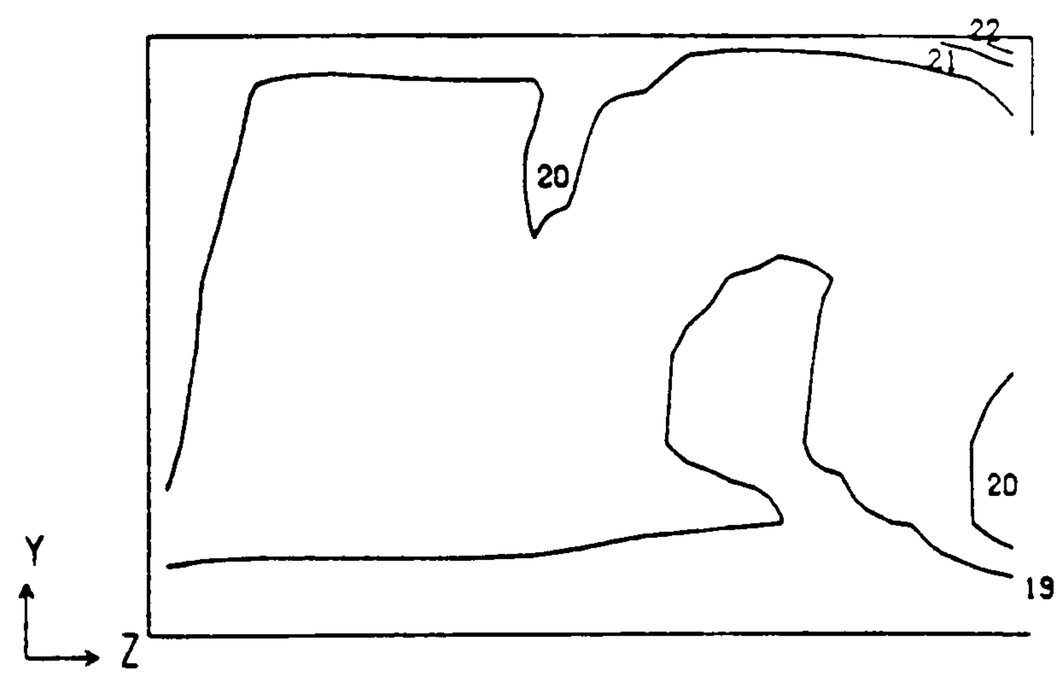

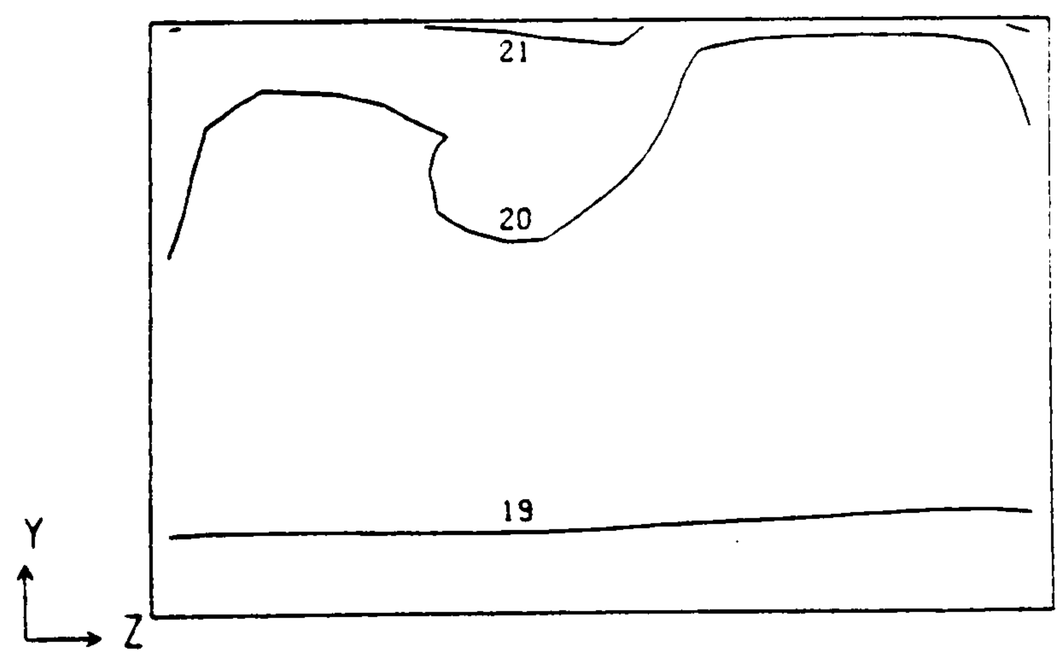

Figure 5.3 Side view of office: predicted gas temperature contours
a) through the fire source
b) 0.165m away from the fire
c) 1.075m away from fire/ 0.145m from the east wall

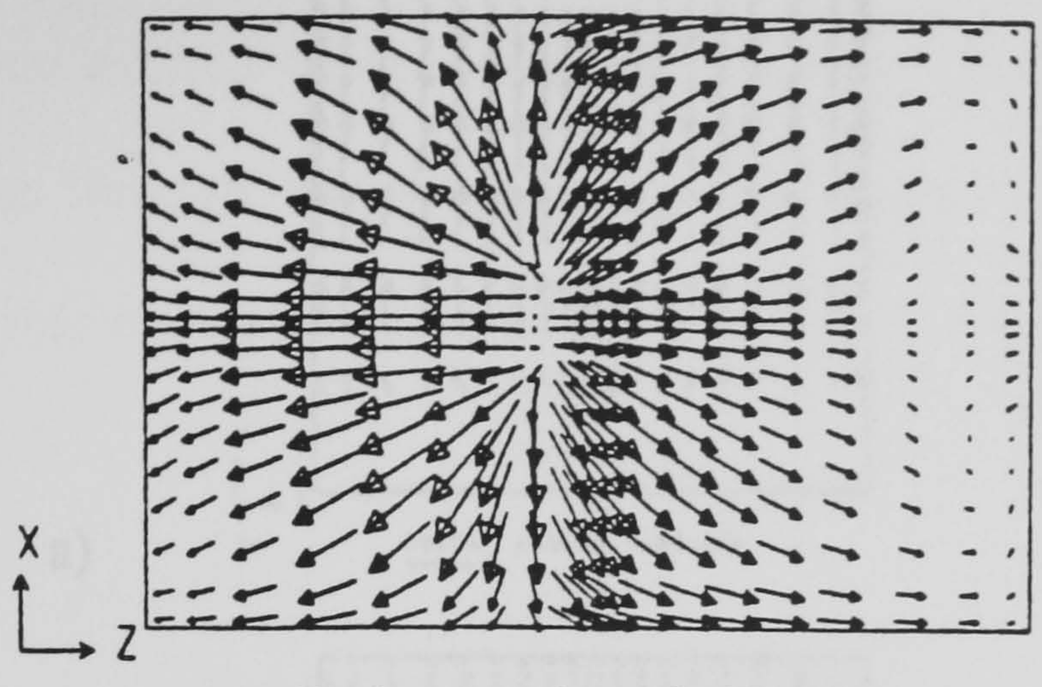

a) Y=2 Vector scale: 2.87 m/s

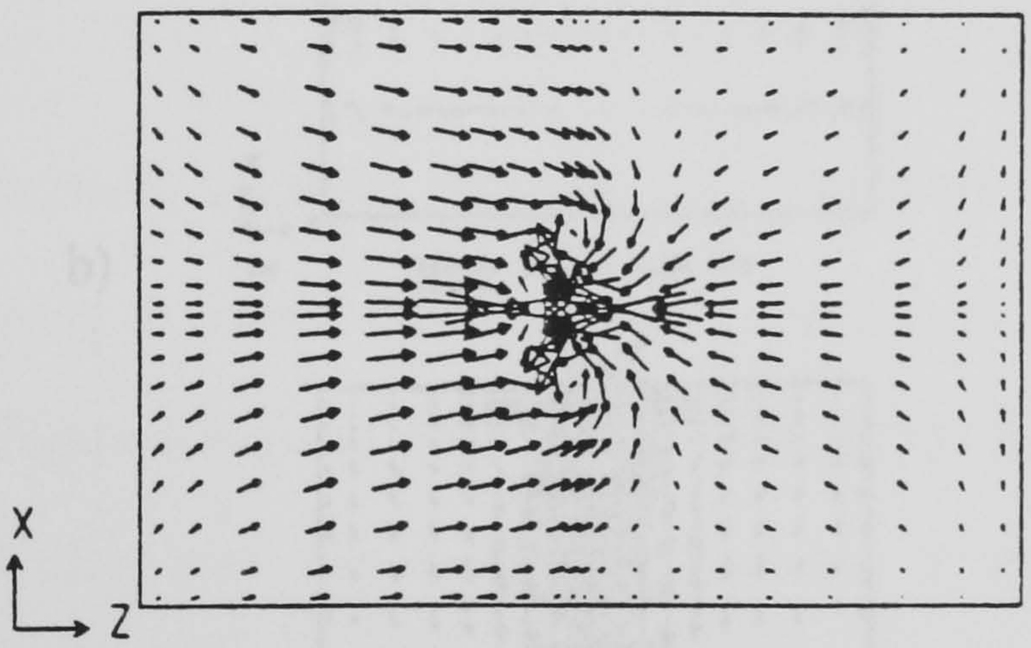

b) Y=9 Vector scale: 2.87 m/s

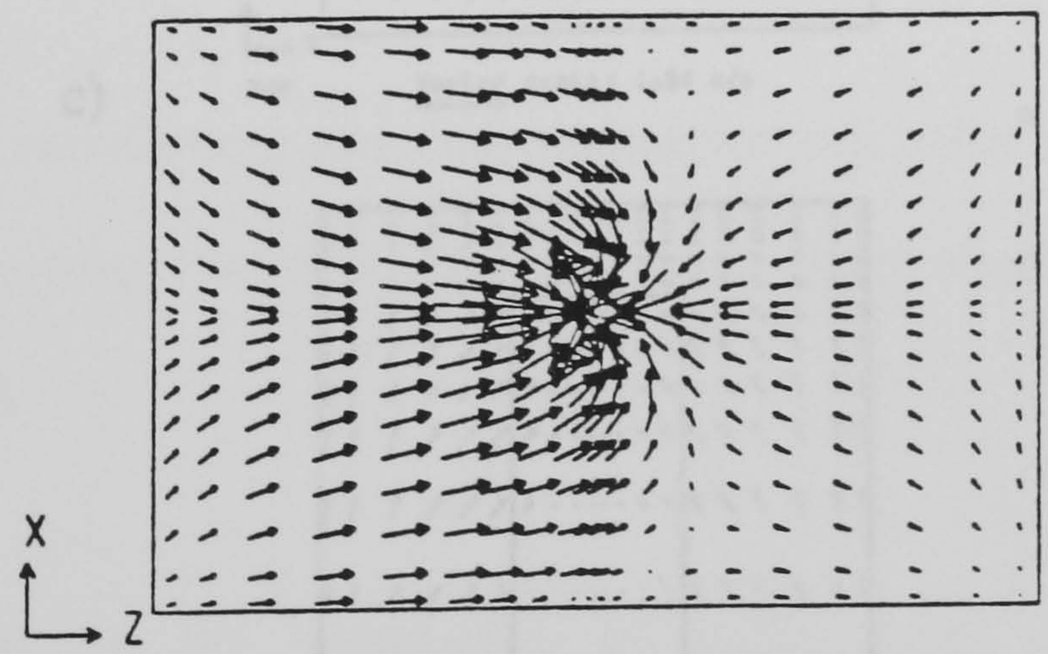

c) Y=12 Vector scale: 2.87 m/s

Figure 5.4 Plan view of office: predicted gas velocity vectors
a) 0.45m above the floor
b) 2.095m above the floor
c) 2.32m above the floor/ 0.12m below the ceiling

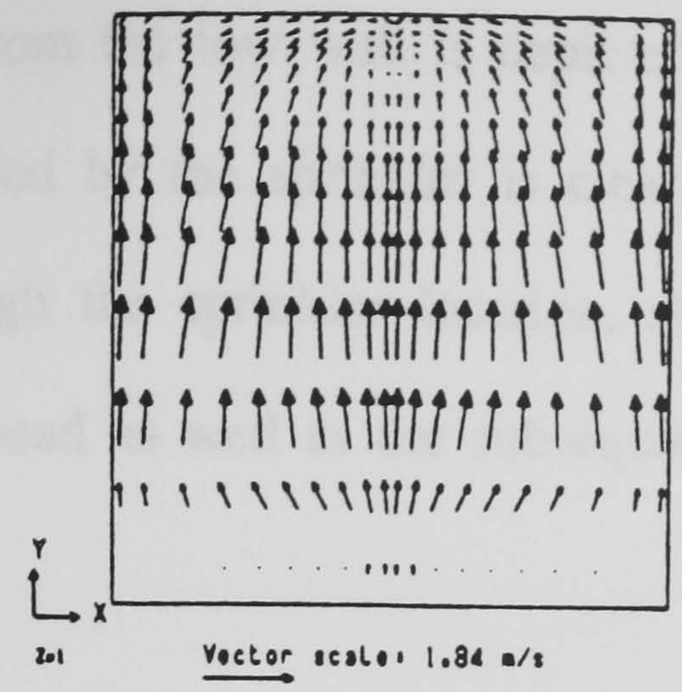

a)

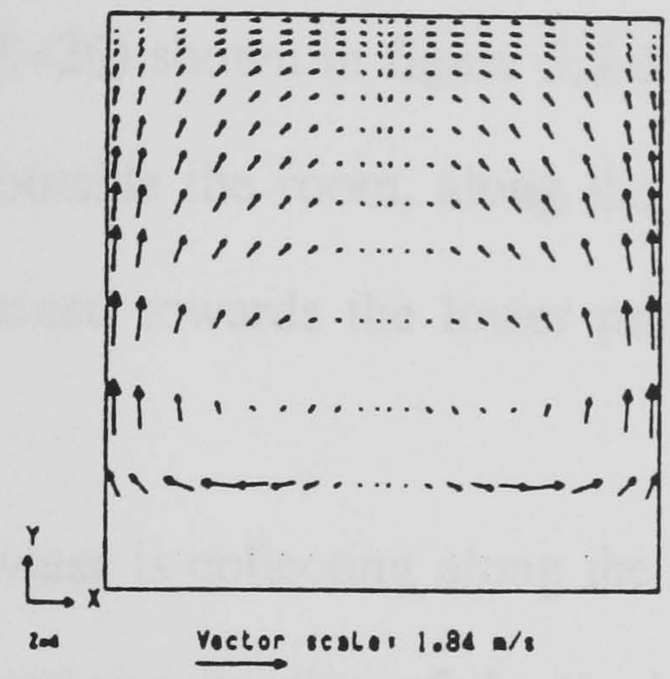

b)

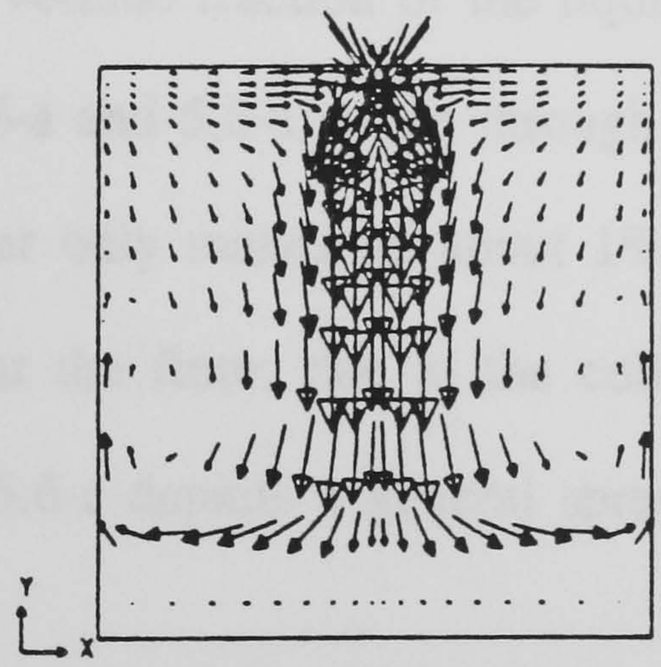

c)

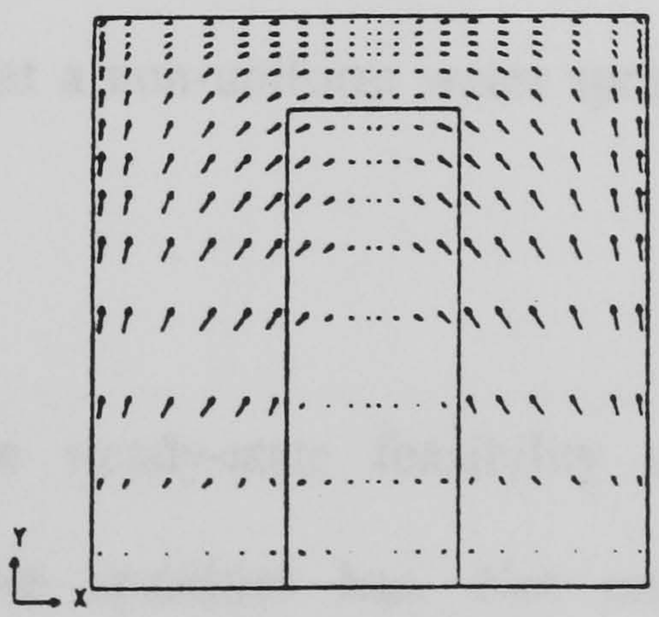

d)

Figure 5.5 Cross view of office: predicted gas velocity vectors
a) through the fire source b) 0.7m away from the fire
c) through the sprinkler plane d) through the doorway

-b where a slice 0.75m from the low wall is depicted (Z=4). The actual strength of the downward force exerted by the sprinkler is clearly shown in figure 5.5-c. This slice (Z=10), taken through the sprinkler location, shows the entrainment near the ceiling and the sprinkler head as well as the subsequent downward movement of the gases.

The effect of an opening (Z=20) shown in figure 5.5-d completes this set. It illustrates the way the air is pushed outside the room, along the sides and upper regions of the doorway whilst air is entrained towards the lower parts.

As previously mentioned, water is collecting along the floor. This is clearly illustrated in figure 5.6, showing the volume fraction of the liquid phase through three different sprinkler planes. Figure 5.6-a and 5.6-c, taken through vertical planes, show that near the sprinkler head the water only makes up about 1% of the volume. However, this is drastically increased near the floor, due to the collection of the water, to around 20%. Furthermore, figure 5.6-c depicts a general spray envelope.

The effect of gas entrainment and their respective velocities are clearly demonstrated in figure 5.6-b, showing that a non-uniform water spray envelope is produced around the sprinkler head.

The above results for the steady-state feasibility study clearly demonstrate the significant effect an active sprinkler has. Not only are the gas temperatures considerably decreased, but the complex circulation pattern which aids this process has been captured. However, the important factor is that it provided initial guidelines as well as confidence for the design of a transient two-phase fire-sprinkler model. The

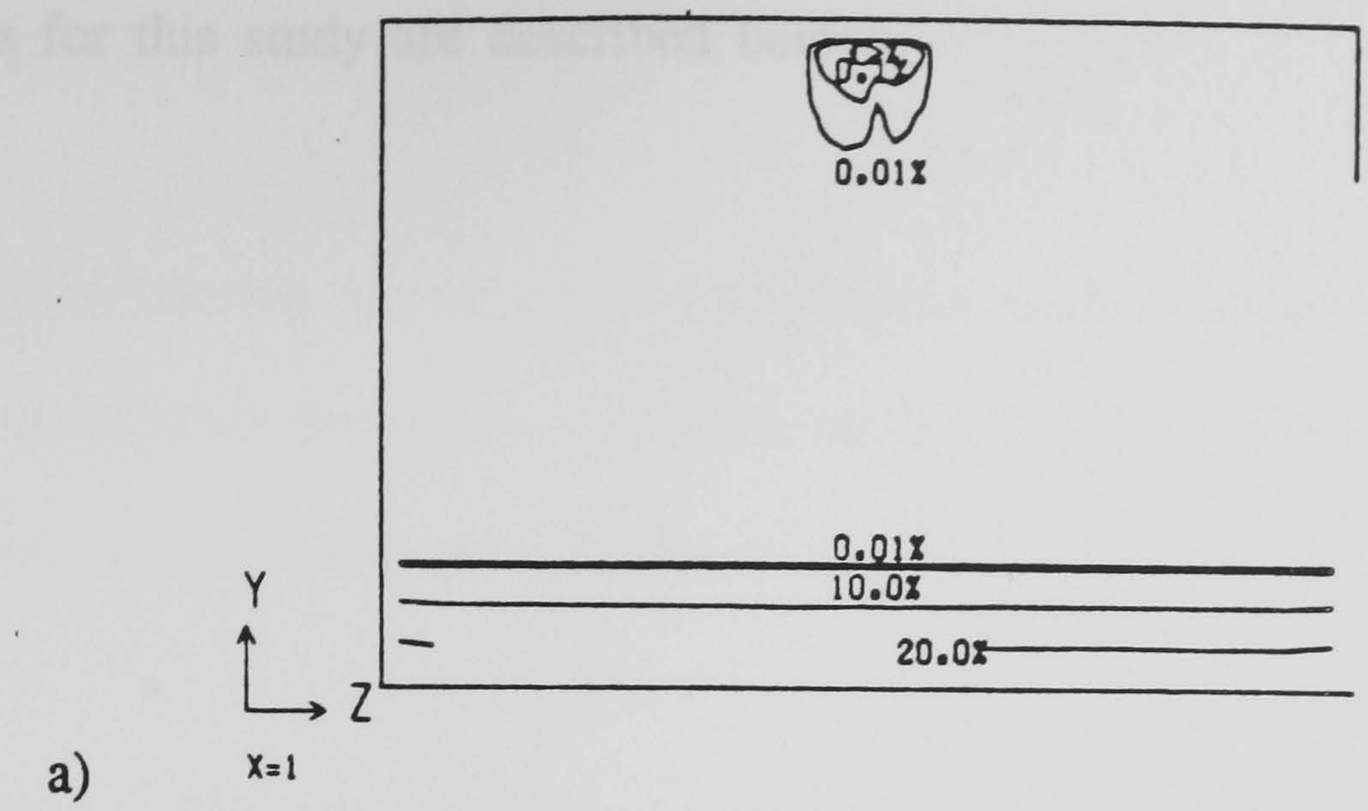

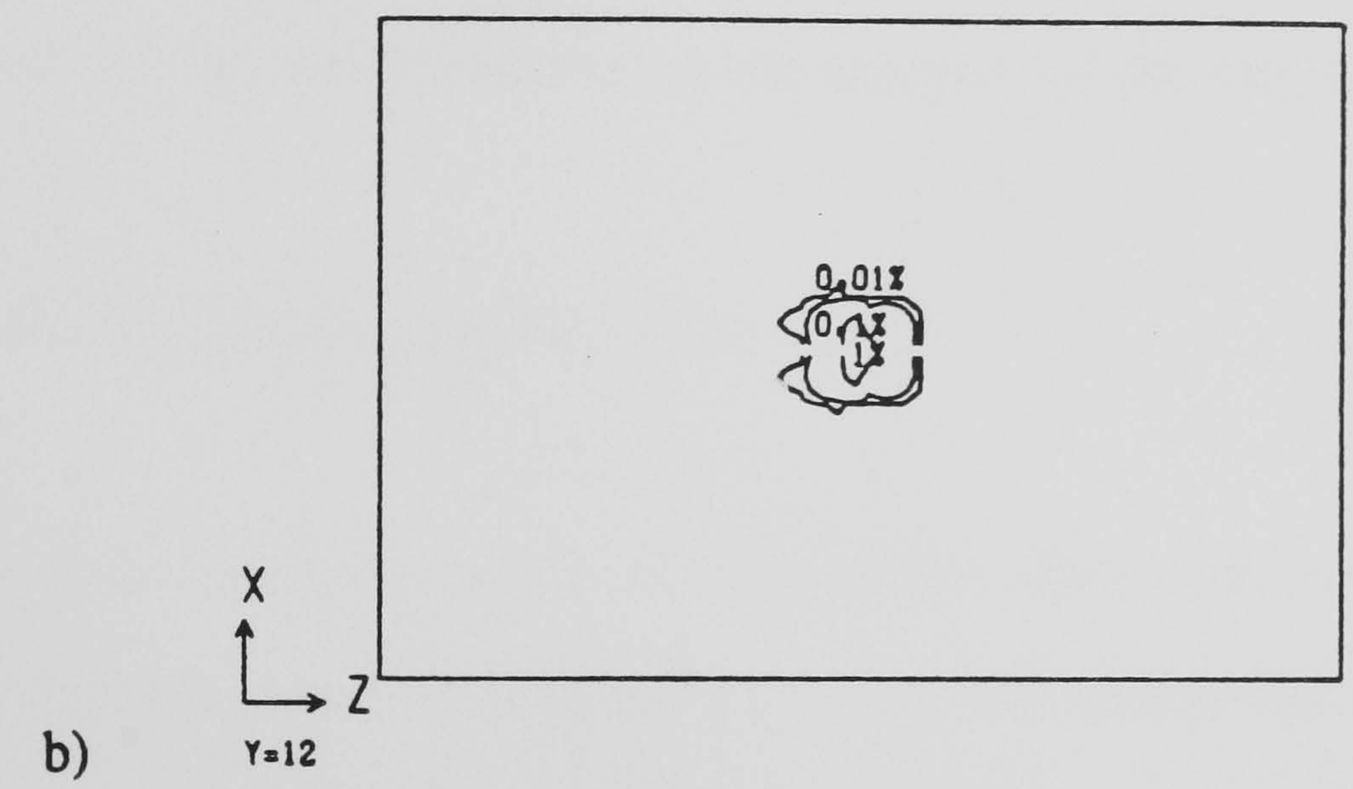

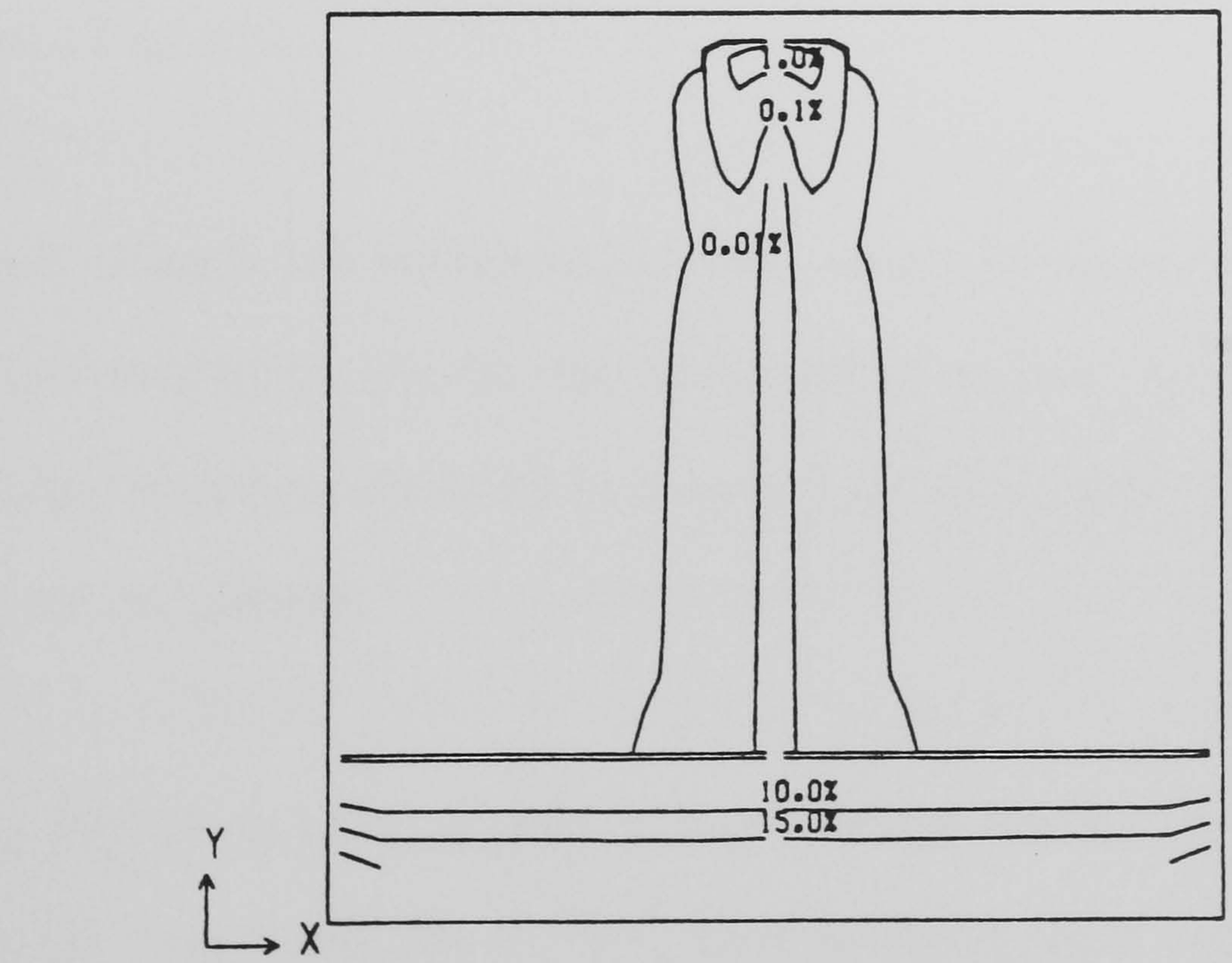

Figure 5.6 Predicted volume fractions of the water phase through the sprinkler planes
a) side view b) plan view c) cross view

results for this study are described below.

5.3 Time Dependent Simulations

The fire scenarios for the office and hospital ward configurations were also used to validate the time-dependent two-phase model. Their respective predictions and results are presented and discussed below.

The overall effect on life safety in terms of the 50°C criteria as highlighted in section 3.3 will also be considered during the analyses of the results.

5.3.1 Office Fire and Sprinkler Scenario

The general description and conditions of the office compartment given for the one-phase fire simulation in section 3.3.1 were not altered for this current simulation. Hence, details of the office schematic and the numerical grid used can be found in figures 3.8 to 3.11.

The only changes and considerations made were with respect to the initial prevailing gas-phase conditions, and the fire and sprinkler sources. As already mentioned, the predictions made and discussed in chapter 3 are used as the initial conditions for the gas-phase calculations.

During the fire-sprinkler scenario it was assumed that the fire was still in progress. Hence, the heat release rate of 40kW used during the final stages of the fire scenario in chapter 3 was utilised.

As no precise details concerning the sprinkler used during the actual experiment were

available, the following statistics for the sprinkler used within the hospital ward were assumed. The sprinkler head which was located within the centre of the room, 0.1m below the ceiling, was assumed to have a diameter of 15mm with a pressure of 0.2 bar at its head. As these factors affect the flow of water through the orifice the flow rate can be determined from the relationship [Smith (1987)]:

$$SQ = K\sqrt{P} \qquad (5.3\text{-}1)$$

where SQ is the water flow rate (l/min), P is the water pressure (bar) and K is a constant determined by the sprinkler construction.

From the above sprinkler details, with K equal to 80 [Spraysafe (1988)], a flow rate of $0.596 \times 10^{-3} m^3/sec$ was calculated. This was released at an angle of 70° from the sprinkler head's line of symmetry, which takes into account the deflector plate of the sprinkler. It was further assumed that droplets with a uniform average diameter of 1mm were produced with an initial release temperature of 10°C.

During the fire-sprinkler scenario the gas temperatures were continued to be monitored at the general locations 'SP' and 'D' as shown originally in figure 3.9. However, due to the interaction of the water particles the locations below the sprinkler could no longer be monitored. As there were no experimental data available meaningful comparisons with the mathematical predictions could not be made.

The thermocouple location 'D', 0.24m below the ceiling, along with the four additional monitoring locations S1 to S4 were unaffected.

Computational Details

The sprinkler was active for 25 seconds. This scenario was simulated using one second time discretisations.

In order to obtain converged solutions, based on the convergence criteria outlined in section 5.2, the number of sweeps required during each time step calculation needed to be adjusted. The resulting range of sweeps necessary was between 250 to 500 sweeps per time-step.

Results

The following two figures are the only two locations where comparisons between predicted and experimental data can be made [Hoffmann et al(1990)].

The first location, which is 0.05m below the ceiling in the centre of the room is depicted in figure 5.7. This diagram, which includes the comparisons prior to sprinkler activation for completeness, illustrates a sudden decrease in gas temperature once the sprinkler was activated. This sharp drop has not only been measured but the correct downward trend has also been captured by the predictions. A slight increase in temperatures predicted after about 190 seconds could possibly be due to some entrainment of hotter gases. The proximity of the cool water source may have affected these predictions. Perhaps finer grid-discretisations could improve the results.

The decrease in gas temperature remote from the sprinkler is as expected not as steep as shown in figure 5.7. The gas temperature comparisons, shown in figure 5.8, are

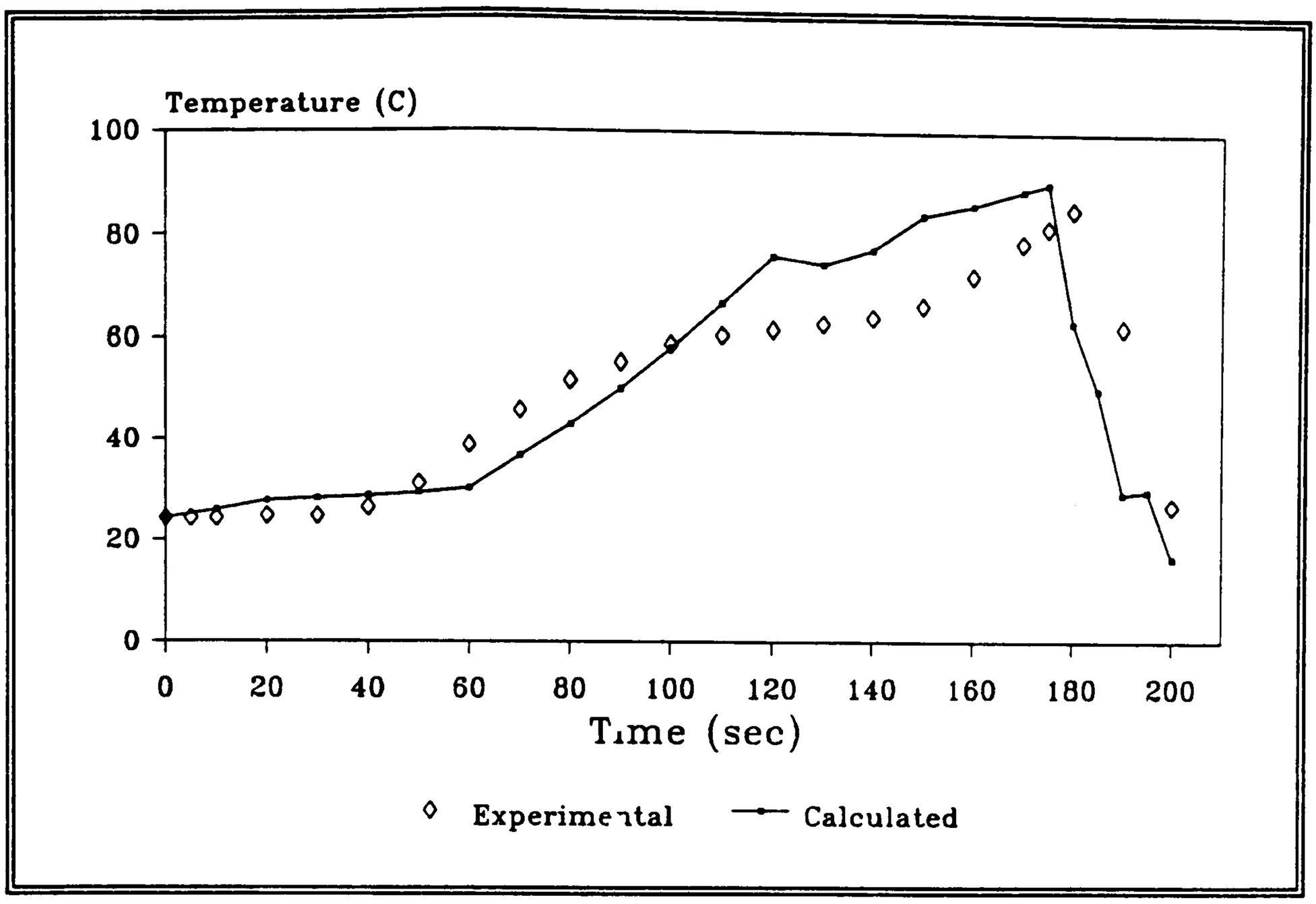

Figure 5.7 Predicted and measured gas temperatures: location towards centre of the room, 0.05m below the ceiling

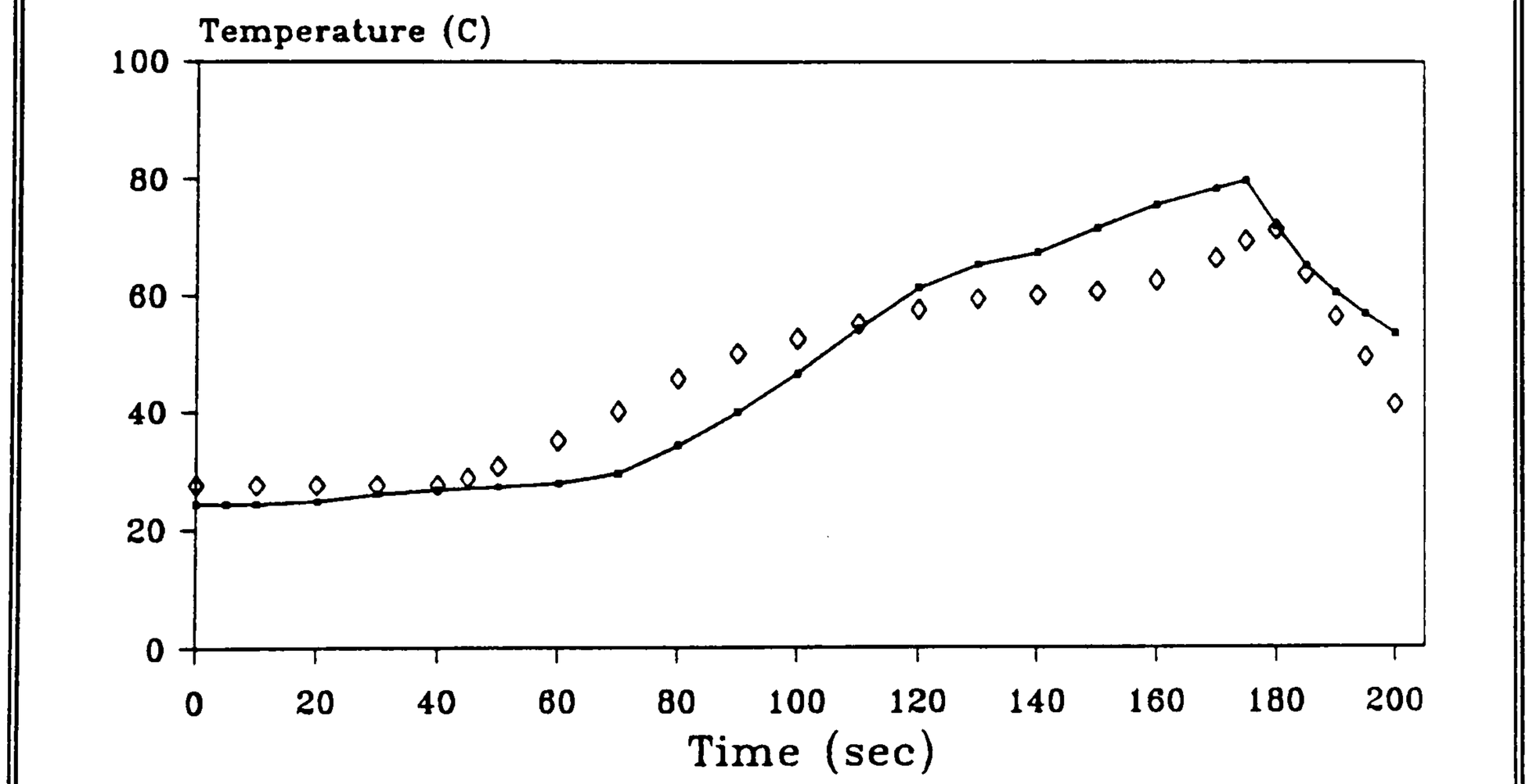

Figure 5.8 Predicted and measured gas temperatures: location near door, 0.24m below the ceiling

at the location near the doorway, 0.24m below the ceiling. Though the gas temperature predictions are decreasing in time and follow the measured trend, the rate at which this cooling is progressing is not as high further into the sprinkler scenario as observed. Hence, the temperature difference between predicted and measured data is at the end of the scenario around 10°C. This discrepancy could be accounted for in the coarseness of the grid existing around this location. Hence, the calculations are not able to capture accurately enough the mixing process of the hot and cold gases in this vicinity.

As in the case for the fire simulation, temperature predictions with height can illustrate important factors from the life safety point of view. The results presented in figure 5.9 depict the temperature variation at the four locations S1 to S4 after 0, 10 and 25 seconds following sprinkler activation. From these very interesting facts concerning the spreading effect of the sprinkler can be observed.

The gas temperatures at S1, figure 5.9-a, initially appear to be little affected as after 10 seconds they still increase near the floor and ceiling. However, after 25 seconds even this location, which is close to the fire, shows an overall reduction in temperature.

Location S2 on the other hand reveals considerable temperature reductions after 25 seconds. However, the interesting feature to point out is that after 10 seconds, gas temperatures above 1.4m from the floor have decreased indicating the overall cooling effect within the upper layer. An increase in gas temperatures observed below that height illustrates the initial mixing of the hot and cold gases as they are pushed downwards by the sprinkler as well as an overall cooling in the upper level. These characteristics are also observed for S3.

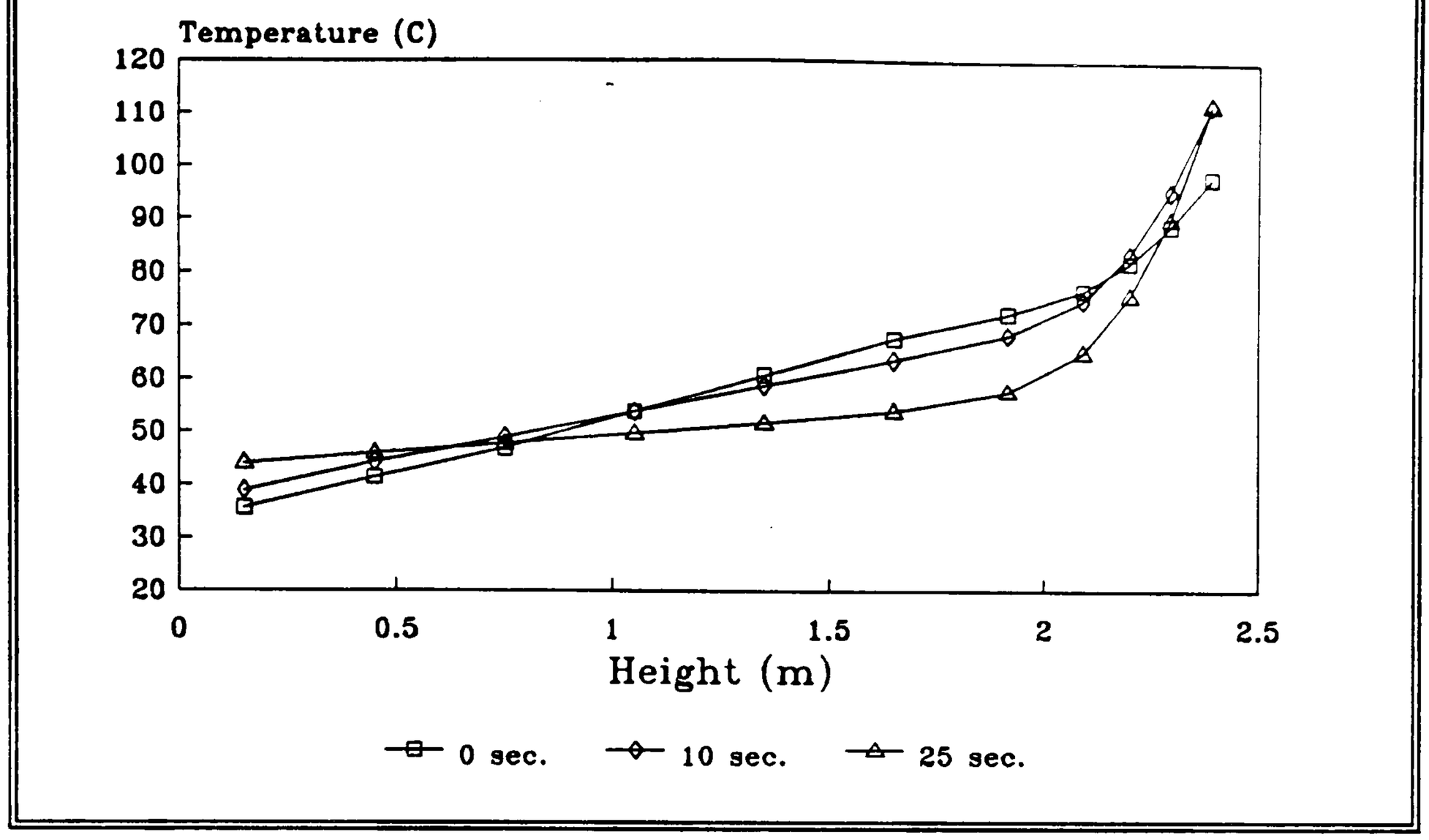

a) Location S1

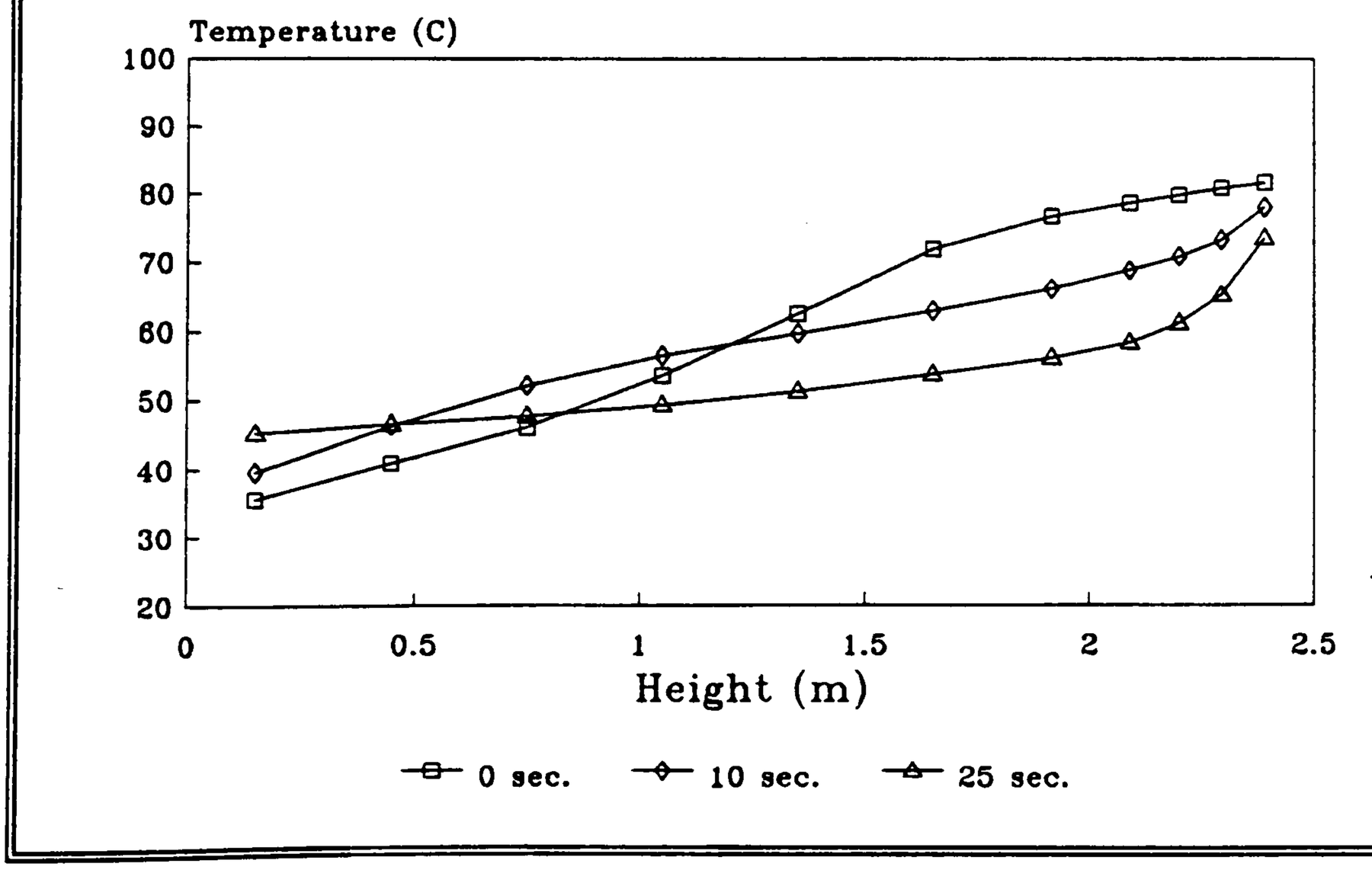

b) Location S2

Figure 5.9 Predicted gas temperature variations with height

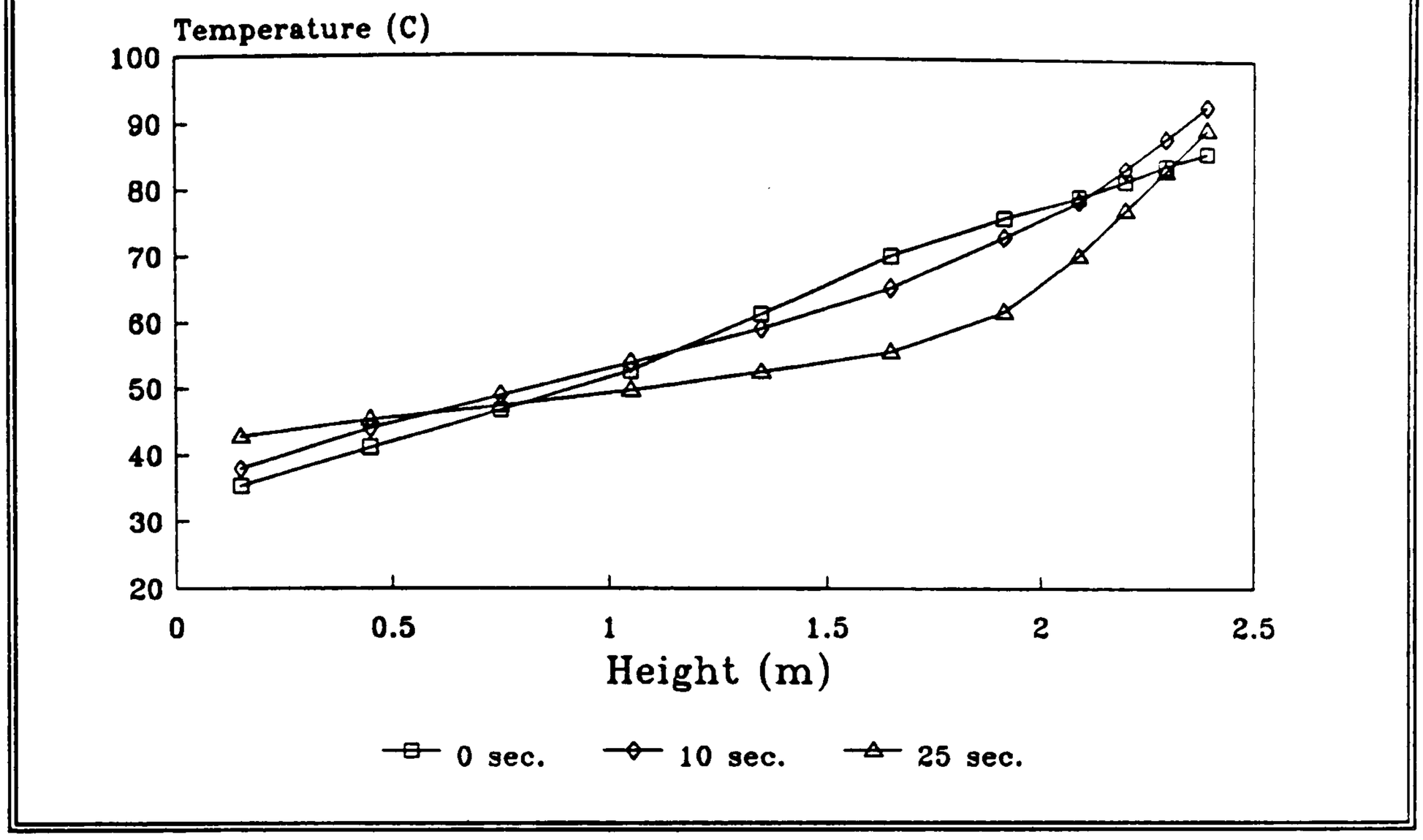

c) Location S3

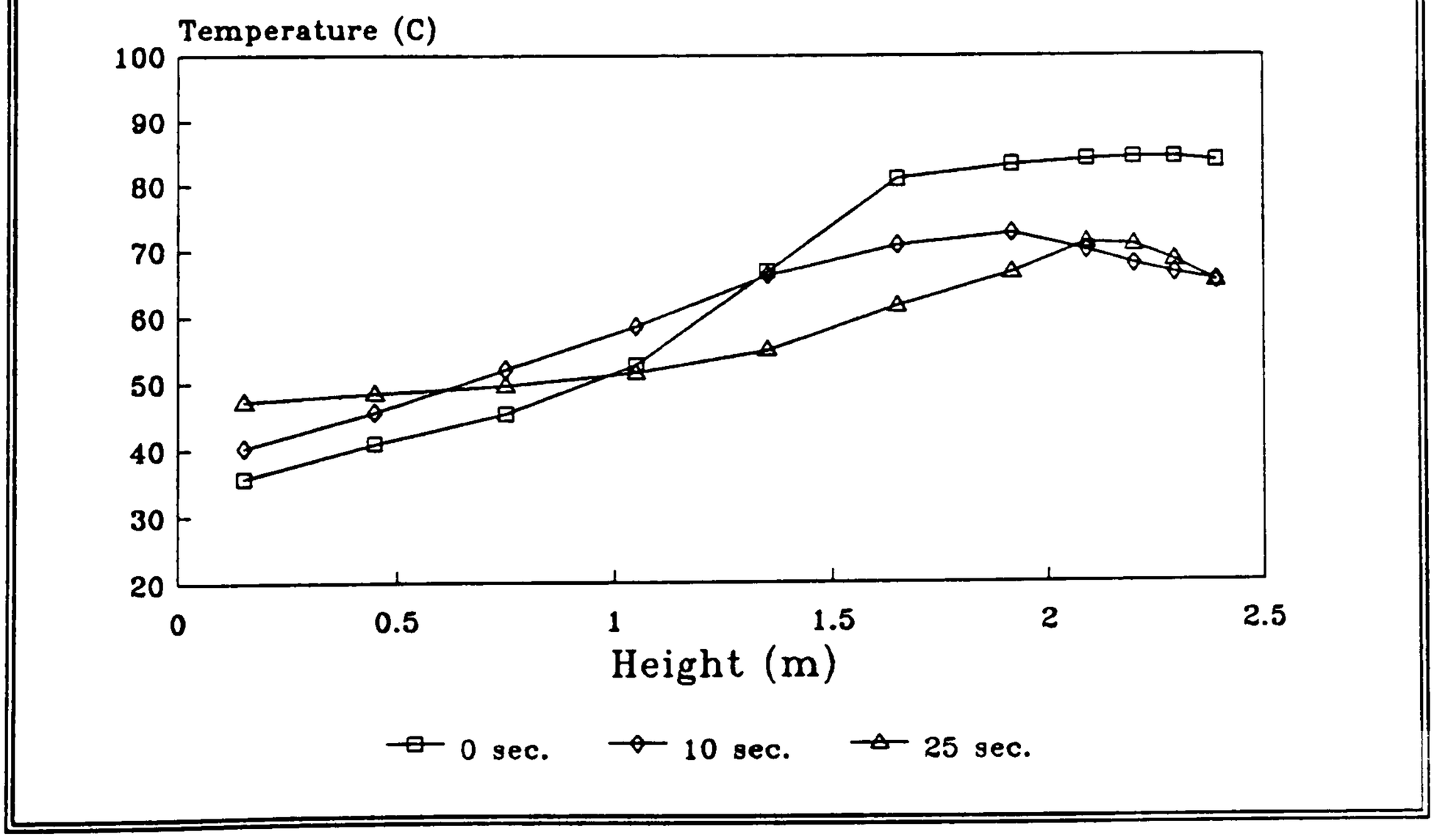

d) Location S4

Figure 5.9 Predicted gas temperature variations with height (continued)

However, the most pronounced effects are displayed by location S4. As this location is along the major air current the cooling effect of the sprinkler is felt the earliest. Hence, the gas temperatures are drastically reduced within the upper layer after only 10 seconds. However, the mixing of the gases increases the temperatures below the 1.4m level. This trend is continued during the rest of the scenario.

A summary of the temperatures after 25 seconds, shown in figure 5.10, further show the relatively even mixing of the gases and hence, even temperatures up to a height of 1.4m. Above this level the cooling effect of the sprinkler in terms of positioning within the general circulation pattern is clearly demonstrated. Location S1, between the fire and prior to the sprinkler has the highest gas temperatures compared to S4, which monitors the gas temperatures following the cooling by the sprinkler. The maximum temperature difference between these two locations is about 50°C.

The following figures which cannot be compared with experimental data, are used to illustrate the general conditions within the compartment and the way in which they vary in time. Gas temperature contours and velocity vectors are used to show the growth of the hot upper layer and the circulation pattern at distinct planes and times within the room. The time intervals shown are 0, 10 and 25 seconds after sprinkler activation, whereby the first diagram is used to show more clearly the effect of the sprinkler.

The first set of figures, 5.11 and 5.12, are taken along the west wall and through the fire source (X=1). The temperature contours, depicted in figure 5.11, not only show how the fire is still increasing in strength, but more importantly that they are with time cooled down within the upper layer. The hot gases created by the fire are also

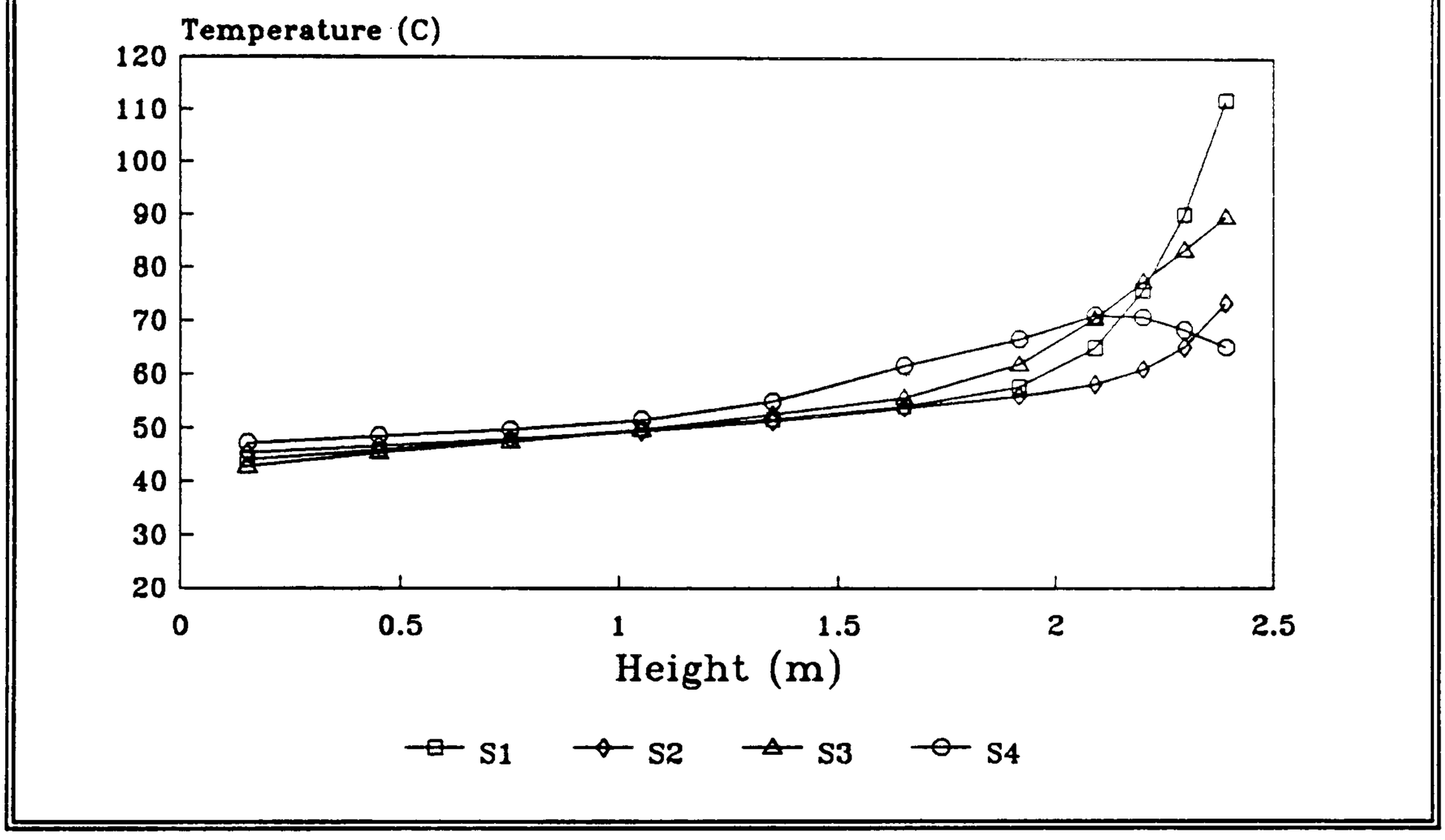

Figure 5.10 Gas temperature predictions with height after 25 seconds at the four monitoring locations

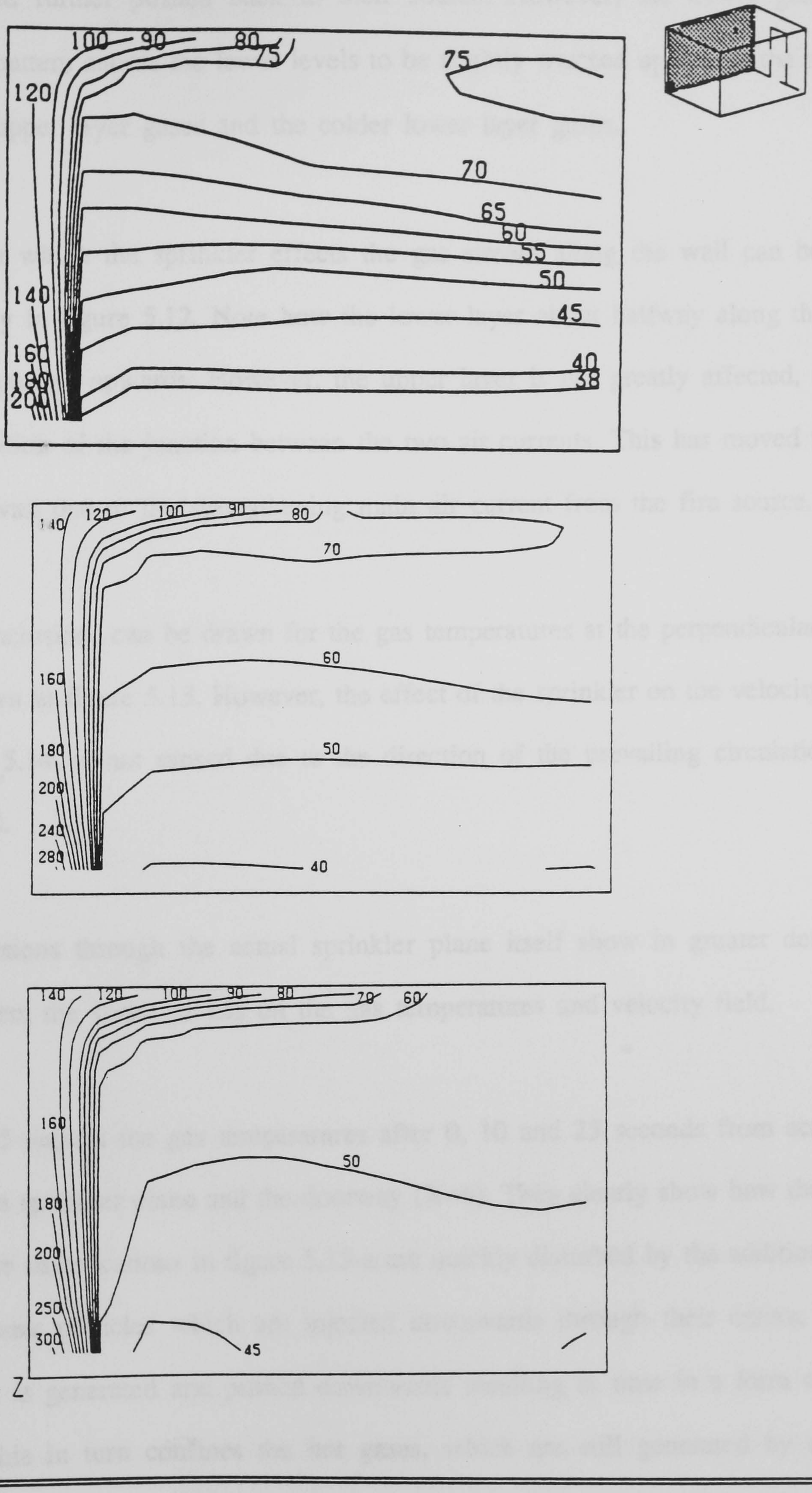

Figure 5.11 Side view of office: predicted gas temperature contours along the west wall through the fire source (X=1)
a) 0 sec. b) 10 sec. c) 25 sec.

confined and further pushed back to their source. However, the newly generated circulation pattern causes the lower levels to be slightly warmed up due to the mixing of the hot upper layer gases and the colder lower layer gases.

The way in which the sprinkler effects the gas stream along the wall can be seen more clearly in figure 5.12. Note how the lower layer about halfway along the wall is in time pushed upwards. However, the upper layer is not greatly affected, except for the location of the junction between the two air currents. This has moved further along the wall due to the strengthening main air current from the fire source.

Similar conclusions can be drawn for the gas temperatures at the perpendicular plane (Z=1) shown in figure 5.13. However, the effect of the sprinkler on the velocity field, see figure 5.14, is not sensed due to the direction of the prevailing circulation, see figure 5.18.

The predictions through the actual sprinkler plane itself show in greater detail the overall effect the sprinkler has on the gas temperatures and velocity field.

Figure 5.15 depicts the gas temperatures after 0, 10 and 25 seconds from activation through the sprinkler plane and the doorway (X=6). They clearly show how the stable temperature stratifications in figure 5.15-a are quickly disturbed by the addition of the cooling water particles which are injected downwards through their centre. Hence, cooler gas is generated and pushed downwards resulting in time in a form of water curtain. This in turn confines the hot gases, which are still generated by the fire, whilst cooling down the gases near the escape route - the open doorway.

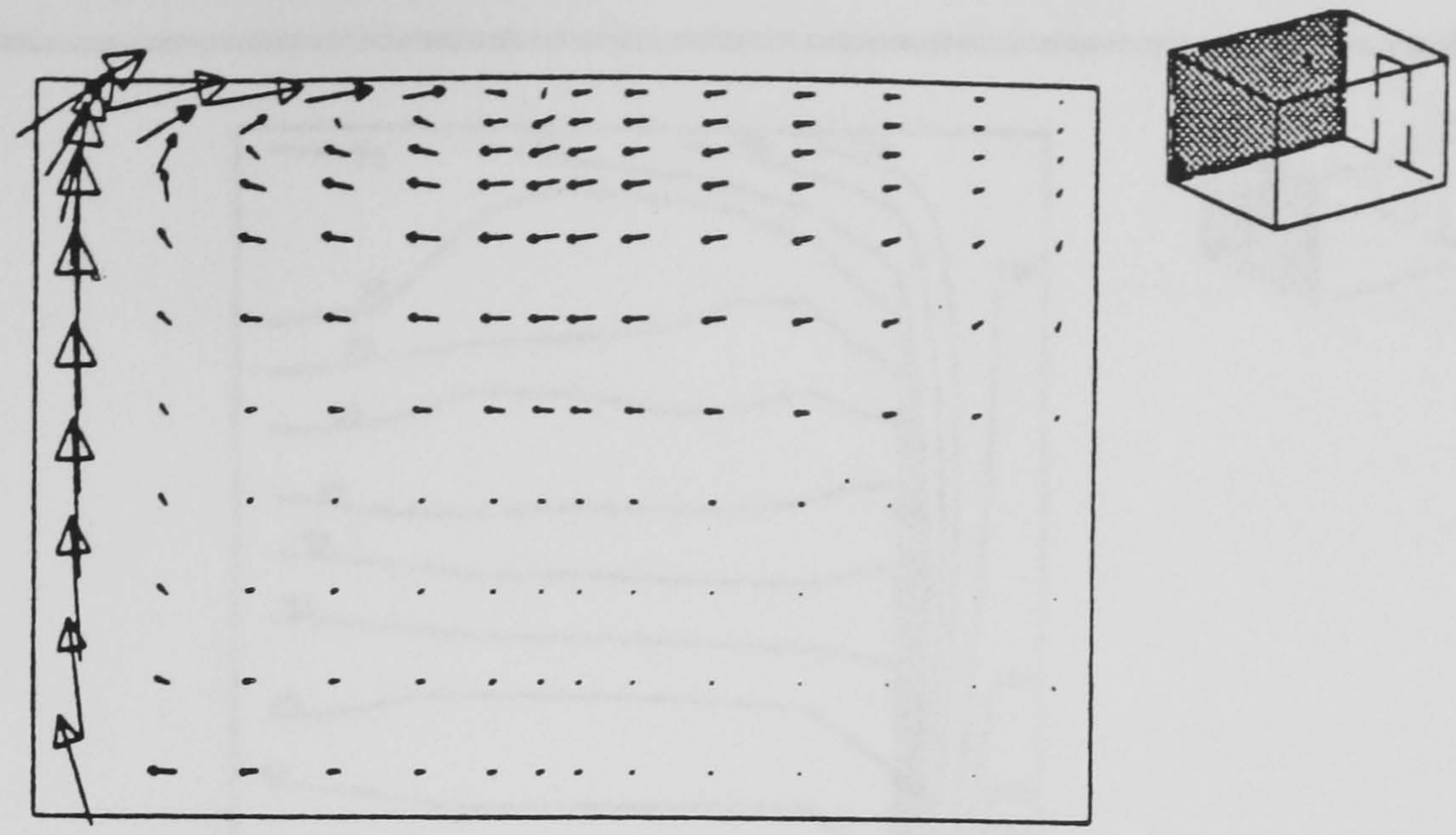

Figure 5.12 Side view of office: predicted gas velocity vectors along the west wall through the fire source (X=1)
a) 0 sec. b) 10 sec. c) 25 sec

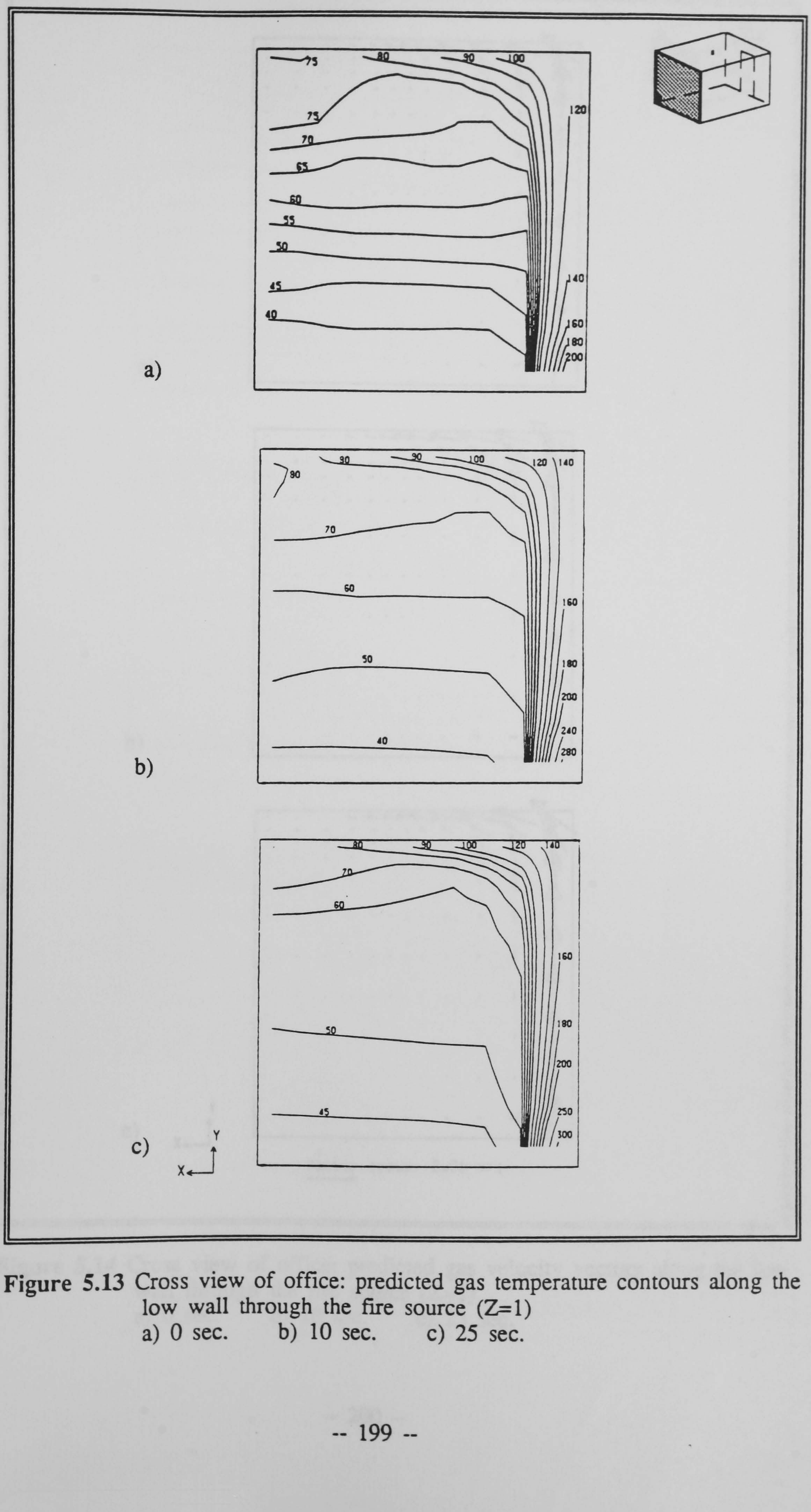

Figure 5.13 Cross view of office: predicted gas temperature contours along the low wall through the fire source (Z=1)
a) 0 sec. b) 10 sec. c) 25 sec.

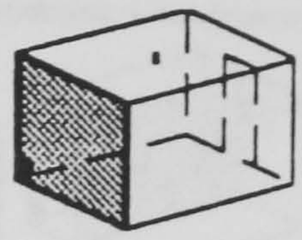

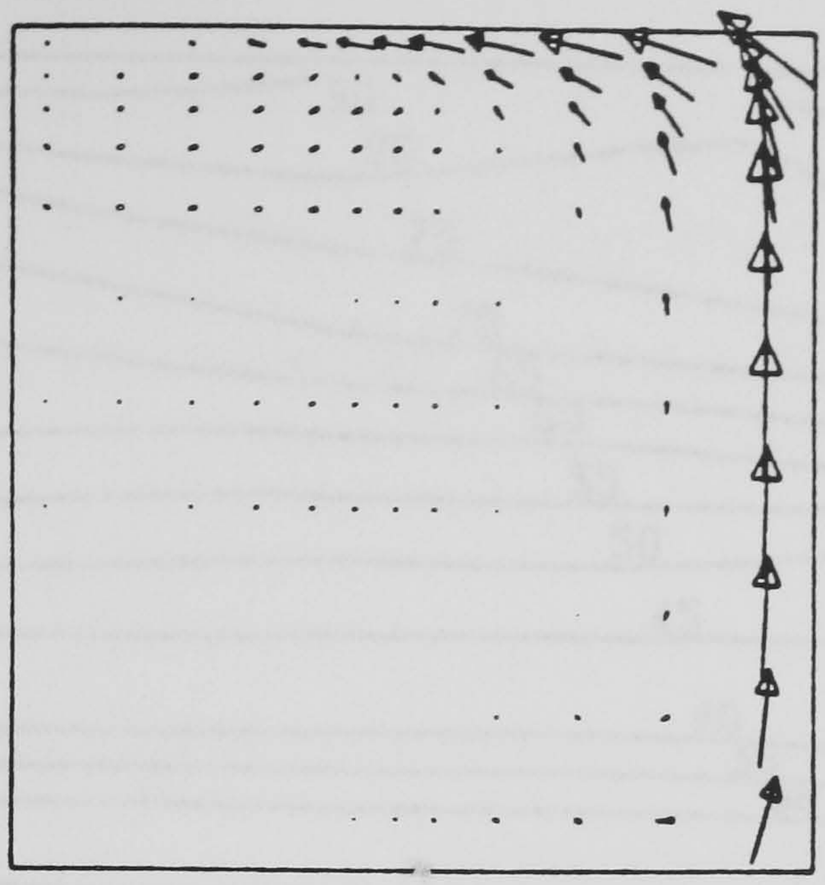

a)

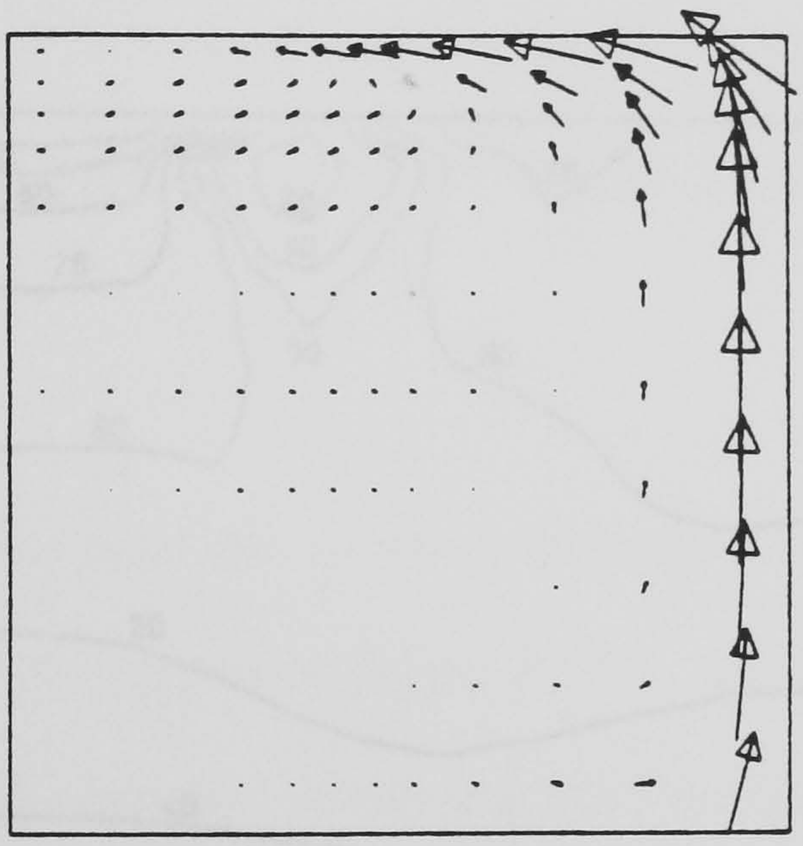

b)

c)

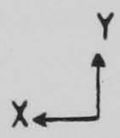

Vector scale: 2.01 m/s

Figure 5.14 Cross view of office: predicted gas velocity vectors along the low wall through the fire source (Z=1)
a) 0 sec. b) 10 sec. c) 25 sec.

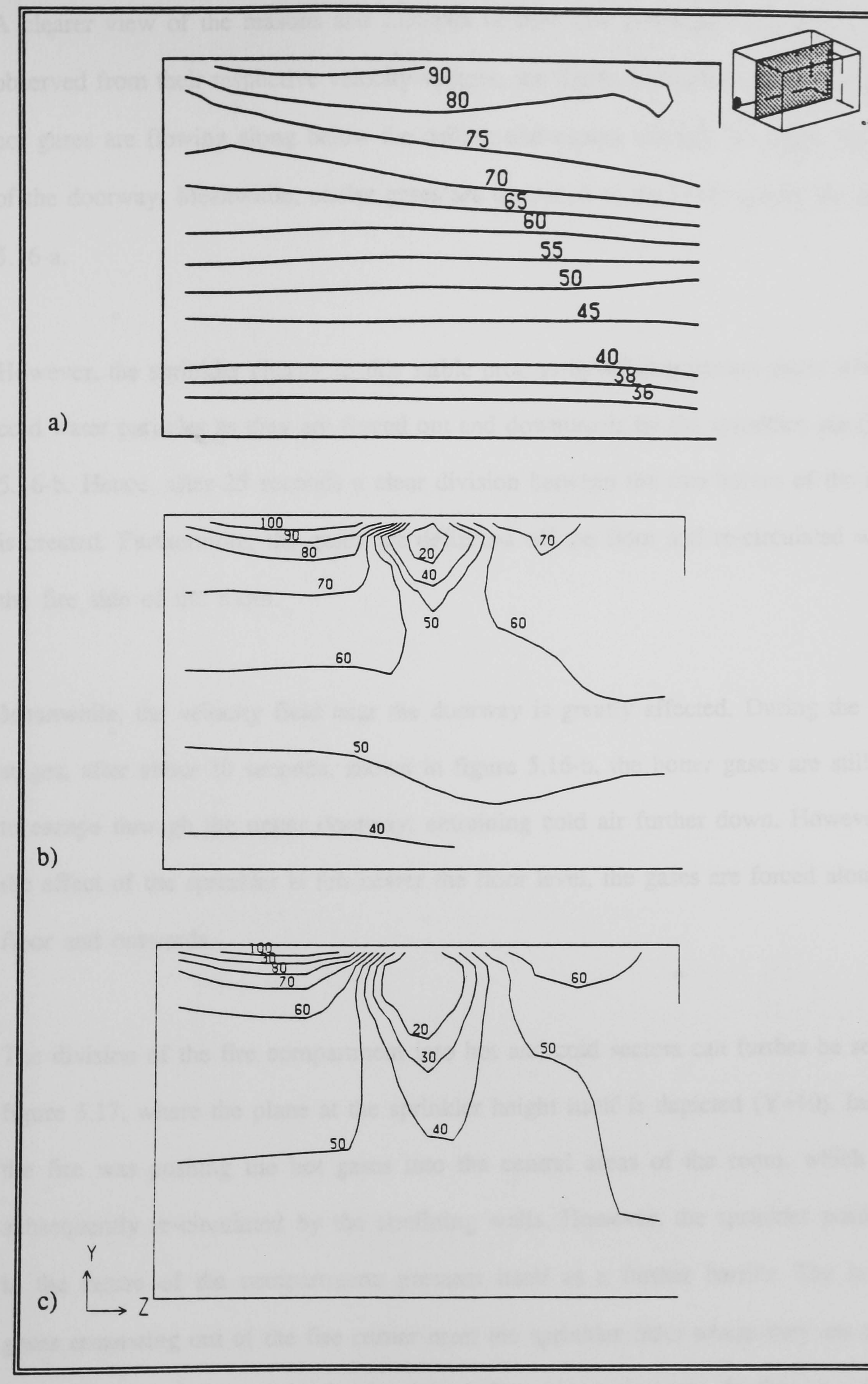

Figure 5.15 Side view of office: predicted gas temperature contours on the vertical plane through the sprinkler and doorway (X=6)
a) 0 sec. b) 10 sec. c) 25 sec.

A clearer view of the reasons and methods of how this processes is created can be observed from their respective velocity vectors, see figure 5.16. Note how initially the hot gases are flowing along below the ceiling and escape through the upper portions of the doorway. Meanwhile, cooler gases are entrained at the lower levels, see figure 5.16-a.

However, the sprinkler churns up this stable process by mixing the hot gases with the cold water particles as they are forced out and downwards by the sprinkler, see figure 5.16-b. Hence, after 25 seconds a clear division between the two halves of the room is created. Furthermore, the gases are deflected off the floor and re-circulated within the fire side of the room.

Meanwhile, the velocity field near the doorway is greatly affected. During the early stages, after about 10 seconds, shown in figure 5.16-b, the hotter gases are still able to escape through the upper doorway, entraining cold air further down. However, as the effect of the sprinkler is felt nearer the floor level, the gases are forced along the floor and outwards.

The division of the fire compartment into hot and cold sectors can further be seen in figure 5.17, where the plane at the sprinkler height itself is depicted (Y=10). Initially the fire was pushing the hot gases into the central areas of the room, which were subsequently re-circulated by the confining walls. However, the sprinkler positioned in the centre of the compartment, presents itself as a further barrier. The hot fire gases emanating out of the fire corner meet the sprinkler from where they are cooled down. Hence, cooler gas is circulated back into the upper layer. In that way further aiding the cooling process. However, the interesting fact to emerge is that the overall

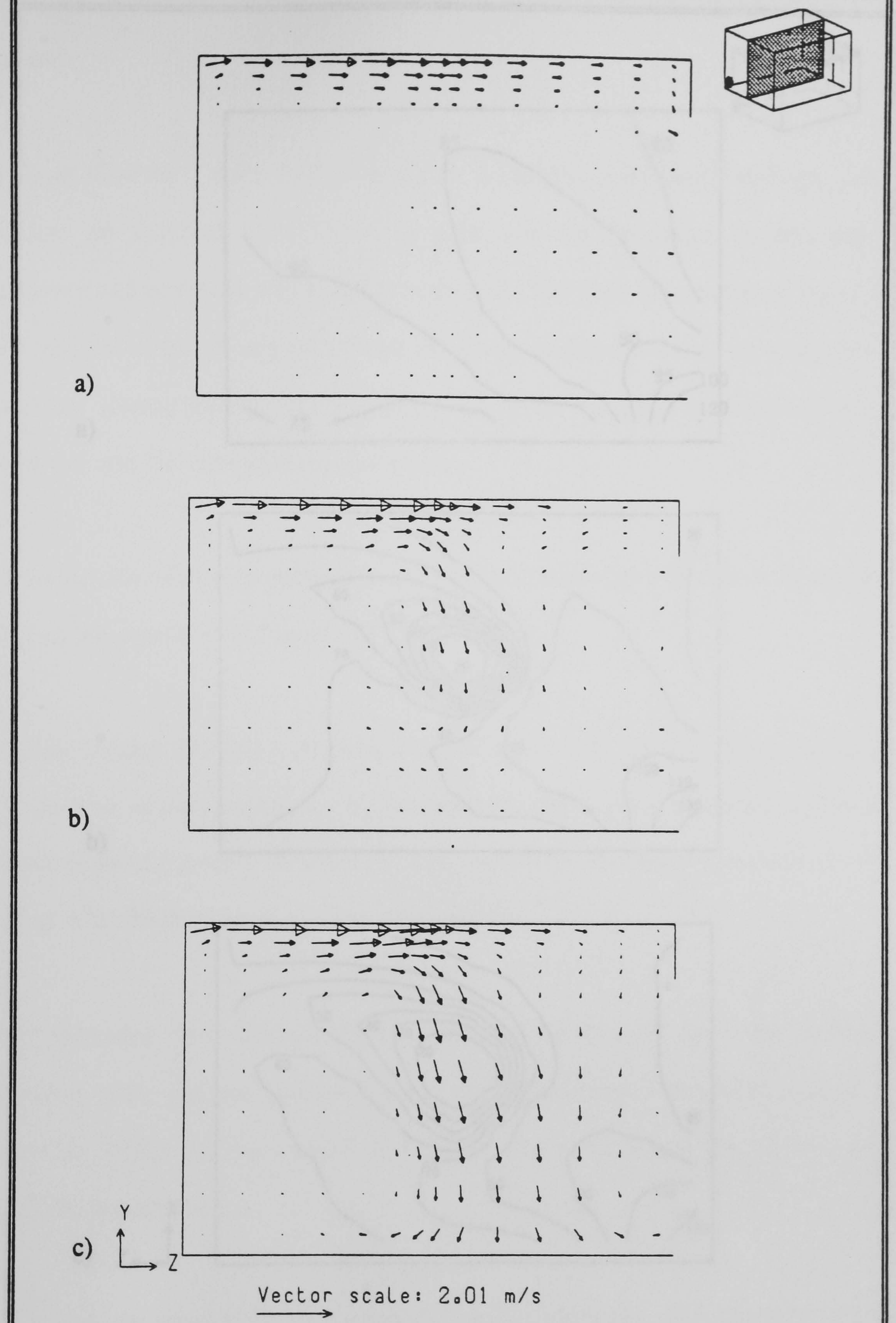

Figure 5.16 Side view of office: predicted gas velocity vectors on the vertical central plane through the sprinkler and doorway (X=6)
a) 0 sec. b) 10 sec. c) 25 sec.

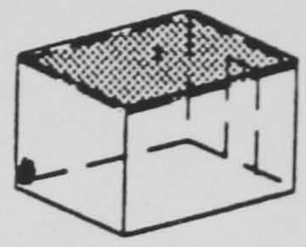

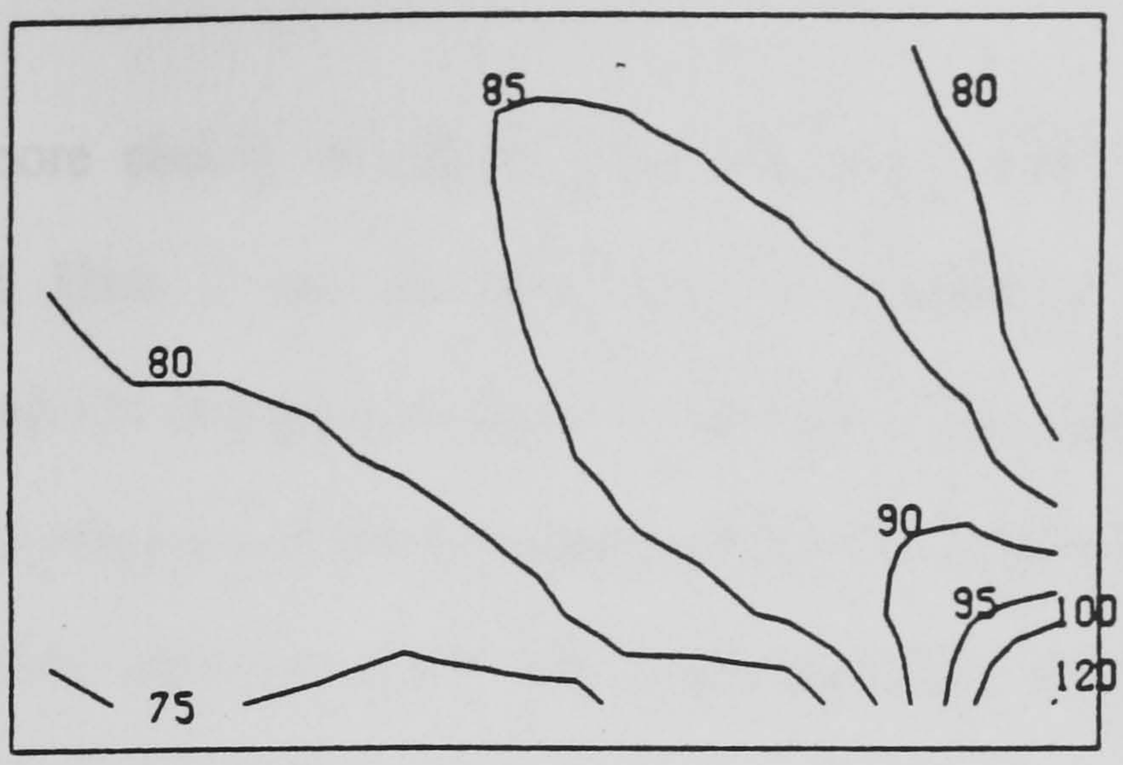

a)

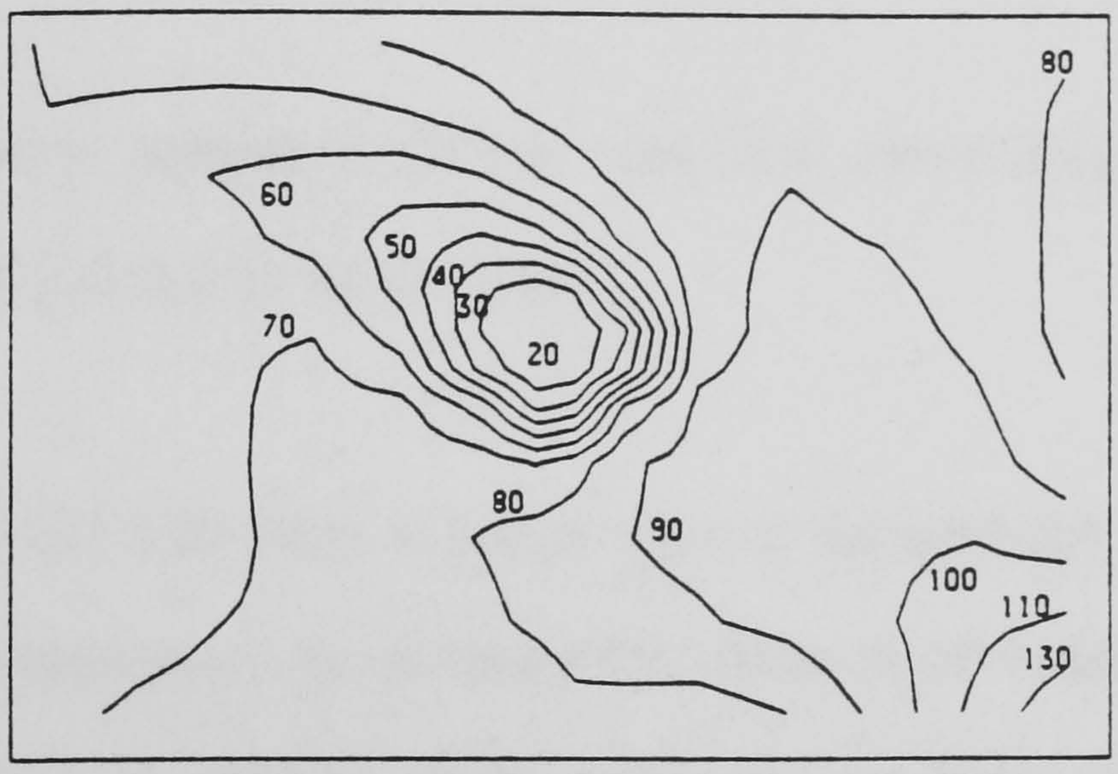

b)

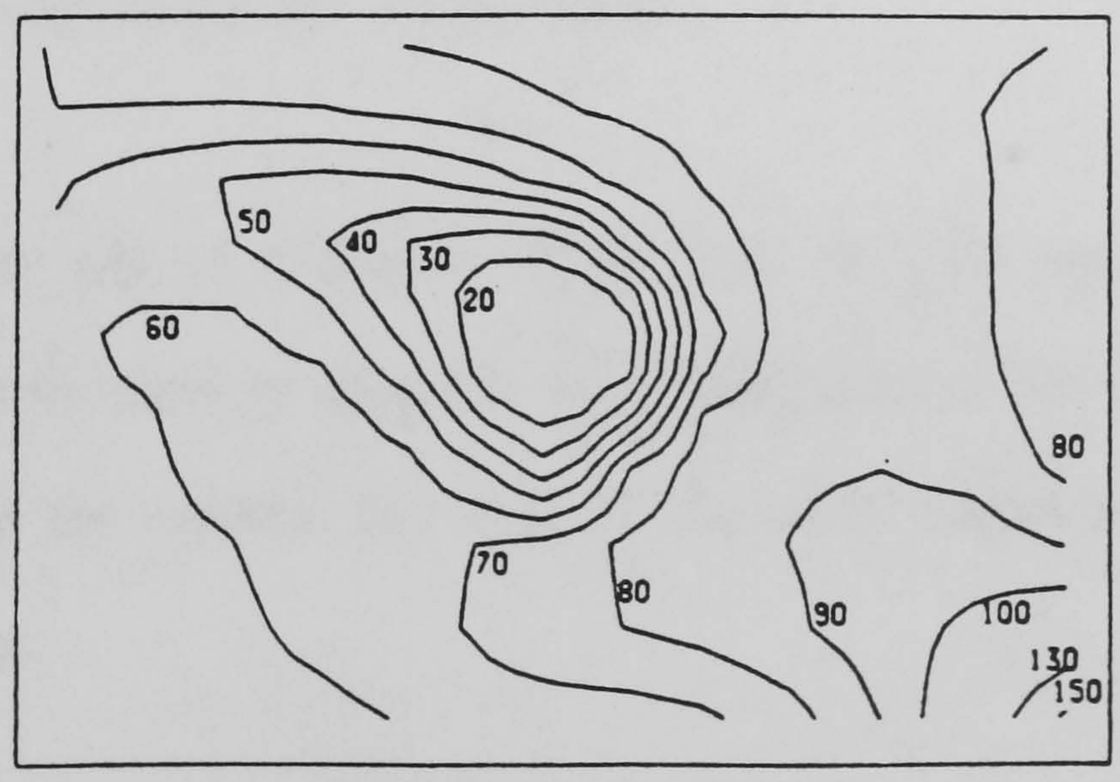

c)

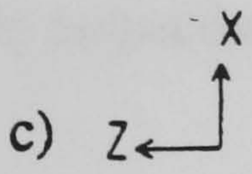

Figure 5.17 Plan view of office: predicted gas temperature contours through a horizontal plane, 0.145m below the ceiling (Y=10)
a) 0 sec. b) 10 sec. c) 25 sec.

direction of the gas stream still appears to be from the fire to the top left hand corner.

This is illustrated more clearly in figure 5.18, where the associated gas velocity vectors are depicted. Here it can be seen how the circulation patterns near the doorway and west wall are changing in time. As had been seen earlier in figure 5.12, the location of the convergence of the gas stream and re-circulating air along the west wall has slightly shifted, which is partly due to the shrinking re-circulation near the doorway and the strengthening fire plume.

However, the circulation patterns in the top right hand corner appear to be unaffected due to the overall directionality of the flow.

Finally, figures 5.19 and 5.20 show a further view of the sprinkler plane, to highlight the division of the compartment by the sprinkler. These slices which are perpendicular to the plane of figures 5.15 and 5.16 (Z=8), emphasise the newly generated circulation along with the cooling of the gas temperatures.

The following three sets of diagrams, figure 5.21 to 5.23, are taken through the sprinkler plane and are used to illustrate the propagation of the water particles. The contours shown are the volume fractions of the water phase after 5, 15, and 25 seconds respectively.

Note how the spray is spreading outwards unsymmetrically. This could be attributed to the evaporation of the water particles as well as the direction of the main gas flow. A certain amount of grid-dependence can also be observed in the sharp corners of the

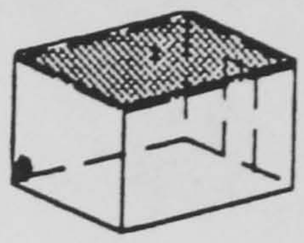

a)

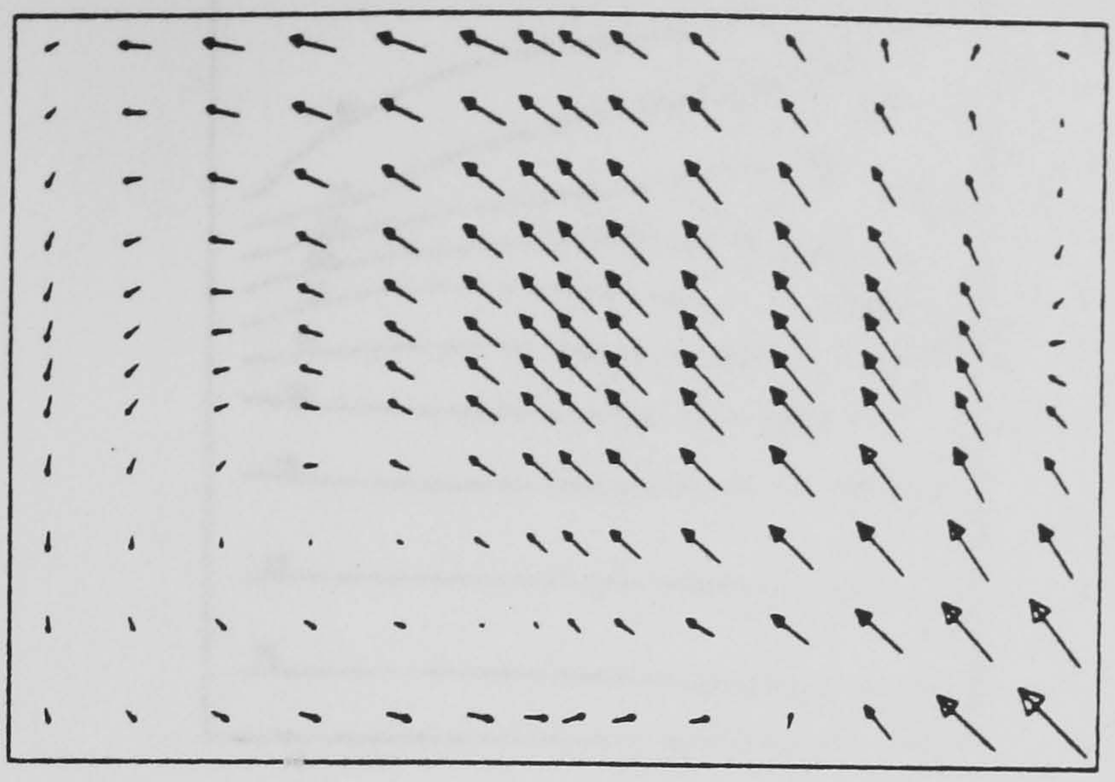

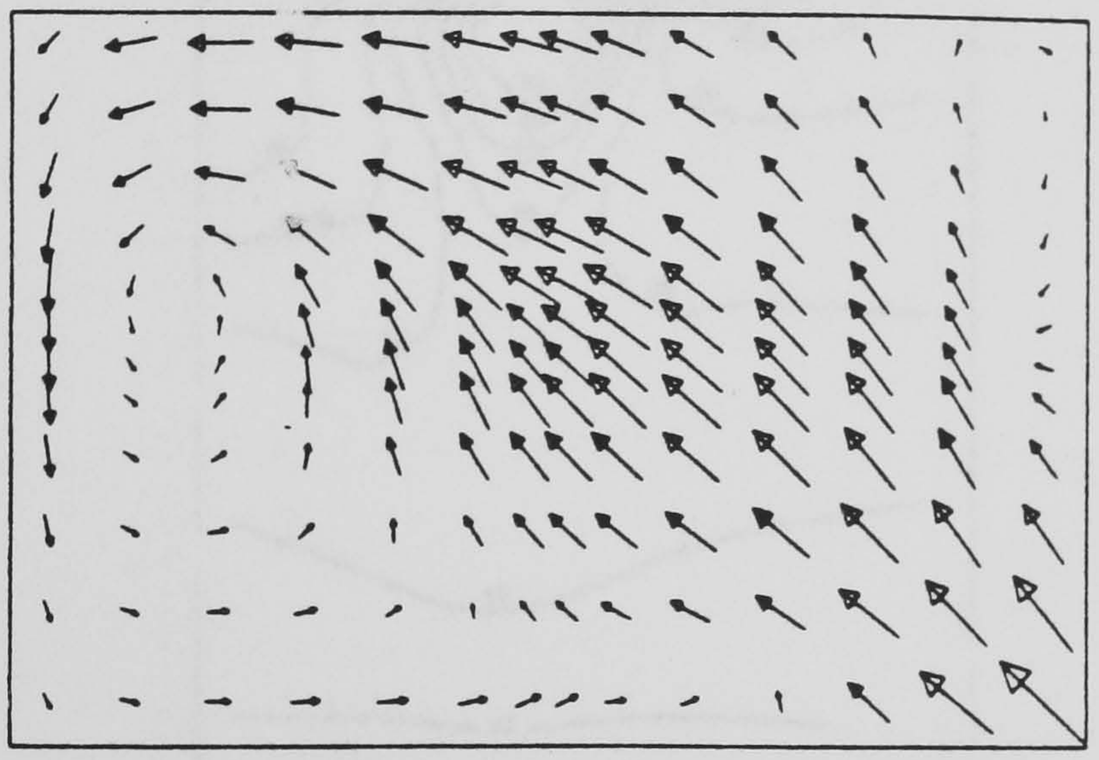

b)

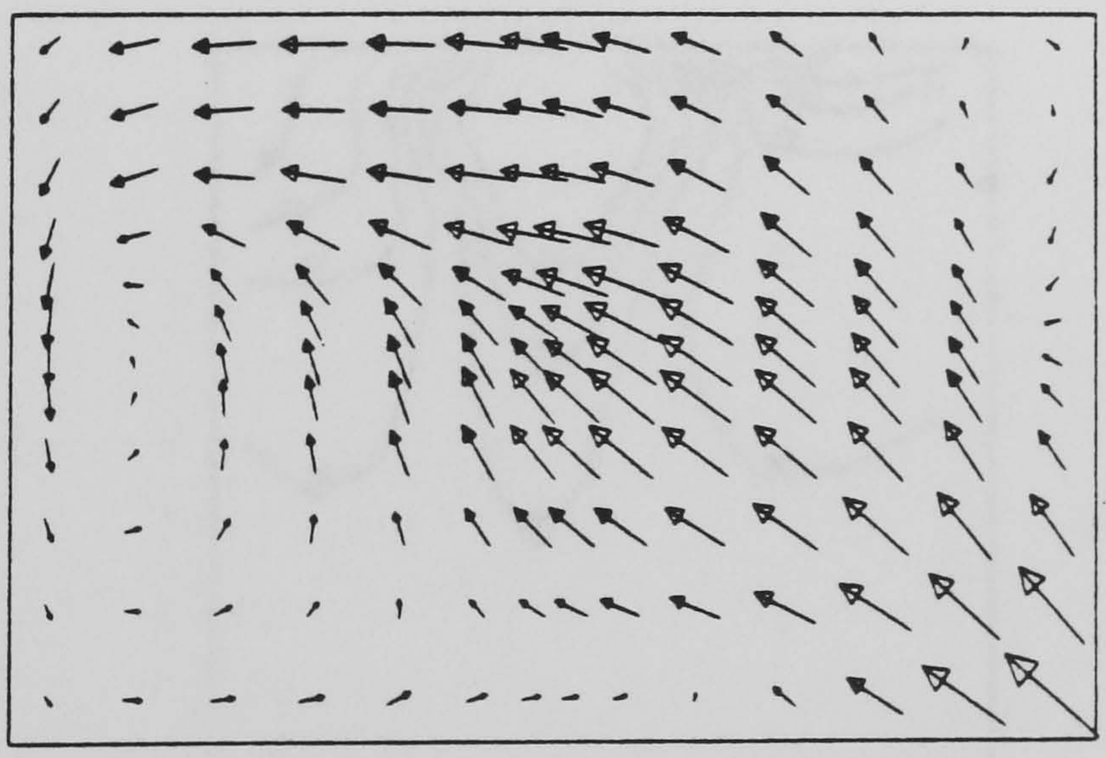

c)

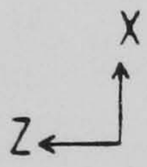

Vector scale: 2.01 m/s

Figure 5.18 Plan view of office: predicted gas velocity vectors through a horizontal plane, 0.145m below the ceiling (Y=10)
a) 0 sec. b) 10 sec. c) 25 sec

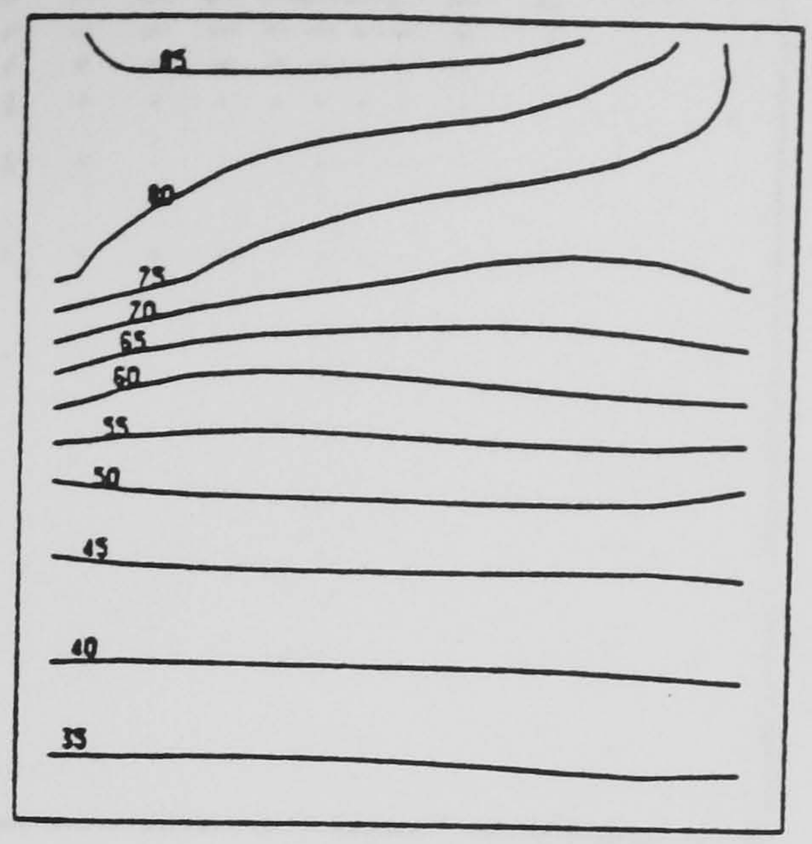

a)

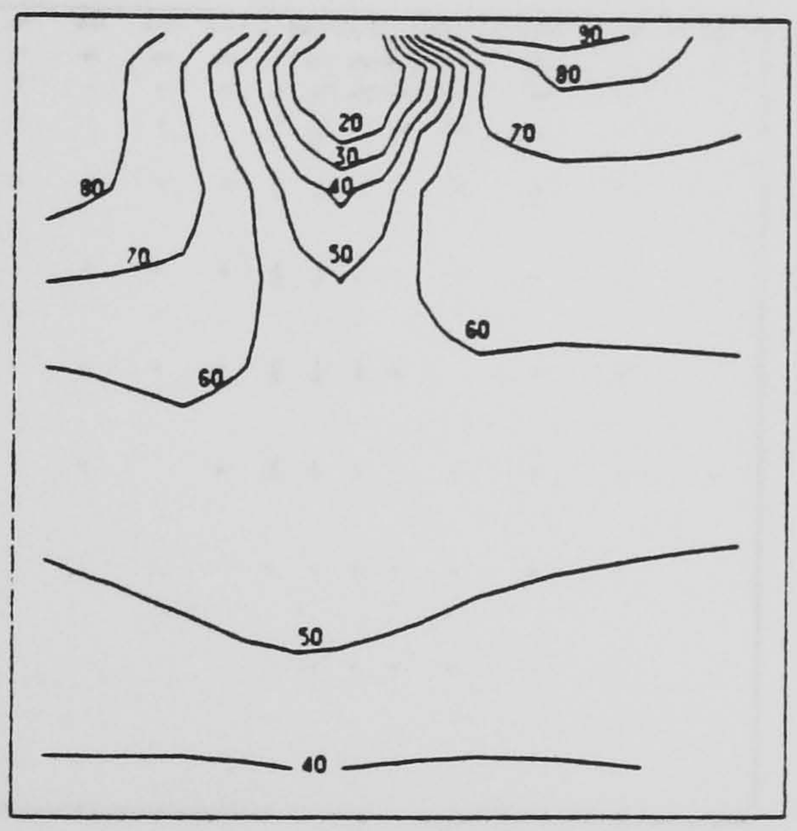

b)

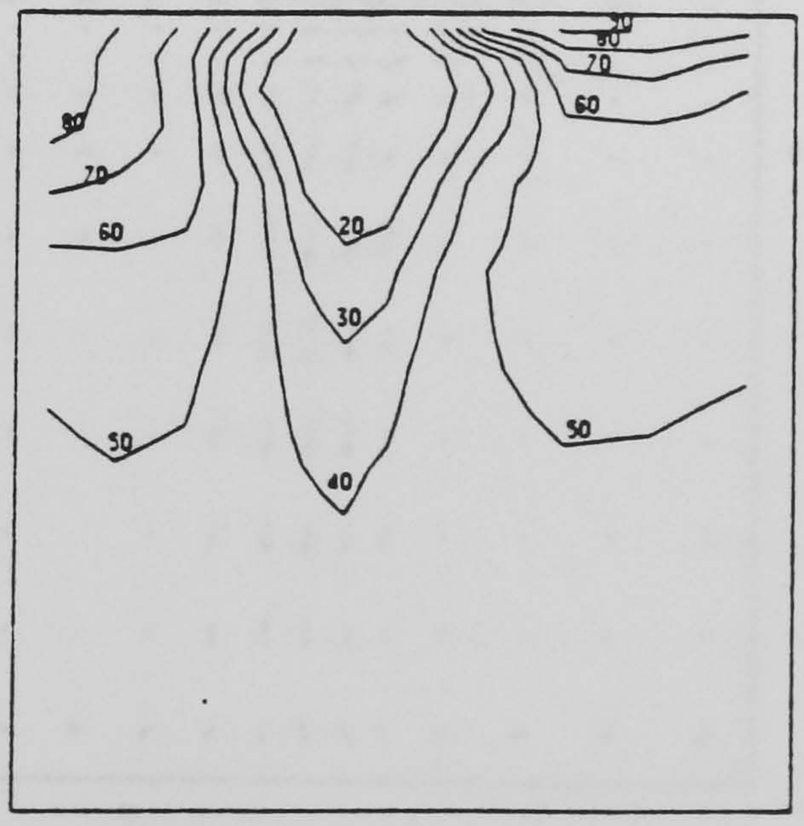

c)

Figure 5.19 Cross view of office: predicted gas temperature contours through the centre of the room and the sprinkler (Z=8)
a) 0 sec. b) 10 sec. c) 25 sec.

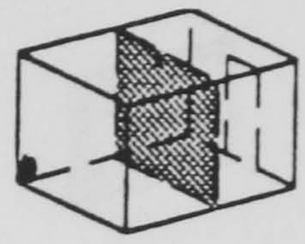

a)

b)

c)

Y
X

Vector scale: 2.01 m/s

Figure 5.20 Cross view of office: predicted gas velocity vectors through the centre of the room and the sprinkler (Z=8)
a) 0 sec. b) 10 sec. c) 25 sec.

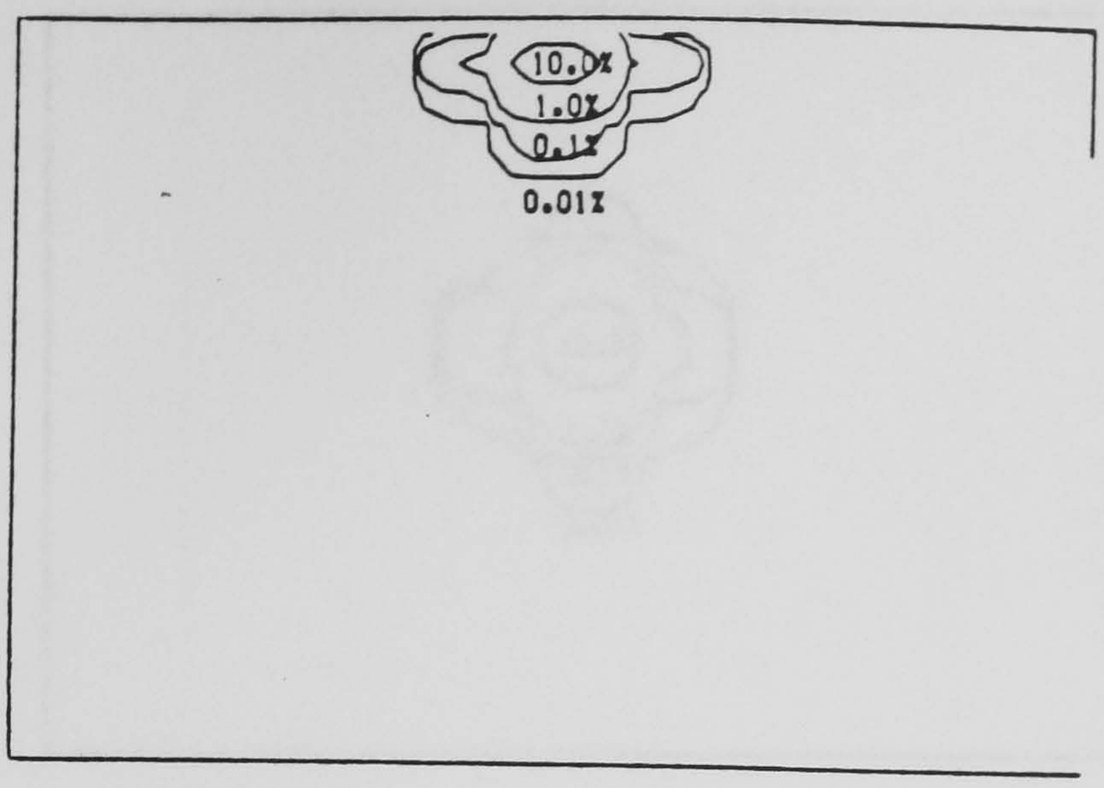

a)

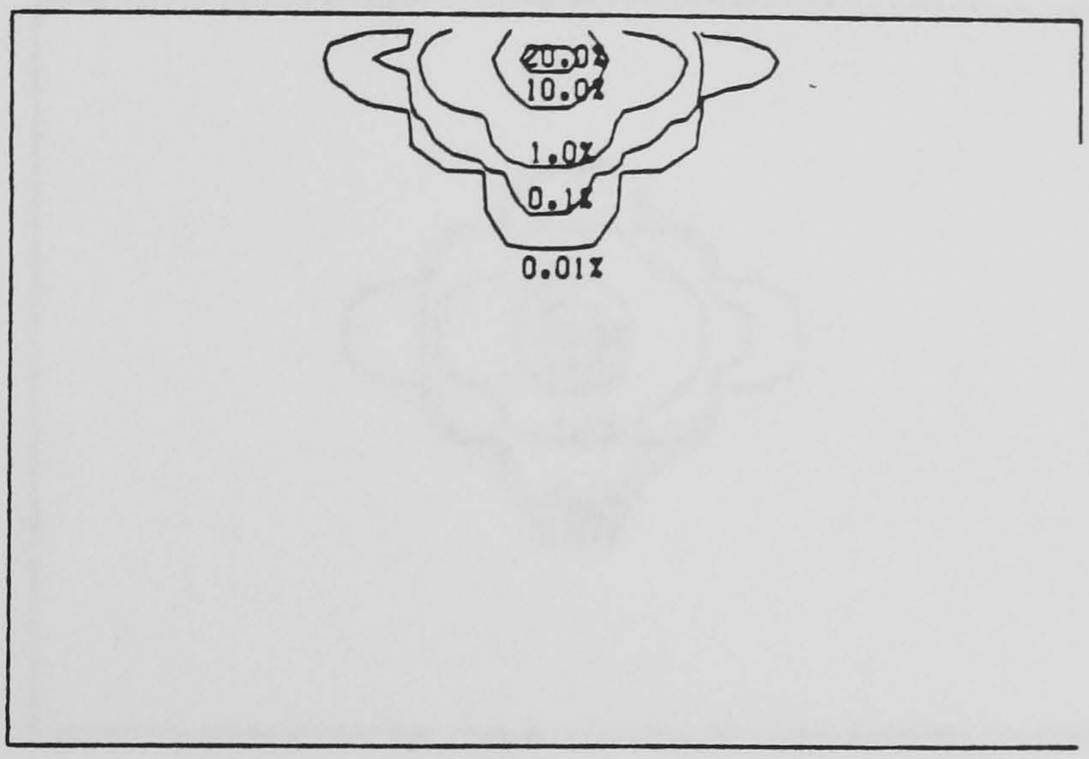

b)

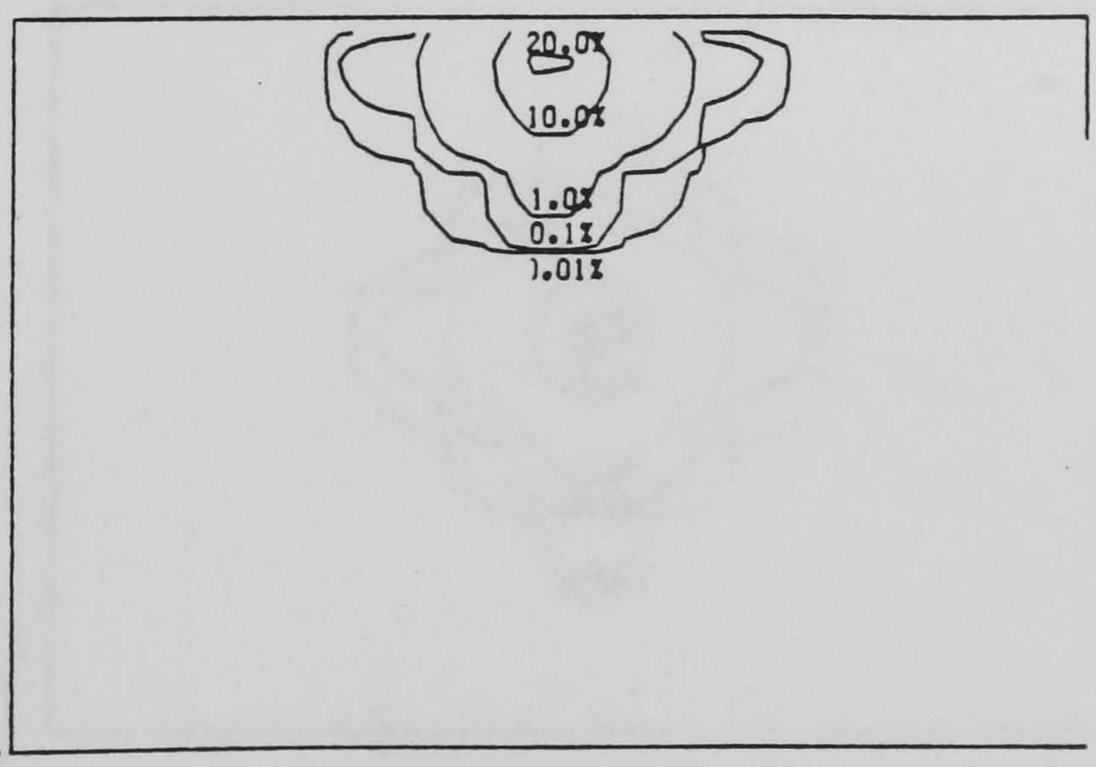

c)

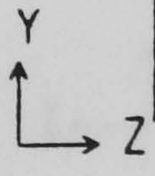

Figure 5.21 Side view of office: predicted volume fractions of water phase on the vertical central plane through the sprinkler and doorway (X=6)
a) 5 sec. b) 15 sec. c) 25 sec.

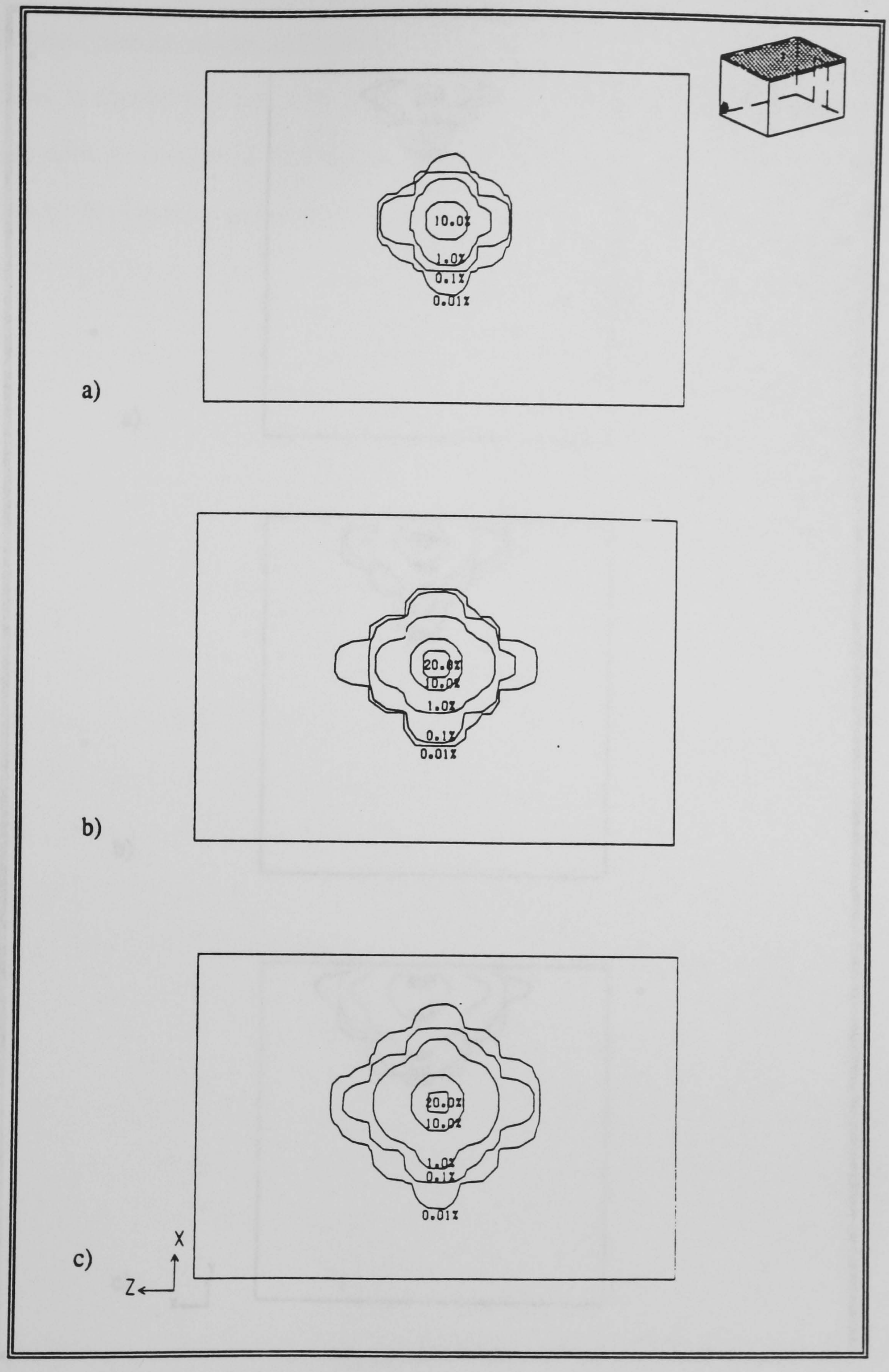

Figure 5.22 Plan view of office: predicted volume fractions of water phase through the horizontal plane sprinkler plane (Y=10)
a) 5 sec. b) 15 sec. c) 25 sec.

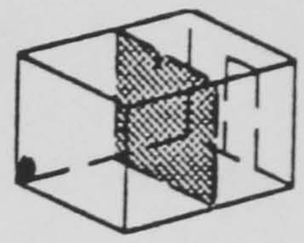

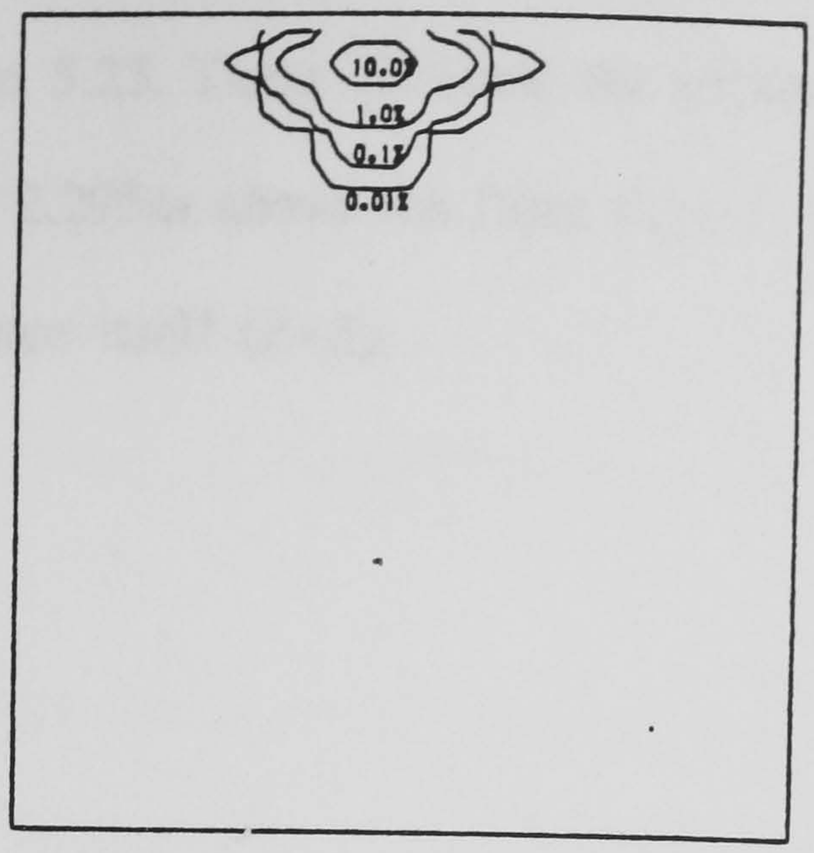

a)

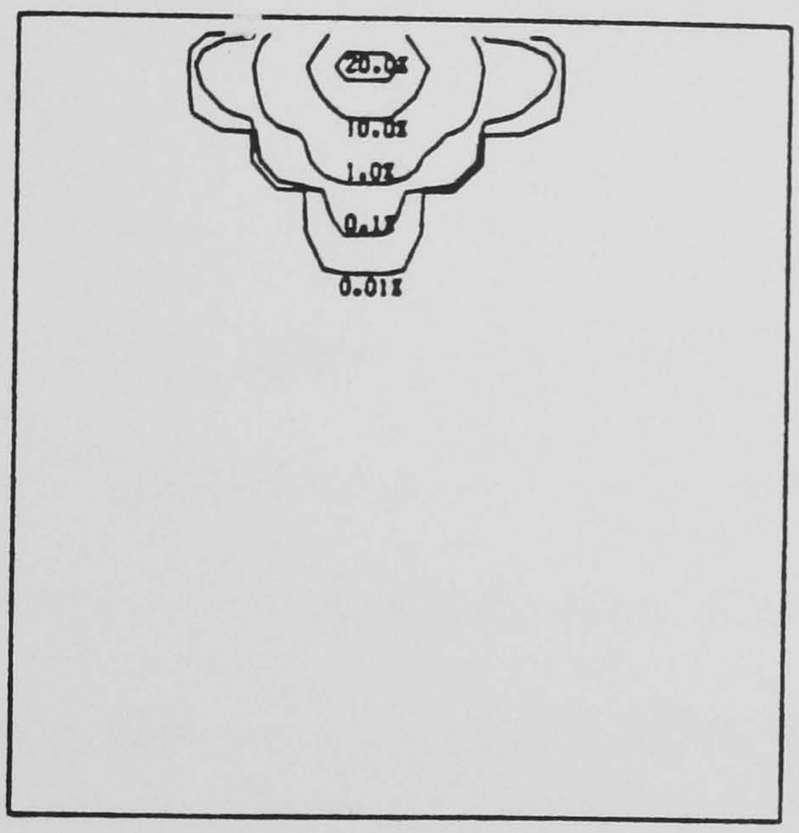

b)

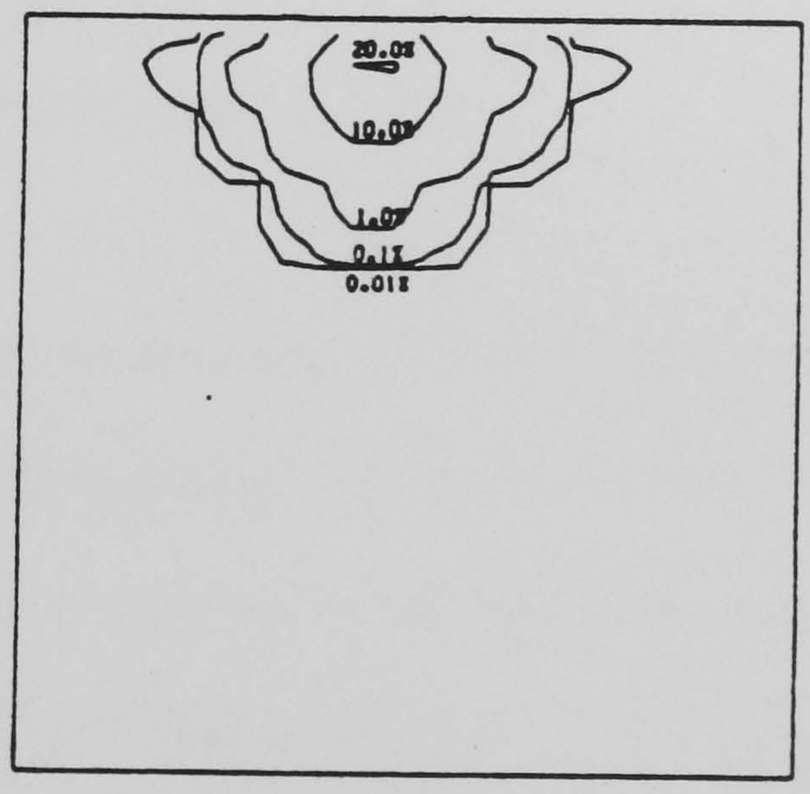

c)

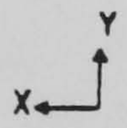

Figure 5.23 Cross view of office: predicted volume fractions of water phase through the centre of the room and the sprinkler plane (Z=8)
a) 5 sec. b) 15 sec. c) 25 sec.

contours. Similar results and conclusions can be observed for the other two views shown in figures 5.22 and 5.23. These illustrate the volume fraction contours from a plan view at a height of 2.295m above the floor (Y=10) as well as along the room through the sprinkler source itself (Z=8).

5.3.2 Hospital Ward Fire and Sprinkler Scenario

The general design of the hospital compartment, as described within chapter 3, was unchanged for the current simulation. Hence, reference is made to figures 3.31, 3.32 and 3.34 for the schematic view and numerical grids of the ward, respectively.

For the current simulation it was assumed that the fire was still in progress, releasing heat at the same rate as used at the end of the fire simulation; 40.0kW. This was assumed due to lack of further information concerning the diminishing power of the fire source.

The sprinkler was located 0.353m below the ceiling and 0.895m away from the east wall along the centre line of the bed. The sprinkler used during the experiment had the same characteristics as the office sprinkler, see section 5.3.1. It was assumed to have a diameter of 15mm with a pressure of 0.2 bar at its orifice. This resulted in a water flow rate of 0.596×10^{-3} m^3/sec released at an angle of 70° from the sprinkler's line of symmetry. The droplets were assumed to have an uniform average diameter of 1mm with an initial temperature of 10°C.

During the second part of the experiment the gas temperatures within the ward were only monitored at seven thermocouple, T1 and T3 to T8. The temperature predictions made at T2, the location just above the sprinkler are not valid in this case due to their closeness and subsequently tight linkage to the sprinkler conditions. The four additional monitoring locations S1 to S4 were unaffected. Their locations can be found in figure 3.32.

Computational Details

This sprinkler simulation lasted for 120 seconds, whereby calculations were made at one second time-intervals.

These calculations were accepted once the convergence criteria outlined in section 3.3 were satisfied. This in turn is reflected in the number of sweeps necessary per step. The resulting range was between 100 to 250 sweeps per time-step.

Results

In order to be able to have confidence in the predictions made by the model the gas temperatures varying with time at the thermocouple locations, T1 and T3 to T8, were monitored. The seven resulting comparisons of predicted and measured data are shown in figure 5.24. The fire scenario data, shown in chapter 3 are also displayed in order to demonstrate more effectively the consequences of an active sprinkler on the gas temperatures in the originally hot upper layer.

From these comparisons, as in the case of the fire scenario, it can be observed that the right *trends* have been obtained for all seven monitoring locations throughout the compartment. In fact the predictions for locations T1 to T5, are between 1.2% to 27.5% of the measured data. However, the rate of temperature decrease *felt* further afield from the fire and sprinkler, at locations T6, T7 and T8, appear to have been less than measured. The reason for this could be due to the spreading of the water particles within the room and reaching the near wall locations. Hence, the predicted direction of the main flow is questioned along with the numerical grid employed.

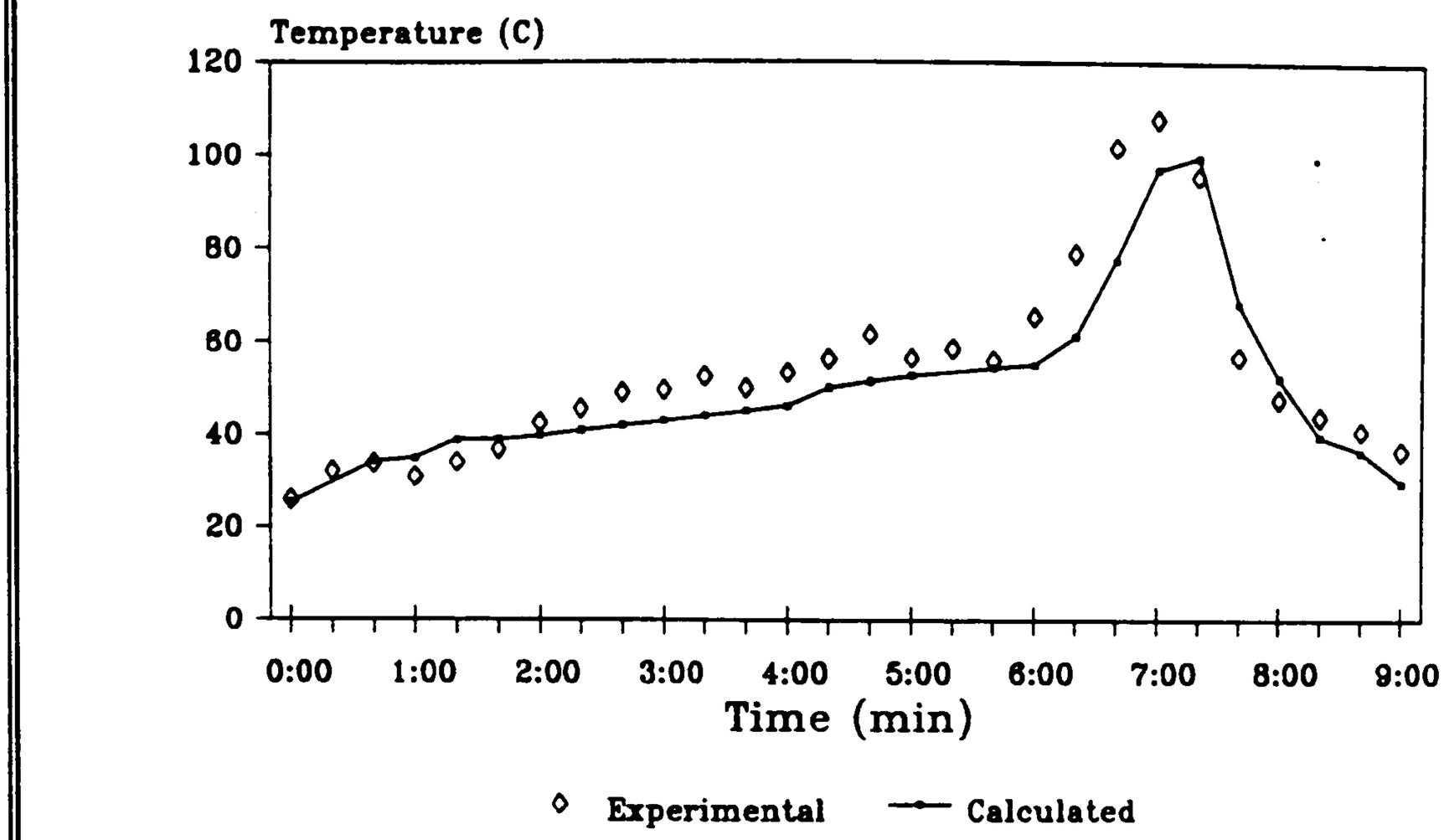

a) T1 location

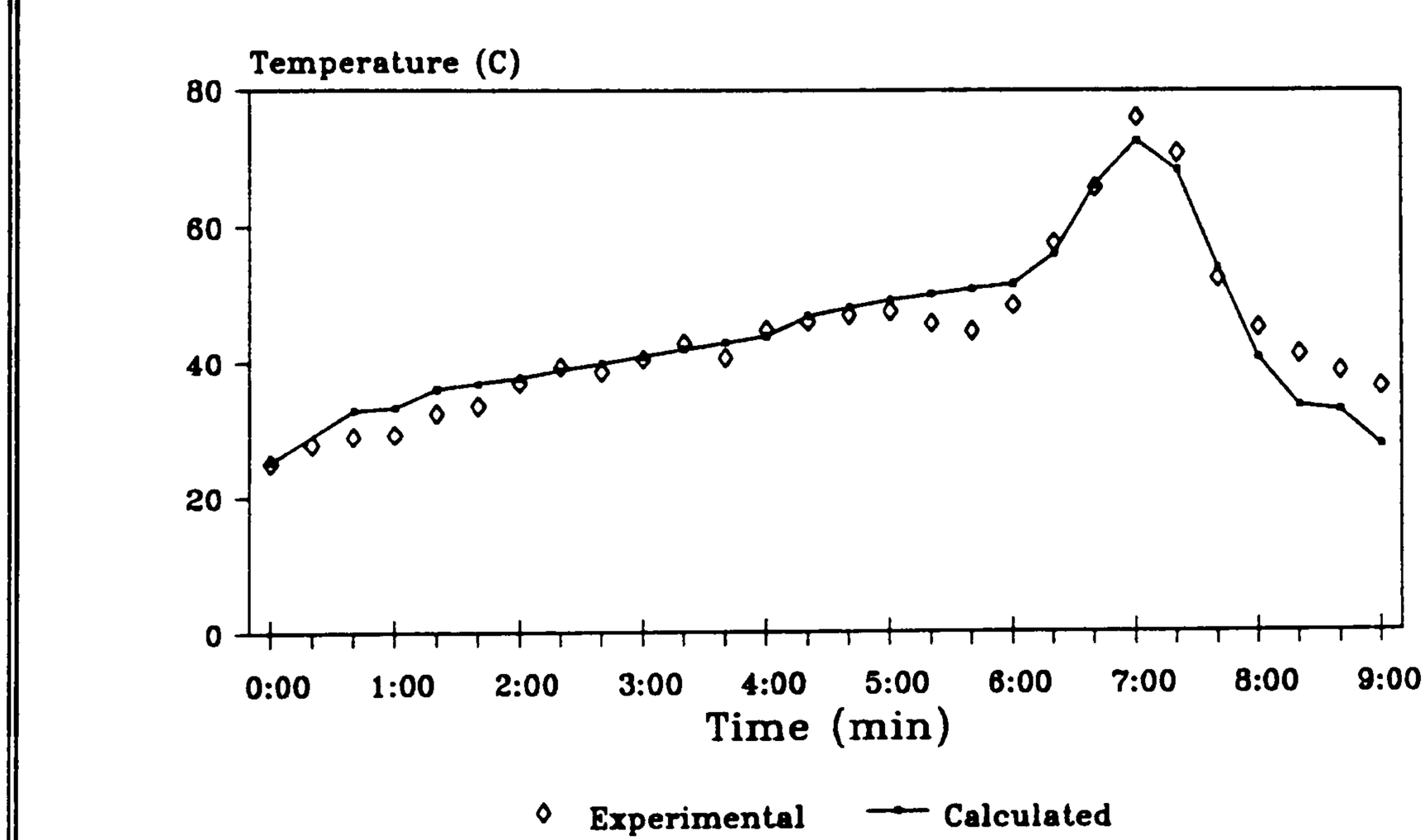

b) T3 location

Figure 5.24 Predicted and measured gas temperatures at seven thermocouple locations, 0.075m below the ceiling

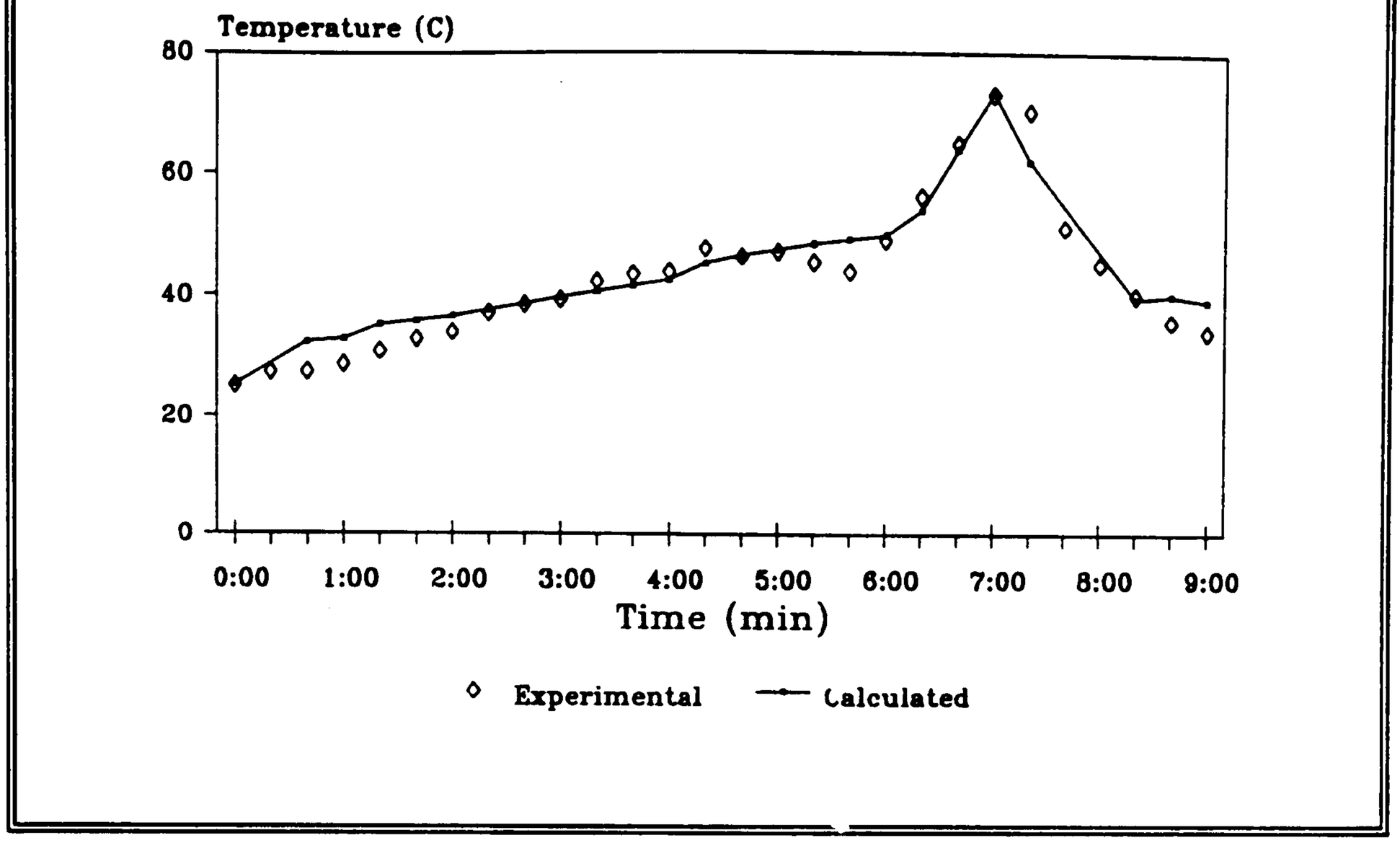

c) T4 location

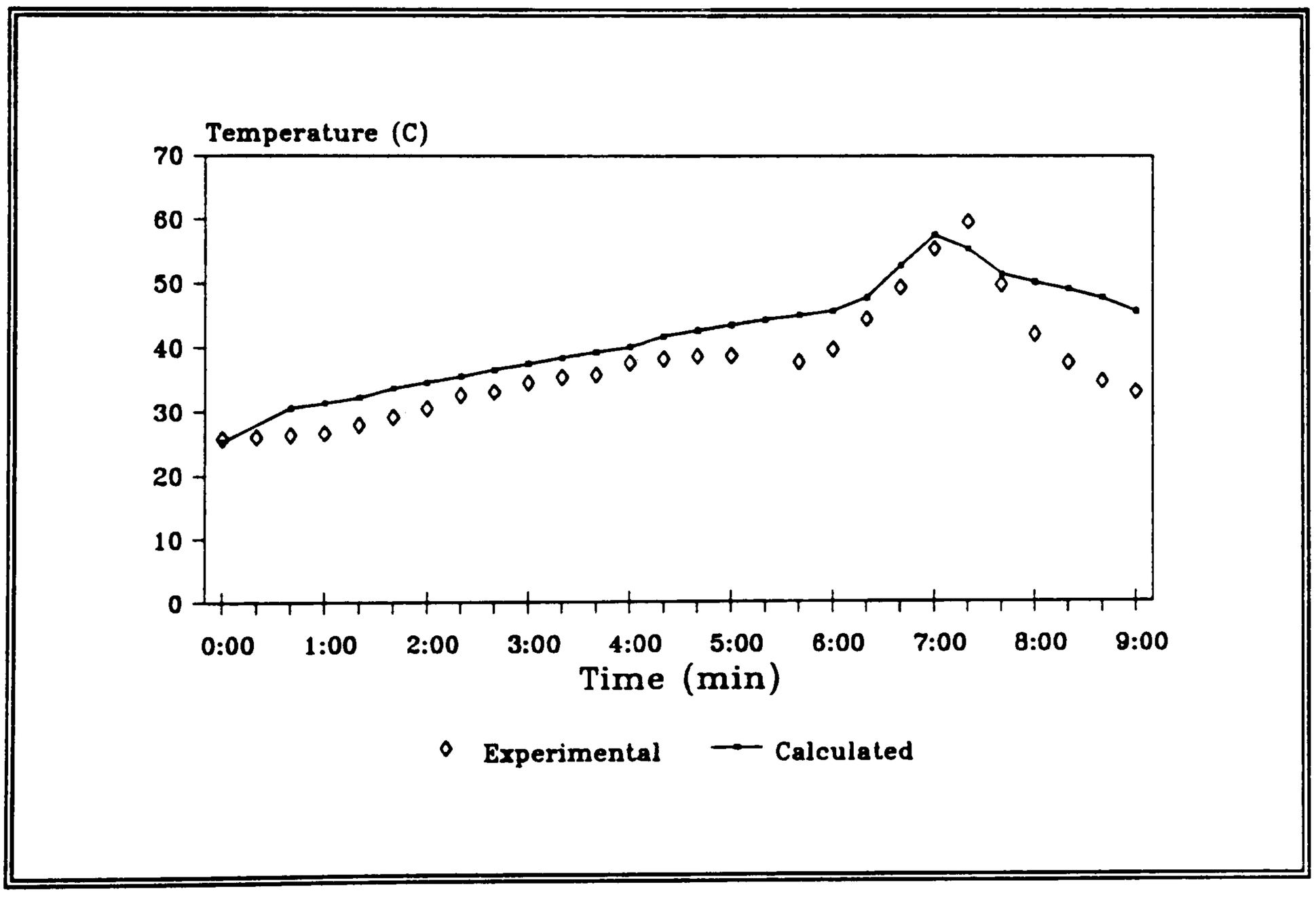

d) T5 location

Figure 5.24 Predicted and measured gas temperatures (continued)

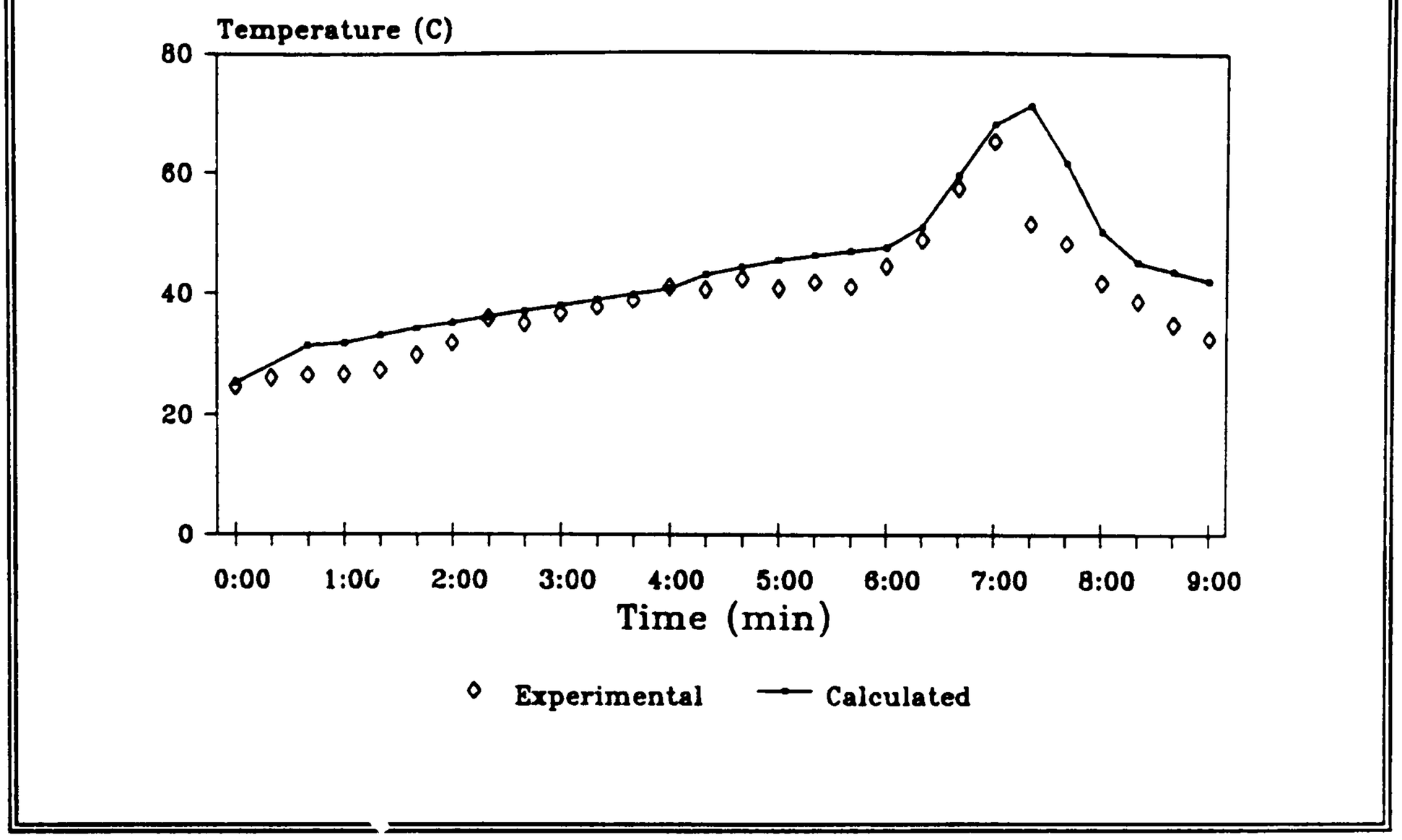

e) T6 location

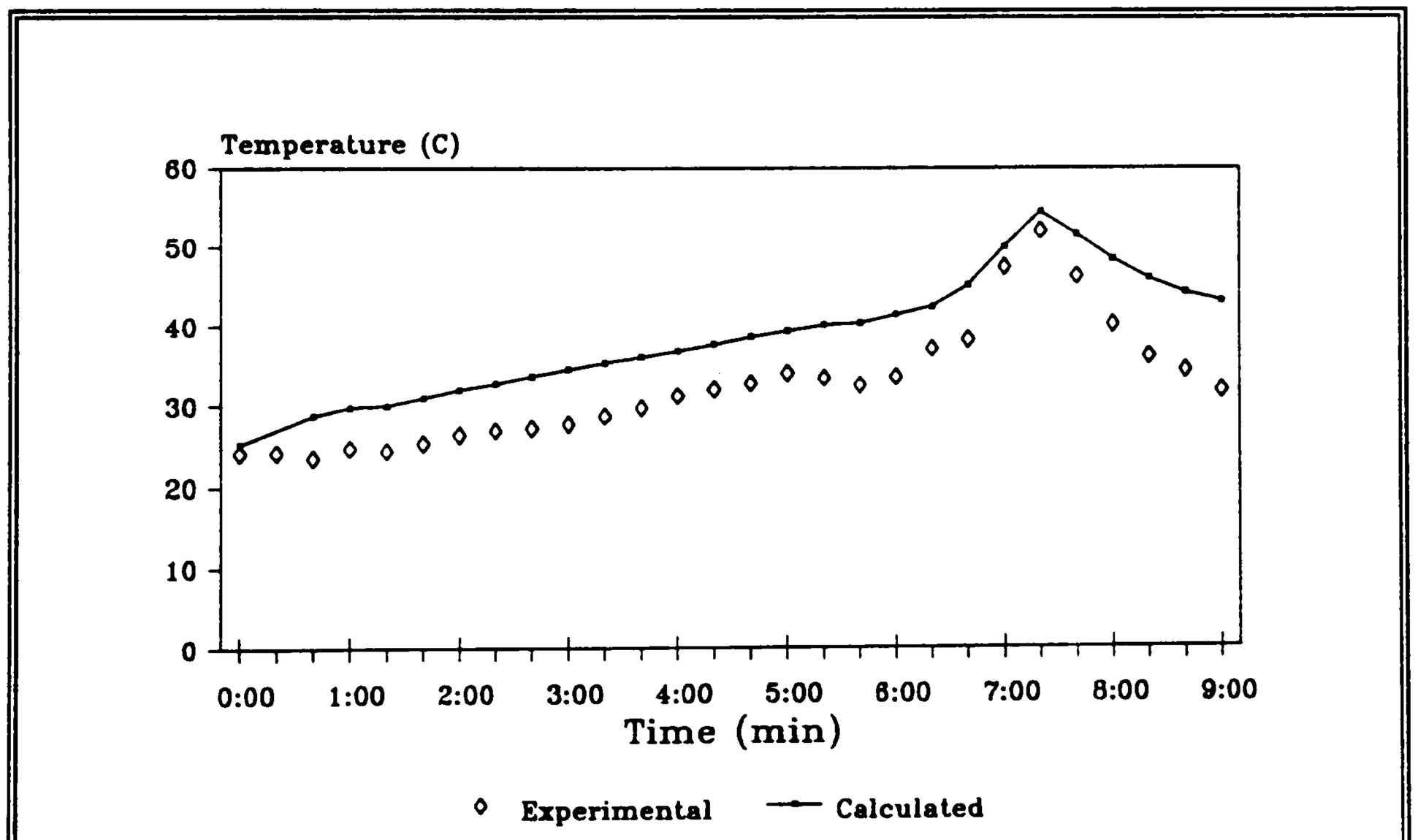

f) T7 location

Figure 5.24 Predicted and measured gas temperatures (continued)

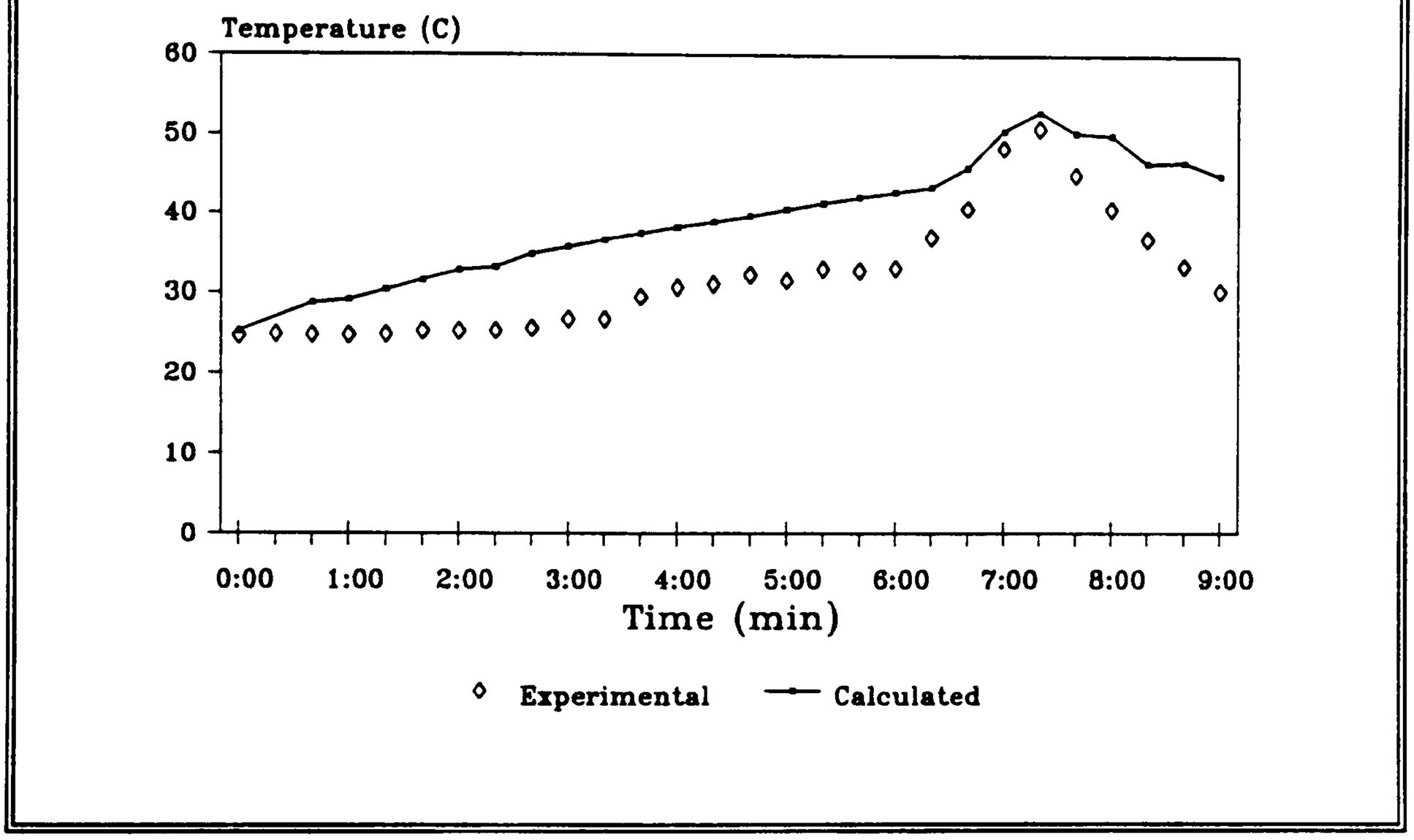

g) T8 location

Figure 5.24 Predicted and measured gas temperatures (continued)

Further investigations need to be carried out to discover if there is a link between the grid-size and the accuracy of the predictions of the spread of the water particles.

The variation of the temperature at specific times with respect to height were continued to be monitored during the sprinkler scenario at the locations S1 to S4 (see figure 3.32) though no experimental values were available for comparisons. The predictions made at these positions are shown in figure 5.25 after 0, 60 and 120 seconds following the sprinkler activation.

As was the case in the office predictions, these results reflect the effect of distance from the locations to the fire and sprinkler sources, as well as the dominant direction of the air flow. Hence, S2 experiences the cooling effect of the water droplets the earliest. Upper layer temperatures have decreased by a maximum of 10.8°C after 60 seconds compared to only a maximum temperature decrease of 4.7°C at S1. Location S3 appears to exhibit the second largest temperature drop with 7.2°C. From further comparisons of these three locations it can be seen that temperatures initially decreased in the upper and lower regions, whilst slightly increasing or remaining unaltered towards the middle section. The reason for this might be the mixing of the hot and cold gases. However, the importance of an additional sixty seconds from the life safety point of view are clearly demonstrated, as all the gas temperatures up to a height of 1.5m have been reduced to below 50°C.

Figure 5.26 shows a summary of the predictions made at the four monitoring locations after two minutes. It can be observed that the temperatures at locations S1 to S3 are below 47.4°C up to a height of 1.5m. Above that height, at locations S2 and S3 the temperatures are not deviating considerably from these values. Location S4 appears

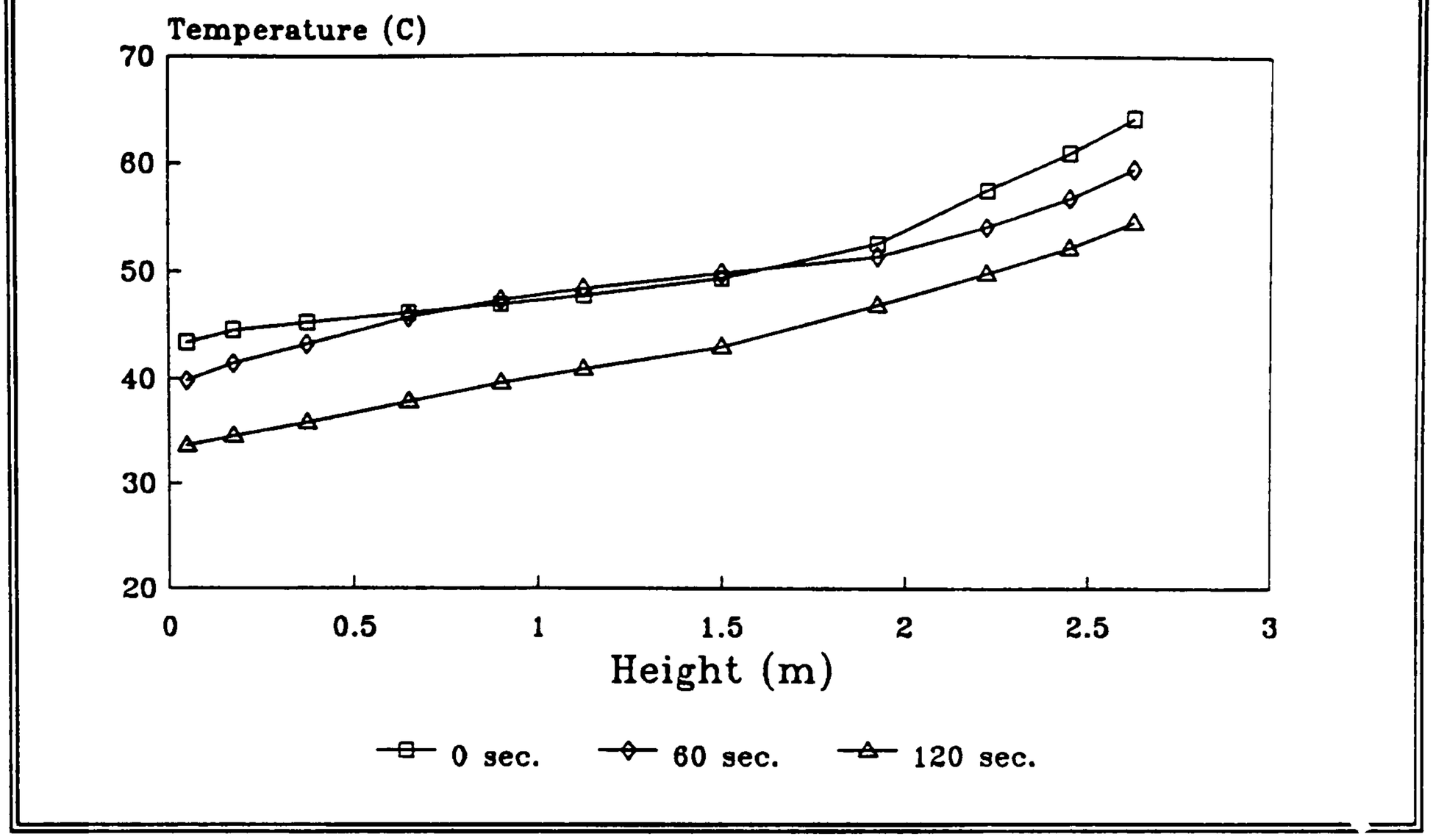

a) Location S1

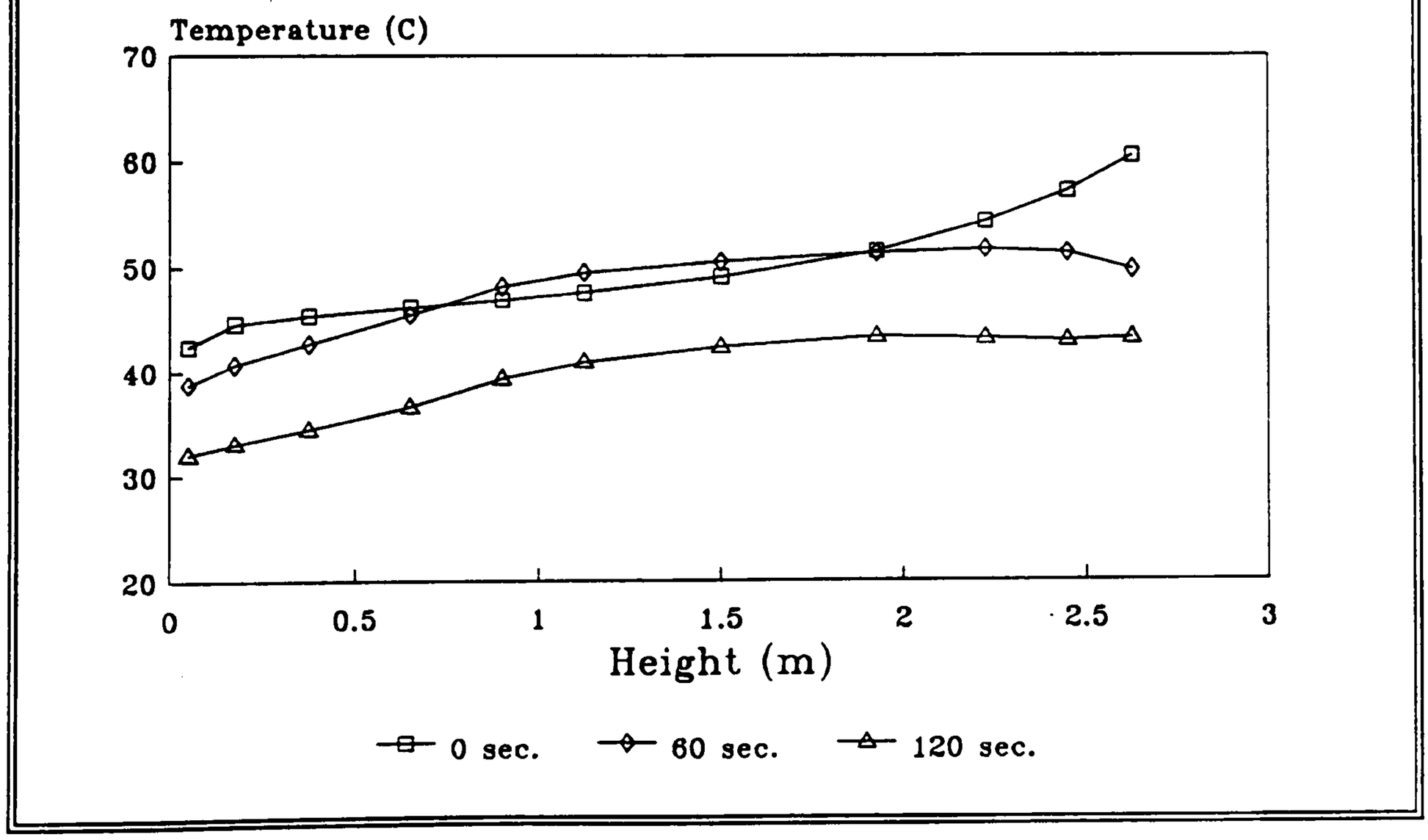

b) Location S2

Figure 5.25 Predicted gas temperature variations with height

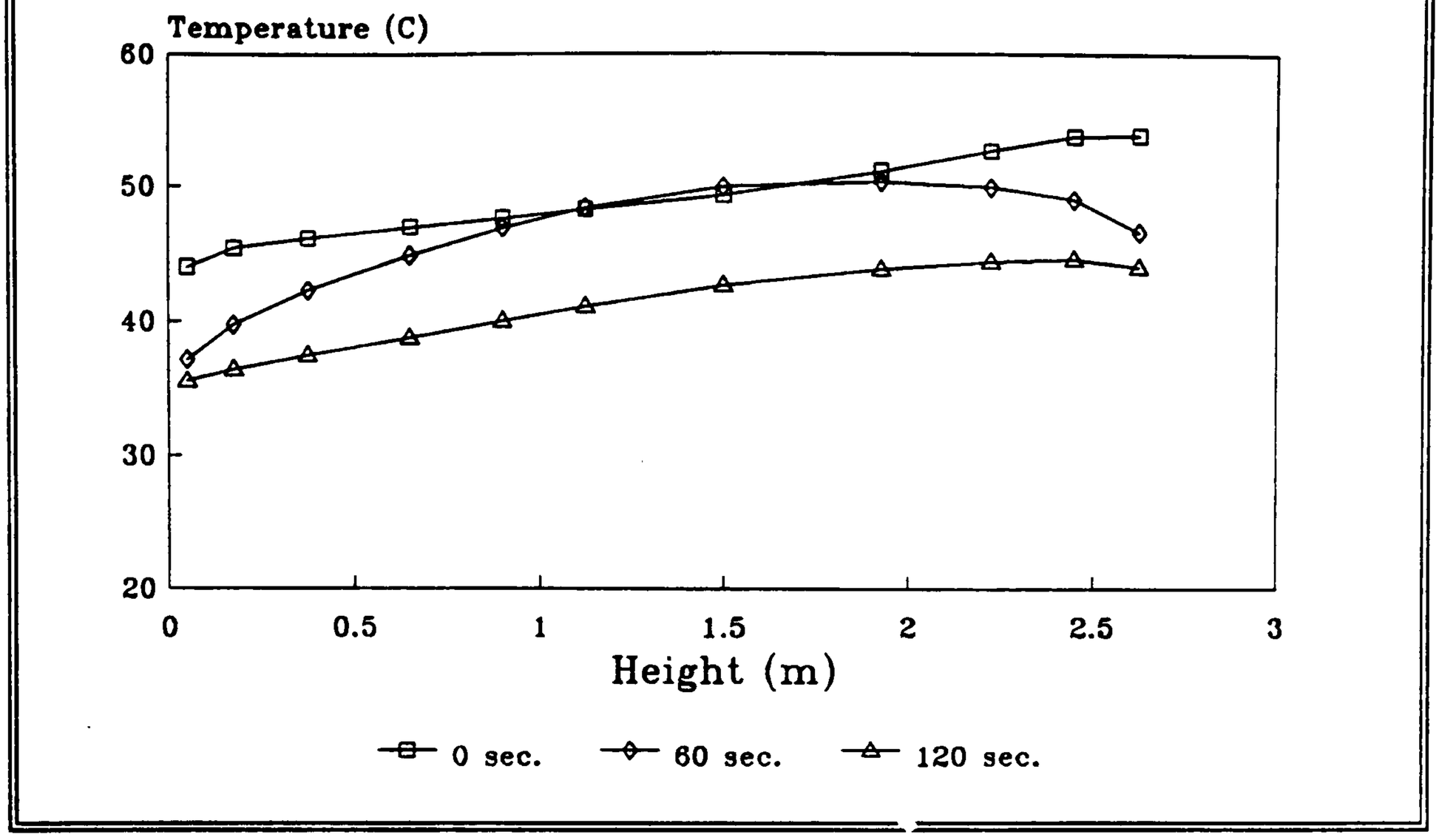

c) Location S3

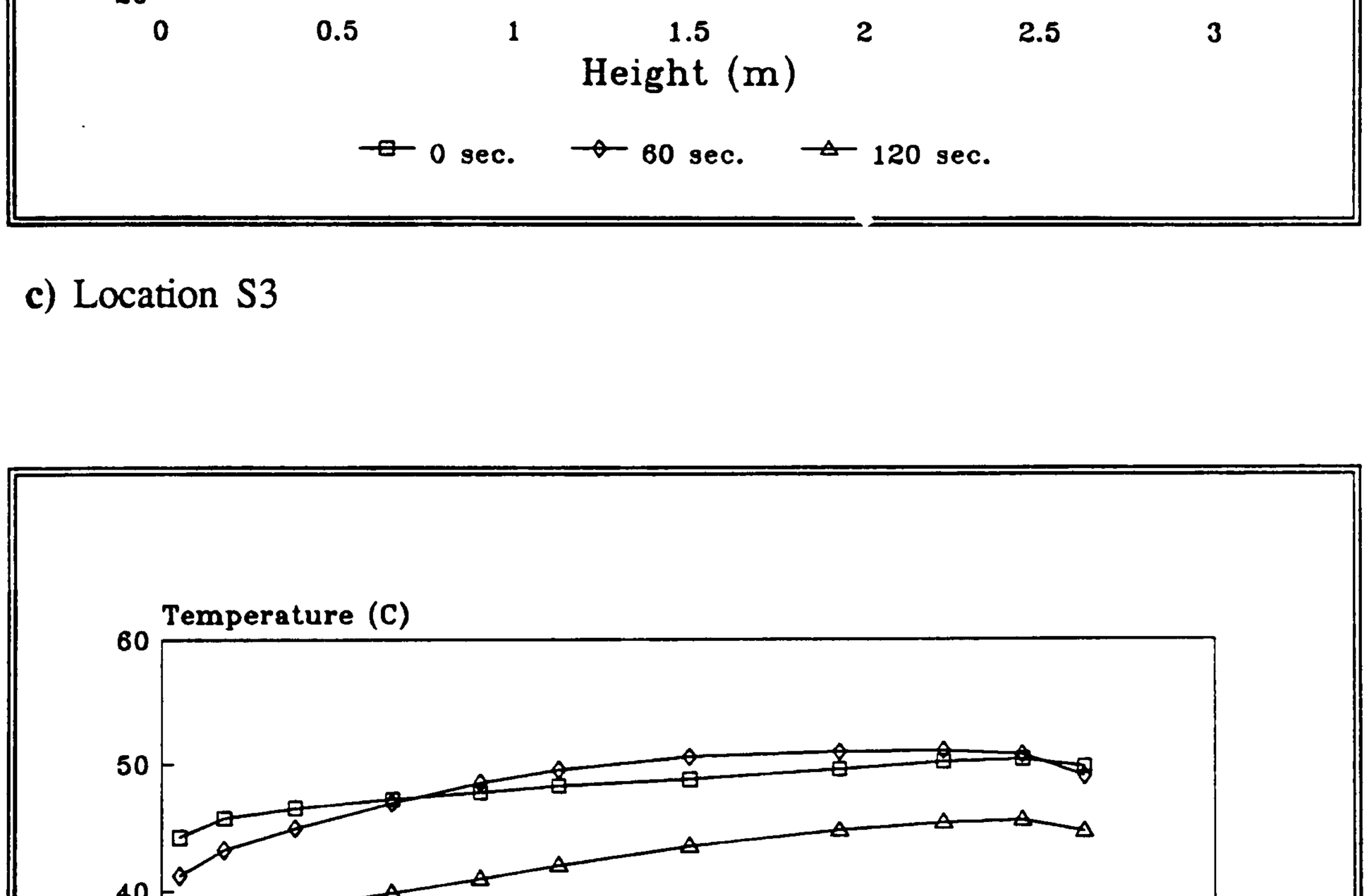

d) Location S4

Figure 5.25 Predicted gas temperature variations with height (continued)

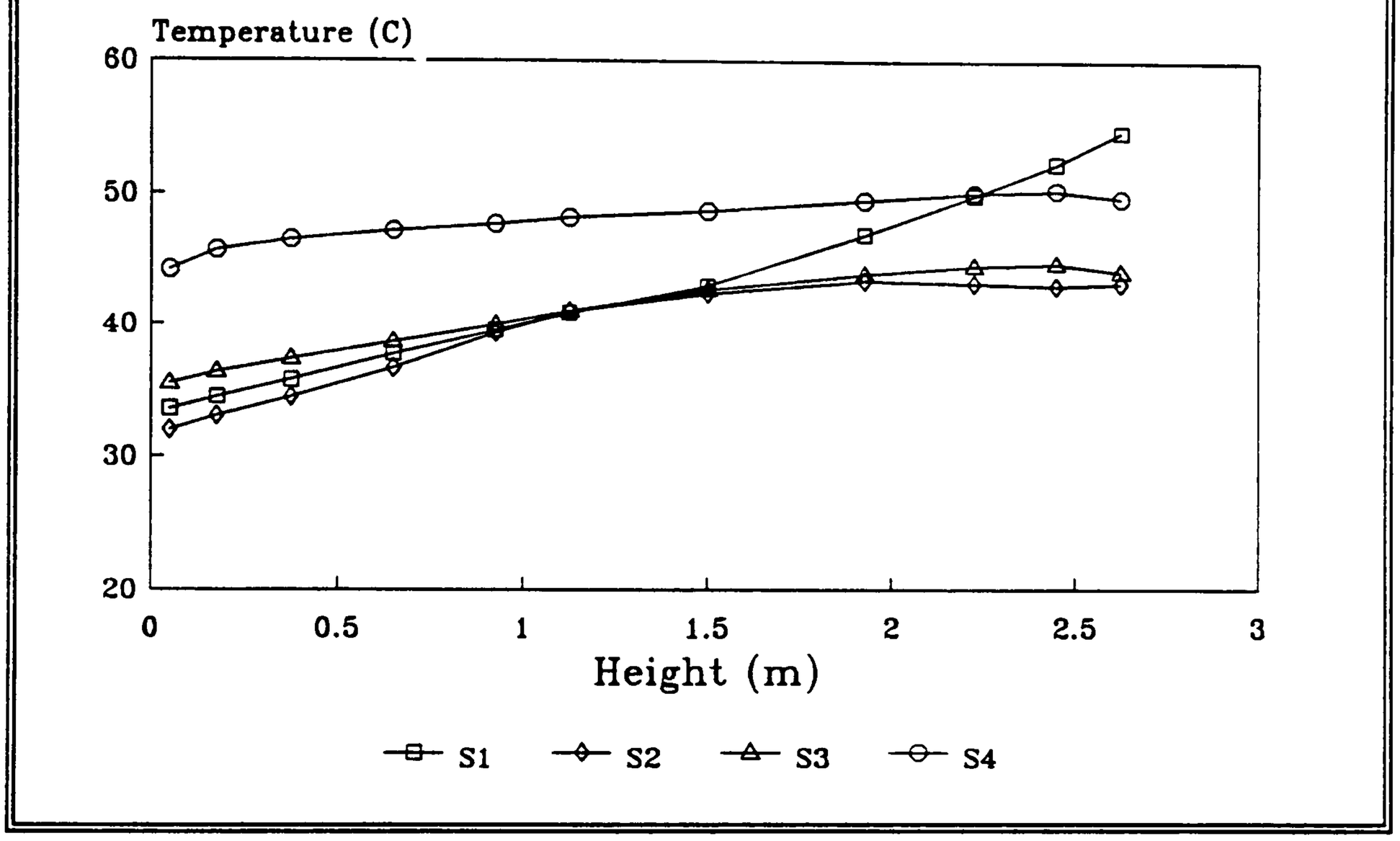

Figure 5.26 Predicted gas temperature variation with height after 120 seconds at the four monitoring locations

to be the point where temperatures have been stopped from increasing above the 50°C limit.

Though the above temperatures are only predictions, they nevertheless are a strong indication of the significant cooling effect on gas temperatures by the evaporating water droplets. The same is true for the following sets of figures which depict the gas temperatures and velocity vectors, as well as the expanding domain of the water spray at distinct moments in time and space through the compartment. The result presented are after 0, 60 and 120 seconds from the activation of the sprinkler respectively. For further comparisons the slices illustrated are taken through the same locations as used in chapter 3; see figures 3.38 to 3.43.

The first slices shown in figure 5.27 and 5.28 are across the room with the heaters on the left and the fire source in the centre, elevated off the floor (X=12). Though this plane is not through the actual sprinkler location the spreading effect of the spray can clearly be identified.

Prior to sprinkler activation the fire plume was able to rise straight upwards and spread outwards along the ceiling. However, the closeness of the sprinkler resulted in a form of barrier which hindered the plume from rising and spreading out. Hence, the hot temperatures are confined to below the sprinkler as well as cooling the surrounding gas temperatures.

Subsequently, after two minutes, the gas temperatures to the right of the bed have cooled down to below 50°C. However, due to the direction of the air flow the area to the left of the bed has been kept much hotter.

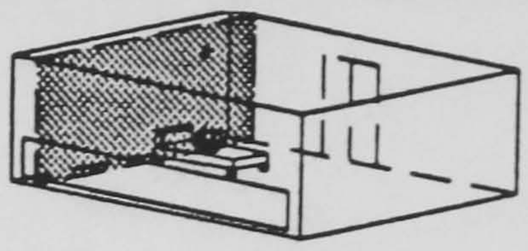

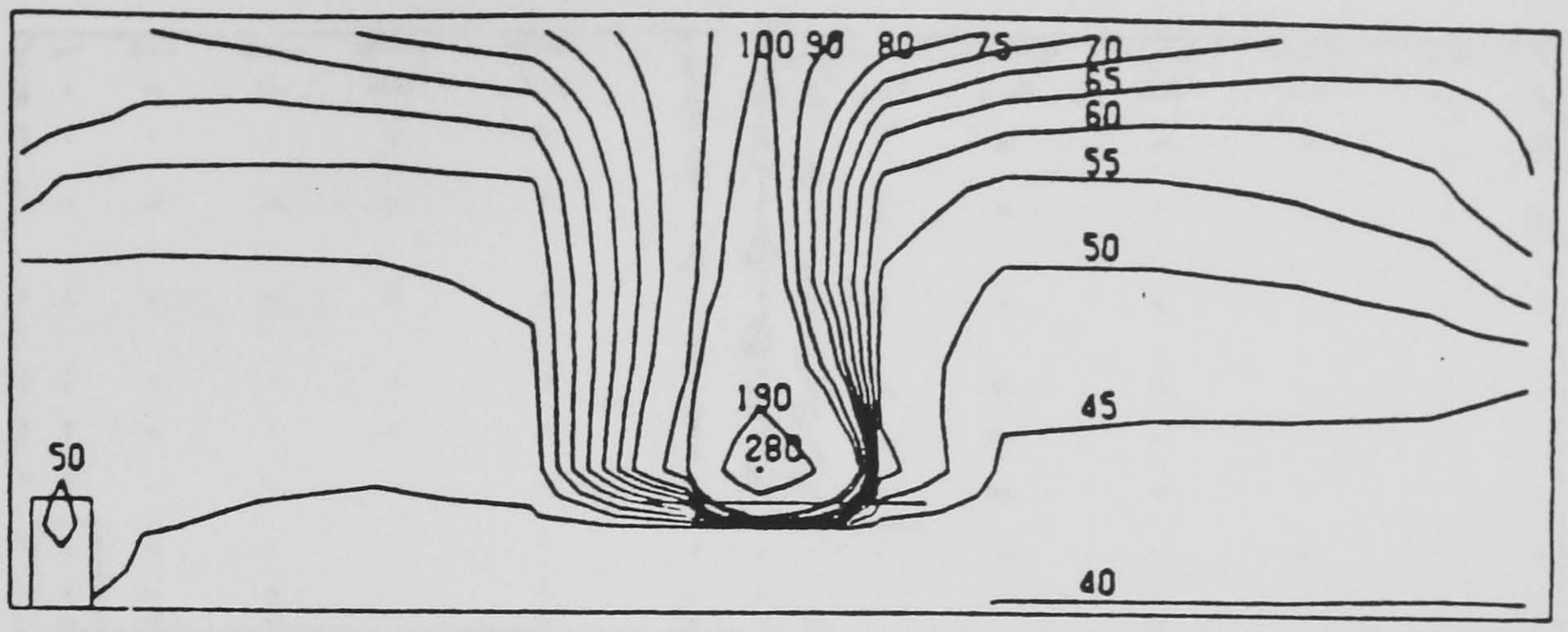

a)

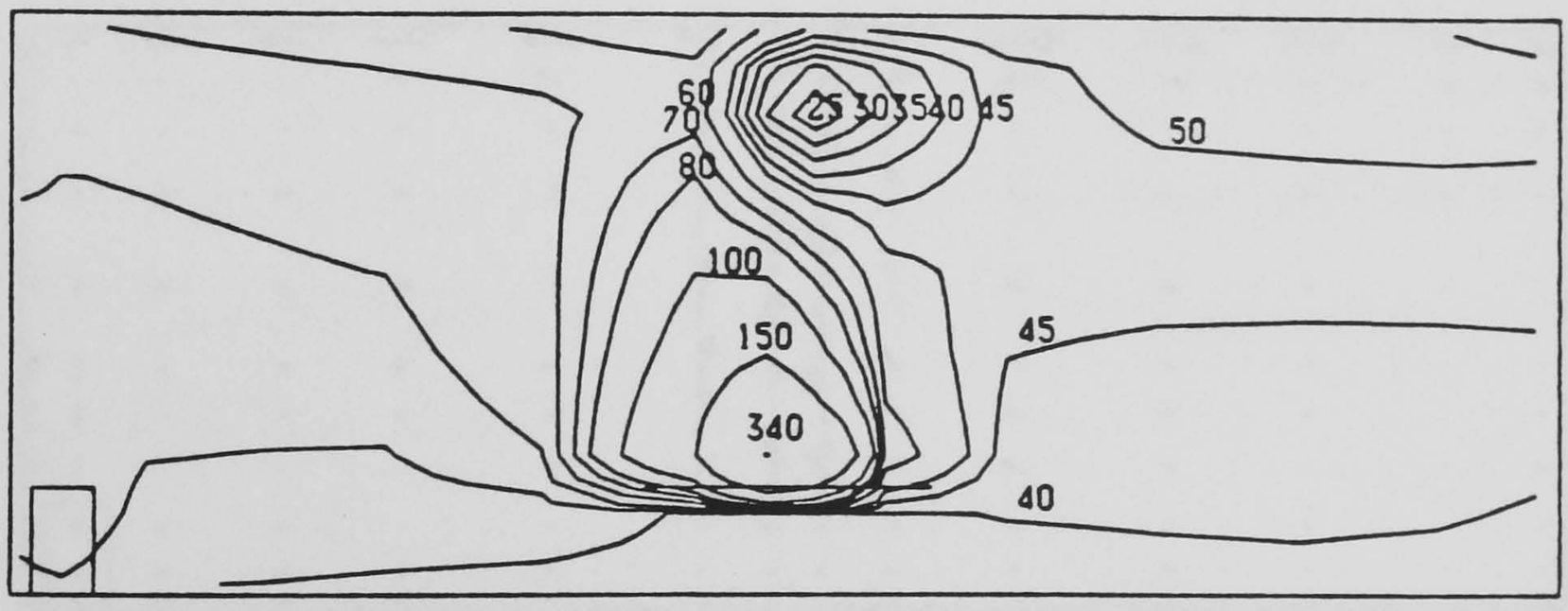

b)

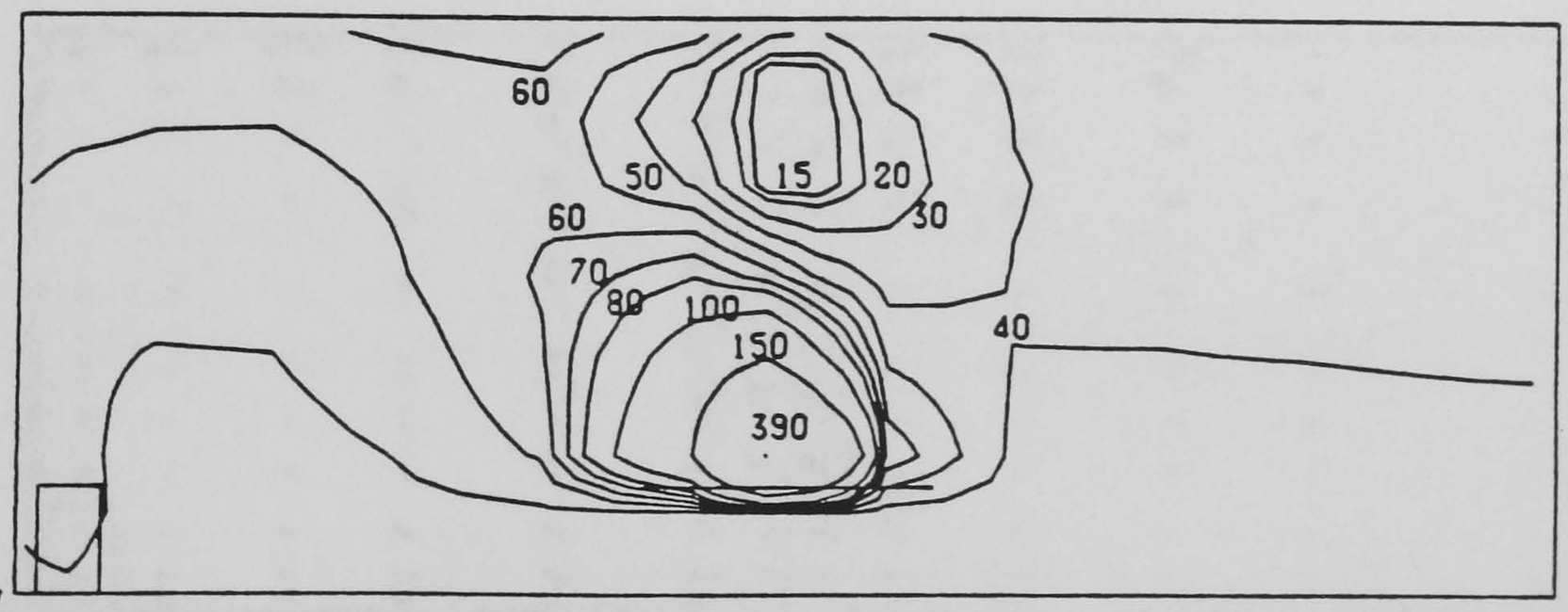

c)

Figure 5.27 Side view of Hospital ward: predicted gas temperature contours along the west wall through the fire source (X=12)
a) 0 sec. b) 60 sec. c) 120 sec.

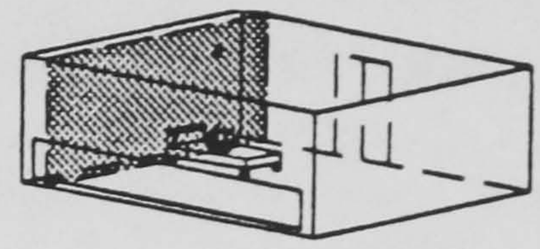

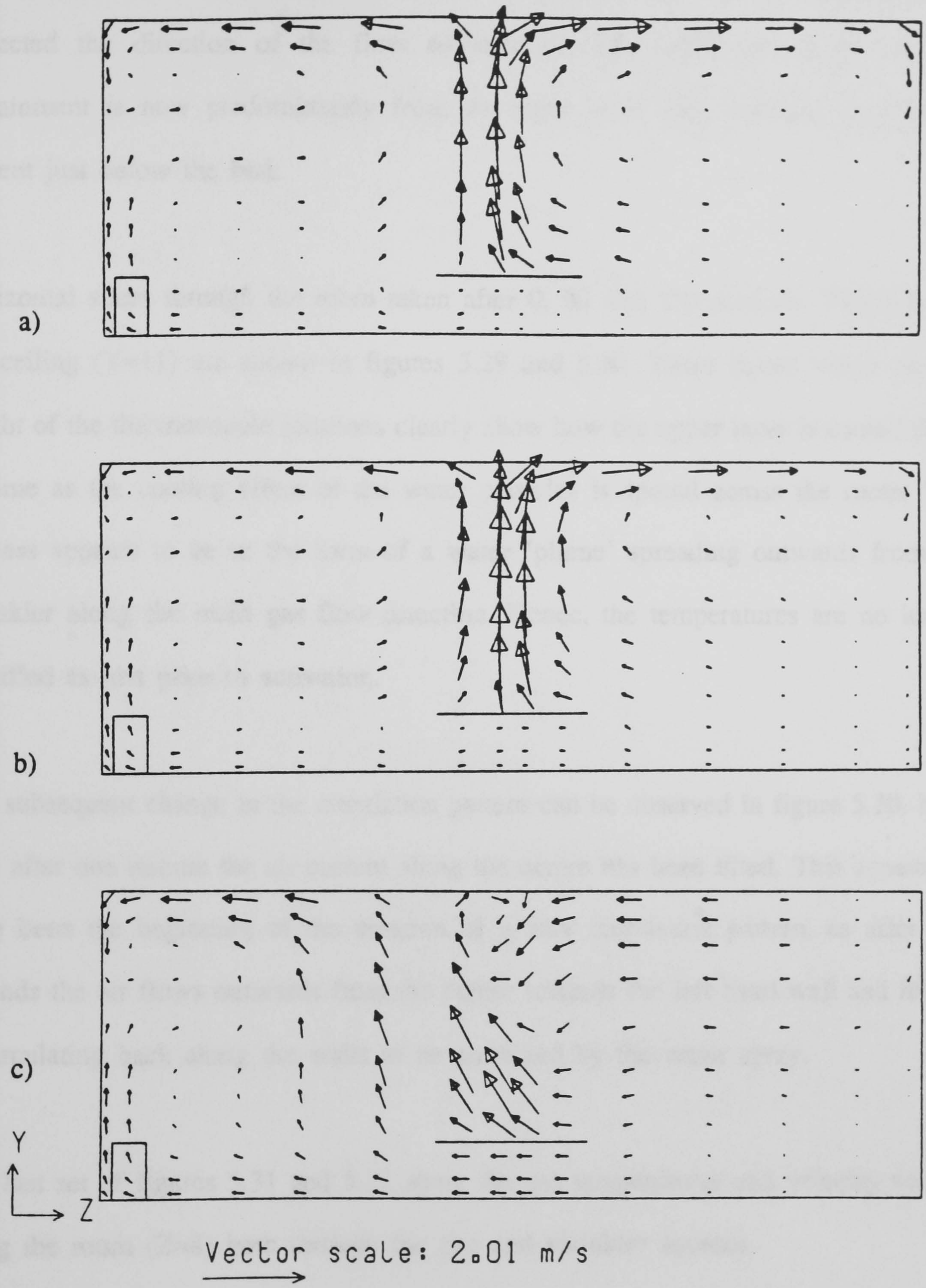

Figure 5.28 Side view of Hospital ward: predicted gas velocity vectors along the west wall through the fire source (X=12)
a) 0 sec. b) 60 sec. c) 120 sec.

The respective velocity vectors of these gas temperatures are shown in figure 5.28. Note how after 60 seconds from release of the water particles the strength of the fire plume has increased. However, after a further minute the water spray has considerably deflected the direction of the flow towards the left hand side. Note how the entrainment is now predominantly from the right hand side, resulting in a strong current just below the bed.

Horizontal slices through the room taken after 0, 60 and 120 seconds, 75mm below the ceiling (Y=11) are shown in figures 5.29 and 5.30. These layers which are the height of the thermocouple locations clearly show how the upper layer is cooled down in time as the cooling effect of the water particles is spread across the room. This process appears to be in the form of a water 'plume' spreading outwards from the sprinkler along the main gas flow direction. Hence, the temperatures are no longer stratified as just prior to activation.

The subsequent change in the circulation pattern can be observed in figure 5.30. Note how after one minute the air current along the centre has been tilted. This appears to have been the beginning of the creation of a new circulation pattern, as after 120 seconds the air flows outwards from the centre towards the left hand wall and hence, re-circulating back along the walls to be entrained by the water spray.

The last set of figures 5.31 and 5.32 show the gas temperatures and velocity vectors along the room (Z=8) both through the fire and sprinkler sources.

Firstly it can be observed from figure 5.31 the way in which the sprinkler creates a water curtain and hence, confining the hot gases to only a small area of the room.

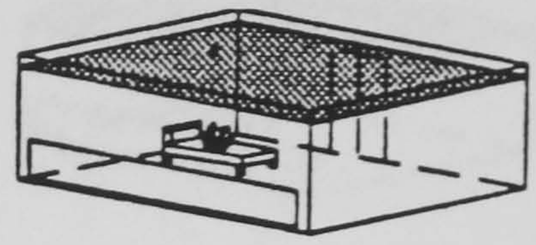

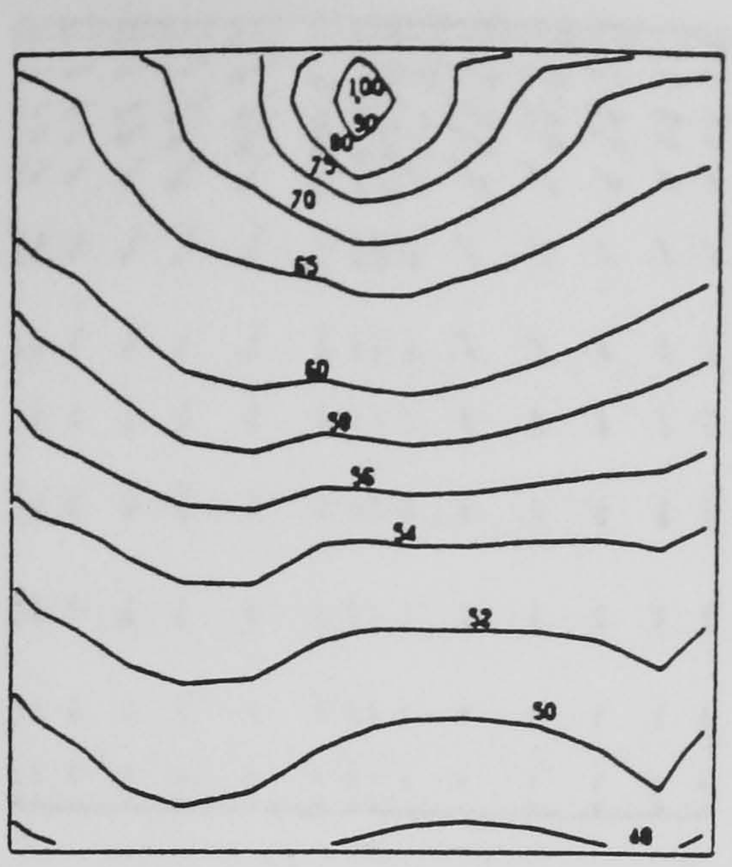

a)

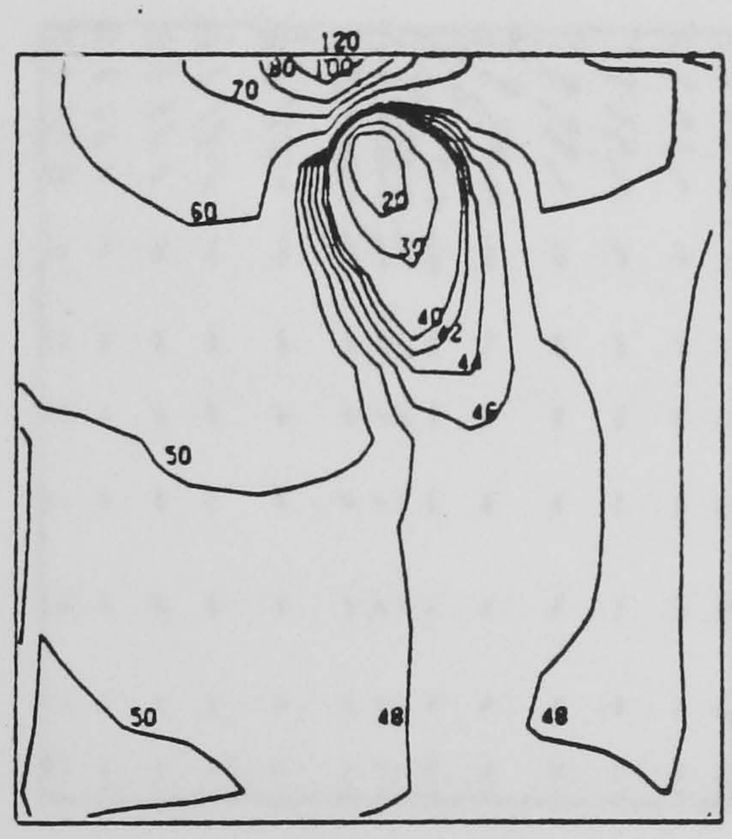

b)

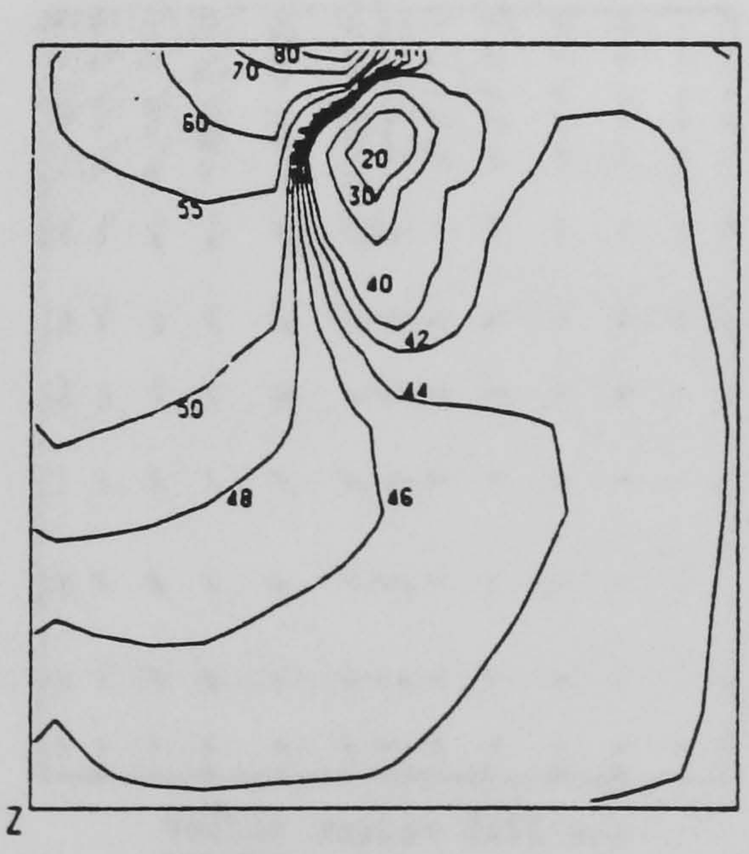

c)

Figure 5.29 Plan view of Hospital ward: predicted gas temperature contours 0.075m below the ceiling (Y=11)
a) 0 sec b) 60 sec. c) 120 sec.

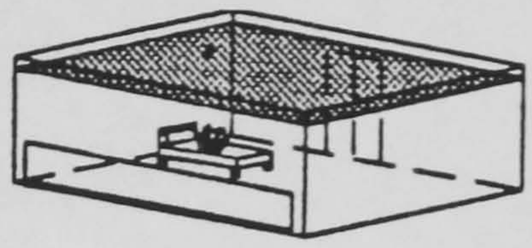

a)

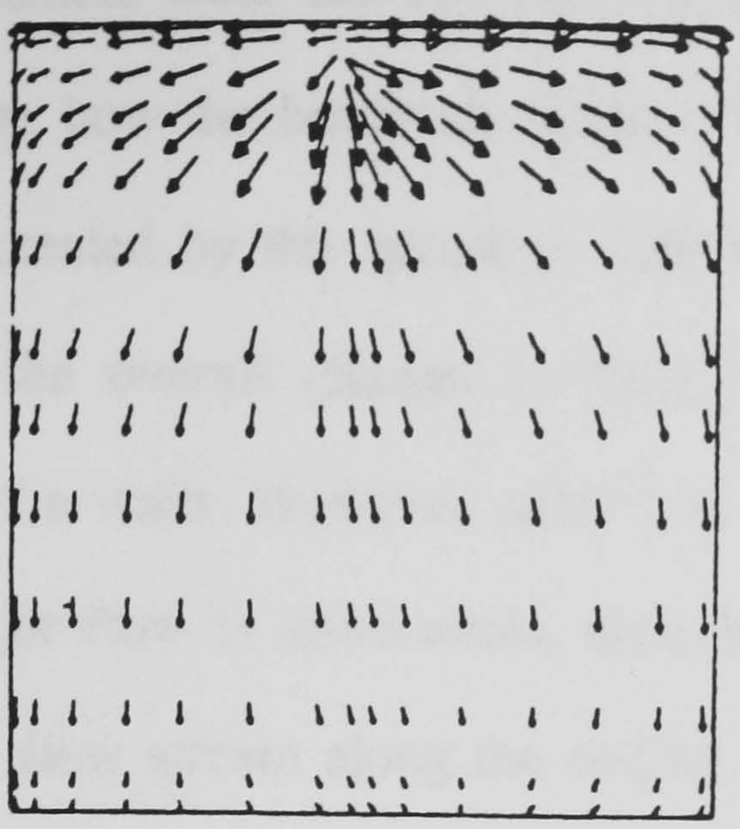

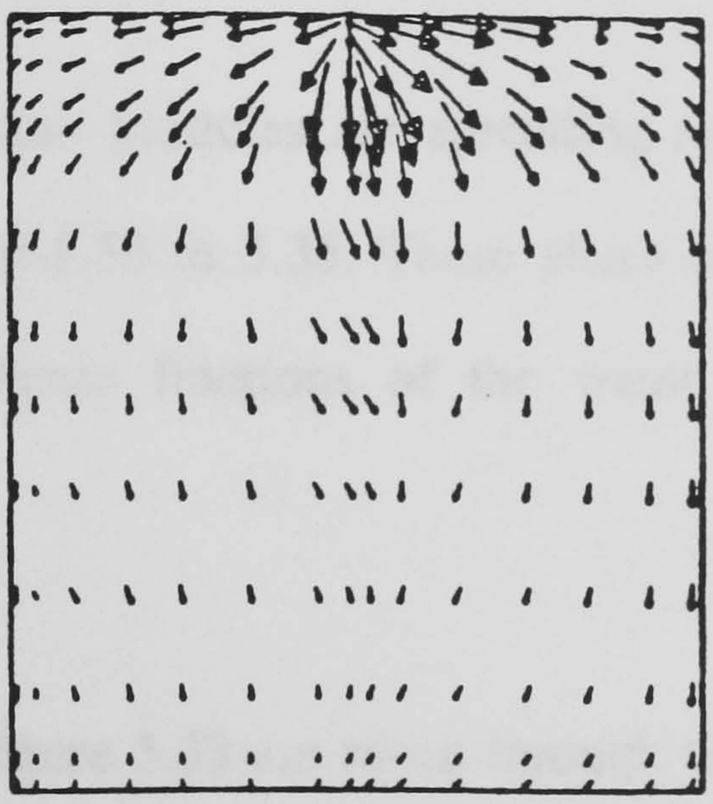

b)

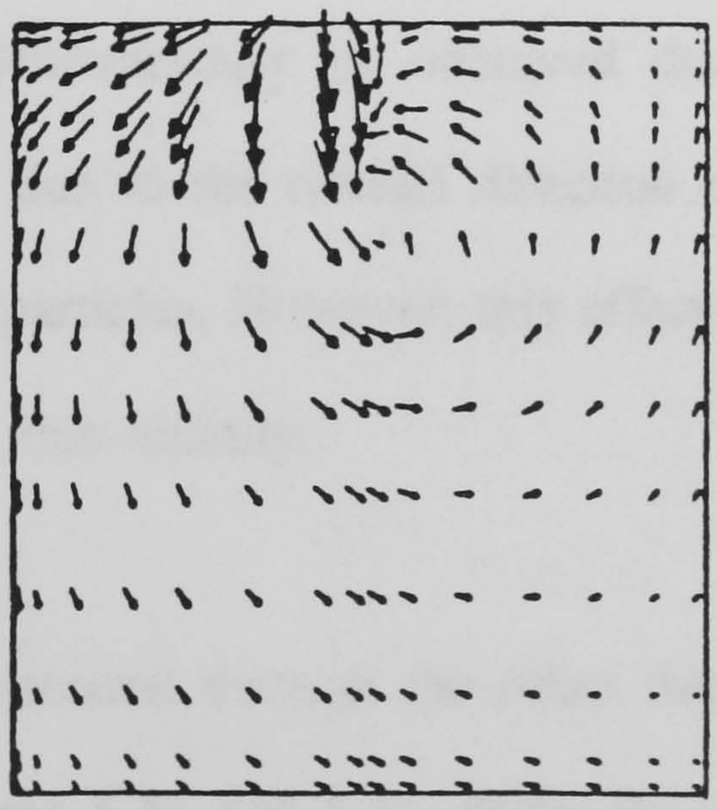

c)

Figure 5.30 Plan view of Hospital ward: predicted gas velocity vectors 0.075m below the ceiling (Y=11)
a) 0 sec b) 60 sec. c) 120 sec.

Subsequently the gases remote from the fire and sprinkler are no longer heated up but are cooled down. Note how the hotter air layers are in fact pushed upwards due to the downwards force created by the sprinkler. This effect is more clearly seen in figure 5.32 along with the overall change in flow pattern. Originally one large circulation moved along the walls. However, after two minutes the resulting current are more varied. The major flow is downwards, deflected off the bed and along the floor. Meanwhile a small flow stream along the ceiling is created. These two current meet towards the centre of the room, aiding the mixing and cooling process.

The way in which the water particles are spreading out within the room are shown in the last three figures of 5.33 to 5.35. These slices are taken through the sprinkler planes and show the volume fractions of the water phase after 30, 60 and 120 seconds.

The volume fractions in figure 5.33 are taken through the sprinkler plane (X=10) with the heaters on the left hand side and the bed in the centre. Note how the spray is spreading outwards unsymmetrically as observed during the office scenario. The reason for this could be due to the overall direction of the gas flow and hence the evaporation of the water particles. However, this effect could also be attributed to the grid spacing used within this vicinity.

Similar patterns are experienced through the other two slices of the sprinkler plane. These, illustrated in figures 5.34 and 5.35, show the volume fraction contours from the plan view at a height of 2.235m (Y=9) above the floor and along the room through the sprinkler source (Z=8).

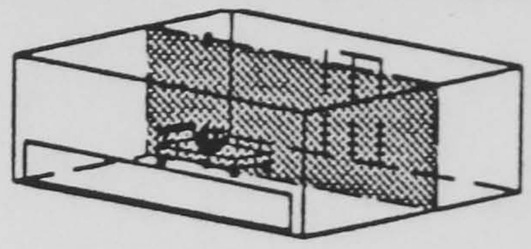

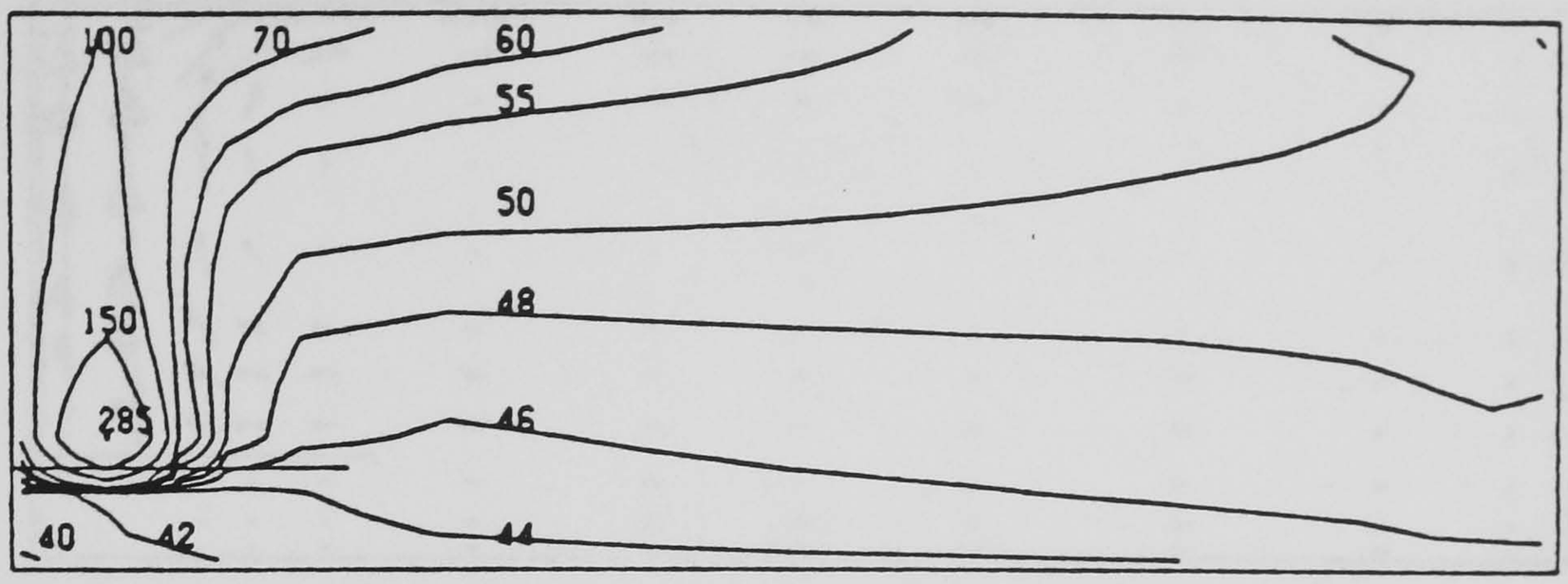

a)

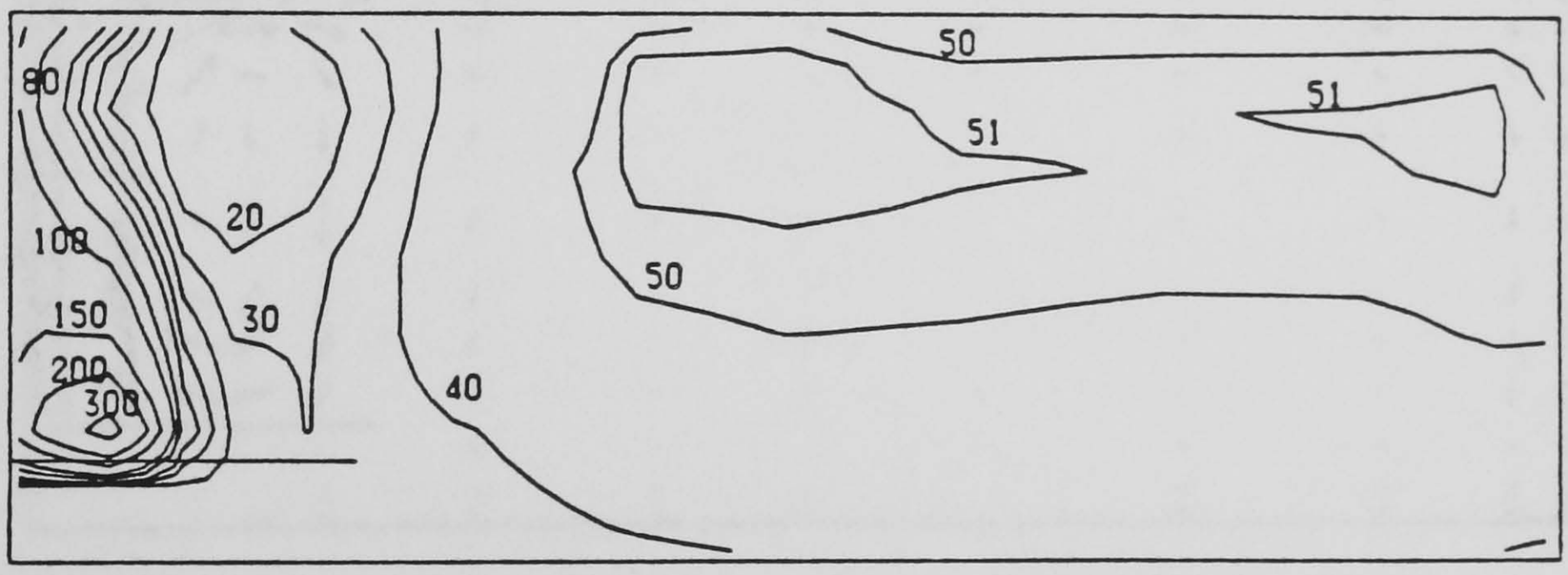

b)

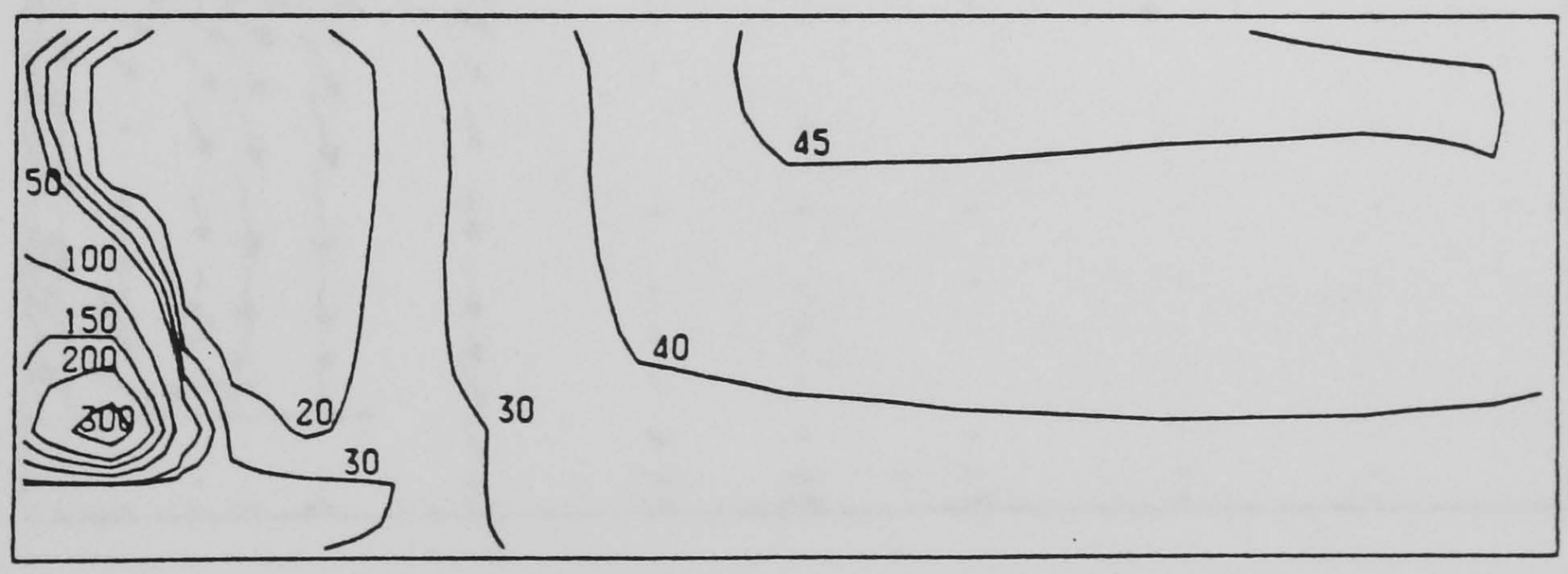

c)

Figure 5.31 Cross view of Hospital ward: predicted gas temperature contours through the centre of the room, fire and sprinkler sources (Z=8)
a) 0 sec. b) 60 sec. 120 sec.

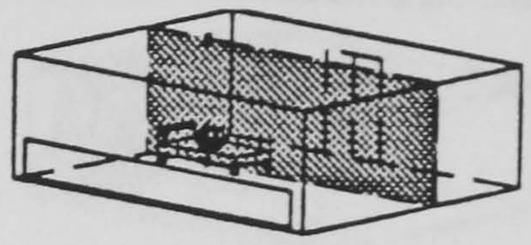

a)

b)

c)

Y

X

Vector scale: 2.01 m/s

Figure 5.32 Cross view of Hospital ward: predicted gas velocity vectors through the centre of the room, fire and sprinkler sources (Z=8)
a) 0 sec. b) 60 sec. 120 sec.

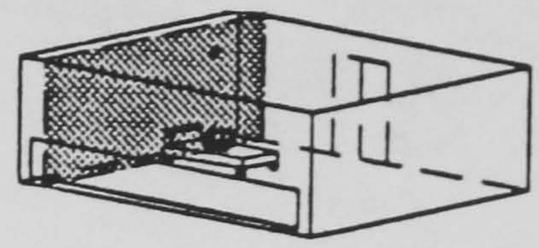

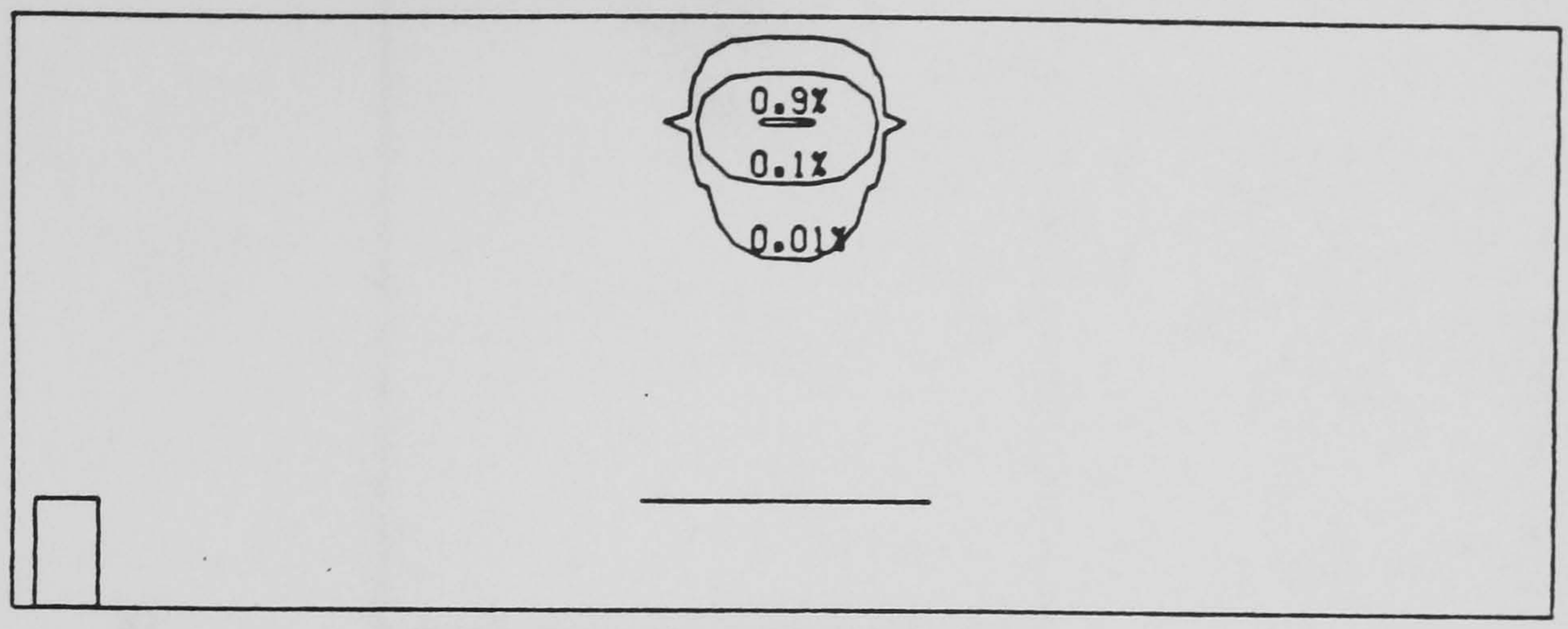

a)

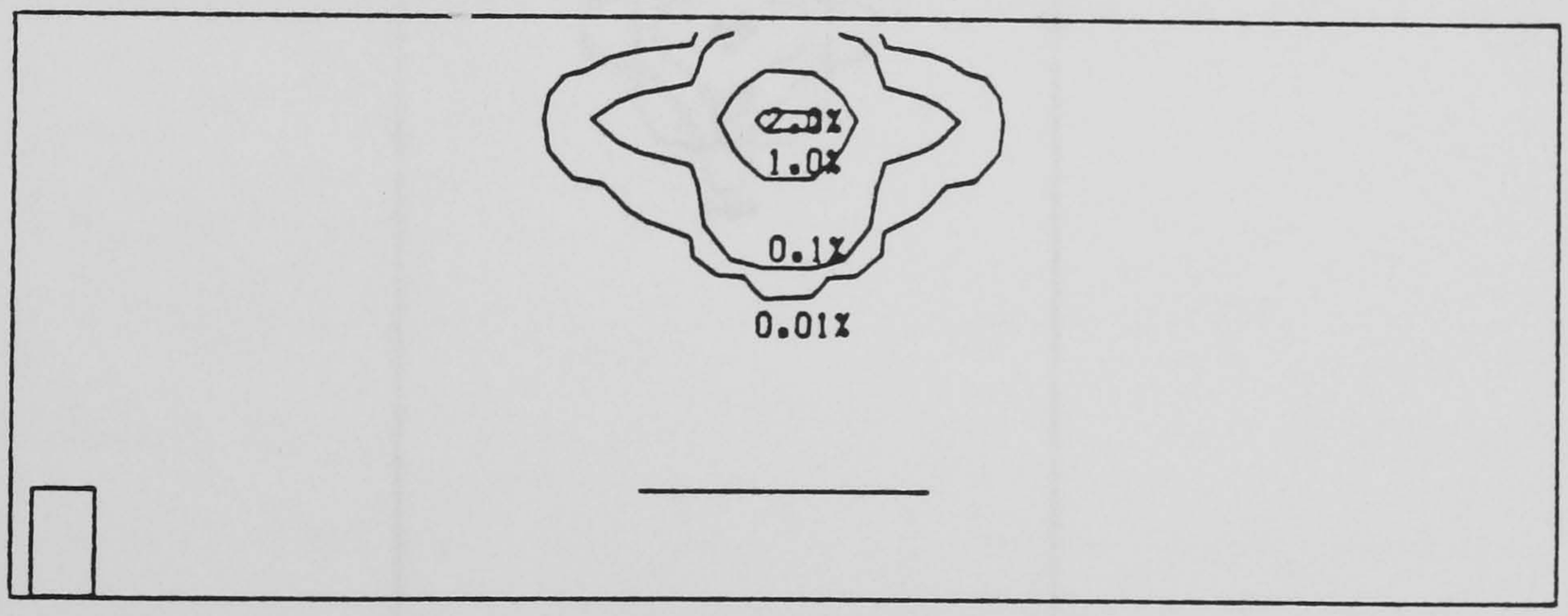

b)

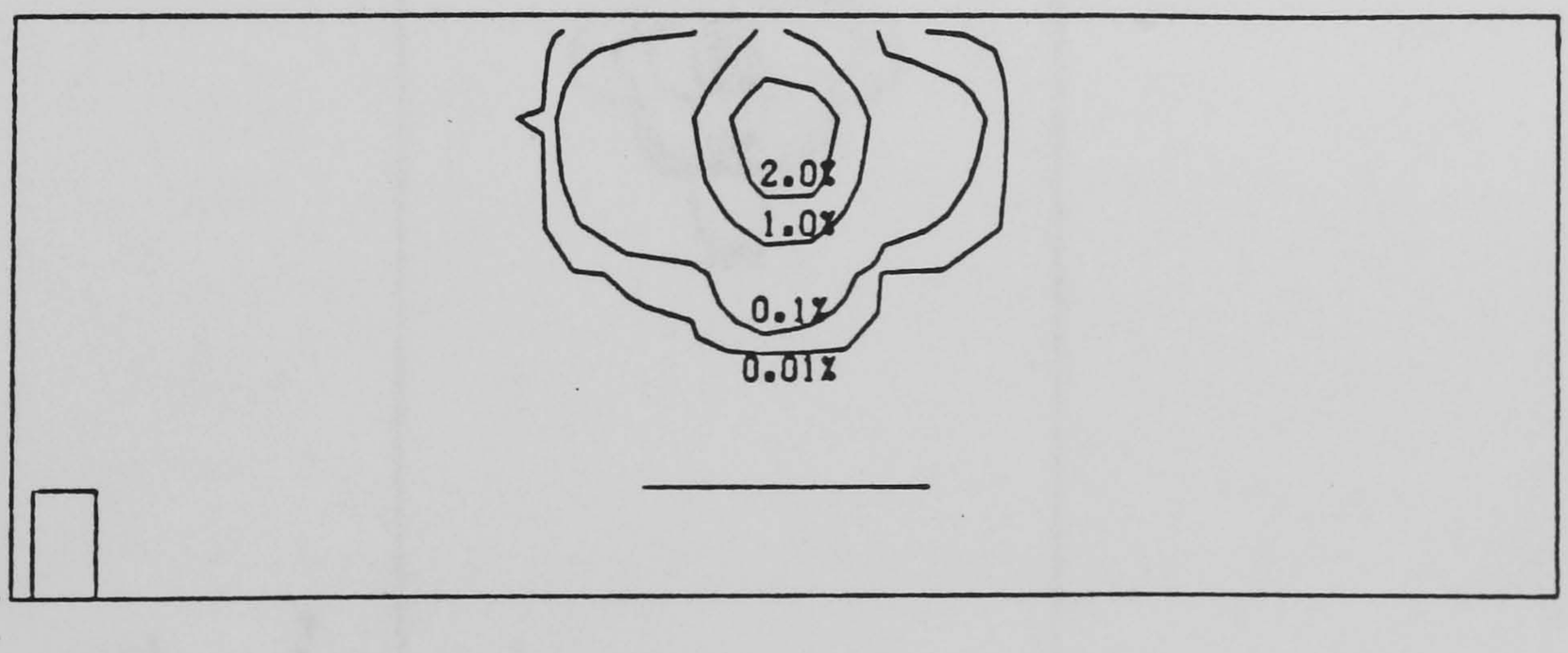

c)

Figure 5.33 Side view of Hospital ward: predicted volume fractions of water phase through the sprinkler plane (X=10)
a) 30 sec. b) 60 sec. c) 120 sec.

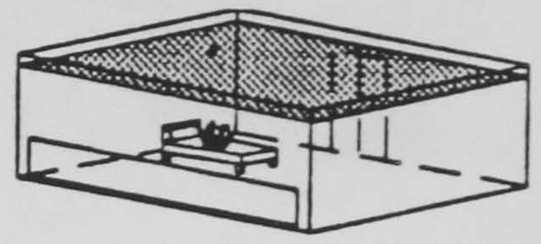

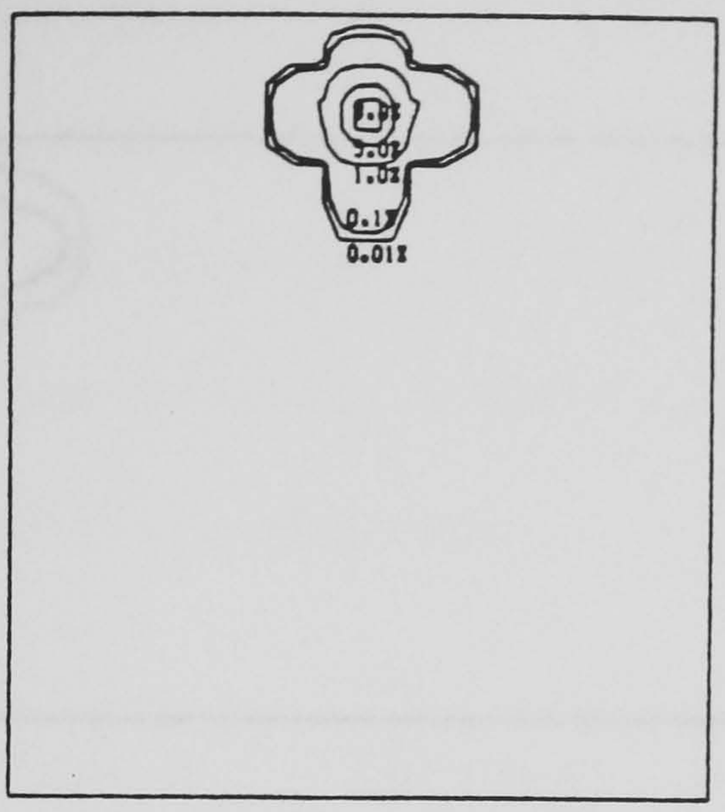

a)

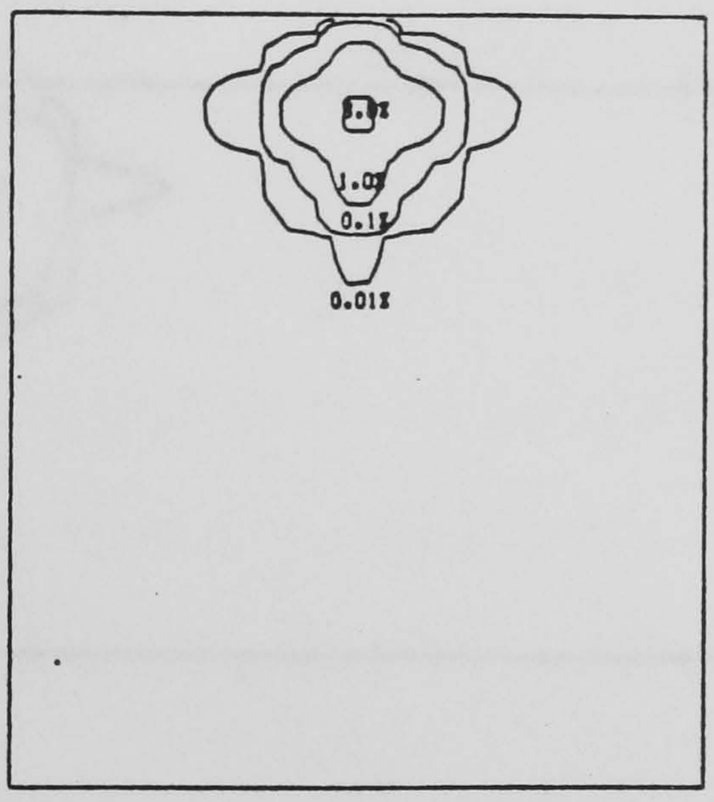

b)

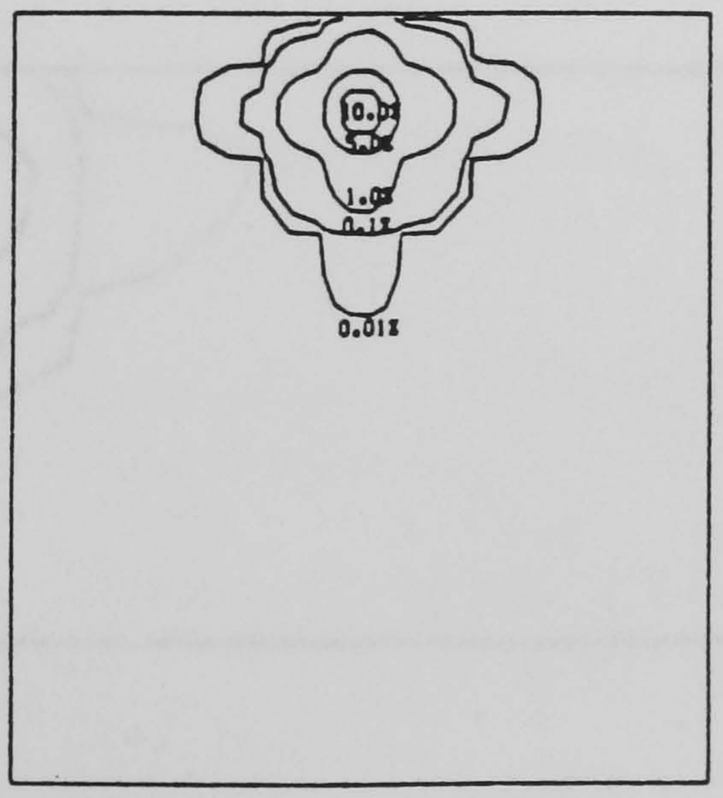

c)

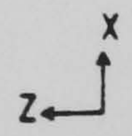

Figure 5.34 Plan view of Hospital ward: predicted volume fractions of water phase through the sprinkler plane (Y=9)
a) 30 sec b) 60 sec. c) 120 sec.

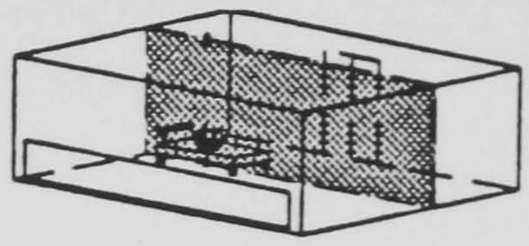

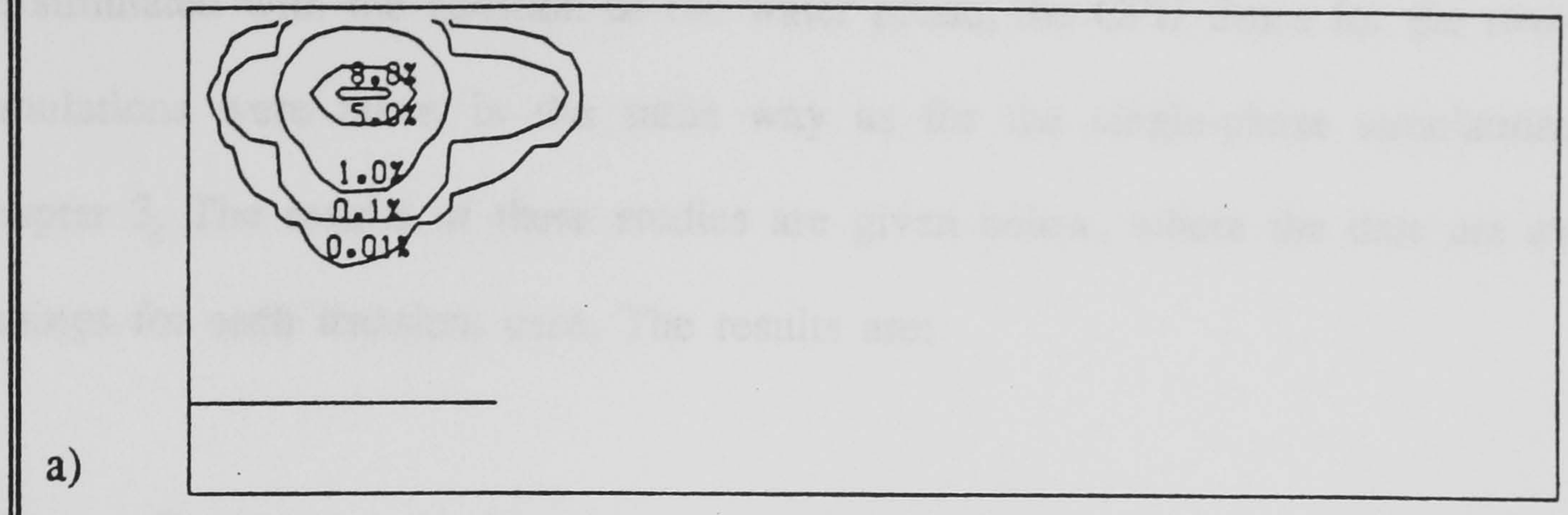

a)

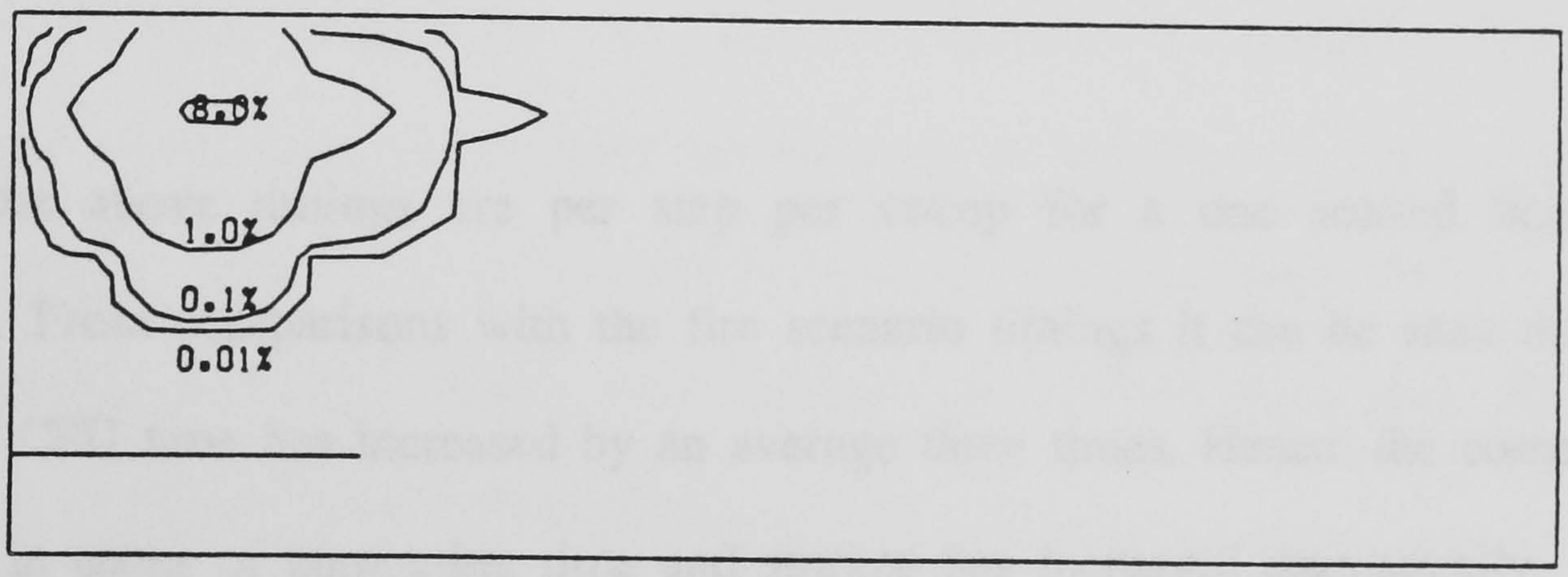

b)

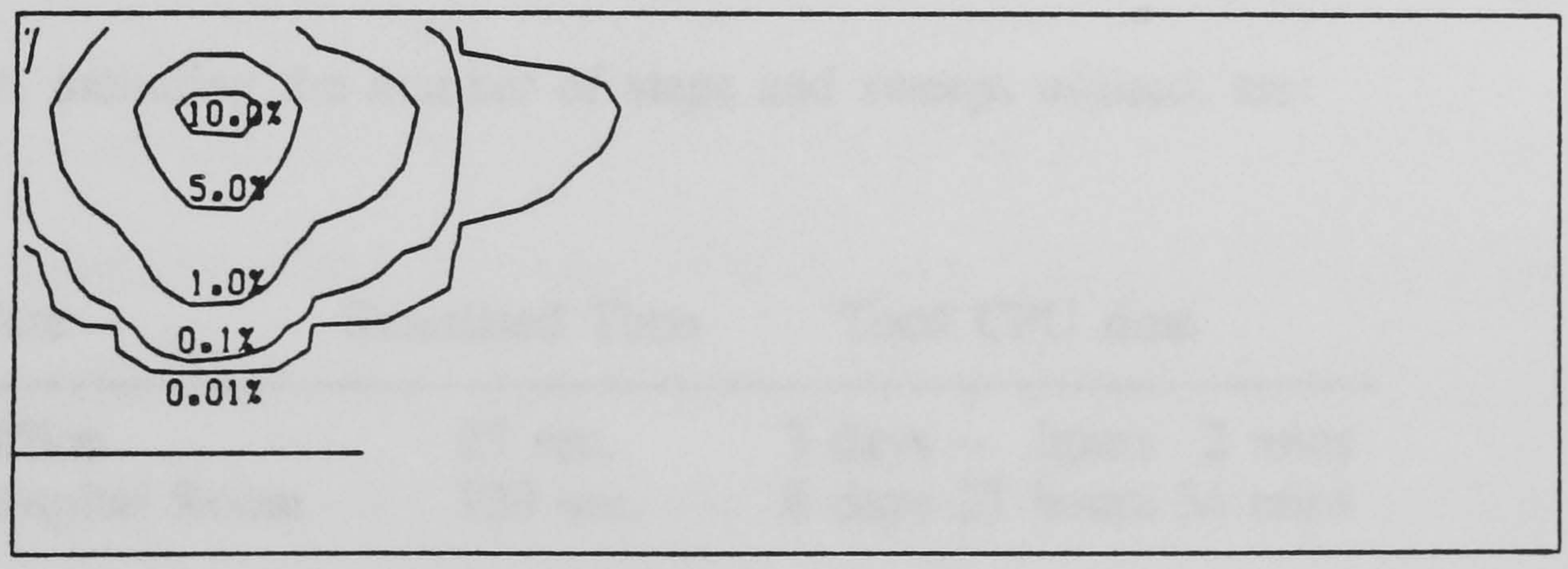

c)

Figure 5.35 Cross view of Hospital ward: predicted volume fractions of water phase through the sprinkler plane (Z=8)
a) 30 sec. b) 60 sec. 120 sec.

5.3.3 Timings

In order to be able to obtain a clearer ideaof the increasing scale of the problem to be simulated with the addition of the water phase, the CPU times for the two-phase simulations were taken in the same way as for the single-phase simulations; see chapter 3. The results of these studies are given below, where the data are average timings for each transient case. The results are:

Case	No. of cells	CPU time
Office	2244	34.5 seconds
Hospital Room	2310	43.0 seconds

whereby the above timings are per step per sweep for a one second time-step simulation. From comparisons with the fire scenario timings it can be seen that the amount of CPU time has increased by an average three times. Hence, the computing overheads in terms of computing time and storage has increased dramatically.

Using the above timings the following CPU times for the complete fire-sprinkler simulations, including the number of steps and sweeps utilised, are:

Case	Simulated Time	Total CPU time
Office	25 sec.	3 days -- hours 2 mins
Hospital Room	120 sec.	8 days 23 hours 34 mins

These results clearly indicate that fire-sprinkler simulation performed on a NORSK ND-5900 computer require several days of CPU time for a relatively short real-time simulation.

5.3.4 Grid Refinement

The above CPU times clearly indicate that a two-phase simulation involves a considerable amount of time. Any attempt to perform meaningful grid refinement experiments would greatly increase these timings to an extent which would make them totally impractical. It was therefore decided not to perform a two-phase grid-refinement study for the time being.

5.3.5 Conclusions

The above transient results for two distinct fire-sprinkler scenarios are very encouraging. In both cases qualitatively correct trends in cooling have been predicted. However, further studies need to be carried out in order to investigate the reason for the considerable deviations which have occurred at various times and locations between the predicted and measured data.

As indicated in chapter 4, the model for the two-phase simulations drew on the knowledge from a wide range of disciplines. Individual working groups for interphase heat and mass transfers and drag resulted in a number of models. These are dependent on the conditions for which they were obtained to be satisfied and to be applicable. As far as possible alternative equations were searched for and compared. As yet, in-depth studies into their effect on the predictions have not been carried out. However, with hindsight it has now become apparent that further studies into these areas need to be carried out.

Furthermore, the predictions made were with respect to only one initial droplet

diameter and water flow rate. Hence, the effect on the temperatures and flow patterns needs further investigation by varying these parameters.

These results have highlighted the need for detailed experimental data. This approach generates far more data than can be generally measured. Hence, more detailed experimental data needs to be made available for complete validation studies.

Hence, it appears as if the transient fire-sprinkler model can provide the fire researcher with a tool for the prediction of thermal properties and conditions within open and closed compartments.

5.4 Summary

The results obtained from applying the steady-state and time-dependent fire-sprinkler models to three different fire situations have been presented. These indicate very encouraging results due to the close agreement between predicted and observed data. However, further work needs to be undertaken to improve on results remote from the fire and sprinkler and to study the effect of grid-size on the results.

Chapter 6

Concluding Remarks

Chapter 6 Concluding Remarks

6.1 Introduction

Mathematical models for the study of fire and fire-sprinkler scenarios have been presented. These were for the cases of steady-state and time-dependent situations, and attempts were made to validate them with relevant experimental data.

The following chapter summarises the results of the comparisons performed. Based on these conclusions and research currently carried out into further aspects of the sprinkler system, suggestions for further work and possible extensions to the model are made. As the sprinkler spray is currently an area of great research interest, suggestions are made on how this particular study fits into the wide spectrum of current experimentation.

6.2 Conclusions

In chapters 3 and 5 results were presented for the cases of fire and fire-sprinkler scenarios within single compartments. These were for both steady-state and transient situations. As the steady-state case was undertaken for the purpose of gauging the feasibility of the proposed modelling strategy the conclusions presented below will focus on the time-dependent results. The main conclusions emerging from these studies are outlined below within their respective sections.

More than a decade of research has already been carried out into developing techniques to model the complexities of fires. With the help of these tools a clearer understanding of the processes involved during compartment fires can be more clearly understood. In fact unforeseen effects such as the 'trench effect' experienced during the King's Cross fire in 1987 [Fennell (1988)] was discovered with the aid of computer models.

During the transient office fire simulation the effect on the flow within the doorway, due to a corner fire also presented itself as something very noteworthy. The flow was extremely complex, displaying a multi-layered profile. Furthermore, due to the corner position of the fire, offset from the central plane of the doorway, the hot gases escaping through the doorway were at an angle. With hind-sight this prediction appears plausible. However, further studies into the effect of the free boundary conditions and its distance from the open doorway need to be carried out to ensure that this effect was not caused by the numerical method employed. Furthermore, as this compartment configuration is to become the ASTM-standard room further experiments might provide further experimental data, hence either verifying the predictions or providing an alternative gas flow pattern within the doorway.

The complexities of the re-circulating flow structures within the room also proved very challenging, both in terms of their calculation as well as interpretation.

However, taking all these factors into consideration along with the difficulties experienced in using a realistic heat release rate of the fire, the temperature

predictions made were fairly accurate. Correct trends in gas temperature rises were obtained at the two monitoring locations. These, however, could be improved, on using for example as a first step, smaller cell divisions.

A similar picture emerges for the hospital ward fire experiment. Though the compartment was closed, the flow created was made more complex with the addition of the heaters along one wall and the fire elevated off the floor.

The gas temperature predictions obtained were also very encouraging due to their correct temperature rises. In fact, predictions were more accurate closer to the fire than further remote. This reflects once again on the computational grid implemented.

Furthermore, the above two cases illustrate that refinements in the model are required. First of all chemical reactions taking place during a fire are vitally important from a life safety point of view. The movement of lethal products within the compartment need to be tracked in order to provide adequate safety measures for the occupants. This implies that the fires modelled need to be simulated by realistic fuels for which chemical reactions are known. These in turn affect the gas density and temperatures due to the different chemical concentrations. This was not as yet taken into account, and hence subsequent predictions could be affected.

A further area of refinement is concerned with the actual area or volume which the fire source occupies. At present the fire was assumed to occupy a fixed volume throughout the scenario. However, in reality a fire grows both in area and volume as it spreads over solid fuels. Hence, the strength and main location of the fire are affected and in turn the predictions made.

These areas, along with the model for turbulence need further investigation, and subsequent refinements to the outlined fire model presented within chapter 2.

A further area of concern, as outlined in chapter 3, involves the determination of the heat release rate of a fire. Measuring combustion products as during the office fire experiment, or weighing the object involved in the fire as carried out during the hospital ward fire, are not very reliable measures. Hence, the introduction of the cone calorimeter [Anon, viii (1990)] might prove itself to be a new alternative. It is a relatively new tool designed for measuring fire properties of materials and is aimed at becoming a standard to be used in fire tests across Europe.

Fire-Sprinkler Modelling

The development of a fire-sprinkler model was at the heart of this study. With the help of vital experimental data the proposed model outlined in chapter 4, was validated. From the results, presented in chapter 5, one main conclusion is evident: the proposed two-phase model is capable of capturing the cooling effect experienced by the hot gas phase and caused by the evaporation of the water droplets.

However, the accuracy of the predictions made need to be improved on. As they rely on the accuracy of the mathematics as well as the empirical equations describing the physical phenomena these two separate areas need further investigation.

As already highlighted in the previous section, chemical reaction is an important aspect of fire simulation. With the addition of the water phase this situation becomes more critical as further chemical reactions are taking place. Hence, by taking into

account chemical reactions further investigations into the merits of water as an extinguishing agent can be carried out.

The effect of grid-spacing on the results can be identified within the results for the volume-fractions of the water phase, as illustrated in figures 5.6, 5.21 to 5.23 and 5.33 to 5.35. Hence the need for further grid-refinement studies need to be carried out, especially for the case of two concurrently present phases. However, this requires a considerable amount of computer resources especially with respect to the CPU time utilised. Hence, any further studies are envisaged to proceed using the available parallel processing environments as typified by the transputer technology.

Furthermore, studies need to be undertaken to investigate the validity and effect the various auxiliary equations have on the predictions. The basis for the equations currently used within the model are theory or their application within similar simulations. For example the drag coefficient in equation (4.2-10) has already been shown to be adequate in similar simulations dealing with particles within a gas stream.

However, the vitally important interphase heat and mass transport equations need further investigation. Though they currently provide a means to adequately simulate the processes their part during the simulation needs to be more thoroughly understood. Perhaps as new experiments into water sprinklers and their effect on fire environments are carried out specific equations for these situations can be incorporated into the model.

Overall, therefore it can be concluded that while the fire-sprinkler model requires

refinement, it provides the basis for a very promising model for predicting the effect of a cooling water spray within a fire compartment.

6.3 Suggestions for Further Work

It is clear from the present study that there are still many areas of importance to be investigated.

In recent years keen interest has been shown by fire engineers and insurers into the workings and usefulness of a water sprinkler spray. However, it has been realised that though the system has been around for more than a century not enough detail is known concerning its exact mechanism or the effect of sprinkler characteristics on the buoyant smoke layer.

It is clear from the previous conclusions that there are still several areas of concern relating to the fields of mathematical modelling and the physical knowledge of sprinkler technology. Hence, it would only be fair to describe the above mathematical model as a foundation on which further research can be based.

The current situation of fire and sprinkler research is very buoyant and hence experiments carried out can be used to improve the physics used within the model. At present several separate research areas concerning sprinklers exist. Firstly a more thorough understanding of the workings of a sprinkler and its effect on smoke layers is investigated. This work is currently undertaken by Williams (1989) at the Fire Research Station, Borehamwood. Early experimental results suggest that the sprinkler

mass flow rate has a considerable effect on the stability of the smoke layer. Photographs, shown in figures 6.1 to 6.3 were taken during some of her initial studies into the effect of flow rates on the smoke layer. The photographs were taken from two angles of the experimental rig. The first view is looking down the rig with the sprinkler head situated on the left hand side and the fire on the right hand side. The second is a head-on view of the sprinkler location itself.

The first set of photos, shown in figure 6.1, are for the case of a low flow rate of 52 l/min. In figure 6.1-a the depth of the smoke layer can clearly be identified along with the position of the sprinkler. Note how the smoke layer is only slightly affected by the water spray. Furthermore, the collection of the water on the floor is clearly noticeable along with the spray pattern on the surface of the water. This in itself is a re-assuring feature as water collection was predicted during the steady-state simulation, see section 5.2.1. Figure 6.1-b further highlights the relative stability of the smoke layer.

Figure 6.2 shows the effect of increasing the flow rate to 55 l/min. Notice how the smoke layer in figure 6.2-a appears to be dragged down slightly by the water spray. This is illustrated more effectively in figure 6.2-b. The smoke layer has now been pushed down to about 0.5m to 0.8m above the floor.

However, a marked effect is seen in figure 6.3, where the case of a 80 l/min flow rate is illustrated. In this situation the smoke layer is clearly dragged down to the floor level, resulting in heavy smoke obscuration in the lower sections.

These are encouraging early results from the validation point of view, as similar

a) Length view

b) Side view

Figure 6.1 Sprinkler flow rate experiment: Flow rate = 52 l/min

a) Length view

b) Side view

Figure 6.2 Sprinkler flow rate experiment: Flow rate = 55 l/min

a) Length view

b) Side view

Figure 6.3 Sprinkler flow rate experiment: Flow rate = 80 l/min

observations have been made during the simulations.

These three sets of photographs clearly indicate the marked effect that the water flowrate through the sprinkler head has on the smoke layer. From a life safety point of view this appears to play a vital role. Hence, future designs of sprinkler heads and their installation and operation could be affected. Though this has as yet not been taken into account during any part of the study, it is evident that future studies need to include this important aspect. Perhaps future data obtained by Williams could be used to further validate the fire-sprinkler model.

A further point of interest are the tests currently conducted by the CAA in conjunction with the Fire Research Station. These tests are investigating the value of installing sprinkler sprays within aircraft cabins (see Appendix 1). The sprinklers tested produce a much finer spray of water droplets than the conventional sprinklers, hence providing a larger surface area for heat transfer. This experimental data is of particular interest as it not only provides further data for model validation but also presents itself as a very challenging fire scenario.

It is envisaged that the sprinkler model could be coupled with the aircraft cabin-fire model developed by Galea and Markatos (1989), in order to predict the experimental data. It is for these situations in particular that chemical combustion plays a vital role. Burning aircraft interiors release a lethal cocktail of poisonous fumes including acid gases such as hydro-chloric acid (HCl). As already mentioned, the speed at which these gases spread out is vital for life within the compartment. Perhaps valuable seconds for safe egress can be obtained by 'washing' these fumes using the fine water

spray and hence lowering the gas concentrations.

However, in order to check the validity of this statement a major hurdle needs to be overcome concerning the availability of the necessary computer resources. As shown in chapter 5 the two-phase sprinkler model needed more than 72 hours CPU time to simulate 25 seconds of experimental time using a cartesian grid of 2640 cells. Per time-sweep calculation, this was 2.76 times slower than for the single-phase fire simulation, see chapter 3. Galea (1989) required in excess of 64 hours for a single-phase fire simulation for a body-fitted solution domain of 20328 cells and for 240 seconds of actual fire data. This would imply that a 25 second sprinkler simulation within an aircraft cabin would take around 554 hours.

This amount of time is clearly unacceptable, as model development and parametric studies would become too involved. However, current research carried out at Thames Polytechnic into transputer technology [Cross et al(1989)] could provide a way to reduce this time. Early results from using a parallel version [Cross and Johnson (1990)] of AEA Harwell's FLOW-3D package [Burns et al(1989)] reveals that on test problems involving up to 17,640 cells, efficiency of over 86% can be achieved. On a 15 processor transputer system this results in a 13-fold speed-up. Translating this performance to the office fire-sprinkler scenario it is expected that the 92 hours simulation time could be reduced to around seven hours using 15 transputers.

It is clear from the current areas of research outlined above that this study only marks the beginning.

Nomenclature

a	= heat transfer coefficient	(W/m^2 K)
A	= total surface area in control cell	(m^2)
A_p	= total projected surface area	(m^2)
b	= mass transfer coefficient	(m/s)
c	= concentration of water vapour	(kg/m^3)
C_D	= drag coefficient	
Cp	= specific heat	(J/kg K)
d	= droplet diameter	(m)
D	= thermal diffusivity	(m^2/s)
f	= diameter of fire source	(m)
F	= interphase friction force	(N)
g	= mass flow rate	(kg m^3/s)
hum	= relative air humidity	(%)
H	= enthalpy	(J/kg)
k	= kinematic turbulence kinetic energy	(m^2/s)
K	= sprinkler constant	
l	= fire length	(m)
L	= latent heat	(J/kg)
$\dot{m}$	= rate of mass transfer	(kg/s)
M	= molecular weight	(kg/kmol)
n	= number of particles in control cell	(-)
p	= gas pressure	(atm)
P	= water pressure at sprinkler head	(atm)
$\dot{q}$	= rate of heat transfer	(W/s)

Q	= total fire heat release	(W)
r	= volume fraction of phase considered	
R_u	= universal gas constant = $8.314*10^3$	(J/kmol K)
S	= source term	
SQ	= water flow rate	(l/min)
t	= time	(s)
T	= temperature	(K)
u	= velocity in the x-direction	(m/s)
v	= velocity in the y-direction	(m/s)
V	= velocity vector	
Vol	= volume of control cell	(m^3)
V_{slip}	= slip velocity	(m/s)
w	= velocity in the z-direction	(m/s)

Greek

Γ	= diffusion coefficient	
δ	= normal distance from wall	(m)
ε	= turbulence dissipation rate of k	(m^2/s)
κ	= von Karman constant	
λ	= thermal conductivity	(W/m K)
μ	= dynamic viscosity	(kg/m s)
ν	= laminar kinematic viscosity	(m^2/s)
ρ	= density	(kg/m^3)
τ	= wall-shear stress	
Φ	= general dependent variable	

Subscripts

eff = effective viscosity (see k-ε model)

g = gas phase

i = refers to phase in question; g or l

l = liquid phase

lam = laminar (see k-ε model)

s = surface

sat = saturation

t = turbulence (see k-ε model)

w = wall

0 = initial condition

n,s,e,w = values evaluated at north, south, east, west, high or low faces of control

h,l volumes

Non-Dimensional Numbers

Nu = Nusselt number

Pr = Prandtl number

Re = Reynolds number

Sc = Schmidt number

Sh = Sherwood number

Mathematical Symbol

∂ = partial differential

div F = ∇.F = divergence (cartesian)

given any vector function F(x,y,z) which defines a vector field

$= (\partial F_u/\partial u) + (\partial F_v/\partial v) + (\partial F_w/\partial w)$

grad S = ∇S = gradient (cartesian)

given a scalar quantity S in cartesian co-ordinate x,y,z

$= (\partial S/\partial x)\underline{i} + (\partial S/\partial y)\underline{j} + (\partial S/\partial z)\underline{k}$

where $\underline{i}$, $\underline{j}$, $\underline{k}$ are unit vectors.

References

Abou Ellail M.M.M. and Khalil E.E. (1980)
A Mathematical Model for Gas-Liquid Interaction in the Turbulent Reacting Flows
Applied Mathematical Modelling; Vol. 4; 1980; pp.136-138

Ahmadzadeh J. and Harker J.H. (1974)
Evaporation from Liquid Droplets in Free Fall
Trans. Inst. Chem. Eng.; Vol.52; 1974; pp.108-111

Alpert R.L. and Mathews M.K. (1979)
Calculation of Large-Scale Flow Fields induced by Droplet Sprays
Factory Mutual Research Report, FMRC J.I. 0E0J4.BU; Dec. 1979

Alpert R.L. (1985)
Numerical Modelling of the Interaction between Automatic Sprinkler Sprays and Fire Plumes
Fire Safety Journal; Vol. 9; 1985; pp.157-163

Alpert R.L. (1986)
Calculated Spray Water-Droplet Flows in a Fire Environment
Factory Mutual Research Report; FMRC J.I. 0J0J1.BU; 1986

Anon,i (1984)
Advances in Sprinkler Technology
Fire Prevention; Vol. 171; 1984; pp.38

Anon,ii (1984)
American Survey shows High Success Rate for Sprinklers
Fire Prevention; Vol. 170; 1984; pp.30-33

Anon,iii (1989)
Safer sprays take the heat out of burning aircraft
New Scientist; No. 1670; 24-June-1989; pp.39

Anon,iv (1989)
Aircraft Sprinklers to be tested on Boeing
Fire Prevention; Vol. 220; June 1989; pp.7

Anon,v (1989)
Sprinklers under study
New Scientist; Vol. 1672; 8-July-1989; pp.43

Anon,vi (1989)
Water Sprays in Passenger Aircraft Fires
BRE News of Fire Research; July 1989

Anon,vii (1989)
Sprinkling Safety around the Home
Fire Prevention; Vol. 225; 1989; pp.5

Anon, viii (1990)
The Future of Fire Research
Fire Prevention; No. 226 (Jan/Feb); 1990; pp.14-15

Beard A.N. (1984/85)
A Stochastic Model for the Number of Deaths in a Fire: Further Considerations
Fire Safety Journal; Vol. 8; 1984/85; pp.201-226

Bird R.B, Stewart W.E. and Lightfoot E.N. (1960)
Transport Phenomena
John Wiley and Sons; New York; 1960

Blomqvist J. and Andersson B. (1985)
Modelling of Furniture Experiments with Zone Models
Fire and Materials; Vol. 9 (2); 1985; pp.81-87

Boysan F., Ayers W.H. and Swithenbank J. (1982)
A Fundamental Mathematical Modelling Approach to Cyclone Design
Trans. Inst. of Chem. Eng.; Vol. 60; 1982; pp.222-230

Bradshaw P. (1978)
Introduction
Turbulence; Topics in Applied Physics, Vol. 12; Ed. by Bradshaw P.; Springer-Verlag, Berlin; 1978; pp.1-44

Burns A.D., Jones I.P., Kightley J.R. and Wilkes N.S. (1989)
Harwell FLOW-3D, User Manual; 1989

Chopra I.S. (1986)
UL Tests the On-Off Sprinkler for Listing
Fire Journal; Nov. 1986; pp.19-22

Clift R. and Gauvin W.H. (1971)
Motion of Entrained Particles in Gas Str ams
The Canadian Journal of Chem. Eng.; Vol. 49; 1971; pp.439-448

Cooper L.Y. (1982)
Convective Heat Transfer to Ceilings above Enclosure Fires
19th Int. Symposium on Combsution; The Combustion Inst.; 1982; pp.933-939

Cooper L.Y. and Stroup D.W. (1982)
Calculating Available Safe Egress Time (ASET) - A Computer Program and User's Guide
National Bureau of Standards Report, NBSIR 82-2578; 1982

Cooper L.Y., Rockett J.A., Mitler H.E. and Stroup D.E. (1985)
A Program for the Development of a Benchmark Compartment Fire Model Computer Code
National Bureau of Standards Report, NBSIR 85-3252; 1985

Cooper L.Y. and Stroup D.W. (1987)
Test Results and Predictions for the Response for the Near-Ceiling Sprinkler Links in a Full-Scale Compartment Fire
National Bureau of Standards Report, NBSIR 87-3633; Sept. 1987

Cooper L.Y. and Forney G.P. (1987)
Fires in a Room with a Hole: A Prototype application of the Consolidated Compartment Fire Model (CCFM) Computer Code
Proceedings of The Combustion Inst; Nov. 1987

Cote A.E. (1987)
QRS: Do you understand the Technology?
Fire Journal; Jan. 1987; pp.27-30,76-77

Cox G. (1983)
A Field Model of Fire and its Application to Nuclear Containment Problems
Specialist Mee ing on Interaction of Fire and Explosion with Ventilation Systems in Nuclear Facilities; Los Alamos, New Mexico; April 1983

Cox G. and Kumar S. (1987)
Field Modelling of Fire in Forced Ventilated Enclosures
Combustion Science and Technology; Vol. 52; 1987; pp.7-23

Cox G. (1987)
Simulating Fires in Buildings by Computer - The State of the Art
Forensic Science Society; 1987; pp.175-188

Cox G. (1990)
Private Communication, Fire Research Station; 1990

Cross M., Johnson S. and Chow P. (1989)
Mapping Enthalpy-Based Solidification Algorithms onto Vector and Parallel Architecture
Applied Mathematical Modelling; Vol. 13; Dec. 1989; pp.702-709

Cross M. and Johnson S. (1990)
Mapping CFD algorithm onto fine grained parallel architecture
In preparation; 1990

Crowe C.T. and Pratt D.T. (1972)
Two-Dimensional Gas-Particle Flows
Proceedings of the 1972 Heat Transfer and Fluid Mechanics Institute, Stanford University; 1972; pp.386-398

Crowe C.T., Sharama M.P. and Stock D.E. (1975)
The Particle-Source-in-Cell (PSI-Cell) Model for Gas-Droplet Flows
ASME; 75-WA/HT-25; 1975

Crowe C.T. (1982)
REVIEW - Numerical Methods for Dilute Gas-Particle Flows
Journal of Fluis Engineering; Vol. 104; 1982; pp.297-303

Daly K. (1989)
Firespray
Flight International; 21-Jan-1989; pp.42-46

Dundas P.H. (1974)
The Scaling of Sprinkler Discharge: Prediction of Dropsize
Factory Mutual Technical Report; FMRC Serial No. 18792; RC73-T-40; 1974

Durst F., Milojevic D. and Schönung B. (1984)
Eulerian and Lagrangian Predictions of Particulate Two-Phase Flows: A Numerical Study
Applied Mathematical Modelling; Vol. 8; 1984; pp.101-115

Drysdale D. (1985)
An Introduction to Fire Dynamics
J.Wiley and Sons Ltd.; Chichester; 1985

Emmons H.W. (1979)
The Prediction of Fires in Buildings
17th Symposium on Combustion; 1979; pp.1101-1111

Emmons H.W. (1983)
The Analysis of a Tragedy
Fire Technology; Vol. 19; 1983; pp.115-

Evans D.D. and Stroup D.W. (1985)
Methods to Calculate the Response Time of Heat and Smoke Detectors installed below large unobstructed ceilings
National Bureau of Standards Report, NBSIR 85-3167; 1985

Evans D.D. and Stroup D.W. (1986)
Methods to Calculate the Response Time of Heat and Smoke Detectors installed below large unobstructed ceilings
Fire Technology; Vol. 22; 1986; pp.54-65

Fenech K.A. (1987)
Analysing Aspects of the Performance of an Iron Blast Furnace
PhD Thesis; Thames Polytechnic, London; 1987

Fennell D. (1988)
Investigation into the King's Cross Underground Fire
Department of Transport; Her Majesty's Stationary Office; 1988

Fire Protection Handbook
16th Edition; Section 18; Chapters 3 and 7

Fleming R.P. (1988)
Applications/ Limitations of QRS Technology
Fire Safety Journal; Vol. 14; 1988; pp.75-88

Galea E.R. and Markatos N.C. (1987,i)
Predictions of Fire Behaviour in Aircrafts
2nd Int. PHOENICS Users Conference, London 1987; CHAM Publication; 1989; pp.308-328

Galea E.R. and Markatos N.C. (1987,ii)
A Review of Mathematical Modelling of Aircraft Cabin Fires
Applied Mathematical Modelling; Vol. 11; June 1987; pp.162-176

Galea E.R. (1989)
On the Field Modelling Approach to the Simulation of Enclosure Fires
Journal of Fire Prot. Eng.; Vol. 1 (1); 1989; pp.11-22

Galea E.R. and Markatos N.C. (1989)
Forced and Natural Venting of Aircraft Cabin Fires - A Numerical Simulation
73rd Symposium on Aircraft Fire Safety, NATO - AGARD; Portugal; May 1989; AGARD-CP-467; pp.17-1 to 17-9

Gardiner A.J. (1988)
The Mathematical Modelling of the Interaction between Sprinklers and the Thermally Buoyant Layers of Gases from Fires
PhD Thesis; South Bank Polytechnic, London; 1988

Garner F.H. and Lane J.J. (1959)
Mass Transfer to Drops of Liquid suspended in a Gas Stream Part II: Experimental Work and Results
Trans. Inst. Chem. Eng.; Vol. 37; 1959; pp.162-172

Gordon G.D. (1959)
Mechanism and Speed of Breakup of Drops
Journal of Applied Physics; Vol. 30 (10); 1959; pp.1759-1761

Gosman A.D. and Pun W.M. (1973)
Calculation of Recirculating flows
Lecture Notes, Imperial College of Science and Technology; December 1973

Gosman A.D., Li K.H. and Samaraweera D.S.A. (1976)
A Numerical Calculation Procedure for Two-Phase Recirculating Flows
5th Int. Conference on Numerical Methods in Fluid Dynamics; 1976; pp.212-219

Gupta A.K., Kumar S. and Singh B. (1988)
One-Dimensional Mathematical Modelling of Enclosure Fire Dynamics
Fire and Materials; Vol. 12; 1988; pp.51-60

Harlow F.H. and Welch J.I. (1965)
Numerical Calculation of Time-Dependent Viscous Incompressible Flow of Fluid with Free Surface
Phys. Fluid; Vol. 8; 1965; pp.2182-2189

Harlow F.H. and Nakayama P.I. (1967)
Turbulent Transport Equations
Phys. Fluids; Vol. 10; 1967; pp.2323-2332

Harmathy T.Z. (1988)
On the Economics of Mandatory Sprinklering of Dwellings
Fire Technology; Aug. 1988; pp.245-261

Heskestad G. and Bill R.G. Jr. (1988)
Quantification of Thermal Responsiveness of Automatic Sprinklers including Conduction Effects
Fire Safety Journal; Vol. 14; 1988; pp.113-125

Hoffmann T.W. and Gauvin W.H. (1962)
Analysis of the Radiative Heat Absorption in the Boundary Layer surrounding an Evaporating Drop
Canadian Journal of Chemical Engineering; Vol. 39; 1962; pp.252-259

Hoffmann N. and Markatos N.C. (1988)
Thermal Radiation Effects on Fires in Enclosures
Applied Mathematical Modelling; Vol. 12; 1988; pp.129-140

Hoffmann N., Galea E.R. and Markatos N.C. (1988)
A Computer Simulation of Fire-Sprinkler Interaction: A Two-Phase Phenomena
Presented at the 12th IMACS World Congress; Paris, France; July 1988

Hoffmann N., Galea E.R. and Markatos N.C. (1989)
Mathematical Modelling of Fire Sprinkler Systems
Appl. Math. Modelling; Vol. 13 (May); 1989; pp.298-306

Hoffmann N., Galea E.R. and Markatos N.C. (1990)
A Transient Two-Phase Fire-Sprinkler Simulation
presented at the IASTED Int. Symp. on Modelling, Simulation and Optimisation; Montreal, Canada; May 1990

Hruby J., Steeper R., Evans G. and Crowe C.T. (1988)
An Experimental and Numerical Study of Flow and Convective Heat Transfer in a Freely Falling C :rtain of Particles
Jl. of Fluids Eng., Transactions of ASME; Vol. 110 (June); 1988; pp.172-181

Ishii M. and Zuber N. (1979)
Drag Coefficient and relative velocity in bubbly, droplet or particulate flows
American Inst. Chem.Eng.J.; Vol. 25(5); Sep. 1979; pp.843-855

Kircaldy D. and Markatos N.C. (1982)
Spray Cooling of Combustion Products
CHAM Technical Report 1371/1; London; 1982

Kostamis P. (1987)
Computer Modelling and Analysis of Particulate Laden Gas Flows
PhD Thesis; Thames Polytechnic, London; 1987

Kreith F. and Black W.Z. (1980)
Basic Heat Transfer
Harper and Row Publishers; New York; 1980

Kumar S. (1983)
Mathematical Modelling of Natural Convection in Fire - A State of the Art Review of the Field Modelling of Variable Density Turbulent Flow
Fire and Materials; Vol. 7 (1); 1983; pp.1-24

Kumar S. (1985)
Private Communication, Fire Research Station; 1985

Kumar S. and Cox G. (1985)
Mathematical Modelling of Fires in Road Tunnels
5th Int. Symposium on Aerodynamics and Ventilation of Vehicle Tunnels; Lille, France; May 1985; pp.61-76

Kumar S., Hoffmann N. and Cox G. (1986,i)
Some Validation of JASMINE for Fires in Hospital Wards
Numerical Simulation of Fluid Flow and Heat/Mass Transfer Processes
Ed. by N.C. Markatos, D.G. Tatchell, M. Cross and N. Rhodes; Springer Verlag, Berlin; 1986; pp.159-169

Kumar S., Hoffmann N. and Cox G. (1986,ii)
Mathematical Modelling of Fires in Hospital Wards
14th National Conf. on Fluid Mechanics and Fluid Power; Roorkee, India; Jan. 1986

Kumar S. and Cox. G. (1988)
Radiant Heat and Surface Roughness Effects in the Numerical Modelling of Tunnel Fires
6th Int. Symposium on Aerodynamics and Ventilation of Vehicle Tunnels; Durham, England; Sep. 1985

Lane W.R. (1951)
Shatter of Drops in Streams of Air
Industrial and Engineering Chemistry; Vol. 43 (6); 1951; pp.1312-1317

Launder B.E. and Spalding D.B. (1972)
Mathematical Models of Turbulence
Academic Press, London; 1972

Launder B.E. and Spalding D.B. (1974)
The Numerical Computation of Turbulent Flows
Computer Methods in Applied Mechanics and Engineering; Vol. 3; 1974; pp.269-289

Lee B.T. (1972)
Laboratory Scaling of the Fluid Mechanical Aspects of Large Fires
Combustion Science and Technology; Vol. 4; 1972; pp.233-239

Leggett P. (1990)
Private Communication; Thames Polytechnic, London; 1990

Lie T.T. (1972)
Fire and Buildings
Applied Science Publishers; Barking, England; 1972

Leschziner M.A. (1989)
Modelling Turbulent Reacting Flows by Finite-Volume Methods - Current Status and Future Directions
Int. J. Heat and Fluid Flow; Vol. 10 (3); Sept. 1989; pp.186-202

Lockwood F.C., Salooja A.P. and Syed S.A. (1980)
A Prediction Method for Coal-Fired Furnaces
Combustion and Flame; Vol. 38; 1980; pp.1-15

Low S.C. and Baruah P.C. (1981)
One-Dimensional Unsteady Air and Droplets Flow Model which includes Evaporation, Heat Transfer and Drag
I. Mech E.; Conference on Gas-Borne Particles; Oxford, England; 1981; pp.37-46

Lumley J.L. (1978)
Two-Phase and Non-Newtonian Flows
Turbulence; Topics in Applied Physics, Vol. 12; Ed. by Bradshaw P.; Springer-Verlag, Berlin; 1978; pp.290-323

Markatos N.C., Malin M.R. and Cox G. (1982)
Mathematical Modelling of Buoyancy-Induced Smoke Flow in Enclosures
Int. Journal of Heat Mass Transfer; Vol. 25 (1); 1982; pp.63-75

Markatos N.C. and Cox G. (1982)
Turbulent Buoyant Heat Transfer in Enclosures containing a Fire Source
7th Int. Heat Transfer Conference; Munich, W. Germany; 1982; pp.373-379

Markatos N.C. and Kircaldy D. (1982)
Analysis and Computation of Three-Dimensional, Transient Flow and Combustion through granulated Propellants
Fluids Engineering Division of the ASME; 82-FE-9; 1982

Markatos N.C. and Kircaldy D. (1983)
Analysis and Computation of Three-Dimensional Transient Flow and Combustion Through Granulated Propellants
Int. Journal of Heat Mass Transfer; Vol. 26 (7); 1983; pp.1037-1053

Markatos N.C. (1984/5)
Computer Simulation Techniques for Turbulent Flows
Encyclopedia of Fluid Mechanics; Ed. by Cheremisinoff N.P.; Vol. 6; Gulf Publishing Corp.; 1984/85

Markatos N.C., Pericleous K.A. and Cox G. (1986)
A Novel approach to the Field Modelling of Fire
PhysicoChemical Hydrodynamics; Vol. 7 (2/3); 1986; pp.125-143

Mason D.J., Markatos N.C. and Reed A.R. (1987)
Numerical Simulation of the Flow of Gas-Solids Suspensions in 'Acceleration' Regions of Pipelines
2nd Int. PHOENICS Users Conference, London; 1987

Migdal D. and Agosta C.V. (1967)
A Source Flow Model for Continuum Gas-Particle Flow
J. Applied Mechanics, Trans of ASME; Vol. 35 (4); 1967; pp.860-865

Mitler H.E. (1978)
The Physical Basis for the Harvard Computer Code
Home Fire Project Tech. Report No. 34; Harvard University; 1978

Mitler H.E. (1984)
Zone Modelling of Forced Ventilation Fires
Combustion Science and Technology; Vol. 39; 1984; pp.83-106

Mitler H.E. (1985)
The Harvard Fire Model
Fire Safety Journal; Vol.9; 1985; pp.7-16

Mitler H.E. and Rockett J.A. (1987)
User's Guide to FIRST, a Comprehensive Single-Room Fire Model
National Bureau of Standards Report, NBSIR 87-3595; Sep. 1987

Mugele R.A. and Evans H.D. (1951)
Droplet Size Distribution in Sprays
Industrial and Engineering Chemistry; Vol. 43 (6); 1951; pp.1317-1324

Nash P. (1973)
The History of Sprinklers
Fire Surveyor; Vol. 2 (2); 1973

Nash P. (1978)
The Essentials of Sprinkler and other Water Spray Fire Protection Systems
Practical Studies from the Building Research Establishment, Fire Control; The Construction Press Ltd; 1978; pp.65-77

Nash P. and Young R.A.,i (1978)
The Performance of the Sprinkler in the Extinction of Fire
Practical Studies from the Building Research Establishment, Fire Control; The Construction Press Ltd; 1978; pp.78-84

Nash P. and Young R.A.,ii (1978)
The Performance of the Sprinkler in Detecting Fire
Practical Studies from the Building Research Establishment, Fire Control; The Construction Press Ltd; 1978; pp.25-39

Patankar S.V. (1980)
Numerical Heat Transfer and Fluid Flow
McGraw Hill Book Company; Hemisphere Pub. Corp.; 1980

Patankar S.V. (1981)
Computer Analysis of Fluid Flow and Heat Transfer
Recent Advances in Numerical Methods in Fluids, Vol. 2; Ed. by Taylor C. and Morgan K.; Pineridge Press Ltd.; 1981; pp.223-252

Patel M.K. and Cross M. (1989)
The Modelling of Fluidised Beds for Ore Reduction
Numerical Method' in Laminar and Turbulent Flow; Ed. by Taylor C., Gresho P., Sani R.L. and Hauser J.; Proceedings of the 6th Int. Conference, Swansea; Vol. 6 (2); 1989;pp. 2051-206.

Patel M.K., Wade K. and Cross M. (1989)
Multiphase approach to CFD Algorithms and Applications
Numerical Methods in Laminar and Turbulent Flow; Ed. by Taylor C., Gresho P., Sani R.L. and Hauser J.; Proceedings of the 6th Int. Conference, Swansea; Vol. 6 (2); 1989;pp. 2080-2090

Pericleous K., Worthington D.R.E. and Cox G. (1987)
The Field-Modelling of Fire in an Air-Supported Structure
2nd Int. Symposium of Fire Safety Science; 1987; pp.871-880

Ranz W.E. and Marshall Jr. W.R. (1952,i)
Evaporation from drops: Part I
Chemical Eng. Progress; Vol. 48; No. 3; 1952; pp.141-146

Ranz W.E. and Marshall Jr. W.R. (1952,ii)
Evaporation from Drops: Part II
Chemical Eng. Progress; Vol. 48; No. 4; 1952; pp.173-180

Rasbash D.J. (1962)
Heat Transfer between Water Sprays and Flames of Freely Burning Fires
Symposium on the Interaction Between Fluids and Particles; Inst. Chem. Eng.; 1962; pp.217-223

Reeves J.B. and MacArthur C.D. (1976)
Dayton Aircraft Cabin Fire Model, Vol.1 Basic Mathematical Model
FAA-RD-76-120; I; 1976

Reynolds W.C. and Cebeci T. (1978)
Calculation of Turbulent Flows
Turbulence; Topics in Applied Physics, Vol. 12; Ed. by Bradshaw P.; Springer-Verlag, Berlin; 1978; pp.193-229

Rogers G.F.C. and Mayhew Y.R. (1985)
Thermodynamic and Transport Properties of Fluids
Basil Blackwell; Great Britain; 3rd edition; 1985

Rosten H.I. and Spalding D.B. (1986)
PHOENICS Beginner's Guide and User Manual
CHAM TR/100; 1986

Round J. (1987)
Making Sure the Sprinkler System Works
Fire and Security Protection; Jan. 1987; pp.7

Sharma M.P. (1987)
Modelling of Gas-Solid or Gas-Droplet Two-Phase Flows in Oil/Gas Drilling and Production Systems
3rd Int. Conf. on Multiphase Flow; The Hague, Netherlands; May 1987; pp.235-248

Sharma M.P. and Crowe C.T. (1989)
Application of Computer Modelling in the design of Multiphase Flow Metering Systems
Jl. of Fluids Eng., Transactions of ASME; Vol. 111 (June); 1989; pp.184-190

Sirignano W.A. (1986)
The Formulation of Spray Combustion Models: Resolution Compared to Droplet Spacing
Journal of Heat Transfer; Vol. 108; 1986; pp.633-639

Smith P.G. (1987)
Private Communication, Fire Research Station; 1987

Soo S.L. (1967)
Fluid Dynamics of Multiphase Systems
Blaisdell Publishing Company; 1967

Soo S.L. (1975)
Power Spray Cooling - Unit and System Performance
ASME Power Division Meeting; Texas; 1975; 75-WA/Pwr-8

Spalding D.B. (1977)
The Calculation of Free-Convection Phenomena in Gas-Liquid Mixtures
Heat Transfer and Turbulent Buoyant Convection; Hemisphere Pub. Corp.; 1977; pp.569-586

Spalding D.B. (1979)
Combustion and Mass Transfer
Pergamon Press, London; 1979

Spalding D.B. (1980)
Numerical Computation of Multi-Phase Fluid Flow and Heat Transfer
Recent Advances in Numerical Methods in Fluids, Vol.1; Ed. by C. Taylor and K. Morgan; Pineridge Press Ltd; 1980; pp.139-168

Spalding D.B. (1981)
A General-Purpose Computer Program for Multi-Dimensional One- Two-Phase Flow
Prepr. 81-6; Mathematics and Computers in Simulation; North Holland (IMACS); Vol. 23; 1981; pp.267-276

Spalding D.B. (1982)
The *shadow* method of particle-size calculation in Two-Phase Combustion
19th Symposium on Combustion; The Combustion Institute; 1982; pp.941-951

Spalding D.B. (1983)
Developments in the IPSA Procedure for Numerical Computation of Multiphase Flow Phenomena with Interphase Slip, Unequal Temperatures etc.
Numerical Properties and Methodologies in Heat Transfer; Ed. by T.M. Shih; Hemisphere Pub. Corp; 1983; pp.421-436

Spraysafe (1988)
Data Cards
Sraysafe Automatic Sprinklers Ltd.; Gainsborough, Lincolnshire; England; 1988

Swithenbank J., Boysan F. and Ayers W.H. (1987)
Two Phase Flow Calculations
Liquid Atomisation and Spray Systems Course; Skandinavisk Tekniformedling International AB, Sweden; Sept. 1987

Takeda H. (1987)
A Trial of Flashover Prediction in Compartment Fire Modelling
Fire Science and Technology; Vol. 7 (1); 1987; pp.15-23

Teague P.E. (1988)
Residential Sprinklers: An idea whose time has almost come
Fire Journal; Sept./ Oct. 1988; pp.46-61

Theobald C.R. (1987)
Heated Wind Tunnel for Testing Fast Acting Sprinklers
Fire Surveyor; April 1987; pp.9-12

Thorne P.F. (1985)
The Physics of Fire Extinguishment
Phys. Technology; Vol. 16; 1985; pp.263-268

Thorne P.F., Theobald C.R. and Melinek S.J. (1988)
The Thermal Performance of Sprinkler Heads
Fire Safety Journal; Vol. 14; 1988; pp.89-99

Tye J. and Genasis C. (1986)
Small Precautions can Prevent Big Fires
Fire Prevention; July/August; 1986; pp.26-28

Walton W.D., Baer S.R. and Jones W.W. (1985)
User's Guide to FAST
National Bureau of Standards Report, NBSIR 85-3284; Dec. 1985

Waters R. (1986)
Air and Smoke Movement within a Large Enc!›sure
Numerical Simulation of Fluid Flow and Heat/Mass Transfer Processes
Ed. by N.C. Markatos, D.G. Tatchell, M. Cross and N. Rhodes; Springer Verlag, Berlin; 1986; pp.135-147

Whalley P.B. (1987)
Boiling, Condensation and Gas-Liquid Flow
Clarendon Press; Oxford; 1987

Williams F.A. (1969)
Scaling Mass Fires
Fire Res. Abstr. Review; Vol. 11; 1969; pp.1-22

Williams C. (1989)
Private Communication, Fire Research Station; 1989

Wise H. and Agoston G.A. (1958)
Burning of a liquid droplet
Literature of the Combustion of Petroleum; Vol. 20; 1958; pp.116-135

Yao C. and Kalelkar A.S. (1970)
Effect of drop size on sprinkler performance
Fire Technology; 1970; pp.254-268

Yao C. (1988)
The Development of the ESFR Sprinkler System
Fire Safety Journal; Vol. 14; 1989; pp.65-73

You H.-Z. (1984)
Investigation of Spray Patterns of Selected Sprinklers with the FMRC drop size Measuring System
1st Int. Symposium or Fire Safety Science; 1984; pp.1165-1176

Yuen M.C. and Cher L.W. (1976)
On Drag of Evaporating Liquid Droplets
Combustion Science and Technology; Vol. 14; 1976; pp.147-154

Principle Authors Index

Appendix 1

Background into Sprinkler Systems

Appendix 1 Background into Sprinkler Sytems

This appendix is intended to provide further background into the wider aspects of sprinkler systems, such as their activation criteria and main purposes as well as the wide variety of different types of sprinkler systems developed.

There are various types of sprinkler systems using different types of extinguishing media. However, the media of interest here is water released through the automatically operated sprinkler system.

An automatic system consists of pipes connected to valves, which control the water supply. The pipes are fixed at, or are near the ceiling. The sprinkler heads are fitted at intervals along these pipes. They contain a device which is triggered into action when the temperature has risen above a certain level, causing the water spray to be discharged over the area below it. There are strict guidelines for various aspects of sprinkler systems which need to be met when designing a system as outlined above.

The type of occupancy protected by the system is divided into three main classes of risk; extra low hazard (ELH), ordinary hazard (OH), and extra high hazard (EHH). Depending on the compartment and risk level the system is being designed for the densities and area coverage by the sprinklers alters. These are [Nash (1978)]:

Hazard	design density (mm/min)	minimum area (m^2)
ELH	2.25	84
OH	5.0	72 to 360
EHH	7.5 to 30.0	260 to 300

These figures are the minimum requirements for the whole sprinkler system. However, each system is made up of many similar sprinklers which are all fed from the same water supply. So in order for the minimum density to be achieved the sprinklers are arranged in the form of *arrays*, which can be square, oblong, triangular, or staggered so that the sprinkler covers a similar area of floor as the requirements specify [Nash and Young,i (1978)]. The water supply and pipe network must therefore be designed to achieve the minimum performance requirements for the appropriate hazard levels.

The type of sprinkler heads used within an automatic sprinkler installation are thermo-sensitive, designed to react at a pre-determined temperature, as well as independently from one another. They consist of a body which screws into the pipe network and an orifice. The orifice is normally sealed by a valve assembly, which is held in place by a thermally sensitive soldered link, figure A1-1 or glass bulb, figure A1-2. The soldered link type sprinkler is more commonly used in the USA due to the low thermal capacity of the link. In Britain the glass bulb is favoured due to their freedom from susceptibility to corrosive atmospheres. Both activators are colour coded depending on their activation temperature. In the case of the bulb the fluid inside the bulb is coloured whilst for the fusible link the support arm is coded. The colours used, specified by the Fire Offices' Committee are [Nash and Young,ii (1978)]:

Fusible Link Temp (°C)	Colour	Glass Bulb Temp (°C)	Colour
68/74	uncoloured	57	orange
93/100	white	68	red
141	blue	79	yellow
182	yellow	93	green
227	red	141	blue
		182	mauve
		204/260	black

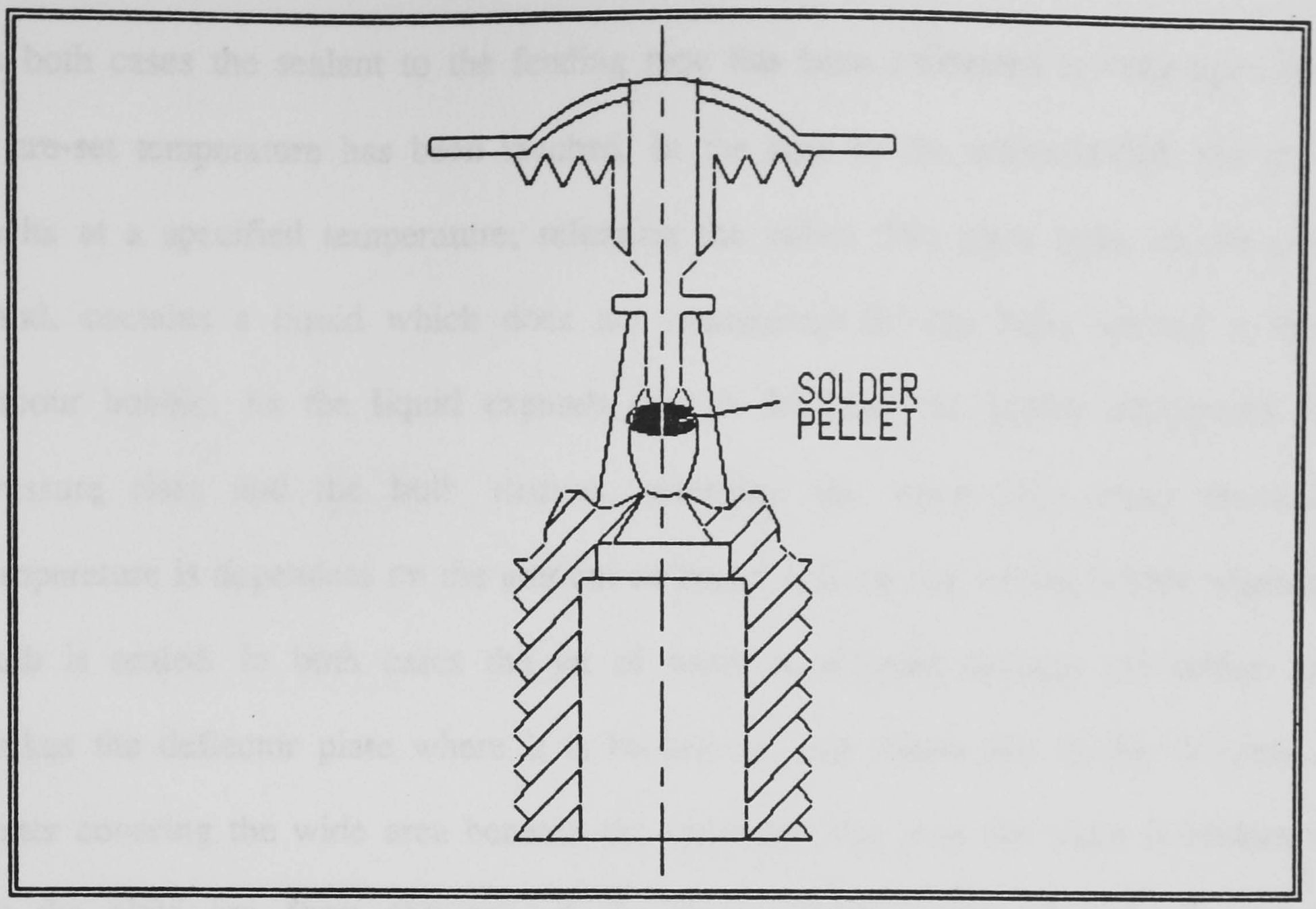

Figure A1-1 Solder Link Sprinkler

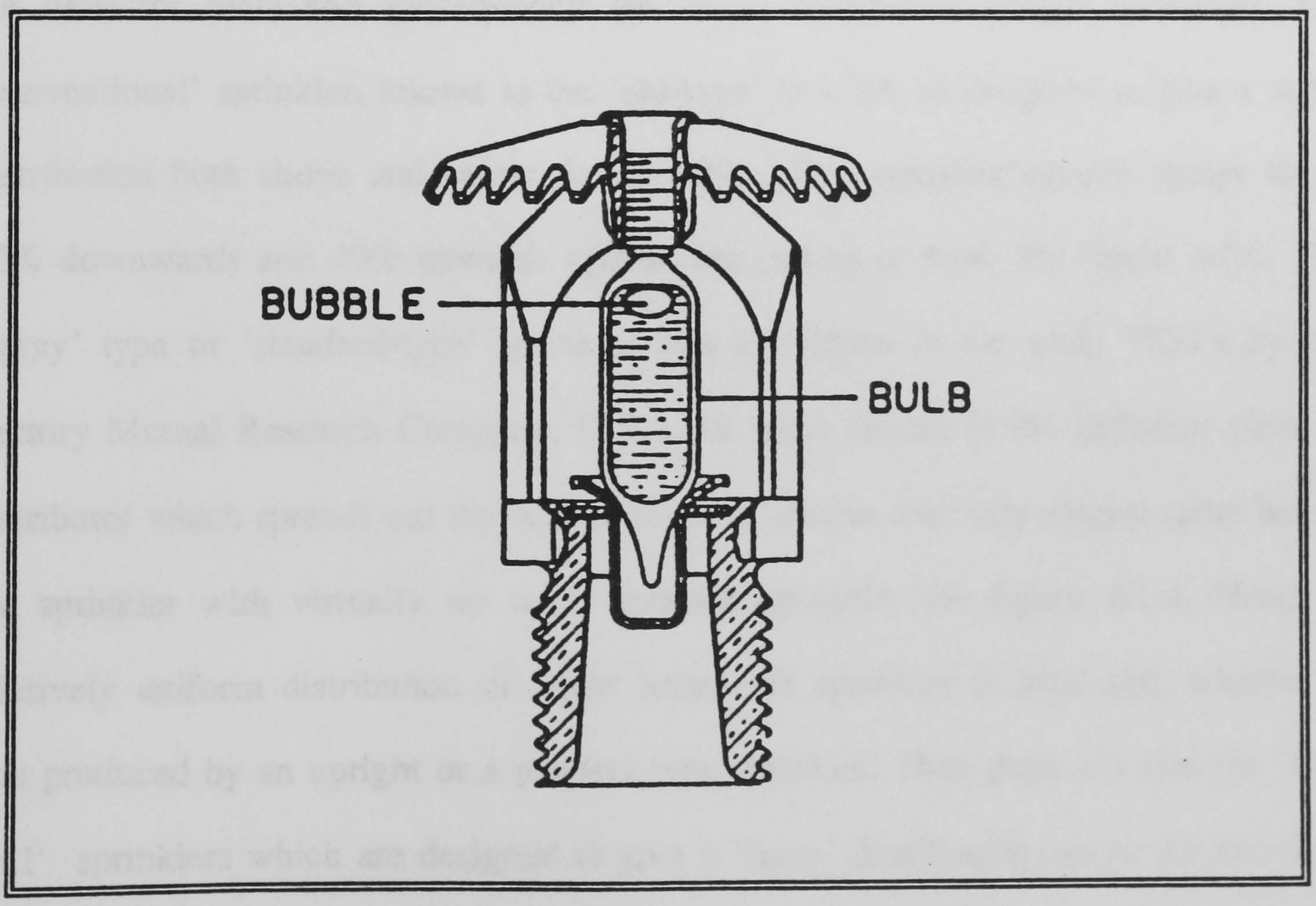

Figure A1-2 Glass Bulb Sprinkler

In both cases the sealant to the feeding pipe has been calibrated to only open once a pre-set temperature has been reached. In the case of the soldered link the solder melts at a specified temperature, releasing the valve. The glass bulb, on the other hand, contains a liquid which does not completely fill the bulb, leaving a small vapour bubble. As the liquid expands due to the heat, the bubble disappears, the pressure rises and the bulb shatters, releasing the valve. The exact operating temperature is dependent on the amount of liquid and the size of the bubble when the bulb is sealed. In both cases the jet of water is released through the orifice and strikes the deflector plate where it is broken up into sheets and finally droplets of water covering the wide area beneath the sprinkler. The way the water is broken up by the plate can form any one of the many distinct types of *umbrella* shaped distribution patterns.

There now exist three main types of sprinkler designs characterised by the shape of the deflector plate and subsequently the water distribution pattern produced. The 'conventional' sprinkler, known as the 'old-type' in USA, is designed to give a water distribution both above and below the sprinkler. This spherical pattern sprays about 60% downwards and 40% upwards against the ceiling or roof; see figure A1-3. The 'spray' type or 'standard-type' sprinkler was developed in the early 1950's by the Factory Mutual Research Company, U.S.A. Its main feature is the deflector plate or distributor which spreads out the stream of water into an *umbrella* shaped spray below the sprinkler with virtually no water sprayed upwards; see figure A1-4. Hence a relatively uniform distribution of water below the sprinkler is produced, whether it was produced by an upright or a pendent type sprinkler. Then there are also the 'side wall' sprinklers which are designed to give a 'skew' distribution below the sprinkler for wetting down the walls on one side as well as throwing much of its discharge back into the room [Nash (1978)].

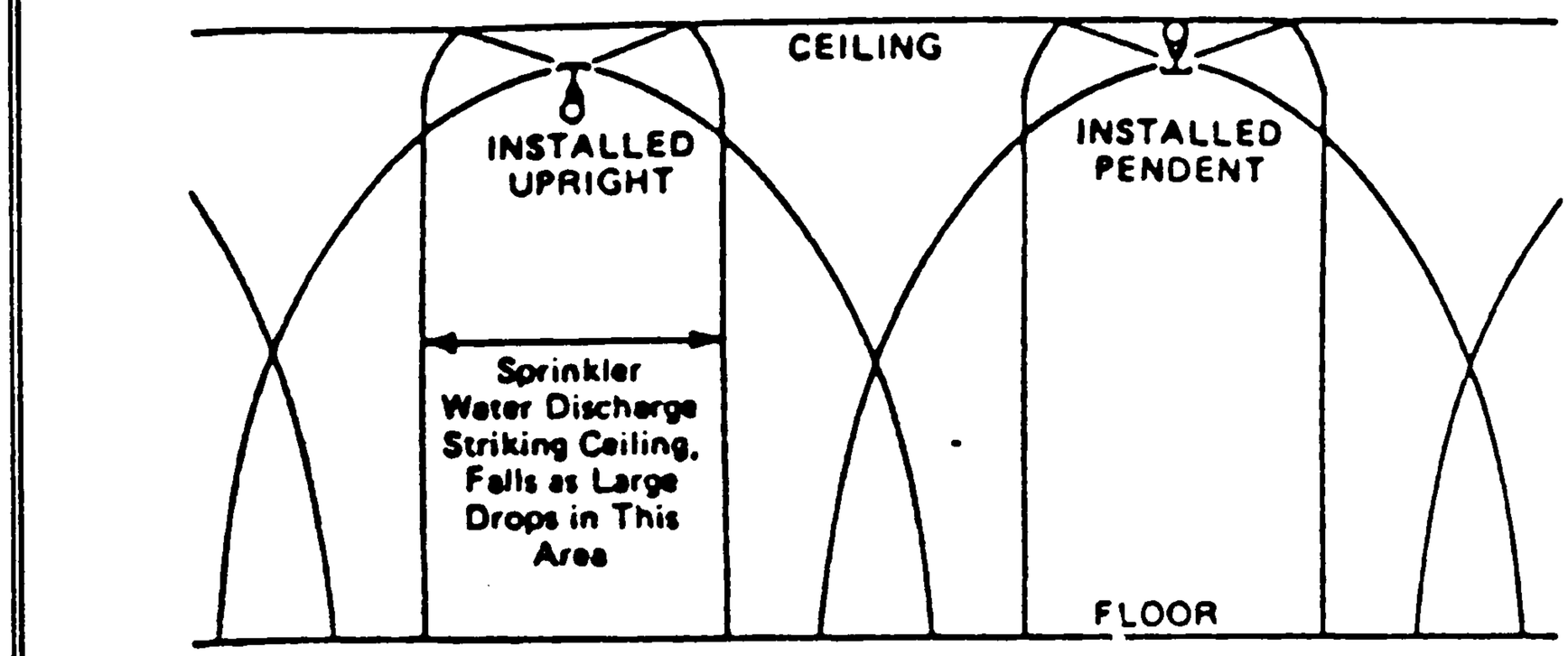

Figure A1-3 Principal Distribution Pattern of water from old sprinklers (pre-1953) [Fire Protection Handbook]

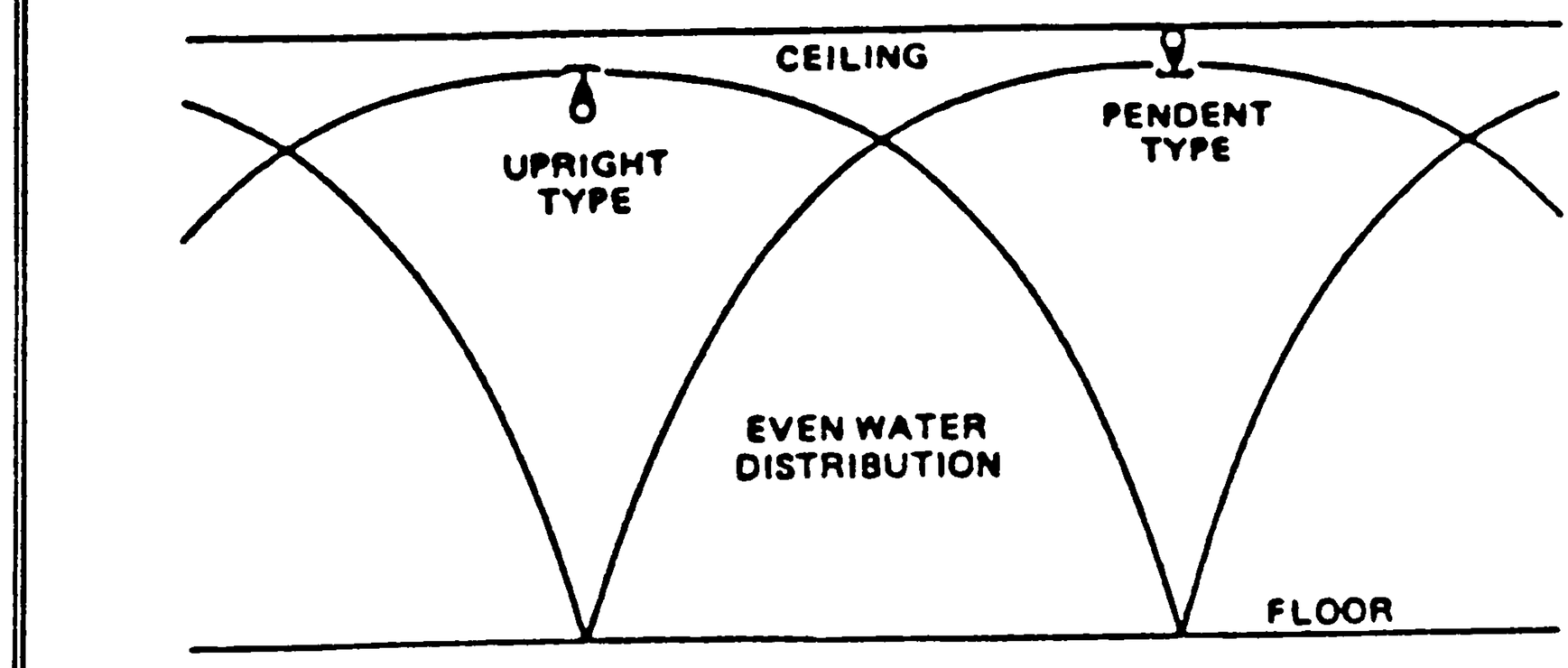

Figure A1-4 Principal Distribution Pattern of water from standard sprinklers (since 1953) [Fire Protection Handbook]

Standards covering the manufacture of these sprinklers do not exist as yet. The National Fire Protection Association (NFPA), U.S.A., and the Fire Offices' Committee, U.K. (now the Loss Prevention Council) do however insist that only listed sprinklers by reputable product evaluation organisations be used in sprinkler systems. (For a detailed description of the different types of automatic sprinkler head designs and their operating principles see the Fire Protection Handbook).

From its humble beginnings the sprinkler system is currently enjoying a more widespread interest across the world. Current research interests vary from developing tests for sprinkler sensitivity analysis like the plunge test [Thorne et al(1988), Theobald (1987)], to new types of sprinkler such as the quick-response sprinkler [Cote (1987)], the on-off sprinkler [Chopra (1986)], the residential sprinkler [Cote (1987)], and sprinklers in aircraft [Daly (1989), Anon,iii,iv,v,vi (1989)].

But in order to be able to develop these new types of sprinklers interest is not only focused on the actual mechanism of the sprinkler, but more importantly on what is being released through the orifice, such as the droplet size distribution, the throw of the water, and the water density.

Fire is a chemical reaction system involving combustion. In order for this combustion to proceed three main factors need to be present to form the fire 'triangle', figure A1-5 [Thorne (1985)]. This triangle consists of fuel, oxidant, and an adequate level of temperature. Hence, if one of the legs of the triangle was to be removed the fire would be extinguished. There are several mechanism which may be involved, such as:

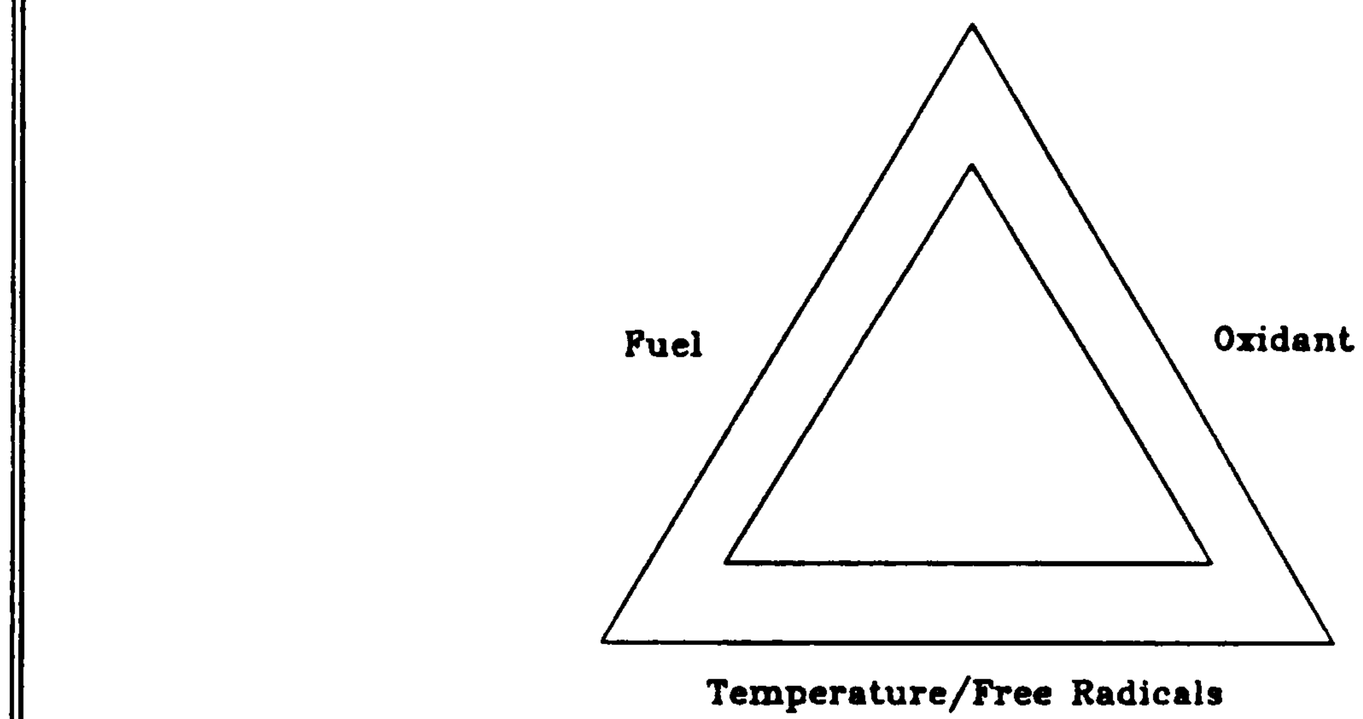

Figure A1-5 Fire 'Triangle' [Thorne (1985)]

1. Cooling of the combustible surface so as to, in the case of a liquid, reduce the vapour pressure and, in the case of a solid, reduce the rate of pyrolysis.

2. Covering the fuel surface with a barrier to reduce emission of fuel vapour. This barrier will also interrupt thermal feedback from the flame.

3. Cooling of flame zone itself. This will have the consequence of reducing the concentration of free radicals.

4. Inhibiting the flame zone by introducing material which will act as a 'sink' for free radicals.

5. Inerting the air feeding the flame by reducing the oxygen partial pressure by the addition of an inert gas.

6. Dilution of a flammable liquid to reduce the partial pressure of flammable vapours.

The principal materials used to implement the above mechanisms are mainly water, foam, halogenated hydrocarbons (Halons), powders and inert gases.

Of these water is the commonest cooling material. It has a high absorption capability due to its very high latent heat of vaporisation and a high specific heat for both its liquid and gas phases. It is especially useful for combustible solids if applied as a spray to minimise 'run off' losses. Fine sprays of water also have an additional cooling effect on the flame zone. The efficiency can be enhanced by a wetting agent to assist penetration of porous surfaces.

In order to reduce the temperature of the fuel the spray must be capable of abstracting heat from the fuel at a rate greater than the rate at which the fuel will take up sensible heat.

The criterion of extinction of a flame by heat abstraction inside the flame is that the combustion products, as they leave the reaction zone, should not exceed the

temperature they would have for lower limits flame. If a spray is capable of removing all the heat of combustion from the flame, then the flame will be extinguished.

The factors which control the penetration of the water to the seat of a fire are the drop size and the thrust of the spray, the thrust of the flame and the evaporation of the water within the flames.

There are two major factors which determine the quality of a sprinkler - its cooling efficiency and its delivery rate. However it is the optimum droplet size which is of prime importance to the fighting efficiency and effectiveness of the sprinkler.

The basic function of a sprinkler system is to extinguish a fire as quickly as possible or at least to control it in the best possible way. It is also essential to use as few sprinkler heads as are absolutely necessary in order to minimise water damage. Hence the droplets to be released through the orifice need to be able to perform three main tasks [Yao and Kalelkar (1970)]:-

1. they need to be able to penetrate the rising fire plume to extinguish the burning surface

2. cool the flame and ambient atmosphere, especially under the ceiling to prevent an excessive number of sprinklers from opening.

3. wet and cool immediately surrounding combustibles that are subject to direct exposure to the fire.

There is therefore a dichotomy. If greater penetrability of the drops through the plume is required large sized droplets should be used, but cooling is obtained from smaller droplets which give rise to larger surface areas.

The size of droplets released through a sprinkler head is dependent on the geometry of the orifice as well as the flow rate of the water [You (1984)]. It is this latter factor which also plays a vital role in the extinguishing phenomena.

Investigations have shown that a spherical water droplet released at high velocities decelerate to take up a terminal velocity, the point when the drag forces balance the gravitational force. Therefore, if the velocity of the hot gases is larger than the terminal velocity, the motion of the drop will be reversed. Even if the release velocity was to be increased, large droplets (> 6mm) become unstable and break up.

Another point to consider is that the water droplets are evaporating as they penetrate the hot layer and the plume. Hence the gravitational force acting on the drop is decreasing as the mass is decreasing. However, the drag force opposing the motion of the drop is increasing.

In a given situation, some drops will penetrate the plume and others will not. Hence the larger the drop the larger the mass, and consequently the gravitational force acting on it is larger. This implies that larger drops have a greater penetrability, but only if their droplet size is stable in terms of break up. The optimum droplet size for fire extinguishment is 4-5 mm in diameter [Yao and Kalelkar (1970)].

Quick response sprinklers

Quick Response sprinklers (QRS) are hailed as one of the major new advances in the field of fire protection. The difference between them and standard sprinklers is their

response or sensitivity. QR sprinklers are designed to have less of a 'thermal lag' and hence to operate much faster than standard sprinklers. This can best be seen when comparing the response time index (RTI) [Heskestad and Bill (1988)], whereby the smaller the index the faster the operation. Some typical RTI levels are [Fleming (1988)]:

standard sprinkler	100-400 $s^{1/2}$ $m^{1/2}$
QR sprinkler	25-55 $s^{1/2}$ $m^{1/2}$

There are currently three types of QRS sprinklers under active development: residential, quick response standard and early suppression fast response (ESFR).

Residential Sprinklers

Nowadays, the reality and fatal consequences of house fires are constantly being pressed into our minds through the media. Hardly a week goes by without the shocking news of another house being totally gutted by a fire within seconds not allowing enough time for the occupants to escape. The usual consequence being that either young toddlers and children or their parents are killed in the tragedy. In fact 75% of U.K. fire deaths occur in the home [Anon,vii (1989)].

Following this type of destruction the fire chiefs are always very quick at pointing out that the lethal fumes given off by the burning P.U. foam furniture were the cause of mortality. However vital seconds necessary for safe egress might be gained by the installation of smoke detectors which are now widely available. These smoke detectors will then be able to save lives. But what about the further consequences of fires - the destruction of property?

The installation of sprinkler systems within buildings has always been seen as effective means of reducing fire losses. The activation of sprinklers reduces the number of deaths and injuries, direct property loss and indirect fire loss [Harmathy (1988)]. The concept of residential sprinklers was first conceived in the early 1970s with sprinkler developed specifically for the use in residential occupancy such as one- and two-family houses and mobile homes.

These new sprinklers not only are more sensitive and react faster than standard sprinklers but their spray patterns have also been changed. As they will generally be operating as single sprinklers within a room the spray needs to be more uniform as there will be no areas of overlapping which can be relied upon. As the sprinklers also need to protect the boundaries such as curtains, the spray pattern needs to be able to throw the water to these areas [Cote (1987)].

As yet these sprinklers have only found a market in the U.S.A. where the insurance companies are encouraging their installation by offering a 10% discount on a homeowner policy [Teague (1988)]. The economics of mandatory sprinkler installation though is a 'proposition not supportable on economic grounds' [Harmathy (1988)]. However a potentially new market has recently been found in Britain where they are now seen as a favoured means of backing up fire detection. Their importance was clearly demonstrated in an article in Fire Prevention [Anon,vii (1989)]. The Hampton Court fire in 1986 needed 525000 gallons of water to fight it. It is now believed that a single domestic sprinkler could have sufficed. The building is still drying out.

Early Suppression Fast Response (ESFR)

Recent advances in sprinkler technology has resulted in a new system termed ESFR (Early Suppression Fast Response). This system has been initially designed for the challenge of high-storage fire protection. Emphasis was placed on early suppression with fast response only acting as the means to accomplish it [Yao (1988)]. The basic concept behind ESFR is that sufficient amount of water is delivered during the early stages of the fire in order to suppress it quickly before a severe situation is reached. In that way fewer sprinklers will operate and hence less fire and water damage will result.

On-Off sprinklers

As in the case for the types of QRS sprinklers, standards are also reviewed for an alternate sprinkler design; the on-off sprinkler. This system has been designed to shut off water supply after the ceiling temperature has dropped to below a certain safety level of about 35 °C. If the fire should flare up again the sprinkler is re-activated once a pre-determined critical level has been reached. Though there are different designs amongst on-off sprinklers, their main mode of operation is a bi-metallic disc which changes shape depending on the temperature. The advantages of these sprinklers are numerous [Chopra (1986)]. The most obvious though is that they conserve water and hence reduce the amount of water damage.

Sprinklers in aircraft

Following the 1985 Manchester airport disaster, considerable interest has been focused on developing a sprinkler system for use in aircraft. SAVE (Safety Aircraft and Vehicle Equipment) company has developed a water-mist cabin fire suppression system which they claim is "the first system to kill fire, cool temperatures, wash air, and maintain visibility".

Their system, which was tested at Teeside Airport in 1988, was able to keep the temperatures within the cabin survivable and hindered fire penetration through sprayed areas. However, the highly toxic levels given off during cabin fires still remained significant [Daly (1989)].

Following these early tests the Civil Aviation Authority is funding further investigation into the system during an 18-month study at the Fire Research Station, Borehamwood, to obtain the first quantitative data on how well the new system performs [Anon,iii,iv,v,vi (1989)]. British Petroleum is also currently involved in the development of a prototype aircraft sprinkler system. Though they reveal little, the major difference between their and Save's system is that BP use a water/compressed air mixture in the spray rather then just water.

Appendix 2

General Fluid Properties

Appendix 2 General Fluid Properties

For completeness the equations and constants of the gas and water properties used within chapters 2 to 5 are given within this appendix.

Gas Density

When modelling the smoke flow generated by a fire one important fluid property that needs to be considered is the density. As air is warmed up it becomes lighter and hence its density decreases. This inverse relationship between density and temperature is taken into account in the following equation:

$$\rho = 1.0 / \alpha * H_s \qquad \text{(A2-1)}$$

where α is a constant, $2.8347*10^{-6}$, determined by assuming an initial enthalpy of $2.88*10^{5}$ (~15°C), and an initial density of 1.227. As combustion was not taken into account the above density relation is only applicable to uncontaminated air.

Water Density

The density of water is taken to be:

$$\rho = 1000.0 \qquad \text{(A2-2)}$$

Kinematic Viscosity

The kinematic viscosity, a ratio between absolute viscosity, μ, and density, ρ, was taken for the single phase model as:

$$\nu = 2.235*10^{-5} \qquad \text{(A2-3)}$$

For the two-phase calculations a relationship was obtained using statistical analysis, between the kinematic viscosity and temperature. The relation obtained and used is:

$$\nu = -9.991*10^{-6} + 6.534*10^{-8}*T_g + 6.203*10^{-11}*T_g^2 \qquad \text{(A2-4)}$$

Prandtl Number

For the single phase calculations the laminar Prandtl number of the gas phase was taken to be a constant of 0.7. However, for the two-phase calculations a relation between the Prandtl number and the temperature was obtained from statistical analysis. The relation obtained and used is:

$$Pr = 0.790282 - 4.283411*10^{-4}*T_g + 5.180381235*10^{-7}*T_g^2 - 1.787353489*10^{-10}*T_g^3 \qquad \text{(A2-5)}$$

The turbulent Prandtl number used for the k-ε model, see Tables 1 and 2, was taken to be 0.9.

Appendix 3

The SIMPLEST Algorithm

Appendix 3 The SIMPLEST Algorithm

SIMPLEST is an extension to the SIMPLE algorithm (Semi-Implicit Method for Pressure-Linked Equations) [Patankar (1980)]. The difference between the SIMPLE and SIMPLEST algorithms is that the coefficients A_E, A_W, A_N, A_S, A_H, and A_L of the momentum equation (2.4-13) now only contain the diffusion contribution. The convection terms are added to the source terms. Hence, the resulting momentum equation discretisations remain to be of the same form.

These momentum equations are solved for with an estimated pressure field p^*. Unless the correct pressure field is employed the resulting velocity field will not satisfy continuity and thus be denoted by an intermediate velocity field; u_i^*, v_i^* and w_i^*. This velocity field results from the solution of the following equations:-

$$
\begin{aligned}
(A_P - S_{uP}^P)\,(u)_e^* &= \Sigma\, A_j\,(u)_j^* + S_{uP}^C V_C + (p_P^* - p_E^*)\,A_e \\
(A_P - S_{vP}^P)\,(v)_e^* &= \Sigma\, A_j\,(v)_j^* + S_{vP}^C V_C + (p_P^* - p_N^*)\,A_n \\
(A_P - S_{wP}^P)\,(w)_e^* &= \Sigma\, A_j\,(w)_j^* + S_{wP}^C V_C + (p_P^* - p_H^*)\,A_h
\end{aligned}
\qquad \text{(A3-1)}
$$

The next step is to improve the guessed pressure, p^*, using a pressure correction term, p', so that the correct pressure is given by:

$$p = p^* + p' \qquad \text{(A3-2)}$$

Following this pressure correction the velocities need to be corrected in a similar manner. The corresponding velocity corrections are given by:

$$u = u^* + u' \quad v = v^* + v' \quad w = w^* + w' \tag{A3-3}$$

Expressions for the velocity corrections can be obtained by subtracting equations (2.5-1) from equations (2.4-13) respectively. These corrections are as follows:

$$(u)'_e = (p'_P - p'_E)\, A_e / (A_P - S^P_{uP})$$
$$(v)'_n = (p'_P - p'_N)\, A_n / (A_P - S^P_{vP})$$
$$(w)'_h = (p'_P - p'_H)\, A_h / (A_P - S^P_{wP}) \tag{A3-4}$$

These expressions for the velocity corrections can now be used to construct equations for the velocity components. These are:

$$(u)_e = (u)^*_e + \frac{(p'_P - p'_E)}{A_P - S^P_{uP}} A_e$$
$$(v)_n = (v)^*_n + \frac{(p'_P - p'_N)}{A_P - S^P_{vP}} A_n$$
$$(w)_h = (w)^*_h + \frac{(p'_P - p'_H)}{A_P - S^P_{wP}} A_h \tag{A3-5}$$

Finally a pressure correction equation can be derived from the continuity discretisation equation (2.4-15) for the time dependent case in order to solve for p'. Substituting all the velocity equations of (2.5-6) for all the velocity components in the continuity equation (2.4-15) gives the pressure correction equation for p' as:

$$A_P p' = A_E p'_E + A_W p'_W + A_N p'_N + A_S p'_S + A_H p'_H + A_L p'_L + b \tag{A3-6}$$

where

$$A_E = \frac{(A^2\,\rho)_e}{A_P - S_{V_P}^P} \qquad A_W = \frac{(A^2\,\rho)_w}{A_P - S_{V_P}^P}$$

$$A_N = \frac{(A^2\,\rho)_n}{A_P - S_{V_P}^P} \qquad A_S = \frac{(A^2\,\rho)_s}{A_P - S_{V_P}^P}$$

$$A_H = \frac{(A^2\,\rho)_h}{A_P - S_{V_P}^P} \qquad A_L = \frac{(A^2\,\rho)_l}{A_P - S_{V_P}^P}$$

$$A_P = A_E + A_W + A_N + A_S + A_H + A_L$$

$$b = (\rho A u^*)_w - (\rho A u^*)_e + (\rho A v^*)_s - (\rho A v^*)_n + (\rho A w^*)_l - (\rho A w^*)_h$$

The equations described in the above section are solved for in the following sequence:

1. guess starting pressure p^*
2. using the momentum equations (A3-1) solve for $(u)^*$, $(v)^*$ and $(w)^*$
3. evaluate the pressure-correction using equation (A3-6)
4. calculate for a new pressure p using equation (A3-2)
5. calculate the new velocity components u, v and w using equation (A3-5)
6. solve for the enthalpies using the discretisation equation (2.4-9)
7. use the new pressure p as a starting value for p^*
8. return to step 2 and continue until the convergence criterion has been satisfied

Appendix 4

Interphase Transport settings in PHOENICS

Appendix 4 Interphase Transport settings in PHOENICS

The two-phase, time-dependent study presented within chapter 5 used PHOENICS 84, version 1.3, as its main equation solver. The equations it solved are detailed in their respective section within the chapter. However, the main aim of this appendix is to clarify how the interphase processes, vital for this particular study, where implemented within the guidelines set by PHOENICS.

The setting of the interphase transport equations within PHOENICS is performed in exactly the same manner as is used to set up boundary or special conditions, namely source terms. These source terms are of the general form:

$$S_P = C_P * (V_P - \Phi_P) \qquad \text{(A4-1)}$$

Using PHOENICS terminology, the interphase sources set are:

$$S_{\Phi,1} = (FIP * CINT(PHI1) + \max(0,\dot{m}))*(PHINT(PHI1) - \Phi_{P,1})$$
$$S_{\Phi,2} = (FIP * CINT(PHI2) + \max(0,-\dot{m}))*(PHINT(PHI2) - \Phi_{P,2}) \qquad \text{(A4-2)}$$

where FIP is the interphase friction force. It should be noted that the friction force, equation (4.2-7), and the mass transfer rate, equation (4.3-13), need to be modified prior to using them within PHOENICS in order to account for the volume of the control cell over which the force is calculated.

The definition and use of CINT and PHINT have proven themselves to be at the heart of this study. Due to their importance the following section aims to clarify their use.

The application of CINT and PHINT

In the case of simultaneous heat and mass transfer between two phases, the processes taken into consideration can be seen in figure A4-1. The notation used has the following meanings:

$\mathring{q}_{1,i}$,$\mathring{q}_{2,i}$ - heat transfer rate between the bulk of the phases and the interface

h_1^*, h_2^* - the values of phase 1 and phase 2 enthalpy at the interface

$\mathring{m}$ - interphase mass transfer rate (assumption: mass is transferred from the denser to the lighter phase, ie. from phase 2 to phase 1)

whereby $\mathring{q}_{1,i}$ and $\mathring{q}_{2,i}$ are termed in equations (A4-2) as CINT and h_1^* and h_2^* as PHINT.

In chapter 4, the equations for evaluating the particle surface temperature and heat transfer coefficients are given. These were used within the above stated guidelines of CINT and PHINT in the following manner.

CINT

The heat transfer rate between the bulks of the phases and the interface were calculated using the heat transfer coefficients, a_g and a_l, given in equations (4.3-9) and (4.2-22) respectively. These were modified prior to using them within the iterations by taking into account the number of droplets present within a control volume, n, (see equation (4.2-19)) and the size of the control volume currently iterated on. Hence CINT is given by:

$$CINT(i) = a_i * n * Vol \qquad (A4-3)$$

where i refers to the phase in question.

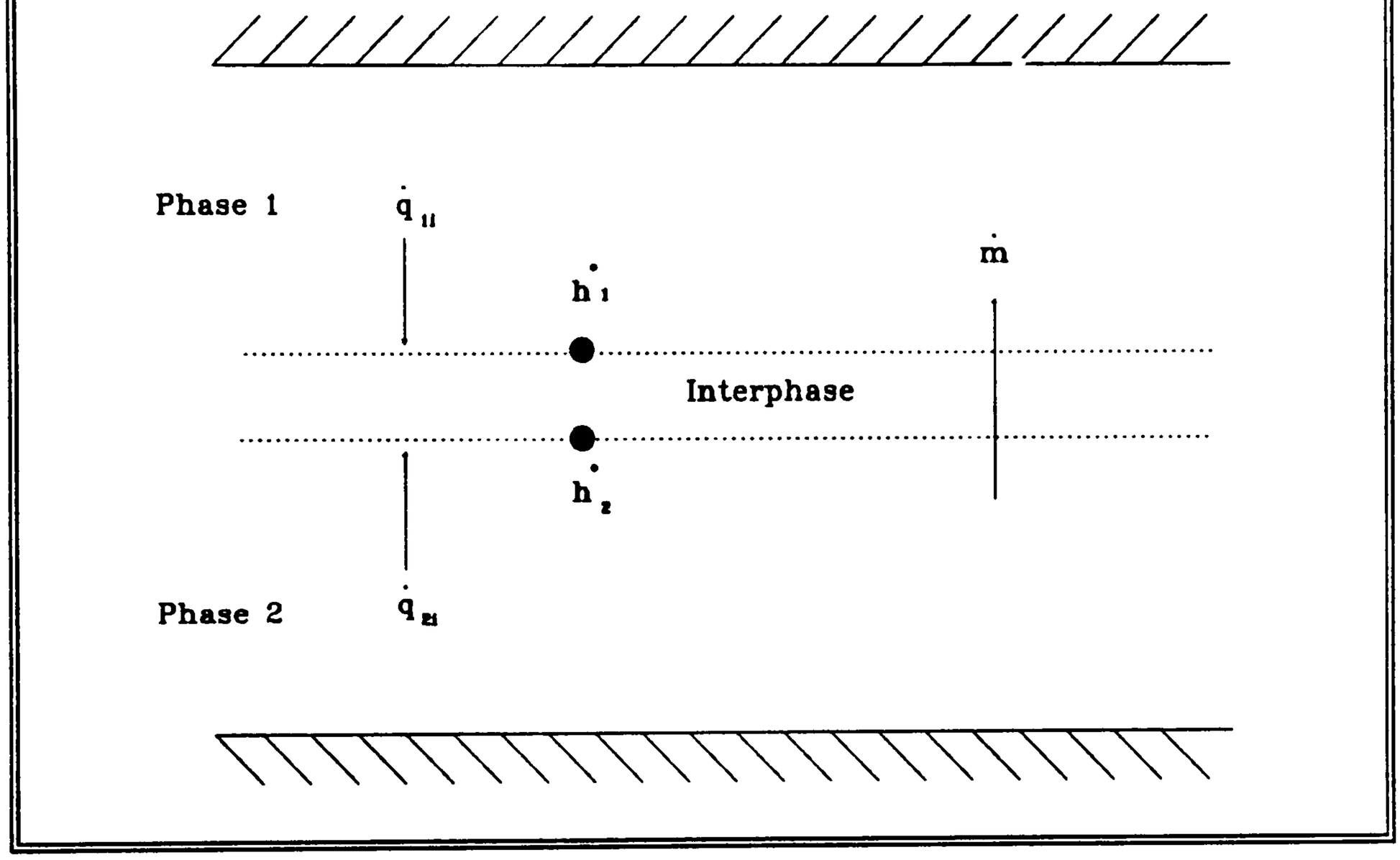

Figure A3-1 Diagram illustrating the interphase settings

PHINT

The value of the enthalpy at the interface for each respective phase was calculated using the interphase temperature, equation (4.3-19). This temperature was converted for each phase into an enthalpy by taking into account the respective specific heat. Hence PHINT is given by:

$$PHINT(i) = T_s * Cp_i \qquad (A4\text{-}4)$$

where i refers to the phase in question.